Multi-resolution physiological modeling for the analysis of cardiovascular pathologies

David Ojeda Avellaneda

ANNÉE 2013

UNIVERSITÉ DE RENNES 1

THÈSE / UNIVERSITÉ DE RENNES 1

sous le sceau de l'Université Européenne de Bretagne

pour le grade de

DOCTEUR DE L'UNIVERSITÉ DE RENNES 1

Mention : Traitement du Signal et Télécommunications

École doctorale Matisse

présentée par

David Ojeda Avellaneda

Préparée à l'unité de recherche INSERM, U1099
Laboratoire de Traitement du Signal et de l'Image
UFR ISTIC: Informatique et Électronique

Multi-resolution physiological modeling for the analysis of cardiovascular pathologies

Thèse à soutenir à Rennes
le 10 décembre 2013

devant le jury composé de :

Catherine MARQUE
PU à l'Université de Technologie Compiègne / *Rapporteur*

Vanessa DIAZ-ZUCCARINI
Lecturer à University College London / *Rapporteur*

Michel ROCHETTE
Directeur de Recherche chez ANSYS / *Examinateur*

Jean-Philippe VERHOYE
PH/PU à l'Université de Rennes 1 / *Examinateur*

Alfredo I HERNÁNDEZ
Chargé de Recherche INSERM, HDR / *Directeur de thèse*

Virginie LE ROLLE
MC à l'Université de Rennes 1 / *Co-directrice de thèse*

Abstract

This thesis presents three main contributions in the context of modeling and simulation of physiological systems. The first one is a formalization of the methodology involved in multi-formalism and multi-resolution modeling. The second one is the presentation and improvement of a modeling and simulation framework integrating a range of tools that help the definition, analysis, usage and sharing of complex mathematical models. The third contribution is the application of this modeling framework to improve diagnostic and therapeutic strategies for clinical applications involving the cardio-respiratory system: hypertension-based heart failure (HF) and coronary artery disease (CAD). A prospective application in cardiac resynchronization therapy (CRT) is also presented, which also includes a model of the therapy. Finally, a final application is presented for the study of the baroreflex responses in the newborn lamb. These case studies include the integration of a pulsatile heart into a global cardiovascular model that captures the short and long term regulation of the cardiovascular system with the representation of heart failure, the analysis of coronary hemodynamics and collateral circulation of patients with triple-vessel disease enduring a coronary artery bypass graft surgery, the construction of a coupled electrical and mechanical cardiac model for the optimization of atrio ventricular and intra ventricular delays of a biventricular pacemaker, and a model-based estimation of sympathetic and vagal responses of premature newborn lambs.

Résumé en français

Les maladies cardiovasculaires représentent la principale cause de mortalité chez les adultes (30% des décès enregistrés en 2004) dans l'ensemble des pays membres de l'Organisation Mondiale de la Santé (WHO, 2008). Les processus impliqués dans les maladies cardiovasculaires sont le plus souvent complexes et multifactoriels. C'est le cas de l'insuffisance cardiaque (IC) qui est une pathologie présentant l'une des plus fortes prévalences dans le monde. Dans l'IC, la réduction significative du débit cardiaque est due à des modifications des propriétés mécaniques du myocarde et est parfois liée à une altération de l'activation électrique (désynchronisation intra ou inter-ventriculaire). De nombreux mécanismes (nerveux ou hormonaux) de régulation sont alors activés, couvrant ainsi des échelles de temps très différentes (de la seconde à la semaine). Bien que ces mécanismes puissent compenser les conséquences de l'IC à court terme, leurs effets peuvent devenir délétères à moyen et long terme, accentuant ainsi les dysfonctionnements ventriculaires. On peut notamment observer une augmentation de la précharge et de la postcharge, un remodelage cardiaque, des œdèmes pulmonaires ou périphériques, une baisse du débit rénal et des difficultés respiratoires.

L'étude de telles pathologies multifactorielles nécessite l'acquisition de données cliniques susceptibles de pouvoir fournir des indicateurs de l'état du patient. Or l'analyse de ces données peut s'avérer complexe car celles-ci peuvent *i)* provenir de différentes modalités d'acquisition, *ii)* être associées à différents organes, *iii)* couvrir différents intervalles temporels, et *iv)* être nombreuses et difficile à analyser et interpréter. Dans ce contexte, une approche à base de modèle pourrait être utile à l'analyse de données cliniques et à la compréhension des évènements impliqués dans un état pathologique. En effet, l'utilisation de la modélisation dans ce contexte peut constituer une aide à l'analyse des phénomènes observés cliniquement à partir des hypothèses incluses dans le modèle et à la compréhension du fonctionnement d'un système physiologique. Par ailleurs, l'utilisation de modèles peut être utile à la prédiction du comportement futur (et des pathologies éventuelles pouvant survenir) et à l'assistance pour la définition de nouvelles thérapies, par exemple dans le cadre des thérapies de resynchronisation cardiaque.

Plusieurs modèles des différents composants de systèmes physiologiques (activité cardiaque, respiration, fonction rénale, système nerveux autonome, etc.) ont été proposés dans la littérature à différents niveaux de détail. L'intégration de ces différents modèles peut permettre de mieux analyser et de mieux comprendre les processus physiopathologiques complexes résultant de leur interaction. Au moins deux types d'intégration peuvent être identifiés : l'intégration structurelle (ou *verticale*) et l'intégration fonctionnelle (ou *horizontale*). La plupart des travaux présentés

aujourd'hui sont basés sur une intégration structurelle exhaustive (de la cellule à l'organe, par exemple), impliquant des modèles complexes, en termes du nombre des variables d'états représentées, d'éléments impliqués, etc. Ces modèles conduisent à des simulations lourdes et sont difficiles à analyser, à identifier et à exploiter dans un contexte pratique. Les modèles qui visent une intégration horizontale fonctionnelle, couplant différents sous-systèmes physiologiques, sont moins présents dans la littérature. Même si ces modèles sont plus aisés à manipuler (numériquement et mathématiquement), ses éléments constituants ne disposent pas du niveau de détail suffisant pour expliquer certains modes de fonctionnement du système à analyser.

Un moyen de contourner ces problèmes est de représenter différentes fonctions à des échelles distinctes, dans une approche multi-résolution. Cela implique la création de modèles intégrant plusieurs composantes physiologiques développées à différents degrés de complexité structurelle en fonction de l'objectif clinique. Cependant, ces modèles peuvent présenter des formalismes hétérogènes (c'est-à-dire modèles continus d'équations différentielles ; modèles discrets, tels qu'automates cellulaires, etc.), plusieurs niveaux de résolutions ou différentes dynamiques temporelles. Le couplage de modèles hétérogènes implique des difficultés techniques et méthodologiques tel que :

- la création d'un environnement approprié basé sur un *modèle de base* (ou « core model ») modulaire et sur des outils spécifiques de modélisation et de simulation de modèles couplés hétérogènes,
- la définition d'une méthode d'interfaçage pour le couplage de ces modèles hétérogènes préservant la stabilité et les caractéristiques essentielles de chaque modèle.

Cette thèse propose des solutions afin de contourner ces problèmes et représenter différentes fonctions à des échelles distinctes, dans une approche multi-résolution, en définissant les interfaces nécessaires à l'intégration de modèles. L'approche proposée pour l'interfaçage de modèles hétérogènes intègre : *i)* la restructuration des modèles devant être couplés, *ii)* l'analyse de sensibilité réalisée sur les modèles, et *iii)* la définition des transformations nécessaires sur les entrées/sorties. L'implémentation de cette approche de modélisation intégrative nécessite l'utilisation d'une librairie de simulation adaptée. Dans ce cadre, un environnement de modélisation et de simulation, précédemment développé au laboratoire, appelé « Multiformalism Modeling and Simulation Library » (M2SL) a pu être utilisé et amélioré. Des outils d'analyse des paramètres (analyses de sensibilité et identification de paramètres) ont notamment pu être ajoutés aux fonctionnalités existantes dans M2SL permettant ainsi de mieux appréhender les caractéristiques de modèles hétérogènes et de faciliter le couplage avec des données cliniques.

Dans cette thèse, la méthodologie concernant l'utilisation de modèles multi-résolution en physiologie a pu être appliquée à plusieurs cas cliniques : *i)* l'étude des conséquences court et moyen terme de l'insuffisance cardiaque, *ii)* la modélisation spécifique-patient des coronaires pour l'étude de la circulation collatérale, *iii)* l'analyse spécifique-patient de modèles cardiovasculaires pour l'optimisation de thérapies de resynchronisation cardiaque, et *iv)* l'évaluation des voies sympathique et vagale chez l'agneau nouveau-né.

La première application traitée dans cette thèse concerne un exemple typique de couplage

entre un modèle d'intégration horizontal couplé avec un modèle de ventricule plus résolu. Le travail pionnier de Guyton (Guyton et al., 1972) sur l'analyse de l'ensemble de la régulation du système cardio-vasculaire a été utilisé et les ventricules non-pulsatiles du modèle de Guyton ont été remplacés par des représentations pulsatiles des ventricules sous forme d'élastance qui s'exécutent à une échelle temporelle plus réduite. Des analyses de sensibilité ont notamment été réalisées pour comparer le modèle original et le modèle pulsatile. Par ailleurs, un épisode d'IC congestive a pu être simulé pour observer les variations des variables de régulation à court et moyen terme. Les variations caractéristiques des pressions artérielles systolique et diastolique ont notamment été observées, ce qui n'est pas possible avec le modèle original.

Ensuite, le cadre de modélisation et de simulation proposé a pu être appliqué à l'étude de la circulation coronarienne afin d'analyser des données cliniques obtenues durant des procédures de pontage coronarien. L'analyse des paramètres du modèle a permis de mettre en évidence l'importance de la circulation collatérale qui est un réseau de vaisseaux alternatifs se développant pour compenser la diminution du flux sanguin du réseau coronaire en cas de sténoses significatives. L'apport principal de ce travail est la création de modèles spécifique-patient dans le cas d'atteinte tritronculaire. Les données cliniques obtenues durant les pontages de dix patients ont pu être reproduites de manière satisfaisante avec le modèle et le développement des vaisseaux collatéraux a pu être évalué.

Une autre application clinique concerne l'étude de la perte de synchronisation cardiaque chez 25% à 50% des patients souffrant d'IC. Dans ce cas, une thérapie de resynchronisation cardiaque (CRT), qui consiste en l'implantation d'un pacemaker, peut être utilisée pour stimuler l'activité électrique cardiaque de manière à restaurer la coordination atrio-ventriculaire et intra-ventriculaire. Le modèle utilisé pour cette application clinique intègre : *i)* un modèle macroscopique de l'activité électrique cardiaque, *ii)* un modèle mécanique des ventricules et des oreillettes, et *iii)* des modèles des circulations systémique et pulmonaire. Le modèle complet intègre donc les activités électrique et mécanique cardiaques basées sur des formalismes différents. Cette application comporte deux apports principaux : la présentation de différentes analyses de sensibilité des paramètres du modèle mettant en évidence les paramètres systoliques ventriculaires, les paramètres reliés à la précharge et ceux en lien avec la description des propriétés diastoliques des ventricules. Ces paramètres ont des effets importants sur les indicateurs cliniques utilisés pour l'optimisation de la CRT ; la création de modèles spécifique-patient de sujets traités par CRT.

La dernière application clinique traitée dans cette thèse concerne l'analyse de l'activité du baroréflexe en néonatologie. En effet, l'activité autonomique est fortement impliquée dans les mécanismes qui mènent aux phénomènes d'apnée-bradycardie observés chez certains nouveau-nés. En effet, le baroréflexe est particulièrement immature durant les premiers jours de vie, particulièrement dans le cas de la prématurité, et il peut être intéressant d'évaluer les activités sympathique et vagal afin de mieux comprendre les mécanismes sous-jacents. Pour mener cette étude, un protocole expérimental a été défini en partenariat avec l'Université de Sherbrooke. Ce protocole a permis l'acquisition de signaux expérimentaux sur 4 agneaux nouveau-nés pendant des manœuvres d'activation du baroréflexe. Une identification récursive des paramètres du modèle

de baroréflexe a pu être réalisée de manière à évaluer les variations des activités des voies vagale et sympathique pendant des injections de vasoconstricteur et de vasodilatateur.

Ainsi, les quatre applications cliniques traitées dans cette thèse mettent en évidence l'applicabilité de la méthode d'intégration de modèles multi-résolution en physiologie. Un apport majeur de cette thèse est la formalisation et la généralisation de la méthodologie nécessaire à cette approche. Cette analyse théorique est accompagnée d'améliorations significatives des outils de modélisation et de simulation précédemment développés au laboratoire. Ces améliorations concernent notamment l'exécution de modèles mathématiques complexes et hétérogènes, ainsi que l'analyse et l'identification des paramètres de ces modèles. Ces outils sont centralisés dans M2SL qui est déjà utilisé dans différents laboratoires et est listé comme l'un des logiciels de simulation dans le réseau d'excellence « Virtual Physiological Human » (VPH NoE). L'application de ces outils pour la modélisation et l'analyse de systèmes physiologiques montre la pertinence de l'approche pour l'étude de problèmes cliniques concrets.

Contents

CHAPTER 1

Introduction

Pathological processes are intrinsically complex, since they are multifactorial and they bring into play a variety of functions and regulatory loops involving different levels of detail (from the sub-cellular to the whole organism, for example) and different physiological sub-systems (cardiac, respiratory, etc.). They are often the result of interactions between a set of local perturbations and the alteration of physiological regulatory feedback loops. Cardiovascular diseases, one of the leading causes of mortality and morbidity worldwide, are an example of these multifactorial pathologies. For instance, heart failure (HF), the pathological state where the heart cannot maintain a proper blood flow to meet the needs of the body, is intrinsically related to the heart. Yet, in order to understand the mechanisms underlying this pathology, a systemic analysis of the complex interactions between the cardiac function, the circulatory system, the autonomic nervous system, the renin-angiotensin-aldosterone system and the respiratory system are needed.

Multivariate biomedical data processing is a crucial aspect for handling this complexity and for improving the understanding of these multifactorial pathologies. The main purpose of these data processing methods is to extract quantitative and objective information from all the available and relevant sources of biomedical data, so as to improve our knowledge on the system under study and provide valuable diagnostic and therapeutic markers. The field of biomedical data processing has significantly evolved during the last decades and a wide variety of methods have been proposed in the literature. However, the appropriate processing and analysis of multivariate biomedical data remains a difficult task and a number of specific research challenges are still to be overcome.

One of the main challenges concerns multivariate data collection. Indeed, biomedical data are often collected asynchronously, in noisy and non-stationary conditions, using a variety of heterogeneous observation modalities (signals, images, textual data, etc.) that carry information at different spatial and/or temporal scales. Data fusion and association methods have shown to be useful for the combined processing of these heterogeneous modalities, but most current developments are still problem-specific. Moreover, although some multi-resolution processing

methods have been proposed, there is still a lack of methodological tools to process data from different observation scales in an integrative manner.

Another major challenge is related to the fact that data acquired from living systems represent an indirect measurement of the phenomena of interest, and carry a mixture of activities from different, intertwined processes (sources) and regulatory mechanisms. Specific source separation methods have been recently proposed for biomedical data and this field is in active development. However, discriminating the useful from the useless sources in these cases is still an open problem, particularly when the number of sources exceeds the number of observations, and in the presence of the significant intra and inter-patient variability, which is a typical characteristic of biomedical data.

A common limitation of most current biomedical data processing methods is that they are based on unrealistic, generic underlying models and on strong hypotheses about the statistical properties of the data, that are difficult to meet in real applications. Only a minority of the proposed approaches integrate explicit biological or physiological a priori knowledge. Previous works on the LTSI SEPIA team have been directed to integrate physiological knowledge on these data processing tasks through the development of novel methodologies for patient-specific physiological modeling and data analysis (HERNÁNDEZ, 2000), (DEFONTAINE, 2006; LE ROLLE, 2006), (FLEUREAU, 2008).

This work is in direct continuity of the previous contributions of our team and is focused on the proposition of new methods for multi-resolution modeling for the analysis and interpretation of physiological signals with applications to various diseases of the cardiovascular system.

This thesis is organized as follows: chapter 2 introduces the modeling and simulation framework and its related concepts, while announcing the main difficulties of modeling applications to physiological systems and the challenges of multi-resolution and multi-formalism simulations. In order to tackle these challenges and to provide new contributions to the simulation of hybrid systems, chapter 3 presents a formalized, general methodology for multi-resolution and multi-formalism modeling that is consistently applied to the clinical applications studied in this thesis. Chapter 4 presents a set of novel tools that have been developed in this thesis in order to integrate the above-mentioned modeling methodology, allowing for its application in concrete clinical problems. In particular, a multi-formalism modeling and simulation library, already developed in our laboratory, has been improved and a set of parameter analysis and parameter identification methods has been implemented and adapted to heterogeneous models.

The rest of this manuscript is dedicated to four clinical applications of the methods and tools described in chapters 2 to 4. In the context of heart failure, chapter 5 shows an example of the integration of several physiological mechanisms relevant to the long-term regulation of blood pressure, improved with a detailed description of the short-term dynamics of a pulsatile heart. Chapter 6 presents a parameter analysis and a patient-specific identification of the coronary circulation hemodynamics for patients with coronary artery disease undergoing a bypass graft surgery. For the particular case of heart failure patients treated with a cardiac resynchronization therapy, chapter 7 shows a prospective application towards an optimized configuration of a

bi-ventricular pacemaker. Finally, chapter 8 presents another prospective study for the analysis of the effect of the autonomic nervous system responses on the heart rate variability, in particular, for the baroreflex response on newborn lambs.

References

Defontaine, A. (2006). "Modélisation multirésolution et multiformalisme de l'activité électrique cardiaque". PhD thesis. Université de Rennes 1.

Fleureau, J. (2008). "Intégration de données anatomiques issues d'images MSCT et de modéles électrophysiologique et mécanique du coeur". PhD thesis. Universite de Rennes 1.

Hernández, A. I. (2000). "Fusion de signaux et de modèles pour la caractérisation d'arythmies cardiaques". PhD thesis. Université de Rennes 1.

Le Rolle, V. (2006). "Modélisation Multiformalisme du Système Cardiovasculaire associant Bond Graph, Equations Différentielles et Modèles Discrets". PhD thesis. Rennes: Université de Rennes 1.

CHAPTER 2

Modeling and Simulation

Résumé

L'objectif du chapitre 2 est de définir un cadre formel à la modélisation et à la simulation qui sera utilisé dans la suite de cette thèse. Ce cadre générique est inspiré et transposé des travaux existants et de la théorie de la modélisation et de la simulation introduite par Zeigler (Zeigler et al., 2000), approfondie par Vangheluwe (Vangheluwe, 2001) et ensuite reprise dans notre laboratoire par (Defontaine, 2006). Ce chapitre permet de définir clairement la terminologie associée à la création et à l'utilisation de modèles. Ce vocabulaire doit être assez générique pour répondre au caractère hautement pluridisciplinaire de la modélisation. De manière à pouvoir appliquer ces concepts dans le cadre de l'étude de systèmes physiologiques, une introduction à la physiologie intégrative est spécifiquement incluse dans ce chapitre afin de relier nos travaux aux projets de modélisation et simulation existants.

The goal of this chapter is to introduce the modeling and simulation framework that is consistently employed throughout this work. This framework was inspired and refined from the existing modeling and simulation theories proposed by Zeigler et al. (Zeigler et al., 2000), subsequently approached by Vangheluwe (Vangheluwe, 2001) and further explored in our previous works in the laboratory, by Defontaine (Defontaine, 2006). This chapter includes the detailed terminology and formalized definitions related to the context of modeling and simulation; an essential formalization for a common notation throughout this manuscript. Additionally, during the description of the simulation process, the problems encountered when modeling systems that are represented with different components are presented. This statement provides an introduction to the multi-formalism contribution detailed in chapter 3.

2.1 Modeling and simulation concepts

Generally, the process of modeling and simulation is a method that permits to obtain knowledge about a mechanism or phenomenon without resorting to an experiment in its real,

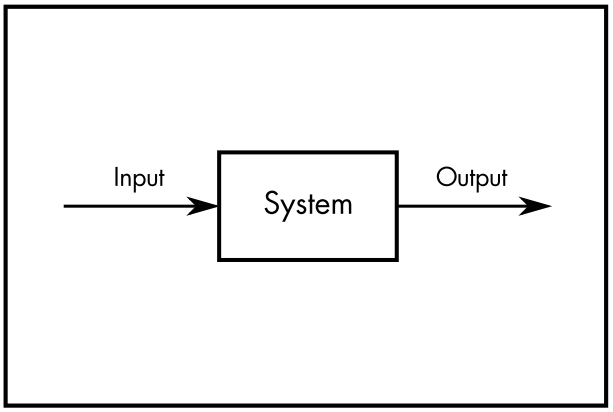

FIGURE 2.1– An input/output system.

physical environment. Modeling consists in the simplified representation of the functioning of a real system, which permits to describe such system as a structure that receives an input and generates a corresponding output, as represented in fig. 2.1. Even though this process is admittedly and purposely a simplification of a system, modeling helps understand the behavior of complex mechanisms.

Modeling and simulation applied to biology and physiology is a well established practice that permits to analyze and learn about the underlying mechanisms that are difficult or impossible to observe, whilst avoiding invasive clinical trials (BEARD et al., 2005). An special comment on this particular subject will be presented later in section 2.3.

There are several goals that can be achieved using modeling and simulation, such as interpretation, explanation or understanding of experimental observations, formal representation and description of current knowledge, prediction of unobserved behaviors, evaluation of hypothesis or configuration scenarios of the system, design of controllers, or simply provide a simplified approach to a problem whose analytical solution is too complex.

In order to formalize the process of modeling, it is important to clearly define some of the concepts that are constantly used in the modeling and simulation literature and throughout this manuscript. These concepts are based on the definitions introduced in (ZEIGLER et al., 2000) and (VANGHELUWE, 2001):

- An **object** is a real world element that features one or various interesting behaviors, which depends on the context in which the real world object is studied.
- A **base model** is a complete representation of the real world object properties and behavior, valid within every context. A base model is a theoretical concept, abstract and nonexistent in practice.
- A **(source) system** is a real world object defined under specific conditions that are of interest to the study. This narrowing of the real world object provides a source of observable data.
- An **experimental frame** is the detailed description of the particular arrangement and situation in which the source system is observed or in which the experiments designed to

observe the system are performed. The experimental frame definition is closely related to the goals of the study.

- A **model**, sometimes termed *lumped* model [1], is a limited representation of the system as a set of rules, instructions, equations or constraints that can generate an input/output behavior. The definition of a model is directly related to the experimental frame. Consequently, a model is a limited representation of a real system, at a specific level of detail that is defined by the experimental frame and the application goals; a model explicitly entails a simplification of a real system and it does not pretend to consider all elements and details of this system, which would be exceedingly complicated.
- A **simulator** is an agent that interprets the model description and generates its behavior, i.e., the model outputs, from a determined input and during a defined time interval.

The basic modeling and simulation concepts are related by various processes, as shown in fig. 2.2, introducing the following complementary elements:

- **Experimentation** is the process that observes or directly manipulates the inputs of a system and monitors the effect on the system outputs. An experiment provides experimental results that can be measured. This data is termed *measurements* or *observations*.
- **Simulation**, which is analogous to the experimentation procedure used to observe a real system, is the process that uses a simulator to feed a model with inputs, and generate the corresponding outputs. The simulation process deserves a detailed description, which will be presented in section 2.2.3.
- The modeling and simulation literature also defines the processes of **verification** and **validation**. Verification, also termed *correctness* in (Zeigler et al., 2000), refers to the evaluation of the consistency of the simulation with respect to the model, while validation can be one of many existing comparisons between the model, system and its experimental frame, as it will be explained later in section 2.2.5.

Until this point, some concepts have been introduced implicitly regarding the elements of a system and its corresponding model. However, for the sake of completeness and coherence with the following sections, it is preferable to specify the following elements:

- An **input**, or input variable is an entrance port of a model or a system which may trigger and influence the behavior of the model or system. Inputs have a defined range, such as the real numbers $\mathbb{R}$, from which they can take a value. Commonly, they are represented by a *trajectory*, a sequence of $\langle \text{time}, \text{value} \rangle$ pairs, ordered by time.
- Correspondingly, an **output**, or output variable is an exit port of a model or system. Outputs are also defined within a range, and they can be represented as a trajectory as well.
- A **state** variable is a value intrinsic to the system, which is not necessarily observable since it is not a port of the system. Yet, it represents some knowledge of an internal mechanism of the system. Indeed, the set of state variables of a system is a sufficient description of

1. It should be clarified that authors that refer to this concept as *lumped model*, such as (Vangheluwe, 2001), do not refer to a lumped parameter model, which is a common term used in modeling to refer to a particular type of simplified models.

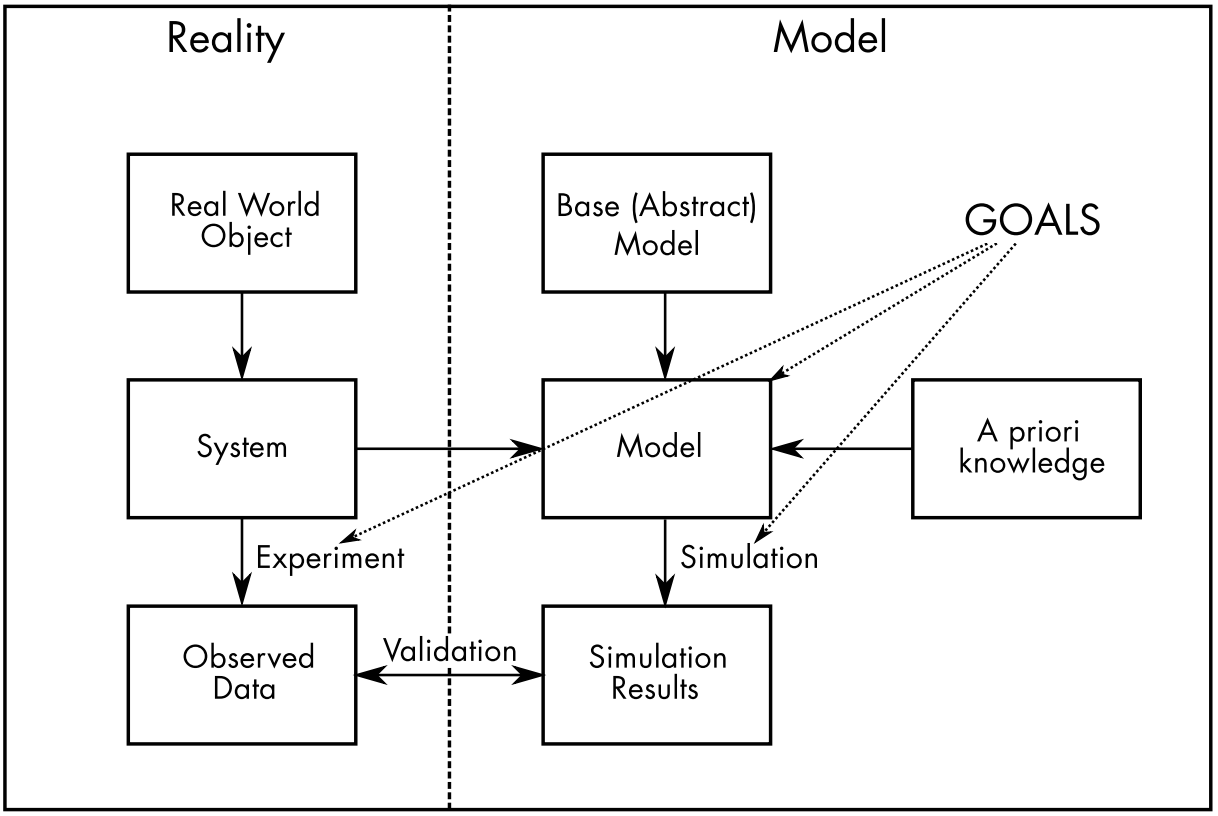

FIGURE 2.2– Modeling and simulation concepts, according to (VANGHELUWE, 2001).

the status of the system to determine its future behavior. Output variables are usually calculated as a function of state variables, parameters and input variables. In the case of a model based on ordinary differential equations, the system is described through the variations (time derivatives) of the state variables.

– A **parameter** is a special kind of input variable that characterizes, defines or sets the conditions of a particular element of a system. As with input, output and state variables, parameters are defined in a range, but they are often used as a constant value for a given simulation. The behavior of a system can be drastically different according to the value of its parameters. Hence, the exploration and analysis of the parameters of a model is very important to the modeling and simulation process, which will be explained thoroughly in section 2.2.4.

2.2 General modeling and simulation framework

As summarized in fig. 2.3, the process of modeling and simulation encompasses several activities other than the creation of a model and its simulation per se. Briefly, this framework consists in the following stages: First, one must define precisely the system that is going to be modeled. In other words, it is necessary to describe the experimental frame and the system of interest, considering which level of detail is necessary to fulfill the application goals and

objectives. Once a system has been specified, its structure is somewhat clearer and a range of mathematical tools can now be selected to describe the system. After the system has been described, we produce a model that can be parametrized: it is possible to control the output response by changing the input and parameters of the model. At this point, we can begin the process of finding a set of model parameters such that the simulation of the models generates some meaningful behavior. This process can be formalized as parameter analysis; it yields a model with a set of corresponding parameter values. Models with parameters are then simulated, performing a virtual experiment that generates *simulated data*. The model can thus be validated, by comparing source system data and simulated data.

Although this description suggests an organized step-by-step procedure, the process of modeling and simulation is rarely this simple. For example, simulations will usually be performed prior to parameter analysis, in order to verify the model description. As depicted in fig. 2.2, each stage provides important knowledge for the subsequent steps. Moreover, after the description of the system it may become evident that the experimental frame must be redefined to include more observable data. Parameter analysis can also reshape the system description, pinpointing elements of the model that need further detail or which parts are unimportant and can be simplified.

In the following sections, each element of the modeling and simulation framework will be explained in detail.

2.2.1 Experimental frame and system specification

The objective of the first step of the modeling and simulation framework is to *i)* characterize the elements of the system that are going to be modeled, and *ii)* define the available knowledge about the system. But before applying a modeling methodology for an investigation, it is necessary to lay out clearly the objectives of such study: What questions about the behavior of the system need to be considered? What are the current and potential applications of the model?

With a clear definition of the goals, the modeling and simulation process starts by the detailed identification of the interesting elements of the system and the conditions in which the researcher wants to investigate a system. In addition to the study objectives, prior knowledge of the system help define which elements of the system need to be manipulated and which elements need to be measured. This information can guide the identification of the inputs and outputs of the system. Finally, one must consider the configuration of the system: Are there any hypothesis that need to be adopted to explain the dynamics of the system? What conditions about the internal structure of the system or regarding the input and output values should be assumed? The definition of these conditions helps determine the valid applications of the model and, more importantly, its limitations.

Despite its outstanding importance to the modeling and simulation process, the abstract nature of the experimental frame makes it difficult to define it appropriately. (Zeigler et al., 2000) acknowledged this and formalized the definition of the experimental frame as five elements shown in fig. 2.4. First, an experimental frame defines two sets of variables, corresponding to

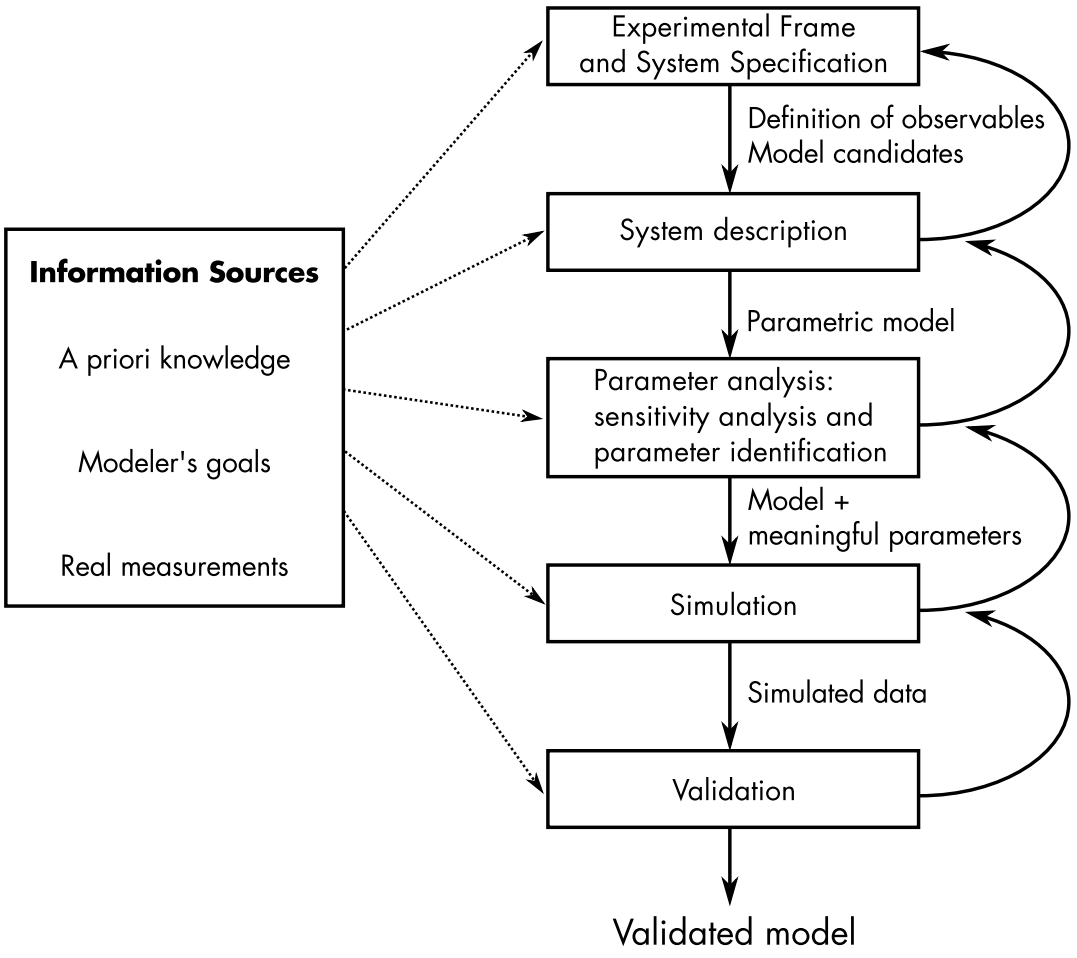

FIGURE 2.3– Model-based design process, adapted from (VANGHELUWE, 2001).

the input and output variables of the system. Second, a *generator* must be described in order to control the stimuli that will produce a matching output, which in turn will be perceived by a *transducer*. Finally, an *acceptor* determines if the input/output of the system matches the experimental frame definition. This last element decides whether the observed data is pertinent with respect to the study objectives.

Once the experimental frame has been defined, one can proceed to model a system, starting with the specification of the system. A system can be specified at different levels, depending on knowledge of the system. These levels are termed *system specification level* (KLIR, 1985; ZEIGLER et al., 2000). Specification levels offer a hierarchical organization of the integrated knowledge of a system in five levels, summarized in table 2.1.Each level is defined by the description of particular features of the system, in addition to the information of previous levels.

The most basic specification level, the *observation frame* (level 0), only includes the definition of the observable inputs and outputs variables of the system. While limited to the definition of these variables, and not their internal functioning, this level is not particularly useful, other than

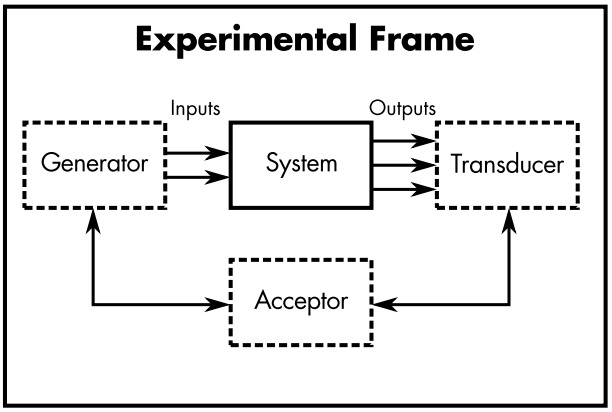

FIGURE 2.4– The experimental frame, its elements and relations with the system, according to the formalization of (ZEIGLER et al., 2000).

TABLE 2.1– Summary of system specification levels.

Level	Name	Available knowledge
0	Observation frame	System time base, inputs and outputs.
1	I/O behavior	Pairs of inputs and outputs, indexed by time.
2	I/O function	A unique association of inputs and outputs given the system initial state.
3	State transition	How the internal state of the system is affected by the input and previous states.
4	Coupled component	Various elements defined in previous levels and how they are coupled.

to define what parts of the systems need to be observed with experiments and what input and output ports need to be included in a model.

When one integrates knowledge regarding the input and output trajectories (i.e. their value over time), the system is specified in *I/O behavior* (level 1). Furthermore, when the initial state of the system is also taken into account, the system is specified in *I/O function* (level 2). At this level, the initial state permits to associate each output to an unique input trajectory.

From this point on, specification levels become an useful description tool because they are often associated with precise families of models. For example, a system specified in level 2 can be described by *black box* models, also known as *data-driven* models (COBELLI et al., 2001). Black box models intend to formulate a system as a function of the inputs that fits the experimental data, but it does not consider any information regarding the internal structure of the system or its real parameters (DEFONTAINE, 2006). Such models are useful in the following cases: *i)* when there is insufficient knowledge of the underlying mechanisms of the system, *ii)* when the internal mechanisms are neither interesting nor part of the objectives of the study, or *iii)* when the associated model must be computationally fast, since data-driven I/O functions are usually

implemented with simple mathematical structures that are not computationally expensive. Some examples of this kind of models include linear regressions from experimental data, auto-regressive models (KORHONEN et al., 1996), transfer functions, among others.

Further knowledge can be incorporated to the system specification, in particular, the transitions of internal states and how they respond to the input trajectories. This additional information defines the *state transition* specification (level 3). In contrast to a black box, the system can be considered a *gray box* at this level, since it provides a representation of the underlying processes that explain the system behavior [2]. A system specified in level 3 is particularly useful and full of insight and most modeling descriptions are based on the knowledge provided by this level. However, they show an increased complexity of the model description, which demands more parameters and computational resources. The key of system specification and model descriptions lies on finding a good compromise between the complexity, accuracy and resources. State machines, cellular automata, ordinary and partial differential equations are examples of modeling formalisms that account for the internal evolution of the system.

Finally, the last system specification level is the coupled component specification (level 4), which states that a system is a composition of various interconnected subsystems. The knowledge incorporated by this level is extremely convenient: it permits the construction of complex systems using a hierarchy of simpler components. Thus, the specification of a system can be divided into separate smaller specifications, which could be reused from previous related works. On the other hand, when each component of the system is represented by a different kind of model (including different specification levels), the simulation of such systems must manage this hybrid description. This is a non trivial task that will be explained in section 2.2.3.1.

2.2.2 System description

In the previous section, it was stated that the design of the experimental frame provides the conditions in which the system will be studied. Moreover, it identifies the important elements of the system and suggests a set of tools or structures that can be used to create a model. The creation of such model is the system description. The objective of the description of the system is to create a model M that represents the system dynamics under a certain formalism F.

A formalism is the group of rules, structures and tools that permits to define a model: they express how the input and outputs are related and how the internal states change with respect to the inputs, parameters, etc. In a figurative sense, a formalism can be considered as the *model language* (SANDERS et al., 2003). The choice of the model formalism depends on the available knowledge of the system (as defined in the previous section) and the goals of the modeling application. There are several different formalisms and categorizations that delineate the state of the art of modeling approaches. Before introducing a proper categorization of formalisms, it can be useful to identify two general methods: quantitative and qualitative approaches.

2. The term *white box* is intentionally avoided since the internal dynamics of any real system are highly complicated and their complete specification or description is fundamentally impossible: a model is, by definition, a simplified representation of a system.

Quantitative models represent a system with exact quantities and relationship, often represented with mathematical equations and algebraic equations. On the other hand, qualitative modeling attempts to describe a system by using qualitative reasoning, characterizing relationships in an informal, yet logical way which can be regarded as "common sense". In contrast with quantitative approaches, qualitative modeling deliberately avoids the use of exact values in favor of descriptions that resemble the human reasoning, such as "x increases when y decreases". These models are easy to create and explain and can be useful when the observable data is severely limited. However, they are inherently less accurate and their application is thus limited. They are still interesting at the initial stages of modeling, since the qualitative relationships can help create the quantitative relationships of more complex models. Qualitative modeling is not further discussed because it is not used directly in this work.

Quantitative approaches present a vast choice of formalisms. They can be separated in two complementary groups: continuous and discrete formalisms, according to the time base or the state representation used to specify the model. Continuous formalisms include ordinary differential equations, partial differential equations, transfer functions, bond graphs, among others. Discrete formalisms include multi-agent systems, cellular automata, state machines, Petri nets, etc. This categorization is not unique, model formalisms can be classified in a number of ways, such as deterministic vs. stochastic, linear vs. nonlinear, lumped vs. distributed (Cobelli et al., 2001).

Among the numerous categorizations, we will follow the arrangement proposed in (Zeigler et al., 2000). This classification is based on three categories: differential equation systems, discrete time systems and discrete event systems. The intention of these categories is to introduce an unified, general classification of mathematical formalisms with common structures and tools that are reusable for all models, or at least for all models in the same family. The definition of each group is discussed in the following paragraphs.

Regardless of the group, all models contain the following elements: *1)* a set of input variables, *2)* a set of output variables, *3)* a set of state variables, and *4)* a function that calculates the value of the model outputs at a given time with respect to the input and state variables. The element that separates each model formalism is the definition of some additional functions or behaviors.

Models defined with a differential equation formalism (Zeigler et al. name this group *Differential Equation System Specification*—DESS) are based on a continuous time base and must define a function that calculates the rate of change of variables with respect to time (derivatives) or with respect to other variables (partial derivatives).

Models defined with a discrete time equation formalism (*Discrete Time System Specification*—DTSS) are analogous to DESS models, but defined under a time base that is discrete. In other words, DTSS models are used when the variations of the system occur at regular intervals. The definition of these models is also similar to the DESS, yet in this case they must define a function that performs the transition of the internal states depending on the input and other state variables.

Models defined with a discrete event formalism (*Discrete EVent System specification*–DEVS)

are different from the two preceding formalism groups. These models are not tied to a rigid, regular discrete time base, but to a series of events along time. Further, the internal state of DEVS models are defined along with a specific time duration. When this period ends, or when it is interrupted by an external event, the model may change to another state. Consequently, DEVS models need to define two functions, one that performs the transition of the internal states when the current state period finishes normally, and another function that performs the transition when the current state is interrupted by an external event.

The similarities between each group of formalism is not coincidental. In fact, DTSS and DESS can be considered equivalent (DEFONTAINE, 2006), and in some cases, they can be converted to a particular case of DEVS. The work of ZEIGLER et al. is strongly based on the definition of these three groups and the possible transformation of all model formalisms to a DEVS case, so as to couple all kind of models in a multi-formalism approach. In this work, however, we will not develop further into these transformations, in favor of the co-simulation approach, which will be explained in section 2.2.3.1.

In this thesis, we follow the definition of a model introduced in (DEFONTAINE, 2006):

Definition 2.1 (Formalization of a model)**.** A model M is a tuple denoted $M\left(F, \mathbf{I}, \mathbf{O}, \mathbf{E}, \mathbf{P}\right)$ where **I**, **O** and **E** denote the input, output and state[3] **variable sets**, **P** denotes the **parameter set** of the model, and F is the formalism in which the model is described, which implicitly includes the definition of the corresponding output, transition or derivatives functions, when necessary.

To account for models that represent a system as a set of components and their interactions (system specification level 4), we will complement the definition above with the formalization of two kind of models: atomic and coupled.

Definition 2.2 (Atomic and coupled models)**.** An atomic model M^a is a model exactly as described in definition 2.1, whose dynamics are explained without any sub-components. A coupled model $M^c\left(F, \mathbf{I}, \mathbf{O}, \mathbf{E}, \mathbf{P}, \{M_i\}\right)$ is a model composed of a set of components ($\{M_i\}$), i.e. sub-models, which can be either atomic or coupled as well.

These definitions and their enclosed elements will be used and referenced throughout this manuscript, specially during the presentation of the contribution to multi-formalism and multi-resolution modeling in chapters 3 and 4.

2.2.3 Simulation

According to the diagram of the modeling and simulation framework illustrated previously in fig. 2.3, when the system has been described, resulting in a complete model, an analysis should be performed in order to better understand the effect of the model parameters. However, these analyses use mostly the calculated outputs of the model, which are only known after a simulation. For this reason, it is more practical to explain the simulation process at this point.

3. **E** is deliberately used instead of **S** since the latter will be used in the definition of a simulator.

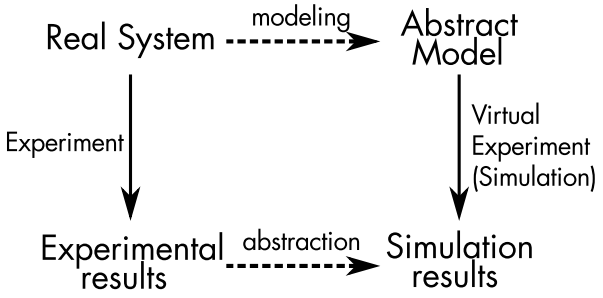

FIGURE 2.5– Mapping between experiment and simulation.

Simulations and models present a parallelism between the real model and experimentation, as illustrated in fig. 2.5. Accordingly, the term *in silico* is often used to refer to an experiment based on a computer simulation, in the same way the terms *in vivo* and *in vitro* experimentation are used in biology or physiology to refer to experiments performed in living organisms and isolated from their natural biological environment. In general, a simulation is the process that interprets the model definition to generate its output. This means that the simulation process must know the trajectories for each of its input variables, the values of each parameter, the initial values of internal states, and the specific definitions of each function according to the model formalism.

The simulation process tackles two distinct problems: *i)* the interpretation of the model specification under its formalism F, and *ii)* the simultaneous simulation of all the sub-systems defined within the model, when the model is composed of several components, as explained in the last level of system specification.The first problem is relevant to the formalism definition; along with the set of rules, relations and equations defined by a formalism, there is a set of devices or algorithms that permit to calculate the model dynamics. Therefore, the simulation process must use the corresponding algorithms to calculate the evolution of the model variables over time. For example, a model based on ordinary differential equations are simulated using a family of numerical integration methods that have been developed to provide a given *accuracy* (i.e. Euler method, the trapezoidal rule, or the Runge-Kutta methods). Hence, a simulator for models defined as a set of differential equations uses numerical methods specifically adapted to this particular formalism. In this example, it was mentioned that the solution to the model equations depend on a given accuracy. Indeed, the process of simulation is often an approximation that depends on an additional set of parameters, the *simulation parameters*, which affect the method that solves the dynamics of the model.

Continuing with the notation introduced in definitions 2.1 and 2.2, in this thesis we will consider the following formalization:

Definition 2.3 (Formalization of simulator and simulation)**.** A simulator is represented by a process $S^h(M^h, P_S, F)$ that calculates the evolution of a model M^h defined with formalism F, using parameters P_S. Here, $h \in \{a, coup\}$ for atomic or coupled models respectively, and

$P_S = [P_{\text{sim}}, I, E_0, P]$ is a vector that defines the values for the simulation parameters (P_{sim}), input trajectories (I), initial conditions (E_0) and the parameter (P) of the model. A simulation, i.e the execution of the process S, produces the outputs of the model, denoted $O = S^h(M^h, P_S, F)$.

2.2.3.1 Multi-formalism simulation

One of the major challenges concerning the simulation of complex models, usually defined at level 4 (coupled models M^{coup}), arises when the model components (its atomic or coupled sub-models) are defined with different mathematical formalisms. The modeling of systems with different formalisms is termed multi-formalism modeling.

From the extensive studies of (DE LARA et al., 2002; VANGHELUWE, 2001; ZEIGLER et al., 2000), two main multi-formalism approaches have emerged: formalism transformation and co-simulation. An additional alternative, the *meta*-formalism approach, is often mentioned in the literature (QUESNEL et al., 2009; VANGHELUWE, 2000), but this case can be considered as a formalism transformation technique.

Formalism transformation: Based on the existence of morphisms between formalisms, this approach proposes that each component of the system must be transformed to a single formalism F_U, for which a simulator is available. The formalism transformation approach has been one of the cornerstones of (ZEIGLER et al., 2000), who defined a universal formalism, the Discrete Event System Specification (DEVS), that permits the coupling of differential equations with discrete-time and event systems. Other candidates include the hybrid differential algebraic equations (hybrid DAE, VANGHELUWE, 2000) or the heterogeneous flow system specification (HFSS, BARROS, 2003). VANGHELUWE developed further this approach, whose contributions are summarized in the *formalism transformation graph* (FTG, cf. fig. 4.1): an exhaustive compilation of formalisms and their possible transformations to either DEVS or to difference equations.

The advantage of the formalism transformation approach is the fact that it only needs one simulator. More importantly, the usage of a common formalism does not require the definition of a particular coupling interface between models. However, this method lacks in practicality because it is difficult to design morphisms between formalisms and a transformed model is more difficult to interpret (DEFONTAINE et al., 2004).

Co-simulation Based on the existence of formalism-specific simulators, this approach suggests that a system can be solved with several coordinated simulators. Avoiding the cumbersome and time-consuming task of formalism transformation, the co-simulation approach proposes that each model shall maintain its original formalism, and each model will be associated with a simulator specialized in this formalism. Consequently, each model is simulated in an independent, distributed fashion, yet the co-simulation must perform a precise inter-component coupling of input and output variables. However, this coupling of input and output variables in the trajectory level is not a straightforward task. Component coupling must contemplate two cases: *i)* when two connected models are simulated with a different temporal scale, and *ii)* when the outputs of a

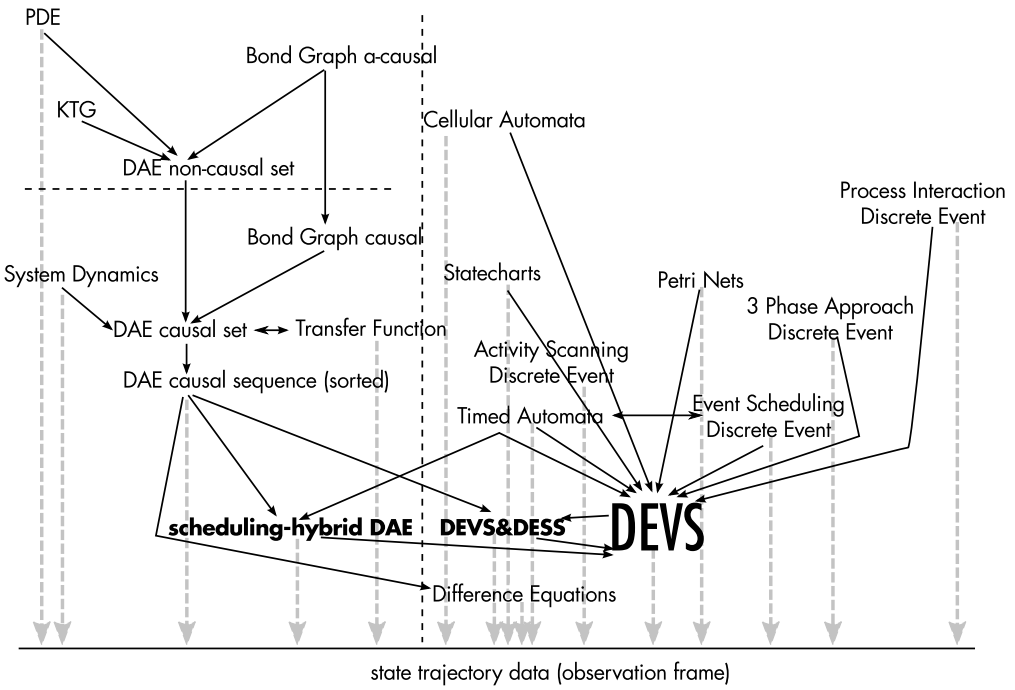

FIGURE 2.6– Formalism Transformation Graph (FTG), introduced by (VANGHELUWE, 2001): solid lines represent an existing morphism that transforms one formalism to another. Gray dashed lines indicate the availability of a simulator for a formalism.

model cannot be directly set as an input of another model because they are expressed in different spatial references or even different mathematical structures. Nevertheless, the co-simulation approach is specially interesting because each model maintains its description, which permits the construction of complex models as a combination of the modeling efforts of different research fields. This combination aspect is interesting when applied to physiological modeling problems, in particular for multi-factorial physiological systems, where the dynamics of the system can only be explained if one considers its internal sub-systems and their intricate interactions.

Presently, multi-formalism simulation with a co-simulation approach is a field still in open research. The management of model coupling has been studied from a temporal-synchronization viewpoint (HERNÁNDEZ et al., 2009) and applied in several multi-factorial physiology applications (DEFONTAINE et al., 2004; LE ROLLE et al., 2011; THOMAS et al., 2008). From the viewpoint of component coupling, (HERNÁNDEZ et al., 2011) considers that the input/output pairing must be studied with an appropriate parameter analysis, e.g. a sensitivity analysis, in order to determine which variables should be considered in this coupling, and to evaluate the impact of such model integration. The modeling contribution of this work can be placed in this domain and it will be explained in detail in chapter 3.

2.2.4 Parameter analysis

As formalized in definition 2.3, the output of the model M are calculated through a simulation S and they depend on the value of the parameters (P) that have been identified during

the system description. Parameters are interesting to modelers and experimenters because, like the model itself, they represent a simplification of a particular element of the real world system. The next logical step of the modeling and simulation process would be to assign meaningful parameter values to the model. This enterprise can be as easy as observing the system and taking measures of some of its observable elements (e.g. measuring length, weight, volume, pressure, etc.). However, parameters are often impossible to observe or difficult to measure accurately; there is always an error associated with the parameter value. Moreover, model parameters may also represent an abstract object which is not physically measurable. Therefore, it is extremely important to acquire knowledge on the relation between the parameters and the outputs of the model.

Parameter analysis is the process that provides insight into the relation between parameters and outputs. It can consist in deductions from the mathematical equations that define the model. Yet, some relations are not evident and can be hidden within the complexity and interaction of different internal structures. Parameter analysis encompasses two different activities: *i)* the characterization of the effect of a parameter on the model dynamics, particularly its outputs, and *ii)* the identification or estimation of meaningful parameter values to the model. These two activities are conceptually independent, yet they are related since they can benefit from the information obtained from each other.

The effect of the system parameters, or more specifically the effect of a change of a parameter over the outputs can be identified when the equations of the model are simple enough to either deduce this or identify some of its properties. For instance, it is important to determine if the model is *time-invariant*, i.e. when the output of a system does not change with time, or if it is a *linear* model, i.e. when the output function satisfies the property of superposition (KARNIEL et al., 1999). Unfortunately, these properties are not easy to verify when the model comprises complex sub-systems and relations, when the model formalism does not admit this analysis, or when the parameters are numerous and highly interconnected. Nevertheless, in this case we will still be interested in the understanding on the effect that changes of the model parameters or inputs have over the model outputs. Keeping with definitions 2.1 and 2.3, this analysis attempts to comprehend $\partial\mathbf{O}/\partial\mathbf{P}$ and $\partial\mathbf{O}/\partial\mathbf{I}$. These questions can be addressed with *sensitivity analysis*, the study of how the alterations of the output of a mathematical model can be apportioned to the alterations in the model inputs or parameters. A review of this field and its related techniques will be presented later in section 4.2.

The second activity included in parameter analysis consists in finding the most adapted set of parameter values that can reproduce a set of experimental data. This process can be formalized as follows: From the perspective of the real system, let O_{obs} stand for an experimental observation of the output of the system under certain conditions. Likewise, in the abstraction of the model and simulation, let O_{sim} denote the simulated observation of the same output of a model M, as formalized in definition 2.3, when simulated using the same conditions. The parameter estimation process consists in the exploration of the parameter space $\mathbb{P}$ in order to minimize a function of distance between the model predictions O_{sim} and the experimental data

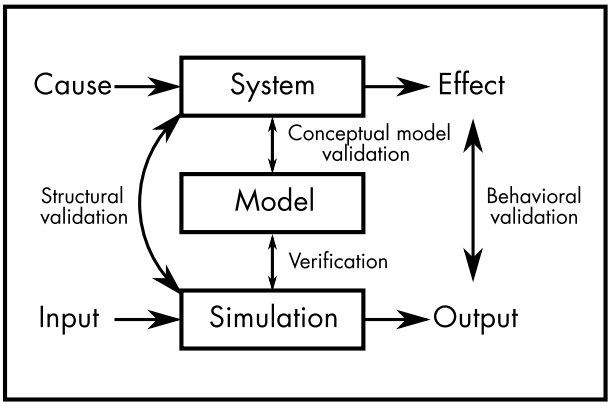

FIGURE 2.7– Validation and verification schemes, according to (VANGHELUWE, 2001).

O_{obs}. In other words, the parameter estimation aims to find the optimal parameter values P_{opt} defined as:

$$\begin{aligned} P_{\text{opt}} = & \underset{P \in \mathbb{P}}{\operatorname{argmin}}\ g_\epsilon(O_{\text{sim}}(P), O_{\text{obs}}) \\ & \text{subject to } h(O_{\text{sim}}(P))\,, \end{aligned} \tag{2.1}$$

where g_ϵ is an error function and h is a generalization for a constraint function that indicates if P is a feasible solution.

The difficulty of parameter estimation resides in three aspects: *i)* the definition of the observable variables and their corresponding simulated outputs, *ii)* the definition of the error function g_ϵ, and *iii)* the choice of the optimization method that solves eq. (2.1). A summary of the available approaches to the definition and selection of the two last elements will be presented in section 4.3.

2.2.5 Validation

Finally, the last stage in the modeling and simulation framework is the validation analysis. This phase, however, is not necessarily the final step of the framework because it can be performed as soon as the system has been specified or described, and the validation results can eventually lead the investigator to restart the whole process.

The validation of the modeling process can occur at different levels, depending on the concept of *validity* used and which elements of the framework are being compared. Additionally, the definition of validation is different among the modeling and simulation literature. In this section, a merged definition of the existing validation concepts will be presented.

Following the identification presented in (VANGHELUWE, 2001), there are four different validation schemes, summarized in fig. 2.7: structural validation, conceptual validation, behavioral validation and simulation verification:

– Behavioral validation is the evaluation of the simulated model behavior with respect to the system observations. This activity is a synonym to the term *replicative validity* of (ZEIGLER

et al., 2000), which can only be affirmed when the experimental data and model output agree within an acceptable tolerance.

- Structural validation is the evaluation of the structure of the model with respect to the structure observed in the system. This validation encompasses two distinct concepts for ZEIGLER et al.: *structural* and *predictive validity*. *Structural validity* refers to an agreement between the state of the system and the model, which requires the observation or inference of this internal information; a difficult task for the system, but potentially easy for the model. A *predictive validity* is achieved when the model can generate outputs for cases where the system has not been directly observed.
- Conceptual validation is the relation between the system and the model in a conceptual level (not the simulation); it evaluates the realism of the model description with respect to the system and the experimental frame.
- Verification refers to the consistency between the model description and the interpretation provided by the simulator. Since simulators are not designed for a particular model, but to a family of models in a certain formalism, the verification, or *simulator correctness* is related with the question of how faithfully a simulation correctly generates the model outputs. Verification also refers to the analysis of the computer program that represents the model; i.e. the evaluation to ensure that the model implementation is correct and does not contain errors introduced by the modeler or programmer.

Although the experimental frame is briefly mentioned in the validation schemes, it is very pertinent during the validation phase. All schemes presented below are to be considered in the context of the experimental frame, in particular the behavioral and structural validation. In consequence, a model taken away from its experimental frame cannot be considered valid or invalid. Moreover, the results of the validation can reshape the experimental frame: when the model does not show replicative validity in some cases can help determine scenarios of the experimental frame that are more complicated than expected. Conversely, a model that shows good predictive validity can enlarge the experimental frame and the potential applications of the model.

While the activities presented below help categorize the validation process, it does not mention the available techniques to reach these validity relations. An extensive description of these techniques are presented in (BALCI, 1994, 2010), which range from informal and manual approaches, to dynamic and advanced testing approaches. The detailed description of these approaches falls out of the scope of this work. However, it is worth mentioning that the sensitivity analysis and parameter identification processes presented in section 4.2 are the main tools that help identify some validity issues of the model.

2.3 Modeling and simulation in physiology

The concepts and definitions described in the previous sections are completely generic and are thus obviously applicable to biological or physiological systems. Indeed, the central role

of modeling and simulation on the analysis of biological or physiological process is now clearly established. Several models of the various components of physiological systems (cardiac activity, respiration, kidney function, autonomic nervous system modulation, etc.) have been proposed in the literature, at different levels of detail, and continue to be improved (Keener et al., 1998). Current research is moving towards the integration of different models, to analyze the complex interactions that govern these biological of physiological systems. This *integrative modeling* approach is central to emerging disciplines such as Systems Biology and Integrative Physiology. It is also the fundamental background of international research initiatives, such as the IUPS Physiome project (Bassingthwaighte, 2000; Crampin et al., 2004; Hunter, 2004) or, at the European level, the *Virtual Physiological Human* (VPH) (STEP Consortium, 2007).

Several research efforts are now focused on a comprehensive *structural integration* (from the cell to the whole organ, for example) involving complex models in terms of the number of state variables represented, or the number of coupled components. These models lead to heavy simulations and in most of the cases neglect the interactions with other organs or systems. Moreover, they are often difficult to analyze, to identify and to exploit in a real clinical setting. Models focused on *functional integration*, by coupling different physiological subsystems, are less present in the literature. Although these models are easier to handle (numerically and mathematically), their components do not have a sufficient level of detail to explain some modes of operation of the system under study. In this sense, the integration of models at different resolutions has been identified as a possible alternative (Bassingthwaighte et al., 2005; Hernández et al., 2009; Hernández et al., 2012). However, several methodological challenges still remain to be solved in order to effectively implement such a multi-resolution approach.

As mentioned before, one of the main objectives of the present work is to provide solutions for some these challenges, in order to build integrated physiological models, combining components which are defined at different resolutions. The following sections will present a formalization of this problem, underlying the main challenges that will be addressed in this thesis.

2.3.1 Integrative modeling in physiology

McCulloch and Huber proposed a graphical representation of the integrative modeling approach, based on three different axes (cf. fig. 2.8) (McCulloch et al., 2002). The *structural integration*(vertical axis or *vertical integration*) extends from the subcellular level to the whole human body and the population level, involving significantly different spatial and temporal scales. The integration of different biological or physiological functions (e.g. cardiac electrical activity, cardiac mechanical activity, autonomic regulation, etc.) is represented in the horizontal axis (horizontal or *functional integration*). The third axis is the level of *knowledge integration*, as represented in the model: one end of this axis corresponds to *black box* models, which are limited to the reproduction of the input-output relationship of the observed system without seeking to represent its underlying mechanisms, and the other end corresponds to *white box* models, incorporating the most detailed biochemical, physical or physiological knowledge available.

Most of the models proposed in the literature can be represented in a single "cell" of this 3D space, since they are usually designed to reproduce a specific function, at a given scale, with a reasonable level of knowledge integration, which depends on the problem to be addressed. We completed this representation by projecting different mathematical formalisms, associated with the modeling of the electrical and mechanical activities of the heart and their regulation by the autonomic nervous system (ANS) (cf. fig. 2.8). An analysis of the literature shows that a relationship exists between the mathematical formalisms used for the development of the models and the position of the models in this space. For instance, the regulation of the cardiovascular activity by the ANS is often considered at system level and modeled using experimental data by means of a transfer function (TF) formalism. The cardiac electrical activity can be modeled at levels spanning from the cell to the whole organ, and these models are commonly represented by ordinary and partial differential equations.

Through projects such as the IUPS Physiome or the Virtual Physiological Human (VPH), research is moving towards the integration of models proposed by different authors for different functions (horizontal integration), at multiple scales (vertical integration) and with various levels of knowledge integration, in order to analyze the complex interactions that govern physiological systems.

An interesting functional integration (or horizontal integration) example is the pioneering work of GUYTON AND COLEMAN on the analysis of the overall regulation of the cardiovascular system (GUYTON et al., 1972). They proposed a mathematical model consisting of a set of *blocks* representing the most important physiological subsystems involved in cardiovascular regulation. The simulation results obtained from this model were used to perform a simultaneous analysis of the main effects caused by several types of stress on the cardiovascular system and even to predict physiological behaviors that could only be observed experimentally years later (GUYTON et al., 2005). It was also used to identify for which part of the system new knowledge was needed, helping to design new experimental research. However, this model is only an overall description of the regulation of the cardiovascular system. The resolution of each of its constitutive blocks was not sufficient to represent most of the pathologies of interest. In this work, a significant effort has been made to the improvement of the Guyton model, by improving the resolution of selected sub-models as a function of the targeted clinical applications (chapters 5 to 8).

Models based on structural integration (or vertical integration) have also been proposed in the literature, particularly in the field of cardiology. For example, representations of cardiac electrical activity incorporating structures at the cellular level to the organ level have been proposed by many different groups (BHATTACHARYA-GHOSH et al., 2012; FENTON et al., 2005; NICKERSON et al., 2006; NOBLE, 2004). Some works include, to some extent, both vertical and horizontal integrations, such as the electro-mechanical models of the cardiac activity (DOU et al., 2009; KERCKHOFFS et al., 2007; NORDSLETTEN et al., 2011; USYK et al., 2003; WATANABE et al., 2004). These models have proven useful in a number of situations, but their complexity and simulation costs jeopardize the application of essential model analysis tasks, such as sensitivity analyses and parameter identification. In addition, the absence of a coupling with other physiological

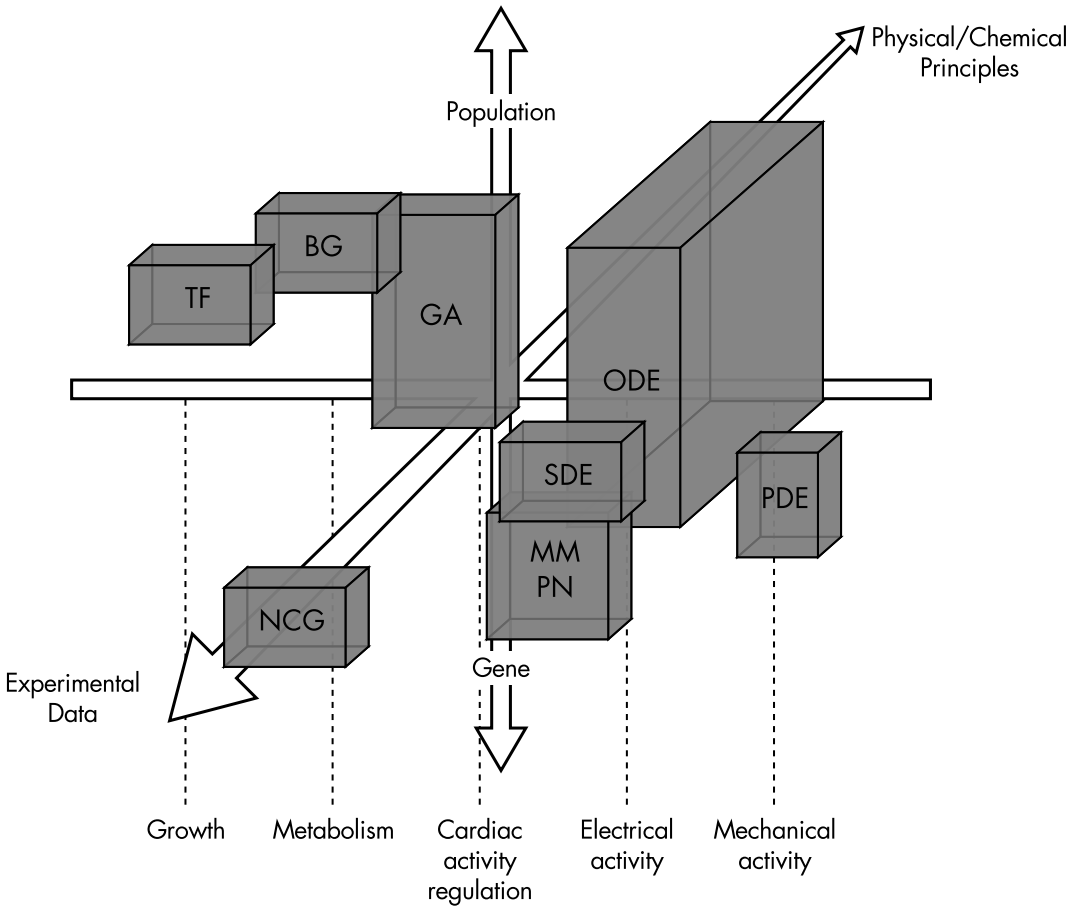

FIGURE 2.8– 3D space formed by the three main axes of the integrative modeling approach proposed by MCCULLOCH AND HUBER. The vertical axis corresponds to the structural integration, the horizontal axis represents the functional integration and the diagonal axis integration of knowledge. We show in this space different formalisms used in the modeling of the cardiovascular system, limited to the representation of the electrical and mechanical activities of the heart and the regulation of the cardiovascular activity by the ANS. Some of the most common formalisms found in the literature are: *NCG*—Network Control Genetics, *TF*—Transfer Functions , *BG*—Bond Graphs, *GA*—Generalized Automata, *SDE*—Stochastic Differential Equations, *MM*—Markov Models, *PN*—Petri Nets, *ODE*—Ordinary Differential Equations and *PDE*—Partial Differential Equations.

subsystems requires the definition of arbitrary and unrealistic boundary conditions. These two drawbacks limit the potential clinical application of such models.

It is obviously impossible to achieve horizontal and vertical integration at the highest resolution level, because it would require unlimited resources. One way around this problem may be thus to represent different functions at different scales in a multi-resolution approach. The application of such an approach also requires the definition of a global physiological model, based on a wide horizontal integration, which can be useful as a *base model* for the integration of sub-models with higher resolutions. This is the concept of a *core model* that some research projects are currently developing. However, the creation of such a model is also a difficult task that requires, among other things:

– the coupling of heterogeneous models in terms of *i)* their mathematical formalism (i.e.

continuous models based on differential equations; discrete models, such as generalized automata, multi-agent systems, etc.), *ii)* their spatial resolution, and *iii)* their dynamics;
- the definition of simplified modular models (via homogenization methods, for instance) preserving the main input-output features of the corresponding detailed models, and
- the creation of a *toolbox* that facilitates the creation, sharing, coupling and simulation of heterogeneous models.

The need for such a generic *toolbox* has been expressed by a number of authors (FENNER et al., 2008) and was one of the main motivations of the VPH Network of Excellence. Some elements of this toolbox are already well advanced, others are still in development or design phases. A particular need has been identified for the modeling tools to deal effectively with the integration of heterogeneous models. The methodological contributions of this thesis, presented in the following chapters, are mainly focused on this point.

2.4 Conclusion

This chapter introduced and formalized the concept and notions of the current theory of modeling and simulation. Modeling is a complex procedure whose ultimate objective is the representation of the dynamics of a system. However, real systems are often complex; a model can only represent the knowledge of a system until a certain level of detail, defined by the research objectives, observable data and previous knowledge. The framework described in this chapter presents the modeling and simulation concepts and structures them in a generalized procedure, designed to help the definition, description and analysis of a model. Additionally, the concepts of model $M\left(F, \mathbf{I}, \mathbf{O}, \mathbf{E}, \mathbf{P}\right)$, atomic and coupled models M^a, M^{coup}, and the process of simulation $O = S^h(M^h, P_S, F)$, were defined, to provide a common notation for the following chapters.

While describing a generalized framework, this chapter enumerated the main challenges associated with modeling and simulation of physiological systems, introducing the concepts of multi-formalism and multi-resolution modeling. The main contributions of this thesis are situated in this field and will be explained chapters 3 and 4.

Finally, the stages of the mentioned framework can profit from other fields related to modeling and simulation. While presenting the modeling and simulation processes used in all the clinical applications of this manuscript, this chapter also introduces the necessity of sensitivity analysis and optimization methods that will be exposed in chapter 4.

References

BALCI, O. (1994). "Validation, verification, and testing techniques throughout the life cycle of a simulation study". In: *Annals of operations research* 53.1, pp. 121–173.

— (2010). "Golden rules of verification, validation, testing, and certification of modeling and simulation applications". In: *SCS M&S Magazine* (4). Ed. by T. S. FOR MODELING and S. I. (SCS), pp. 2010–10.

BARROS, F. J. (2003). "Dynamic structure multiparadigm modeling and simulation". In: *ACM Transactions on Modeling and Computer Simulation (TOMACS)* 13.3, pp. 259–275.

Bassingthwaighte, J. B. (2000). "Strategies for the Physiome Project". In: *Ann. Biomed. Eng.* 28. article antoine, pp. 1043–1058.

Bassingthwaighte, J. B., H. J. Chizeck, and L. E. A. a. H. Qian (2005). "Multiscale Modeling of Cardiac Cellular Energetics". In: *Annals of the New York Academy of Sciences* 1047. article antoine, pp. 395–426.

Beard, D., J. Bassingthwaighte, and A. Greene (2005). "Computational modeling of physiological systems". In: *Physiological genomics* 23.1, pp. 1–3.

Bhattacharya-Ghosh, B., S. Schievano, and V. Díaz-Zuccarini (2012). "A multi-physics and multi-scale lumped parameter model of cardiac contraction of the left ventricle: A conceptual model from the protein to the organ scale". In: *Computers in Biology and Medicine* 42.10, pp. 982 –992. issn: 0010-4825. doi: http://dx.doi.org/10.1016/j.compbiomed.2012.07.010.

Cobelli, C. and E. Carson (2001). "An Introduction to Modelling Methodology". In: *Modeling Methodology for Physiology and Medicine*. Ed. by E. Carson and C. Cobelli. Biomedical Engineering. San Diego: Academic Press. Chap. 1, pp. 1 –13. isbn: 978-0-12-160245-1. doi: http://dx.doi.org/10.1016/B978-012160245-1/50002-7.

Crampin, E. J., M. Halstead, P. Hunter, P. Nielsen, D. Noble, N. Smith, and M. Tawhai (2004). "Computational physiology and the physiome project". In: *Experimental Physiology* 89.1, pp. 1–26.

De Lara, J. and H. Vangheluwe (2002). "AToM3: A Tool for Multi-formalism and Meta-modelling". In: *Fundamental approaches to software engineering*. Springer, pp. 174–188.

Defontaine, A. (2006). "Modélisation multirésolution et multiformalisme de l'activité électrique cardiaque". PhD thesis. Université de Rennes 1.

Defontaine, A., A. Hernández, and G. Carrault (2004). "Multi-formalism modelling and simulation: application to cardiac modelling". In: *Acta Biotheoretica* 52.4, pp. 273–290.

Dou, J., L. Xia, Y. Zhang, G. Shou, Q. Wei, F. Liu, and S. Crozier (2009). "Mechanical analysis of congestive heart failure caused by bundle branch block based on an electromechanical canine heart model." In: *Phys Med Biol* 54.2, pp. 353–371. doi: 10.1088/0031-9155/54/2/012.

Fenner, J. W., B. Brook, G. Clapworthy, P. V. Coveney, V. Feipel, H. Gregersen, D. R. Hose, P. Kohl, P. Lawford, K. M. McCormack, D. Pinney, S. R. Thomas, S. V. S. Jan, S. Waters, and M. Viceconti (2008). "The EuroPhysiome, STEP and a roadmap for the virtual physiological human." In: *Philos Transact A Math Phys Eng Sci* 366.1878, pp. 2979–2999. doi: 10.1098/rsta.2008.0089.

Fenton, F. H., E. M. Cherry, A. Karma, and W.-J. Rappel (2005). "Modeling wave propagation in realistic heart geometries using the phase-field method." In: *Chaos* 15.1, p. 13502. doi: 10.1063/1.1840311.

Guyton, A., T. Coleman, and H. Granger (1972). "Circulation: overall regulation". In: *Annual review of physiology* 34.1, pp. 13–44.

Guyton, A. and J. Hall (2005). "Nervous regulation of the circulation, and rapid control of arterial pressure". In: *Textbook of medical physiology*. 11th ed.

Hernández, A. I., V. Le Rolle, A. Defontaine, and G. Carrault (2009). "A multiformalism and multiresolution modelling environment: application to the cardiovascular system and its regulation". In: *Philos Transact A Math Phys Eng Sci* 367.1908. PTRSA, pp. 4923–4940. doi: 10.1098/rsta.2009.0163.

Hernández, A. I., V. Le Rolle, D. Ojeda, P. Baconnier, J. Fontecave-Jallon, F. Guillaud, T. Grosse, R. G. Moss, P. Hannaert, and S. R. Thomas (2011). "Integration of detailed modules in a core model of body fluid homeostasis and blood pressure regulation". In: *Progress in Biophysics and Molecular Biology* 107, pp. 169–182. doi: 10.1016/j.pbiomolbio.2011.06.008.

Hernández, A. I., J. Dumont, M. Altuve, A. Beucheé, and G. Carrault (2012). "Evolutionary Optimization of ECG Feature Extraction Methods: Applications to the Monitoring of Adult Myocardial Ischemia and Neonatal Apnea Bradycardia Events". In: *ECG Signal Processing, Classification and Interpretation. A comprehensive Framework of Computational Intelligence*. Ed. by A. Gazek and W. Pedrycz. Springer.

Hunter, P. J. (2004). "The IUPS Physiome Project: a framework for computational physiology." In: *Prog Biophys Mol Biol* 85.2-3, pp. 551–69. doi: 10.1016/j.pbiomolbio.2004.02.006.

KARNIEL, A. and G. F. INBAR (1999). "Linear systems description". In: *Modern Techniques in Neuroscience Research*. Springer, pp. 589–625.

KEENER, J. and J. SNEYD (1998). *Mathematical Physiology*. book. Springer-Verlag.

KERCKHOFFS, R. C., M. L. NEAL, Q. GU, J. B. BASSINGTHWAIGHTE, J. H. OMENS, and A. D. MCCULLOCH (2007). "Coupling of a 3D finite element model of cardiac ventricular mechanics to lumped systems models of the systemic and pulmonic circulation." In: *Ann Biomed Eng* 35.1. 0090-6964 (Print) Journal Article Research Support, N.I.H., Extramural Research Support, U.S. Gov't, Non-P.H.S., pp. 1–18.

KLIR, G. J. (1985). "Architecture of systems complexity". In: *Saunders, New York*.

KORHONEN, I., L. MAINARDI, P. LOULA, G. CARRAULT, G. BASELLI, and A. BIANCHI (1996). "Linear multivariate models for physiological signal analysis: theory". In: *Computer methods and programs in biomedicine* 51.1, pp. 85–94.

LE ROLLE, V., D. OJEDA, and A. I. HERNÁNDEZ (2011). "Embedding a cardiac pulsatile model into an integrated model of the cardiovascular regulation for heart failure follow-up". In: *IEEE transactions on biomedical engineering* 58.10, pp. 2982–2986.

MCCULLOCH, A. D. and G. HUBER (2002). "Integrative biological modelling in silico". In: *Novartis Found. Symp.* Vol. 247, pp. 4–19.

NICKERSON, D., S. NIEDERER, C. STEVENS, M. NASH, and P. HUNTER (2006). "A computational model of cardiac electromechanics." In: *Conf Proc IEEE Eng Med Biol Soc* 1, pp. 5311–5314. DOI: 10.1109/IEMBS.2006.260169.

NOBLE, D. (2004). "Modeling the heart." In: *Physiology (Bethesda)* 19, pp. 191–197. DOI: 10.1152/physiol.00004.2004.

NORDSLETTEN, D., S. NIEDERER, M. NASH, P. HUNTER, and N. SMITH (2011). "Coupling multi-physics models to cardiac mechanics". In: *Progress in biophysics and molecular biology* 104.1, pp. 77–88.

QUESNEL, G., R. DUBOZ, and E. RAMAT (2009). "The Virtual Laboratory Environment – An operational framework for multi-modelling, simulation and analysis of complex dynamical systems". In: *Simulation Modelling Practice and Theory* 17, pp. 641–653.

SANDERS, W. H., T. COURTNEY, D. DEAVOURS, D. DALY, S. DERISAVI, and V. LAM (2003). "Multiformalism and Multisolution-method Modeling Frameworks: The Möbius Approach". In: *Proc. of Symp. on Performance Evaluation–Stories and Perspectives,(Vienna, Austria)*, pp. 241–256.

STEP CONSORTIUM (2007). *Seeding the EuroPhysiome: A Roadmap to the Virtual Physiological Human*.

THOMAS, S. R., P. BACONNIER, J. FONTECAVE, J.-P. FRANÇOISE, F. GUILLAUD, P. HANNAERT, A. HERNÁNDEZ, V. LE ROLLE, P. MAZIÈRE, F. TAHI, et al. (2008). "SAPHIR: a physiome core model of body fluid homeostasis and blood pressure regulation". In: *Philosophical Transactions of the Royal Society A: Mathematical, Physical and Engineering Sciences* 366.1878, pp. 3175–3197.

USYK, T. P. and A. D. MCCULLOCH (2003). "Relationship between regional shortening and asynchronous electrical activation in a three-dimensional model of ventricular electromechanics." In: *J Cardiovasc Electrophysiol* 14.10 Suppl, S196–S202.

VANGHELUWE, H. (2001). "Multi-formalism modelling and simulation". PhD thesis. Universiteit Gent.

VANGHELUWE, H. L. (2000). "DEVS as a common denominator for multi-formalism hybrid systems modelling". In: *Computer-Aided Control System Design, 2000. CACSD 2000. IEEE International Symposium on*. IEEE, pp. 129–134.

WATANABE, H., S. SUGIURA, H. KAFUKU, and T. HISADA (2004). "Multiphysics simulation of left ventricular filling dynamics using fluid-structure interaction finite element method." In: *Biophys J* 87.3, pp. 2074–2085. DOI: 10.1529/biophysj.103.035840.

ZEIGLER, B. P., H. PRAEHOFER, and T. G. KIM (2000). *Theory of modeling and simulation: Integrating discrete event and continuous complex dynamic systems*. 2nd ed. Academic Press.

CHAPTER 3

Contribution to multi-resolution modeling in physiology

Résumé

Ce chapitre présente une contribution à la définition des interfaces nécessaires à l'intégration de modèles hétérogènes dans le contexte de la physiologie intégrative. L'objectif est d'intégrer les modèles associés aux différentes composantes d'un même système physiologique, qui peuvent être développés à des niveaux de complexité divers, en fonction de l'objectif clinique visé. Cette intégration est le plus souvent problématique car ces modèles peuvent présenter plusieurs formalismes, être définis à différentes résolutions ou être associés à des dynamiques hétérogènes. La principale contribution de ce chapitre est la formalisation de la méthodologie d'intégration de modèles dans une approche multi-résolution. Afin d'interfacer ses différents modèles, il est nécessaire de : *i)* identifier les entrées/sorties impliquées dans le couplage de modèles hétérogènes, *ii)* réaliser des analyses de sensibilités sur les entrées/sorties et définir les transformations appropriées sur celles-ci, et *iii)* appliquer des méthodes adaptées pour la synchronisation temporelle de ces modèles lors de la simulation.

As stated in previous chapters, the role of modeling and simulation on the analysis of living systems is now clearly established. Emerging disciplines and worldwide research actions are based on an intensive use of integrative modeling and simulation methodologies and tools. A key aspect in this context is to perform an efficient integration of various models representing different biological or physiological functions, at different resolutions, spanning through different scales. However, there is still a lack of tools allowing such an efficient integration of heterogeneous models. Indeed, a recent special issue of the journal *Progress in Biophysics and Molecular Biology* was dedicated to this challenging problem of model interactions (Kohl et al., 2011). The content of this chapter is mainly based on a paper we have published in that special issue (Hernández et al., 2011).

The proposed approach to achieve this efficient model integration is to represent the various components of the physiological system of interest, by separate specific models (or sub-models),

developed at distinct levels of structural complexity, as a function of the targeted clinical application. However, such models are often developed under a variety of mathematical formalisms, use distinct structural resolutions, or show significant differences in their intrinsic dynamics. Coupling these formally heterogeneous models into a multi-resolution approach presents a number of methodological and technical challenges, particularly: *i)* the identification of the appropriate input-output variables involved in the coupling of heterogeneous models (e.g. coupling discrete with continuous variables), *ii)* the definition of appropriate transformations between these variables and *iii)* the creation of efficient methods for the temporal synchronization of these heterogeneous models in an integrated simulation approach.

This chapter is focused on these methodological aspects, for interfacing heterogeneous sub-models into an integrated, multi-resolution model. Section 3.1 extends the notation presented in the previous chapters and formally states the problem of interfacing heterogeneous models. Section 3.2 presents globally the proposed interface approach, while sections 3.3 and 3.4 describe in more detail the proposed input-output coupling method and the temporal synchronization strategies, respectively.

3.1 Notation and problem statement

The formalization introduced in this chapter follows the definitions 2.1 and 2.2 introduced in the previous chapter. For practical purposes, the next paragraph summarizes them.

A given model M of a system S can be formally defined by coupling a set of components (or sub-models) of two types: atomic models (M^a) and coupled models (M^{coup}). Atomic models represent a specific component of the system under study, using a given formalism (for example, a continuous model of a single myocite). Coupled models are composed of a hierarchy of interconnected coupled or atomic sub-models, that may be defined with different formalisms. These atomic and coupled models can be noted as the following tuples:

$$M^a : \quad (F, \mathbf{I}, \mathbf{O}, \mathbf{E}, \mathbf{P}) \text{ and} \tag{3.1}$$

$$M^{coup} : \quad (F, \mathbf{I}, \mathbf{O}, \mathbf{E}, \mathbf{P}, \{M_{G,i}\}), \quad i = 1, \ldots, N\,, \tag{3.2}$$

where F is the mathematical formalism in which each model is represented, $\mathbf{I}$, $\mathbf{O}$, $\mathbf{E}$ and $\mathbf{P}$ are vectors containing, respectively, the input, output, state variables and the parameters of each model, and $\{M_{G,i}\}$ is the set of N atomic or coupled sub-models constituting M^{coup}.

Figure 3.1 shows schematically how such a hierarchical model can be constructed from a given system, which has been previously analyzed and represented in specification level 4, as defined in chapter 2. In this example, a system S has been described as six interacting sub-components A,...,F, including a sub-system R that is also composed of three interacting sub-components (top panel). This system is then represented as a model $M = M_1$, and each one of its component is also represented by a model, yielding six atomic and one coupled sub-model ($M_2, \ldots, M_8$). Moreover, the interactions of the original system are now translated as connected input and output ports of the models (middle panel). The atomic and coupled model hierarchy can be

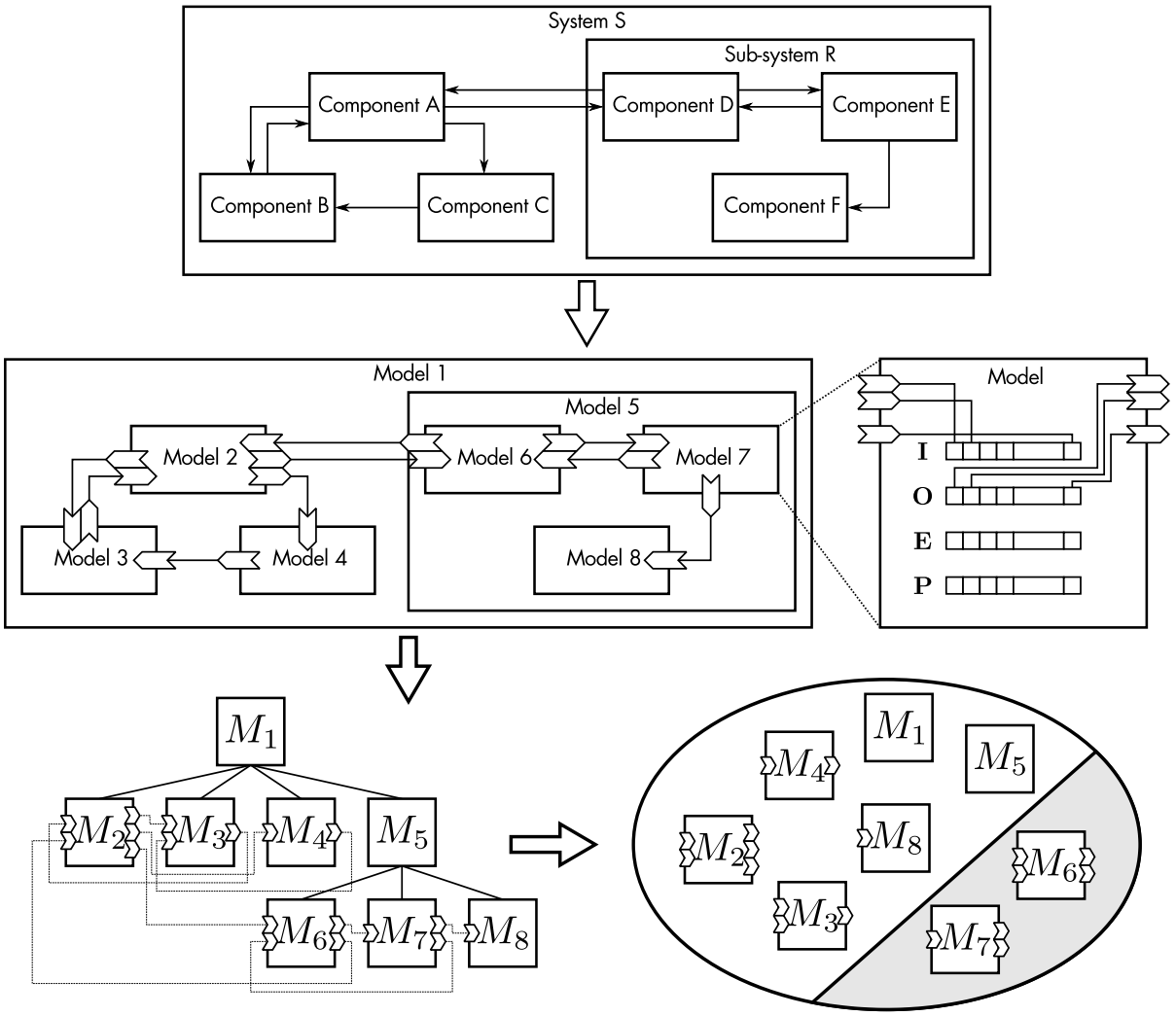

FIGURE 3.1– Schema of the transformation from a system to the model notation used in this chapter. In the top panel, a system is represented in specification level 4 (see chapter 2). The left middle panel shows the equivalent model structure with input/output ports, detailed in the right panel. The bottom panel translates the previous representation with a hierarchy that follows the model organization used later in chapter 4. Finally, the grouping at the bottom right is the notation used in this chapter.

also represented as a tree (bottom left panel). The objective here is thus to replace some of the original sub-modules of the model M_1 (for instance, models M_6 and M_7) by new models with a higher temporal or spatial resolution, while preserving the stability and the essential characteristics of the overall, integrated model.

3.2 Proposed sub-model interfacing approach

In order to formalize the sub-model interfacing method, we may define several model sets (see fig. 3.2). As proposed in the previous section, M_G represents the set of N original atomic or coupled sub-models constituting the global model M. This set, represented in fig. 3.2 as an ellipse, can be partitioned into two subsets: $\{M_{R,j}\} \subseteq \{M_{G,i}\}, j = 1, \ldots, N_R$, defines the sub-models

that we wish to replace (gray part of the ellipse in fig. 3.2(a)), and $\{M_{C,l}\} = \{M_{G,i}\} - \{M_{R,j}\}, l = 1, \ldots, N_C$, $N_C = N - N_R$, contains the sub-models that will be conserved from the original model (white part of the ellipse). Furthermore, let $\{M_{D,k}\}$ (truncated ellipse with segmented lines in fig. 3.2(a)) be the set of $k = 1, \ldots, N_D$ new, more detailed models that we wish to integrate instead of M_R. We may also define the following vectors: $I_{U,v}$, $O_{U,v}$, $E_{U,v}$ and $P_{U,v}$ (see eqs. (3.1) and (3.2)) containing input, output, state variables, and parameters of each model $v \in M_U$, where $U \in \{G, R, D, C\}$ for the original, replaced, detailed and conserved model sets, respectively. These vectors will be useful for the definition of the interface between models in different sets. The proposed approach for replacing M_R by M_D and for interfacing M_D with M_C involves the following steps:

Step 1: Identification of the interaction variables in models M_C, M_R and M_D.

Step 2: Whole-model and module-based sensitivity analyses.

Step 3: Input-output coupling of heterogeneous models.

Step 4: Temporal synchronization of heterogeneous models.

The following sections describe each one of these steps.

3.2.1 Identification of the interaction variables in models M_C, M_R and M_D

Six sets can be defined in this step, from the analysis of vectors $I_{U,v}$ and $O_{U,v}$. These sets contain the inputs and outputs of a given model set, which depend on outputs and inputs of models pertaining to a different set (boxes containing arrow-shaped ports in fig. 3.2(b)).

$$\mathcal{I}_R = \{I_{R,j}(n) \mid I_{R,j}(n) \text{ depends on } O_{C,l}(m)\}, \tag{3.3}$$
$$\mathcal{O}_R = \{O_{R,j}(m) \mid I_{C,l}(n) \text{ depends on } O_{R,j}(m)\}, \tag{3.4}$$
$$\mathcal{I}_D = \{I_{D,k}(n) \mid I_{D,k}(n) \text{ depends on } O_{C,l}(m)\}, \tag{3.5}$$
$$\mathcal{O}_D = \{O_{D,k}(m) \mid I_{C,l}(n) \text{ depends on } O_{D,k}(m)\}, \tag{3.6}$$
$$\mathcal{I}_C = \{I_{C,l}(n) \mid I_{C,l}(n) \text{ depends on an element in } \mathcal{O}_R\}, \tag{3.7}$$
$$\mathcal{O}_C = \{O_{C,l}(m) \mid \text{ an element in } \mathcal{I}_R \text{ depends on } O_{C,l}(m)\}, \tag{3.8}$$

where n and m are the indexes of each input or output vector, respectively.

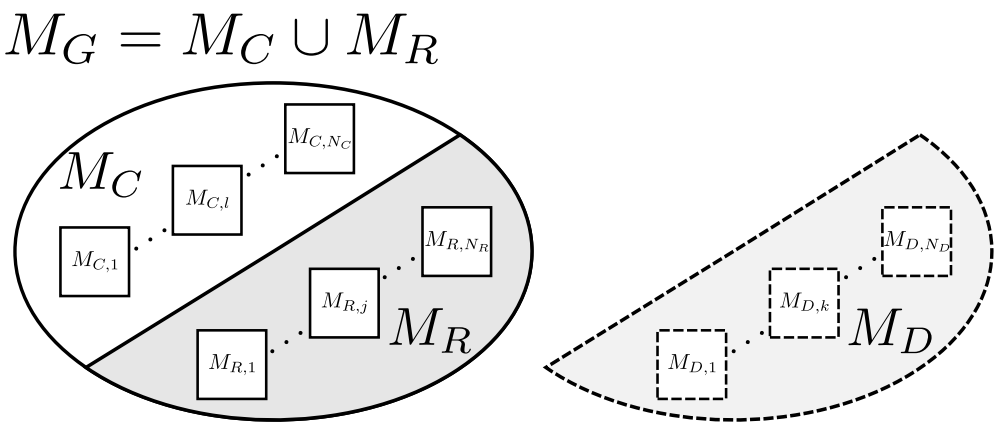

(a) Notation of the different model sets. The original model set (M_G) is represented with an ellipse and is the union of two subsets: a subset containing the models that will be preserved (M_C), and a subset of models that will be replaced (M_R, in grey). The M_D set (light gray, segmented lines) includes detailed models that will be used to replace models in M_R.

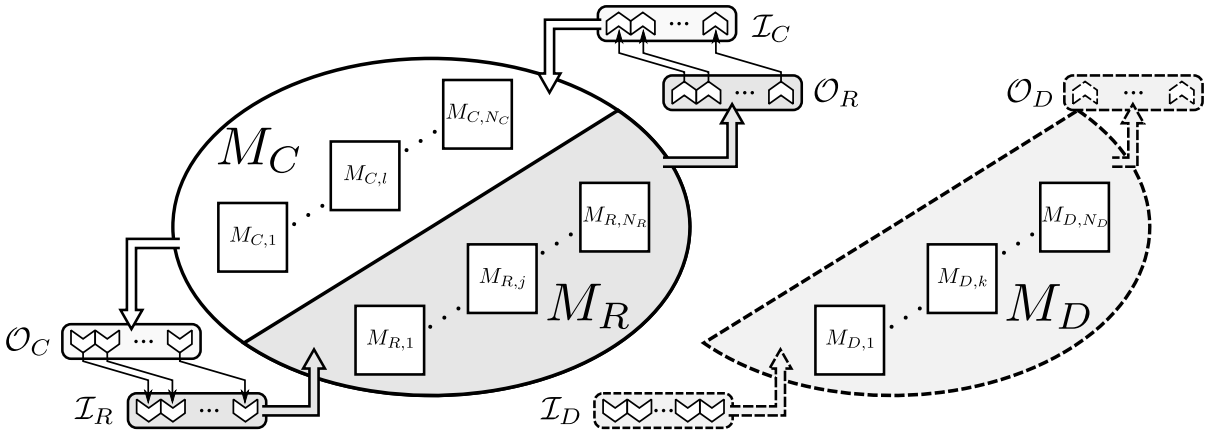

(b) Representation of the input and output variable sets (rounded boxes with arrow-like glyphs representing input/output ports) defined in eqs. (3.3) to (3.8).

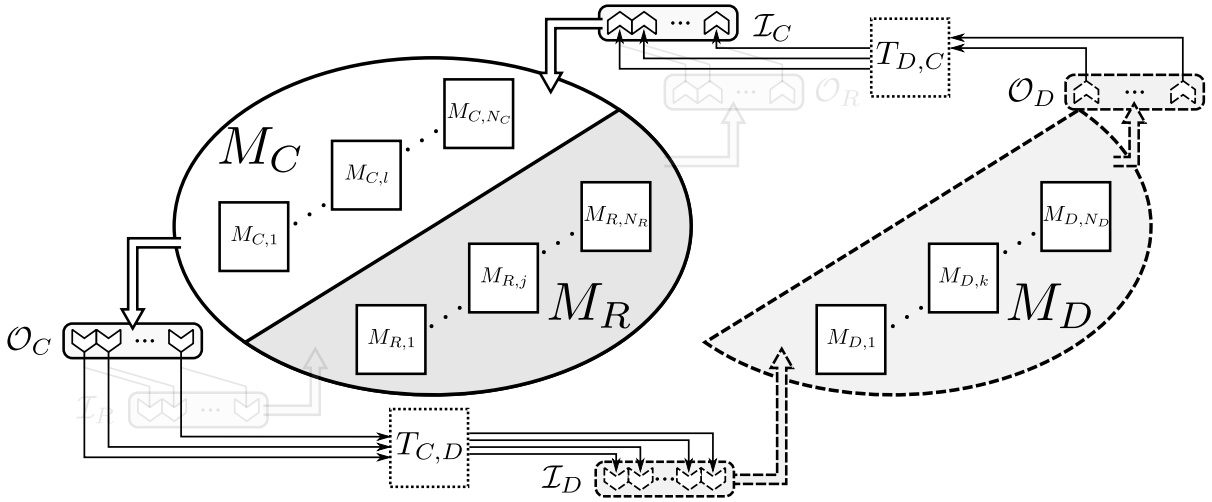

(c) Transformations functions $T_{C,D}$ and $T_{D,C}$ provide input/output interfaces between models in M_C and M_D.

FIGURE 3.2– Graphical representation of the sub-model interfacing method.

These sets can also be defined using an alternative notation:

$$\mathcal{I}_R = \left\{ \begin{array}{c} \text{All } \textbf{input variables} \text{ in } M_R \\ \text{connected with an } \textbf{output variable} \text{ in } M_C \end{array} \right\}, \tag{3.3}$$

$$\mathcal{O}_R = \left\{ \begin{array}{c} \text{All } \textbf{output variables} \text{ in } M_R \\ \text{connected with an } \textbf{input variable} \text{ in } M_C \end{array} \right\}, \tag{3.4}$$

$$\mathcal{I}_D = \left\{ \begin{array}{c} \text{All } \textbf{input variables} \text{ in } M_D \\ \text{that will be connected with an } \textbf{output variable} \text{ in } M_C \end{array} \right\}, \tag{3.5}$$

$$\mathcal{O}_D = \left\{ \begin{array}{c} \text{All } \textbf{output variables} \text{ in } M_D \\ \text{that will be connected with an } \textbf{input variable} \text{ in } M_C \end{array} \right\}, \tag{3.6}$$

$$\mathcal{I}_C = \left\{ \begin{array}{c} \text{All } \textbf{input variables} \text{ in } M_C \\ \text{connected with an } \textbf{output variable} \text{ in } M_R \end{array} \right\}, \tag{3.7}$$

$$\mathcal{O}_C = \left\{ \begin{array}{c} \text{All } \textbf{output variables} \text{ in } M_C \\ \text{connected with an } \textbf{input variable} \text{ in } M_R \end{array} \right\}, \tag{3.8}$$

During the model replacement procedure, the links between $\mathcal{O}_R$ and $\mathcal{I}_C$ and between $\mathcal{O}_C$ and $\mathcal{I}_R$ (depicted as arrows between boxes in fig. 3.2(b)), will be removed. This step can be addressed with completing a level 4 analysis, as presented in chapter 2, of the original and the detailed models. The simulation library used in this work and described in chapter 4, provides tools that use the definition of M_C, M_R and eqs. (3.3), (3.4), (3.7) and (3.8) to automate this initial identification step.

3.2.2 Whole-model and module-based sensitivity analyses

This step requires two kind of analyses: a whole-model sensitivity analysis (on model M) to study the response of their main variables with respect to all the model parameters and a module-based sensitivity analyses on each model in M_R to analyze $O_{R,j}$ with respect to variations in $I_{R,j}$. This step is crucial *i)* to better understand the mathematical properties and limitations of the global model and of each original sub-model, *ii)* to identify parameters and variables presenting the strongest and weakest interactions, since this information is useful to determine the elements in M_R and M_D for a particular problem, and *iii)* to evaluate the impact of the integration of M_D into the whole model, by comparing results of this step with a sensitivity analysis performed after integration of M_D.

Section 4.2 in chapter 4 will describe the methods applied in this thesis for these whole-model and module-based sensitivity analyses.

3.2.3 Input-output coupling and temporal synchronization of heterogeneous models

The general problem in this step is to design, implement, and evaluate an interface between models in M_D and models in M_C. This step is particularly difficult, since it may require the

definition of appropriate input-output transformations ($T_{C,D}$ or $T_{D,C}$) allowing to interface elements in $\mathcal{O}_D$ with elements in $\mathcal{I}_C$ and between $\mathcal{O}_C$ and $\mathcal{I}_D$. These transformations are illustrated as dotted boxes in fig. 3.2(c). Furthermore, specific simulation methods and parameters for models in M_D should also be defined, since they may be developed under different formalisms or present significantly different dynamics.

Sections 3.3 and 3.4 will present in detail the contributions related to this problems. Chapters 5 to 8 will provide examples of the application of all these four steps to development of multi-resolution models.

It should be noted that the method presented above may be applied to any coupled model, even if it is a sub-module of a higher-level coupled model or if models in M_D and M_R contain coupled models.

3.3 Input-output model coupling

As described in section 3.2, the objective of step 3 of the proposed approach requires is to couple models in M_D and M_C by defining specific input-output linear or non-linear transformations:

$$I_{C,l}(n) = T^{l,n}_{D,C}(\mathcal{O}_D, P^{l,n}_{TDC}), \quad I_{C,l}(n) \in \mathcal{I}_C \text{ and}$$
$$I_{D,k}(n) = T^{k,n}_{C,D}(\mathcal{O}_C, P^{k,n}_{TCD}), \quad I_{D,k}(n) \in \mathcal{I}_D,$$

where $P_{T^{\cdot}}$ are the parameters characterizing each transformation. For example, let $\mathcal{O}^{C,l}_D \subseteq \mathcal{O}_D$ be the elements in $\mathcal{O}_D$ connected to $I_{C,l}(n)$. In the simplest case, *i)* when there is only one output to couple, i.e. $\left|\mathcal{O}^{C,l}_D\right| = 1$, *ii)* when the corresponding models are defined under the same formalism, and *iii)* when these variables share the same physical units and temporal resolutions, the application of $T^{l,n}_{D,C}$ is trivial and the corresponding elements l are defined as the identity function. When this is not the case (heterogeneous models), problem-specific transformations have to be designed, although some general cases can be identified. For example, if $\left|\mathcal{O}^{C,l}_D\right| > 1$, such as in the case of different spatial resolutions of the same physical variable, an up-scaling method (such as homogenization or variable aggregation) will be applied, through $T^{l,n}_{D,C}$, to the elements on $\mathcal{O}^{C,l}_D$. A simple example of such a transformation is the application of an instantaneous weighted sum of the elements on $\mathcal{O}^{C,l}_D$, as in (Auger et al., 2000), with the coefficients of this transformation represented in $P^{l,n}_{TDC}$.

A similar approach can be applied when $\left|\mathcal{O}^{C,l}_D\right| = 1$, and when both variables share the same physical units, but the temporal resolution of variables in $\mathcal{O}^{C,l}_D$ is much higher. In this case, the scaling transformation can be applied in the time domain by means of filtering and subsampling (Hernández et al., 2009). Down-scaling methods can be applied when defining $T^{k,n}_{D,C}$, in particular when one output in $\mathcal{O}_C$ should be connected to many inputs in $\mathcal{I}_D$. A variety of up-scaling or down-scaling methods have been proposed in the literature (Auger et al., 2003; Lischke et al., 2007). The complex nature of the physiological systems, however, makes the application of analytic methods difficult, especially when coupling models defined under different mathematical formalisms.

Yet another case is when the physical units of variables in $I_{C,l}(n)$ and $\mathcal{O}_D^{C,l}$ are different. In this case, $T_{D,C}^{l,n}$ will additionally include the unit conversion process. However, in some cases, these variables may be represented in relative or arbitrary units, requiring the estimation of specific parameters $P_{TDC}^{l,n}$ in order to define an appropriate model interaction. Chapter 5 presents several examples of the definition of such transformations, when integrating heterogeneous models within the Guyton models.

3.4 Temporal synchronization of heterogeneous models

The objective of this step is the definition of appropriate simulators and simulation parameters for each model in M_D and M_C. This step is particularly important when the dynamics of these models are significantly different or when the models have been developed under different mathematical formalisms. In order to address this problem, our developments are based on the co-simulation principle, in which each model is associated with a specific simulator, adapted to the mathematical formalism of the corresponding model. These simulators can be represented, according to definition 2.3, as:

$$O_{U,v} = S_{U,v}^{h}(M_{U,v}^{h}, P_{U,v}^{S}, F_{U,v}) \,,$$

where $S_{U,v}^{h}$ is the simulator for model ($M_{U,v}^{h}$, $h \in \{a, coup\}$ for atomic or coupled models, respectively, and $P_{U,v}^{S}$ is a vector defining the simulation parameters (including specific model parameter values, initial conditions, integration step-size for continuous models, etc.). Each $S_{U,v}^{a}$ may thus use a different simulation method, with different simulation time-steps. The coupling of all atomic models is performed within the M^{coup} model that contains them, through a $S_{U,v}^{coup}$.

Consider the coupled model depicted in fig. 3.3, in which all atomic models (M_i^a, $i = 2, \ldots, n$) are represented in a continuous formalism and a hierarchy of continuous atomic simulators (S_i^a, $i = 2, \ldots n$), each one with its own fixed or adaptive integration step-size ($\delta t_{a,i}$). The input-output coupling of atomic models ($M_2^a, \ldots, M_n^a$) is performed by M_1^c and S_1^c at fixed or adaptive intervals, denoted δt_c, in which a temporal synchronisation of all atomic models occur, and outputs of the S_1^c coordinator are calculated.

Three different schemes for synchronizing $\delta t_{a,i}$ and δt_c, noted *ST1*, *ST2*, and *ST3*, have been proposed (cf. fig. 3.4):

- *ST1*: Simulation and synchronization with a unique, fixed time-step fig. 3.4(a)). In this approach, the simulation step is $\delta t_{a,i} = \delta t_c$ for all the elements, regardless of their local dynamics. This is the simplest way, which is indeed the same used in centralized simulators that update all the state-variables of the model in a single simulation loop. This approach does not correctly handle the heterogeneity of the local dynamics associated with each component of the model.
- *ST2*: Adaptive atomic simulation and synchronization at the smallest time step required by any of the atomic models (fig. 3.4(b)). The simulation time-step for each atomic model, $\delta t_{a,i}(t)$ and the coupling time-step $\delta t_c(t)$ are adaptive, and are updated after each coupling

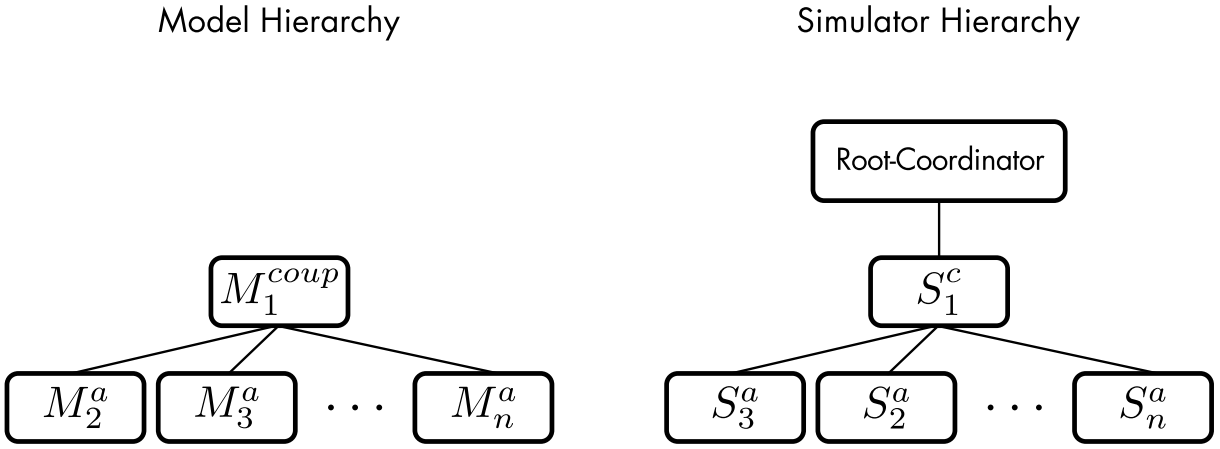

FIGURE 3.3– Functional diagram of an example coupled model M_1^c composed of n atomic models and its corresponding simulator hierarchy.

step with $\delta t_c(t) = \min_i [\delta t_{a,i}(t)]$ and $\delta t_{a,i}(t) = \delta t_c(t), \forall i$. This scheme is a completely adaptive approach, requiring minimum user interaction. However, the benefits of this method are only observed when the dynamics of atomic simulators are similar and when these dynamics show significant differences through time.

– *ST3*: Synchronization at a fixed time-step and atomic simulation with independent, adaptive time-steps (fig. 3.4(c)). Here, each atomic simulator S_i^a evolves with its own adaptive simulation step $\delta t_{a,i}(t)$ and all simulators are coupled at fixed intervals δt_c. The objective is to exploit the different dynamics of the atomic models in order to improve the efficiency of the simulation. For instance, if model M_2^a shows slower dynamics than model M_3^a, $\delta t_{a,2}$ will be greater than $\delta t_{a,3}$. This approach benefits from the heterogeneity of the dynamics in each atomic simulator, but the value of δt_c should be chosen carefully, with $\delta t_c(t) \geq \max_i [\delta t_{a,i}(t)]$.

Classical algorithms for the adaptation of the simulation time-step can be used with methods *ST2* and *ST3*. It should be noticed that, in a typical centralized method, equivalent strategies for *ST1* and *ST2* can be applied. However, implementation of *ST3* is only possible using a distributed co-simulation architecture.

3.5 Conclusion

With the emergence of integrative physiology, an increasing interest exists today towards the integration of different physiological models, which may cover different functions and be developed at various scales, under distinct mathematical formalisms. This chapter presented a contribution to the formalization of the seldom-covered problem of the appropriate definition of the interfaces required to perform this model integration. It also proposes an approach to interface such heterogeneous models, by *i)* restructuring and modularizing the different models to

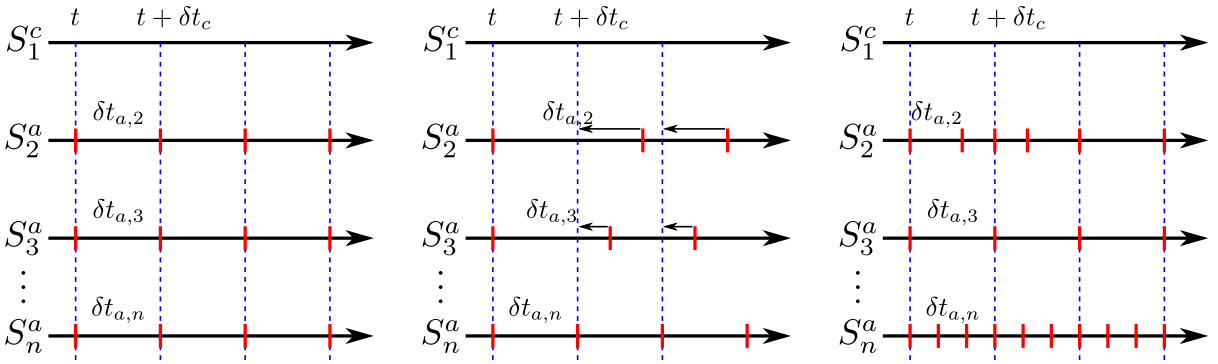

(a) Fixed-step method.

(b) Adaptive synchronization and simulation, with the smallest atomic timestep.

(c) Synchronization at a fixed timestep (δt_c) and atomic simulation with independent, adaptive timesteps $\delta t_{a,i}$.

FIGURE 3.4– Graphical representation of the time synchronization schemes, based on the example of coupled models on fig. 3.3.

be coupled, *ii)* analyzing their input-output sensitivity and *iii)* defining appropriate input-output transformations and simulation methods. Moreover, although described here in the context of integrative physiology, the proposed methods are completely general and can be used for multi-resolution modeling of any kind of system.

In order to apply the methods proposed in this chapter, they have to be implemented and integrated into a complete software framework allowing for the representation, handling, sharing and simulation of heterogeneous models. The next chapter will present the contributions made during this thesis for the continuous development of such a framework (M2SL toolkit).

Finally, chapters 5 to 8 will present concrete clinical applications in which the proposed methodological approach for heterogeneous model interactions has been applied, through the use of the M2SL toolkit.

References

AUGER, P. and R. BRAVO DE LA PARRA (2000). "Methods of aggregation of variables in population dynamics". In: *Comptes Rendus de l'Académie des Sciences-Series III-Sciences de la Vie* 323.8, pp. 665–674.

AUGER, P. and C. LETT (2003). "Integrative biology: linking levels of organization". In: *Comptes Rendus Biologies* 326.5, pp. 517–522.

HERNÁNDEZ, A. I., V. LE ROLLE, A. DEFONTAINE, and G. CARRAULT (2009). "A multiformalism and multiresolution modelling environment: application to the cardiovascular system and its regulation". In: *Philos Transact A Math Phys Eng Sci* 367.1908. PTRSA, pp. 4923–4940. DOI: 10.1098/rsta.2009.0163.

HERNÁNDEZ, A. I., V. LE ROLLE, D. OJEDA, P. BACONNIER, J. FONTECAVE-JALLON, F. GUILLAUD, T. GROSSE, R. G. MOSS, P. HANNAERT, and S. R. THOMAS (2011). "Integration of detailed modules in a core model of body fluid homeostasis and blood pressure regulation". In: *Progress in Biophysics and Molecular Biology* 107, pp. 169–182. DOI: 10.1016/j.pbiomolbio.2011.06.008.

KOHL, P., P. HUNTER, and R. WINSLOW (2011). "Model interactions: 'It is the simple, which is so difficult'". In: *Progress in Biophysics and Molecular Biology* 107.1. <ce:title>Experimental and Computational Model

Interactions in Bio-Research: State of the Art</ce:title>, pp. 1 –3. ISSN: 0079-6107. DOI: http://dx.doi.org/10.1016/j.pbiomolbio.2011.07.003.

Lischke, H., T. J. Löffler, P. E. Thornton, and N. E. Zimmermann (2007). "Model up-scaling in landscape research". In: *A Changing World*. Springer, pp. 249–272.

CHAPTER 4

Novel tools for multi-formalism modeling, simulation and analysis

Résumé

Ce chapitre présente les outils mis en œuvre pour l'intégration de modèles dans une approche multi-résolution. La définition d'une librairie de simulation adaptée est notamment nécessaire afin de faciliter l'implémentation de l'approche de modélisation intégrative définie au chapitre précédent. Un environnement de modélisation et de simulation a été précédemment développé au laboratoire (M2SL : « Multiformalism Modeling and Simulation Library »). Les améliorations apportées à M2SL, afin de faciliter l'intégration de modèles, sont présentées dans ce chapitre. Les approches proposées pour l'analyse de sensibilité et l'identification de paramètres sont notamment décrites après un état de l'art des méthodes existantes.

This chapter presents a set of original approaches and novel tools for multi-formalism modeling, simulation and analysis that have been developed in the context of this thesis in order to ease the application of model-based methods in clinical contexts. The first part, section 4.1, describes a specific tool for the implementation of multi-resolution and multi-formalism models that integrates the methodological contributions cited in the previous chapters. Sections 4.2 and 4.3 are dedicated to sensitivity analysis and parameter identification, respectively. In each section, a brief state of the art is presented, followed by the proposed approach. The combination of these modeling, simulation and analysis tools was the cornerstone for building the clinical applications presented in the following chapters.

4.1 Multi-formalism modeling and simulation

4.1.1 Modeling and simulation tools: state of the art

The extended application of models in different research disciplines has led to a vast choice of modeling and simulation tools. Primarily, industrial processes have driven the development of

most simulation tools, but recent international initiatives in systems biology and physiological modeling, such as the IUPS Physiome (MILLER, 2010) or the Virtual Physiological Human (KOHL et al., 2009), have encouraged the advancement of new modeling tools designed for applications in the life sciences. Unfortunately, describing all recent developments would be prohibitively long. This section summarizes the most important simulation tools, which are readily applicable to modeling and simulation in general, and those specifically useful for applications in physiology.

Generic integrated environments: A set of popular modeling and simulation tools are based on generic, graphical computing environments. In this category, commercial applications, leaded by MATLAB®/Simulink [1], are widespread for providing complete and extensive packages for numerous scientific domains (engineering, electronics, biology, mechanics, etc.). Currently, other commercial competitors offer good alternatives, including Wolfram Mathematica®/System Modeler [2], Dymola [3], MapleSim [4], Stella - Berkeley Madonna [5] and, in a lesser extent, an open-source free alternative, Scilab/Xcos [6].

These environments usually provide an embedded or independent graphical toolkit (such as Simulink, System Modeler, or Xcos) specifically designed for the creation of models using modular interconnected blocks. Only a few of these environments (Simulink, for instance) provide means for coupling different model formalisms (discrete models, ordinary differential equation—ODE models), using specific libraries (such as StateFlow, for discrete models in Simulink) and the employment of advanced parameter analysis methods.

Within this group of generic environments there is a set of tools specifically designed for building multi-physics and multi-scale models. ANSYS [7] solvers, COMSOL Multiphysics® [8] and the ADINA [9] systems stand out as the most popular commercial products. Although mainly applied to the automotive, aerospace, and fluid mechanics fields, these systems have also been successfully used in a number of biomedical applications.

Although powerful and refined, most of these tools do not present an explicit approach to multi-formalism simulations. Simulations are performed using a centralized simulator approach that is specifically optimized for a given formalism, with globally-fixed simulation parameters. In this sense, these generic integrated environments are not optimal for handling formally heterogeneous systems.

Generic modeling languages: In the pursuit of a machine and human readable description of a model, numerous modeling languages have been proposed, along the vast choice of simulation tools. Yet, a particular language emerged from the international cooperation of key authors in

1. http://www.mathworks.com
2. http://www.wolfram.com/system-modeler
3. http://www.dymola.com
4. http://www.maplesoft.com/products/maplesim
5. http://www.berkeleymadonna.com
6. http://www.scilab.org
7. http://www.ansys.com
8. http://www.comsol.com
9. http://www.adina.com

the modeling field, the Modelica Association [10] and the Modelica language: a non-proprietary, equation based modeling language for large hierarchical systems. The Modelica language allows for the definition of continuous (differential algebraic equations—DAE and ODE models) or discrete-time models. It has been applied to multidomain models (robotics, mechanics, aerospace), but rarely to physiological modeling. Several commercial tools implement and profit from Modelica's versatility to define their models, such as Dymola, MapleSim, Wolfram System Modeler, among others. An attractive tool for educational purposes is the open-source implementation OpenModelica [11], providing a large set of tutorials, documentation and parameter analysis tools. Moreover, OpenModelica enjoys from large and very active developer and user communities.

Specific tools for physiological applications: Several simulation tools have been specifically designed for physiological modeling applications. Currently, most major efforts in providing specific physiological modeling tools are listed on the Virtual Physiological Human Network of Excellence website (VPH NoE [12]) or the Physiome Project [13]. Notable examples include the Continuum Mechanics, Image analysis, Signal processing and Signal identification (CMISS [14]) toolkit, and its open source counterpart OpenCMISS, an environment specialized on finite element analysis on bioengineering problems. Continuity 6 [15] also offers a multi-scale modeling environment that has been used for cardiac mechanics and electrophysiology modeling. For fine scale applications on cancer, cardiac and soft-tissue, CHASTE (Mirams et al., 2013) offers a simulation tool that permits the integration from cell to tissue models. However, these tools are not adapted to the integration of system-level physiological models that may be used to refine the boundary conditions of FEM models. Finally, a Java-based simulation system, JSim [16], deserves a special mention, not only due to the fact that it integrates ODE, PDE with discrete event models, but because it has grouped a set of more than 70 000 models in a public online database.

In the particular context of biological and physiological modeling, a set of markup languages have been developed by researchers in order to ease the sharing, curation and testing phases. The most significant effortsts are SBML (Hucka et al., 2003), CellML (Garny et al., 2008) and FieldML (Britten et al., 2013). The Systems Biology Markup Language (SBML) is a XML-based language designed from systems biology concepts that defines models as a description of chemical substances, reactions, parameters and mathematical expressions. CellML is also an XML-based format with a modular structure, which allows for model reuse, defining models as several interconnected components. Each component is defined by a set of variables and

10. http://www.modelica.org
11. http://www.openmodelica.org
12. http://www.vph-noe.eu
13. http://physiomeproject.org
14. http://www.cmiss.org
15. http://www.continuity.ucsd.edu
16. http://www.physiome.org/jsim

mathematical rules expressed in another markup language, MathML [17]. Not constrained to cellular models, as incorrectly implied from its name, a large database of (partially) curated models are part of the CellML tools [18]. Finally, FieldML (CHRISTIE et al., 2009) is an XML representation still under development that seeks to define multivariate field models, which is currently impossible with other markup languages.

Multi-formalism environments: Whereas most modeling environments are specialized in a particular formalism, a group of modeling and simulation tools handle multi-formalism systems explicitly. A special group can be defined for these tools.

The majority of multi-formalism frameworks adopt the formalism transformation approach, following the morphisms introduced by ZEIGLER et al. (ZEIGLER et al., 2000). ZEIGLER focused most of his research on the transformation towards the DEVS formalism, but he also introduced the co-simulation of DEVS and DESS formalisms using interface objects, managed by coordinator objects. His work was continued with the DEVS-suite simulator [19], although this framework is so specialized in DEVS that its multi-formalism features are questionable. Meanwhile, VANGHELUWE (VANGHELUWE, 2001) worked on the formalism transformation concepts further, introducing the formalism transformation graph (FTG, cf. fig. 4.1), illustrating the possible model formalism morphisms, emphasizing the transformation towards a meta-formalism that incorporates DEVS and DESS. VANGHELUWE's initial efforts were concentrated on a declarative modeling language named MSL, which was later renamed WEST++ and commercialized for water treatment plants. Later, his work led to the creation of AToM3 (DE LARA et al., 2002) and to the establishment of Modelica. Other notable simulation environments that use formalism-transformation are OsMoSys (VITTORINI et al., 2004) and the Virtual Laboratory Environment (VLE) (QUESNEL et al., 2009), a framework specialized in DEVS, parallel DEVS, Quantified State Systems (QSS), cellular automata and differential equations.

Among the co-simulation implementations, a prominent effort is the High Level Architecture (HLA), a general purpose architecture designed for distributed computer simulation systems. HLA is not a modeling environment, but a standard (in fact, it has become the IEEE 1516 standard) that defines how computer simulations communicate data and synchronize their actions by introducing coordination time points. Implementations of HLA are called Run-Time Infrastructures (RTI); a number of commercial and non-commercial RTI implementations exist today, although current efforts are mostly oriented to the aspects and computational advantages of large distributed simulations.

The objective of the modeling applications presented in this work is to use and integrate different models proposed by various authors. Each model is usually associated with a particular simulator. Therefore, an important requirement of our works is the simultaneous utilization of different simulators of different formalisms, and not its transformation to an unique formalism,

17. http://www.w3.org/Math
18. http://models.cellml.org
19. http://acims.asu.edu/software/devs-suite

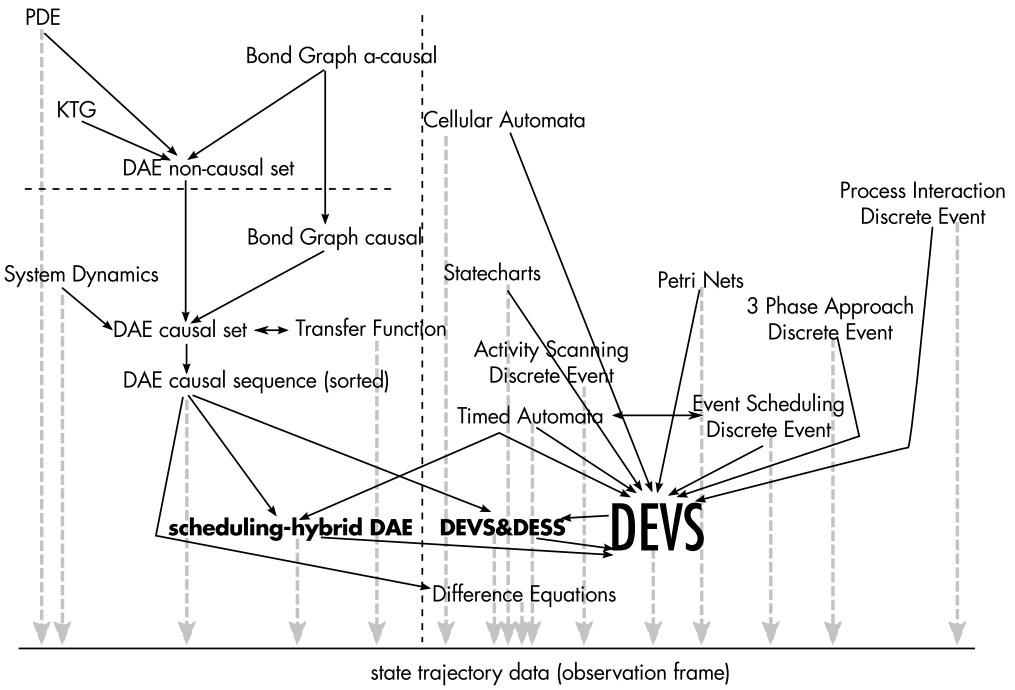

FIGURE 4.1– Formalism Transformation Graph (FTG), introduced by (VANGHELUWE, 2001): solid lines represent an existing morphism that transforms one formalism to another. Gray dashed lines indicate the availability of a simulator for a formalism.

such as DEVS. For this reason, we propose the creation and improvement of a custom multi-formalism library, using a co-simulation approach, as explained in the next section.

4.1.2 Proposed approach: Creation of a custom multi-formalism modeling and simulation library

The modeling and simulation toolkit used for all models in this thesis is the *Multi-formalism Modeling and Simulation Library* (M2SL). This toolkit was originally designed as a library, during the work of (DEFONTAINE, 2006) on the cardiac electrical system. Continuously in evolution since that time, M2SL has been adapted to solve the problems encountered by multi-formalism and multi-scale modeling (HERNÁNDEZ et al., 2009; HERNÁNDEZ et al., 2011). M2SL has been progressively improved, including a variety of coupled formalism-specific simulators, including discrete-time and continuous ordinary differential equations (ODE) (DEFONTAINE, 2006), Bond-Graphs (LE ROLLE, 2006), or low-resolution finite element methods (FLEUREAU, 2008). In order to solve the dynamics of the targeted heterogeneous models, M2SL uses the co-simulation principle. Furthermore, the solutions to the main problems introduced by this approach, (i.e. the input/output coupling and the temporal synchronization), presented in chapter 3, have been implemented in M2SL with the definition of transformation objects and establishing different synchronization strategies. This section presents the technical details of the library, along with the description of the new modules and tools implemented during this thesis, which have been registered with the French Agency of Software Protection.

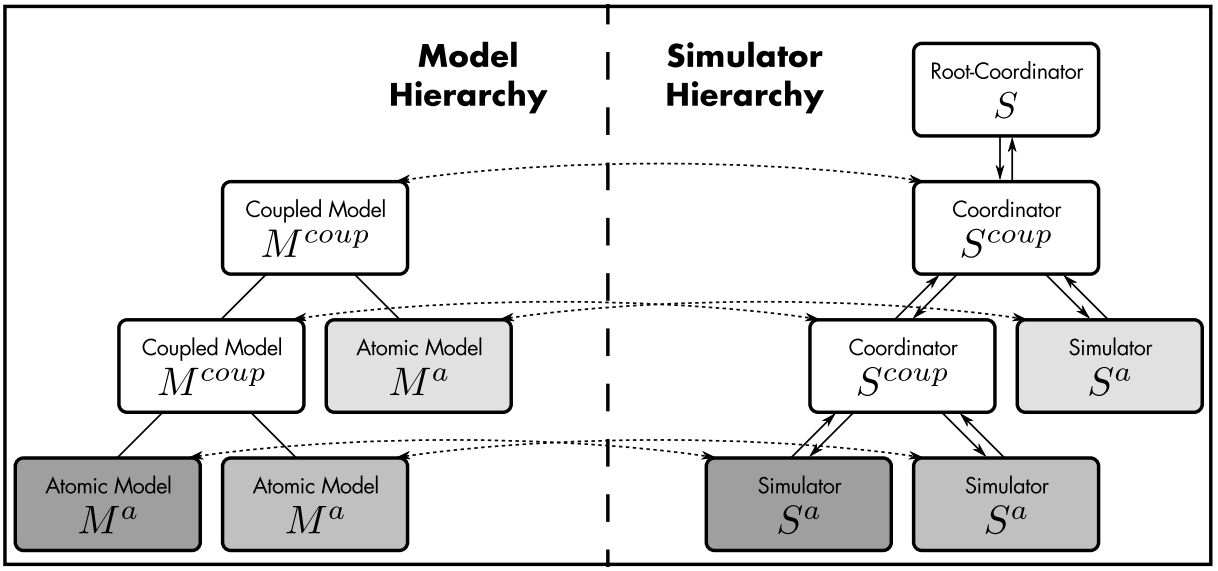

FIGURE 4.2– Hierarchical structure of models and their corresponding simulators. Schema based on (ZEIGLER et al., 2000).

4.1.2.1 Model representation

A model in M2SL is a set of interconnected components; a combination of two types of model objects: atomic models (M^a) and coupled models (M^{coup}), as defined in chapter 2. Atomic models are the description of a specific component of a system using one particular formalism. Coupled models are the composition of two or more models that may be defined under different formalisms and the connections between them. A graphical representation of atomic and coupled models, including their organization, is presented as the model hierarchy in the left part of fig. 4.2.

When a computational model is defined in M2SL, a global simulator S, called the *root coordinator*, is first created. This object analyses the model hierarchy and creates a simulator S_i^a for each atomic model M_i^a. The choice of the appropriate simulator type is automatically handled by the library. In this way, a model with formalism F_i is associated with a simulator designed for the same formalism F_i. For each coupled model M_i^{coup}, a *coordinator* S_i^{coup} is created. Coordinators are a special kind of simulator that handle the connection of the internal components of a complex model and computes model outputs at the coupled level.

Using an object-oriented methodology, models in M2SL are represented with different abstract classes, which define the structural elements of a model and its behaviors. The development of a model in M2SL consists in choosing a base abstract class, defining its data structures and then the programming of its behavior. The available data structures and behaviors of a model depends on the formalism of the model. However, it always follows definition 2.1, introduced in chapter 2: a model is represented as a tuple $M\,(F, \mathbf{I,O,E,P})$. The relation between each element of this tuple and the structures of M2SL is explained below:

Formalism F: The formalism of a model is defined by the abstract class chosen as base class for its implementation. In other words, for each formalism, M2SL provides an abstract class. As of version 1.8.4, the available formalisms are summarized in table 4.1. Following an object-oriented paradigm, a model in M2SL must inherit from one of these classes. Moreover, each formalism requires the implementation of particular behaviors, represented by the methods of each class. These behaviors will be presented later.

Variables I,O,E,P: The variables of a model are organized in four different groups according to their semantic definition: `inputs`, `outputs`, `states`, and `parameters`. Each single variable or parameter can be represented by any data structure provided by the C++ language [20]. Variables and parameters are encapsulated in a class named `GenericVariable`, an object that aggregates metadata regarding the user configuration of each variable (cf. table 4.2).

Components: As explained before, in M2SL, models can be either atomic or complex. To permit the creation of complex models, the `submodels` container is also included in the definition of a model, which accommodates a list of references to other models.

Behaviors: The behavioral definition of a model comprises four different procedures:

- Initialization: the calculation or simple assignment of initial values to all variables of the model.
- Variable synchronization: the update or modification of the internal state of the model due to a change in the input variables.

20. The most natural choice among all C++ data structures would be `int` for any integer value or `double` for real values, but any other data type can be used.

TABLE 4.1– Formalisms supported in M2SL and their corresponding class.

Formalism F	**Class**
Algebraic equations	`GenericModel`
Ordinary differential equations	`OdeModel`
Algebraic equations with discrete time	`DiscreteTimeModel`

TABLE 4.2– Metadata related to variables and parameters.

Property	**Type**	**Relevant to**	**Description**
`label`	String	Any	Unique identifier of the variable
`units`	String	Any	Units of the variable (optional)
`printable`	Boolean	Any	Whether or not to include its trajectory in the output file
`errorScaleFactor`	Number	State variable	Weight used for the error associated with this variable

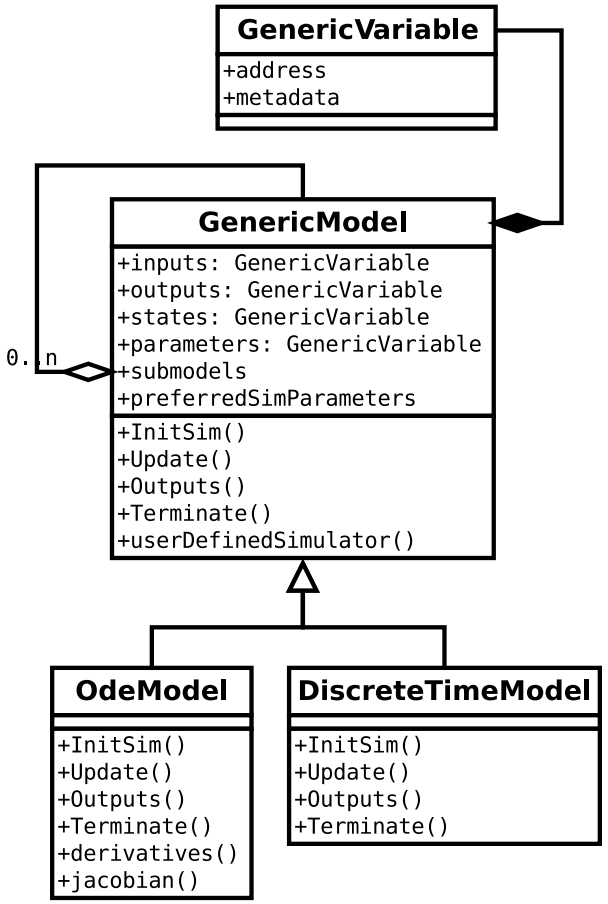

FIGURE 4.3– Object oriented representation of models in M2SL.

– Output calculation: the computation of the output variables from the current internal state and the input variables.
– Termination: the final procedure executed when the simulation ends.

This list serves as the base behavior set for all formalisms in M2SL; more behaviors may complement them when a particular formalism requires it.

4.1.2.1.1 Algebraic equations models

Algebraic equations (AE) models are the most simple type of model available in M2SL. It represents a model whose outputs can be calculated with a mathematical function of the inputs and current states. However, this type of model does not provide any function to account for the internal transitions of the states. Algebraic equation models are implemented by the `GenericModel` class; the base class of all other model definitions, as illustrated in fig. 4.3. One of the design objectives of this class is to provide the object-oriented foundation for all other M2SL classes and any user-defined model. It defines four methods, `InitSim`, `Update`, `Outputs`, and `Terminate` that correspond exactly to the behaviors defined previously: initialization, variable synchronization, output calculation and termination.

4.1.2.1.2 Ordinary differential equations models

Ordinary differential equations (ODE) models represent systems whose internal states that are modified according to their rate of change with respect to time. Formally, an ODE system of n variables can be defined as:

$$\frac{dy_i(t)}{dt} = f_i(t, y_1(t), y_2(t), \ldots, y_n(t)) \text{ for } i = 1, \ldots, n\,, \tag{4.1}$$

where f_i is the derivative function of variable y_i. In M2SL, a variable described by a differential equation is represented by a state variable $e_i \in \mathbf{E}$, $i \in [1, n]$. Therefore, eq. (4.1) can be rewritten as:

$$\frac{de_i(t)}{dt} = f_i(t, e_1(t), e_2(t), \ldots, e_n(t)) \text{ for } i = 1, \ldots, n\,. \tag{4.2}$$

Following the object-oriented paradigm, an ODE model is a specialization of an algebraic equation model, with the addition of a behavior that calculates the derivative function f_i of each state variable. The structure that implements ODE models is the `OdeModel` class. All ODE models must implement the `derivatives` method to calculate each $f_i(t, e_1(t), \ldots, e_n(t))$. Optionally, the `jacobian` can be implemented, which calculates the matrix of all first-order partial derivatives of the state variables:

$$J = \begin{bmatrix} \frac{df_1}{de_1} & \cdots & \frac{df_1}{de_n} \\ \cdots & \ddots & \cdots \\ \frac{df_n}{de_1} & \cdots & \frac{df_n}{de_n} \end{bmatrix}. \tag{4.3}$$

4.1.2.1.3 Discrete time models

Discrete time models define the dynamics of a system as internal transitions that occur at regular intervals. These kind of models can be formalized as:

$$e_i(t+1) = \delta(e(t), i(t))\,, \tag{4.4}$$

where $e \in \mathbf{E}$ represents the state of the model, and δ is a function that calculates the next state from the current states $e(t)$ and input $i(t)$.

A discrete time model in M2SL is a specialization of the algebraic equation model, but for this particular class, the function `Update` is used to perform the operation defined in eq. (4.4).

4.1.2.2 Simulator representation

Simulators in M2SL are represented with the `GenericSimulator` class or one of its specialized classes designed for a particular formalism. Analogously to models, simulators follow definition 2.3, representing a simulator as a process $S^h(M^h, P_S, F)$, with $h \in \{a, coup\}$. Here, M^h is an atomic or coupled model of formalism F associated with a simulator S^h using parameters $P_S = [P_{\text{sim}}, I, E_0, P]$, where P_{sim} represents the simulation parameters.

The representation of these elements in M2SL is explained in the following subsections:

TABLE 4.3– Formalism-specific simulators and their associated model in M2SL.

Simulator	**Model**	**Formalism** F
`GenericSimulator`	`GenericModel`	AE
`OdeSimulator`	`OdeModel`	ODE
`DiscreteTimeSimulator`	`DiscreteTimeModel`	Discrete Time
`Coordinator`	—Any model with submodels—	

Model M^h and formalism F: Each model instance in M2SL is associated with exactly one simulator. The formalism in which the simulator is specialized is exactly the same as the formalism of the model, as prescribed by the co-simulation principles. As with models, the formalism of a simulator is represented by a different class. The list of formalisms and corresponding simulators is summarized in table 4.3.

In order to evolve the dynamics of the model over time according to an input trajectory, the simulator implements a set of basic procedures:

- `initSimulation`: the initialization of all structures related to the simulation (internal variables, temporal data, output files, etc.). It also initializes its associated model M^h using the `InitSim` method of the model.
- `update`: the synchronization of the input values of the model, calculated from the updated values of the outputs of other models, which uses the model `Update` method. Also, this procedure may analyze the dynamics and internal variables of the model to determine an optimal scheme for the next simulation step.
- `simulate`: the calculation of the transitions of the model until a defined time, when the formalism accepts a transition function. In the case of ODE models, this procedure will call the `derivatives` function at least one time.
- `outputs`: the calculation of the outputs of the model using its `Output` function.
- `stop`: the final procedure that performs a clean-up and frees all the resources used for the simulation.

The evolution of the model dynamics is achieved with an organized application of these procedures during the simulation loop, which will be detailed in section 4.1.2.4.

Simulation parameters P_{sim} The behavior of the simulation can be controlled through the simulation parameters P_{sim}, a list of attributes that the user may modify. These parameters are summarized in table 4.4. Each model implemented in M2SL contains a structure `preferredSimParameters` that represents P_{sim}. The implementation of the simulator takes into account these elements as default values when it is created.

4.1.2.2.1 Algebraic equations simulator

The algebraic equation simulator is the most basic simulator available in M2SL. It is represented by the class `GenericSimulator`. It solves the dynamics of an AE model and serves as base class for other simulators, as illustrated in fig. 4.4.

TABLE 4.4– Simulation parameters of M2SL simulators. Parameters associated with algebraic equation models are available for all models, due to the object oriented architecture shown in fig. 4.3.

Formalism	Parameter	Description
AE	`DT`	Preferred simulation step
	`minDT`	Minimum allowed simulation step for adaptative simulations
	`maxDT`	Maximum allowed simulation step for adaptative simulations
	`couplingDT`	Preferred synchronization step
ODE	`absError`	Maximum absolute error allowed
	`relError`	Maximum relative error allowed
	`maxRatio`	Maximum ratio of change for the next simulation step
	`solverType`	Preferred numerical algorithm for the ODE solver

4.1.2.2.2 Ordinary differential equations simulator

This simulator uses numerical algorithms to solve the dynamics represented by an ODE model. Such dynamics are an approximation of the trajectory of the state variables that solve eq. (4.2). M2SL includes three numerical solvers for this task: Euler, Runge-Kutta and Runge-Kutta-Fehlberg. Briefly, these solvers use the current value of the state variables at time t (denoted $\mathbf{e}(t) = [e_1(t), \ldots, e_n(t)]$) to calculate their value at time $t + h$. Euler's method uses the following rule:

$$\mathbf{e}(t+h) = \mathbf{e}(t) + h\mathbf{f}(t, \mathbf{e}(t))\,, \tag{4.5}$$

where $\mathbf{f}$ denotes the derivatives of the function $\mathbf{e}$. Better results can be achieved with a higher-order approach, such as the Runge-Kutta 4th order method, which evaluates $\mathbf{f}$ several times for a closer approximation:

$$\begin{aligned} \mathbf{e}(t+h) &= \mathbf{e}(t) + \tfrac{1}{6}k_1 + \tfrac{1}{3}k_2 + \tfrac{1}{3}k_3 + \tfrac{1}{6}k_4\,, \\ &\quad \text{where} \\ k_1 &= \mathbf{f}(t, \mathbf{e}(t))\,, \\ k_2 &= \mathbf{f}(t + \tfrac{1}{2}, \mathbf{e}(t) + \tfrac{h}{2}k_1)\,, \\ k_3 &= \mathbf{f}(t + \tfrac{1}{2}, \mathbf{e}(t) + \tfrac{h}{2}k_2)\,, \\ k_4 &= \mathbf{f}(t + h, \mathbf{e}(t) + hk_3)\,. \end{aligned} \tag{4.6}$$

As eqs. (4.5) and (4.6) entail, the calculation of the value of state variables involves the evaluation of the derivatives function $\mathbf{f} = [f_1, \ldots, f_n]$. Consequently, the `simulate` procedure of an ODE simulator consists in the organized invocation of the `derivative` function of its associated model, followed by the update of its state variables.

Since the ODE simulator provides an approximation to the solution of a differential equation, the trajectories calculated have a numerical error, denoted ϵ. In order to estimate this error, when the ODE simulator advances a model from t to $t + h$, it performs two integration steps: The first one is an application of a classical method such as Euler or Runge-Kutta. The second one is the application of a method whose order is higher than the method used before. For

example, if the Runge-Kutta method was used, which has order 4, a 5th order method is applied to obtain a better approximation. The absolute value of the difference of the solutions obtained with these two methods is considered as the integration error ϵ.

The integration error calculated by this simulator can be used for the estimation of an optimal simulation step, used for the adaptive simulations explained in section 4.1.2.5. This optimal step $\delta t_{\text{optimal}}$ is calculated as:

$$\delta t_{\text{optimal}} = \delta t \cdot \left(\frac{\epsilon}{\epsilon_{\max}} \right)^{-\frac{1}{5}} , \tag{4.7}$$

where $\epsilon_{\max}$ is the maximum permitted error set by the user.

4.1.2.2.3 Discrete-time simulator

A discrete time simulator provides the same behavior of an AE simulator, but it enforces that the internal transitions of a model occur at a discrete time. In other words, the values of the state and output variables of these models are calculated at points in time with an equal separation. A discrete time simulator with a simulation step s advances the status of a model from time t to $t + h$ by repeatedly calling the model's `Update` method in order to advance its variables to $t + s$. This process is repeated until the time of the model reaches $t + h$.

4.1.2.2.4 User-defined simulators

Since there is a wide choice of algorithms associated with the formalisms included in M2SL, the library has been designed to permit the creation of user-defined simulators. In order to create a user-defined simulator, a child class of `GenericSimulator` needs to be defined, including the implementation of the methods described in section 4.1.2.2 and fig. 4.4. Moreover, the model that uses the customized simulator must override the `userDefinedSimulator` method in order to create an instance of its preferred simulator.

This feature of M2SL is useful for the integration of external libraries. For example, the large choice of ODE solvers included in the GNU Scientific Library (GALASSI et al., 2006) can be used for the simulation of ODE models. In fact, a class `ODEGSLSimulator` has been developed for this matter, but it is not included with M2SL to avoid licensing issues.

4.1.2.3 Transformation objects representation

The function that performs a variable transformation in order to integrate heterogeneous models, as explained in chapter 3, is represented by the `Coupler` class. This class contains references to the source and destination variables, as illustrated in fig. 4.5. The destination variables may be modified during the `convert` method, the procedure that performs the transformation denoted $T_{C,D}$ in chapter 3. This class can be extended by the user, permitting the implementation of custom-made transformations. Otherwise, the `Coupler` class applies the identity function to the output (source) variables and sets the value of the corresponding input (destination) variables.

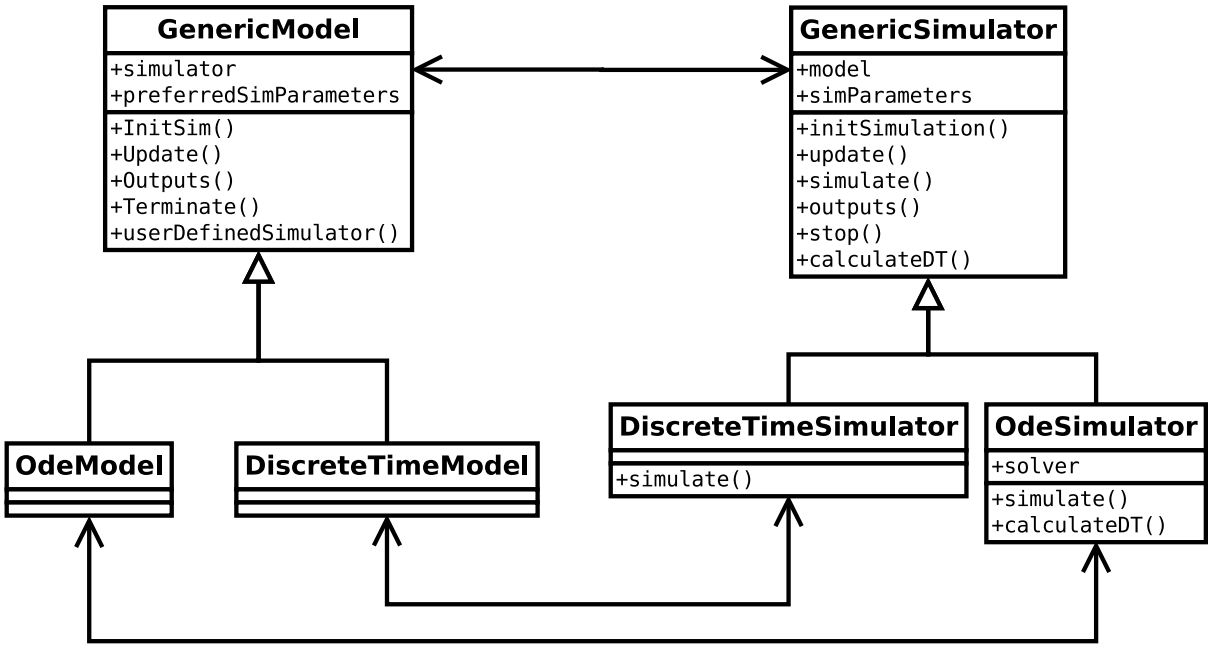

FIGURE 4.4– Object oriented representation of simulators in M2SL and their associated models.

M2SL also provides two example couplers: `IntegerCoupler`, which rounds a floating point value to an integer, and `MeanCoupler`, which calculates the arithmetic mean of the source variable.

4.1.2.4 The simulation loop

All the objects, procedures and relations defined by M2SL are brought together in the simulation loop. A simulation in M2SL is conducted by a root coordinator, represented by the `RootCoordinator` class. This crucial element defines and updates the global time of the simulation, while coordinating the underlying simulators and their local simulation time. It consists of three procedures executed in a sequential fashion: initialization, simulation loop and finalization (fig. 4.6, left side).

First, the initialization step prepares all models and simulators for the simulation, which includes the following activities:

1. creation of a simulator for each model, according to its formalism, and the configuration of each simulator according to its simulator parameters P_{sim},
2. association and linking of all simulators in a hierarchical structure that follows the model hierarchy, as illustrated before in fig. 4.2,
3. initialization of all simulators and models, which entails the `initSimulation` and `initSim` methods,
4. override of variable values, if the user has manually set values to some model variables,
5. initialization of the global time to its initial value, usually 0.

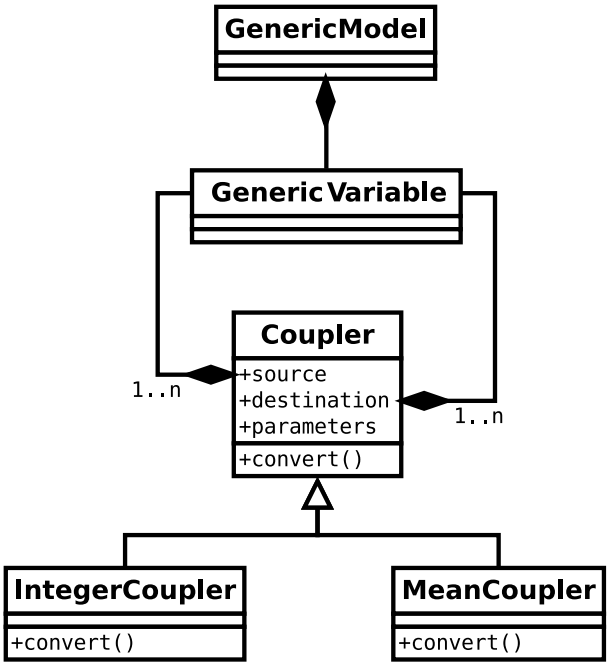

FIGURE 4.5– Object oriented representation of transformation objects in M2SL.

After the initialization step, the simulation loop repeats the following steps, illustrated in fig. 4.6 (right side):

1. Synchronization of models: at this point, all models have updated values for each of their output variables, calculated from the initialization phase or from a previous iteration of the simulation loop. This step performs the transformation of these output values to new input values, according to $T_{C,D}$. Once the input variables have been assigned with new values, all internal values of the model that depend on the inputs should be updated as well.
2. Simulation of models: it calculates the internal transitions of the model in order to advance the local simulation time of one or several time steps, depending on the temporal synchronization procedure. For instance, the adaptive strategies can iterate in this step several times until a target time is achieved, as shown in fig. 4.7.
3. Calculation of outputs: since the previous step modifies the state variables of the model to a new point in time, this step calculates new values of the output variables for all models.
4. Advance global time: this step increments the global simulation time according to the results of the current iteration. Depending on the temporal synchronization procedure, this step can be as simple as an addition, but it may calculate an optimal time step for the next iteration. The behavior of the simulation and the advance of global time phases are different according to the synchronization strategies described in chapter 3.
5. Stopping condition: at the end of each iteration, the target simulation time is evaluated to determine if the simulation should stop. Other elements may be taken into account as well, such as stopping conditions introduced by an external tool like the user interface.

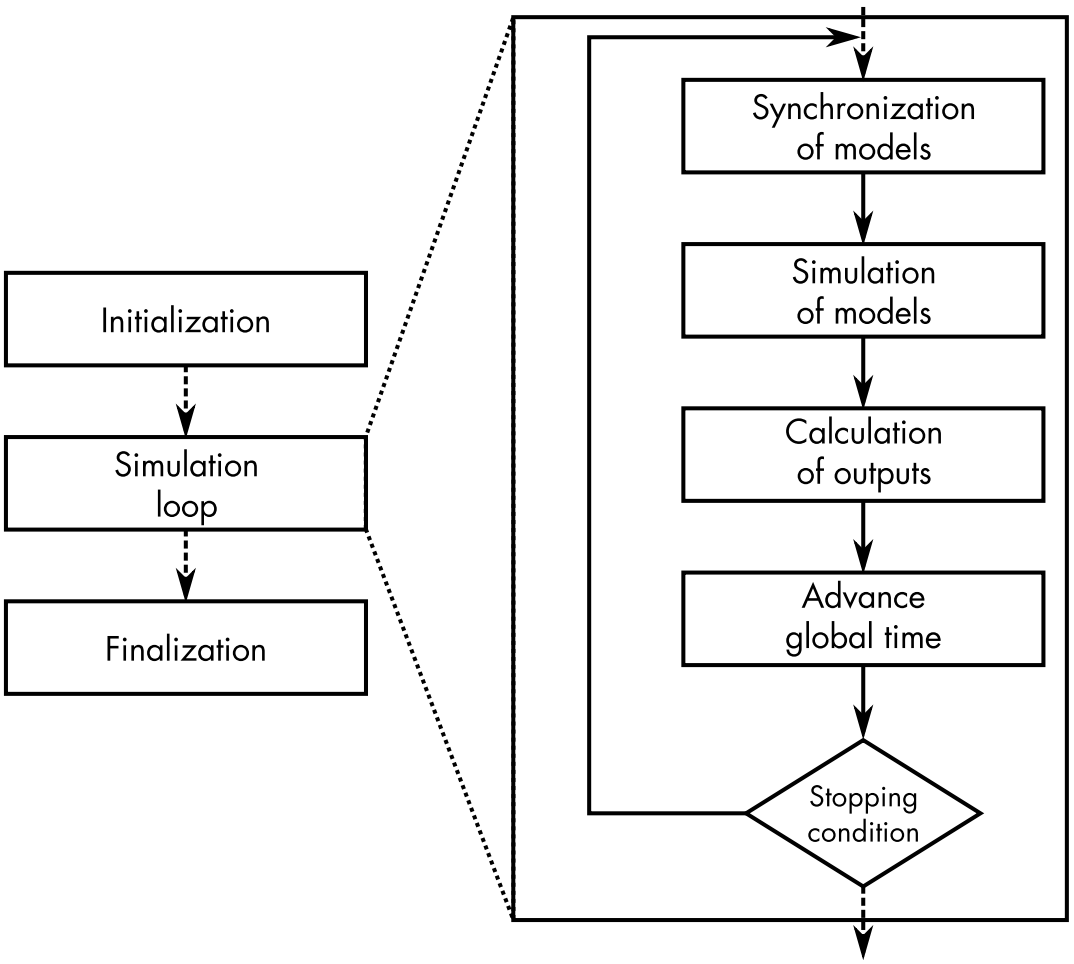

FIGURE 4.6– General execution flow of a simulation in M2SL (left) and its detailed simulation loop (right).

Lastly, when the simulation loop meets the stopping condition, the finalization step releases all resources acquired during the simulation.

4.1.2.5 Adaptive simulation and synchronization

Simulations in M2SL can follow different temporal strategies for the step-by-step advancement of models' dynamics, which affect the internal execution of the simulation loop, as illustrated in fig. 4.7. As explained in chapter 3, there are three possible simulation strategies:

Fixed step simulation (`FIXED`): the user defines a global simulation step `DT` (δt). All simulators advance the state of a model using a single step of the same size. At the end of each simulation step, the synchronization of input and output variables is performed.

Adaptive step with smallest synchronization step (`ADAPT_SMALLEST`): initially, each simulator S_i has an independent simulation step δt_i and the user specifies an initial synchronization step `couplingDT` (δt_c). Each simulator advances with an adaptive step until they all reach δt_c, where the input and output synchronization occurs. At this point, the error

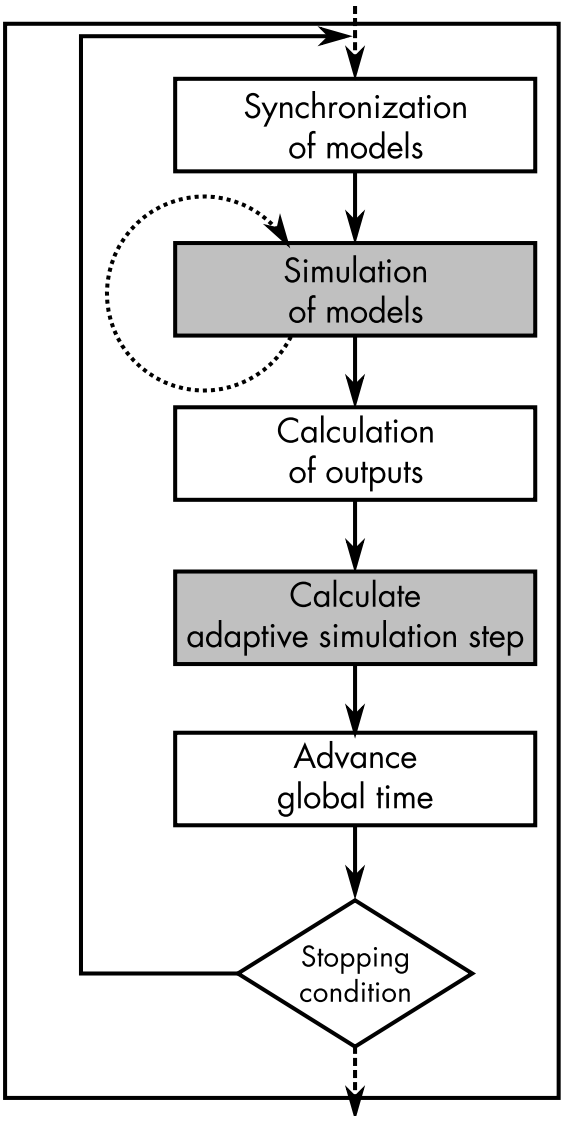

FIGURE 4.7– Simulation loop with adaptive simulation steps. Gray boxes denote the steps that are different from the general simulation loop in fig. 4.6.

of each model is calculated and each simulator determines the minimum simulation step needed to meet the acceptable error ranges (cf. section 4.1.2.2.2). The minimum step throughout all simulators is selected as the next δt_c.

Adaptive step with fixed synchronization step (`ADAPT_FIXED`): each simulator advances with an adaptive δt_i and the synchronization step δt_c is fixed by the user.

4.1.2.6 Additional tools

In addition to the data structures and simulation algorithms provided by the library, M2SL includes a set of tools for parameter analysis, user interface, and an application programming interface (API) that permit the interaction of the models and simulations with external tools. A diagram of the current existing tools and connections is shown in fig. 4.8.

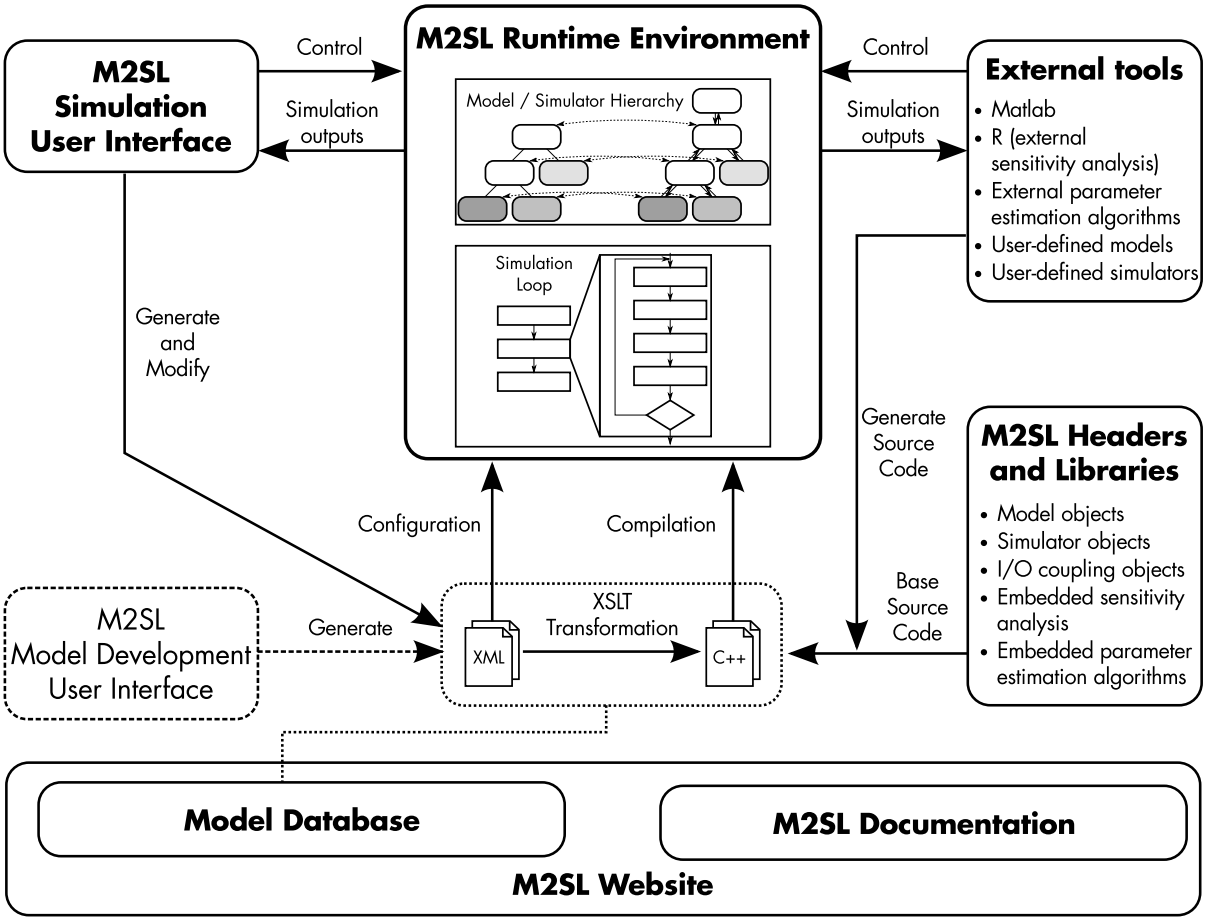

FIGURE 4.8– Diagram of all the components and relations of the tools provided by M2SL.

4.1.2.6.1 Sensitivity analysis tools

Due to the importance of parameter analysis for the multi-resolution approach described in chapter 3, and considering the constant application of sensitivity analyses during the applications presented in chapters 5 to 7, a sensitivity analysis method is implemented in M2SL: the Morris elementary effects method (MORRIS, 1991). All details regarding the elementary effects method are presented in section 4.2.3.

4.1.2.6.2 Parameter identification tools

Parameter identification is also an important part of any modeling and simulation application, as emphasized during chapter 2. M2SL includes a simple optimization method, the Nelder-Mead algorithm (NELDER et al., 1965), adapted for the parameter identification of models. The details of this method are presented later in section 4.3.1.

Furthermore, M2SL can also handle the execution of several concurrent simulations from a list of parameter values, an useful feature for the application of parameter identification algorithms that require the evaluation of several simulations. This feature was designed to ease the implementation of the evolutionary algorithms presented in section 4.3.4.

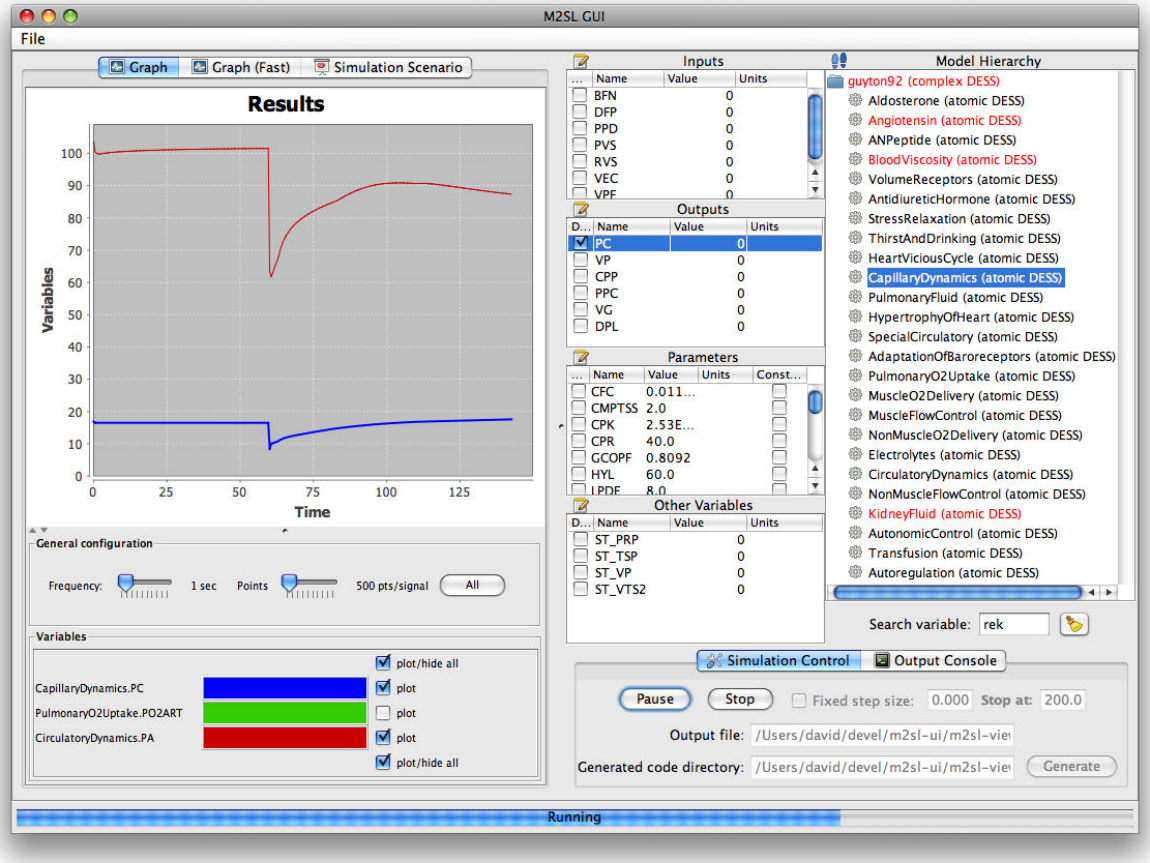

FIGURE 4.9– Screenshot of the simulation graphical user interface. The left part shows the visualization of two model variables. The center panels list all the inputs, outputs, states and parameters of a model. The right panel shows the model hierarchy. The bottom right panel is the simulation control panel.

4.1.2.6.3 User interface

As many modeling and simulation toolkits, M2SL provides an user-interface that permits the control and observation of a simulation, illustrated in fig. 4.9. This basic application implemented in Java provides the following features:

1. Description of models: the interface provides panels that shows the model hierarchy, and four panels that names and values of all input, output, parameters and state variables for each model.
2. Simulation control: an user can start, pause or stop a simulation. He may also control the simulation steps or choose the temporal synchronization strategy.
3. Real time variable plotting: the interface shows a panel with the trajectory of any variable chosen by the user. The trajectory is updated as fast as the simulation advances.
4. Real time parameter modification: during a simulation, it is possible to change the value of a parameter. The interface interacts with M2SL to apply this change and the effect on the variables can be observed in the variable plot.

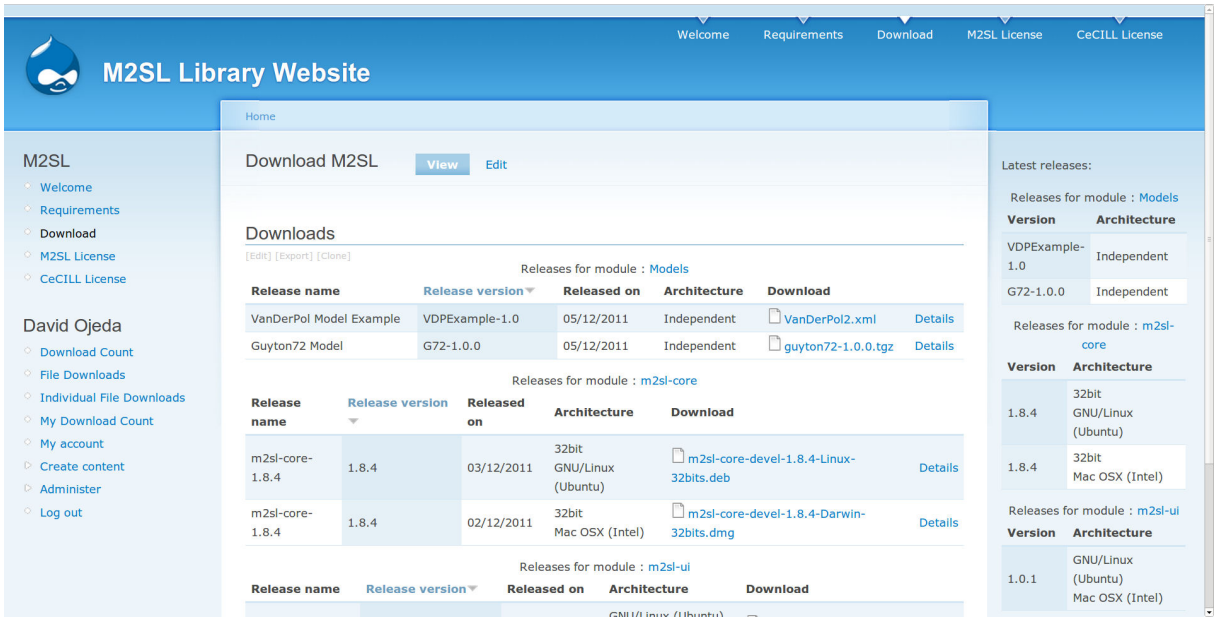

FIGURE 4.10– Screenshot of the M2SL website.

4.1.2.6.4 M2SL website

As M2SL was used during the cooperation with colleagues from different research centers, it became evident the need for an organized distribution system for the continuous development of M2SL and its related tools. A collaborative website was designed with the following objectives:

- Publish information and updated download links about the M2SL library and its associated tools,
- Inform and enforce the licenses for the use of M2SL,
- Provide a centralized location for the user and developer documentation of M2SL,
- Help the modeling community with a site for the interchange and publication of models as C++ source files based on the M2SL API.

During this thesis, a website based on Drupal [21], a content management framework, was developed and customized to meet these objectives. This website has been published at `http://www.ltsi.univ-rennes1.fr/m2sl`.

4.2 Sensitivity Analysis

As underlined in chapter 2, model parameters represent an element of the real system, or rather, a simplification of such element. These parameters can sometimes be measured directly from the system, estimated from the observable data, or even guessed from prior knowledge. In any case, it is highly likely that the parameter value contains an intrinsic error or a level of uncertainty. Then, some questions arise regarding these parameters: What is the effect of this incertitude on the model outputs? Is it possible to measure quantitatively or qualitatively the

21. `http://drupal.org`

effect of changes in parameter values on the outputs? The field of sensitivity analysis, along with the highly related area of uncertainty analysis, provides a set of tools that can answer this questions.

There are many definitions to sensitivity analysis, mainly because it is a technique that has been used by different technical communities and because there are various known approaches. SALTELLI et al. are probably the most influential authors in sensitivity analysis and uncertainty analysis, whose extensive works present, formalize and classify most major sensitivity analysis topics and methods (SALTELLI et al., 2000, 2008). In (SALTELLI et al., 2008) sensitivity analysis is defined as:

> The study of how the uncertainty in the output of a model (numerical or otherwise) can be apportioned to different sources of uncertainty in the model input.

However, in the context the modeling applications presented in this manuscript, it is more appropriate to define sensitivity analysis as the measurement of the effect of changes in input values and model parameters on the outputs of a system.

Sensitivity analysis can provide important information for modeling and simulation applications. The objectives include:

- Factor prioritization: it can determine which inputs or parameters are more important, which can help guide the parameter estimation or motivate further attention in the observation of certain inputs.
- Model simplification: it can identify which elements of the model have little effect and can be replaced with a simpler definition.
- Parameter regions identification: it can pinpoint critical or interesting ranges in the parameter or input spaces.
- Parameter interaction: not only it can measure the effect of changes of one parameter, it can also measure the effect of the interaction of parameters, i.e. the outcome of changes in two or more parameters.

Even though it has been identified as a best practice for modeling guidelines (EPA, 2009), sensitivity analysis methods are not defined around the concepts of modeling and simulation; they are defined for the study of a function $y = f(X)$, where y denotes a single output, and $X = [X_1, X_2, \ldots, X_k]$ is a vector of k inputs or parameters. This notation can be easily translated to modeling notation, as it will be explained in section 4.2.4.

The approach followed by most sensitivity analysis methods is summarized in fig. 4.11. It consists in:

1. The definition of the distribution for each source of uncertainty each input or parameter X_i, or the definition of the relevant parameter space $\mathbb{P}$. For simplicity it will be assumed that there are k parameters denoted $[X_1, X_2, \ldots, X_k]$.

2. The creation of an *experimental design*, which will be denoted D, consisting of n sets of

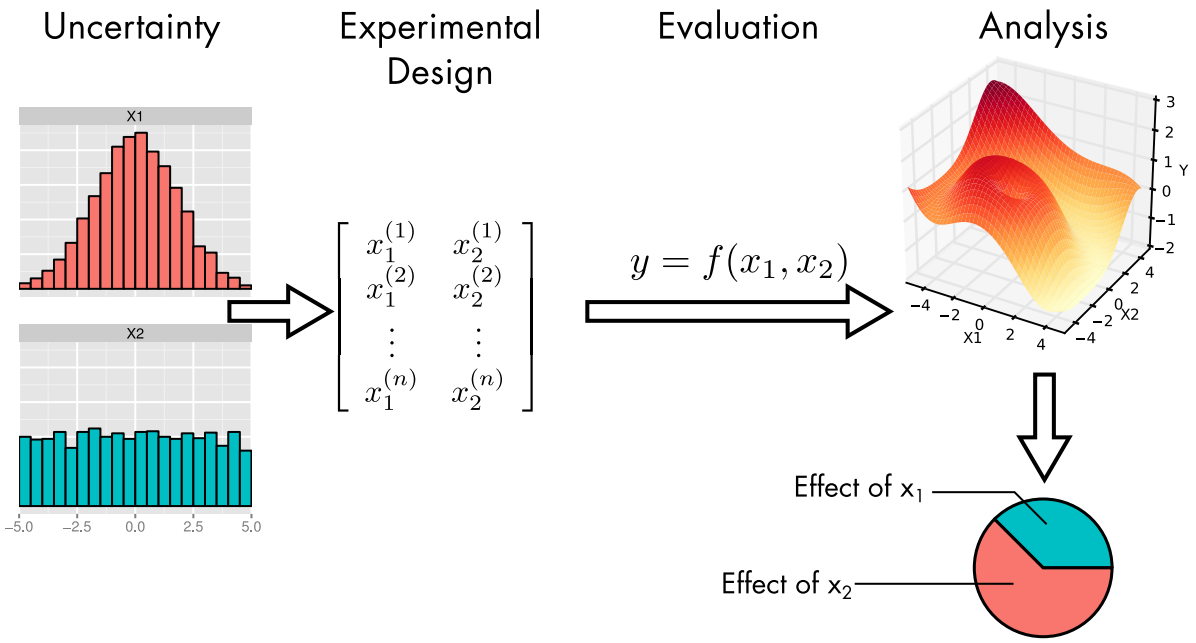

FIGURE 4.11– Simplified diagram of the process of uncertainty and sensitivity analysis, based on (EPA, 2009).

input values [22]:

$$D = \begin{bmatrix} x_1^{(1)} & x_2^{(1)} & \dots & x_k^{(1)} \\ x_1^{(2)} & x_2^{(2)} & \dots & x_k^{(2)} \\ \vdots & \vdots & \ddots & \vdots \\ x_1^{(n)} & x_2^{(n)} & \dots & x_k^{(n)} \end{bmatrix}, \tag{4.8}$$

where a row represents the values for each parameter.

3. The evaluation of each row of the experimental design D, which yields a vector of outputs

$$Y = \left[y^{(1)}, y^{(2)}, \dots, y^{(n)}\right]^T . \tag{4.9}$$

4. The analysis of the outputs Y, identifying and associating the source of the variations in the outputs, with respect to the variations in the parameters.

The variety of the existing methods in sensitivity analysis lies on the diverse schemes to produce an experimental design and to analyze the variability of the evaluated outputs. However, the choice of the sensitivity analysis depends on several factors, such as the assumptions on the parameters of $f(X)$ (linearity, independence or interaction) and the available computational resources for the evaluation of this function. Existing methods can be divided into three groups: local sensitivity methods, global sensitivity methods and screening methods. This categorization is not strict, considering that some methods can be considered as part of more than one of these groups.

22. Normally, this matrix is denoted M. Here, we changed this change of notation in order to avoid confusion with the notation of models M.

4.2.1 Local sensitivity analysis

Local methods represent the most simple form of sensitivity analysis. The term *local* emphasizes the fact that the sensitivity of the parameters are studied in a small region of the parameter space $\mathbb{P}$. A natural approach consists in the selection of a working point $X^{(0)} = [x_0^{(0)}, x_1^{(0)}, \ldots, x_k^{(0)}]$, followed by the evaluation of the function $f(X^{(0)})$ and at other points close to $X^{(0)}$. When the variations are introduced only in one parameter X_i at a time, the approach is termed a one-at-time (OAT) analysis. For example, a typical OAT experimental design for X_i would be:

$$D_i = \begin{bmatrix} x_0^{(0)} & \ldots & x_i^{(0)} & \ldots & x_k^{(0)} \\ x_0^{(0)} & \ldots & x_i^{(0)} + \delta & \ldots & x_k^{(0)} \\ x_0^{(0)} & \ldots & x_i^{(0)} + 2\delta & \ldots & x_k^{(0)} \\ \vdots & & \vdots & & \vdots \\ x_0^{(0)} & \ldots & x_i^{(0)} + (n-1)\delta & \ldots & x_k^{(0)} \end{bmatrix}, \tag{4.10}$$

where δ is a predefined perturbation of parameter X_i. In this example, only the variations in $[x_i^0, x_i^0 + (n-1)\delta]$ are explored, but this range can be defined as evenly spaced variations from the minimum and maximum values of parameter X_i, or as an arbitrary variation of δ.

Once Y is obtained from the evaluation of matrix D_i (cf. eq. (4.10)), the results can be analyzed in several ways. On one hand, the partial derivatives $\partial Y/\partial X_i$ can be estimated or averaged, which can be normalized and compared to the partial derivatives of other parameters $\partial Y/\partial X_j$. On the other hand, the results of the evaluation can be plotted with respect to the different values of the varying parameter, as shown in fig. 4.12. In this case, the effect of the parameter variation can be identified visually, or directly quantified using a linear regression and its coefficient of determination R^2.

Local sensitivity analyses are practical for their simplicity and reduced number of evaluations. However, as their name imply, the parameter space is not fully explored, since it does not consider simultaneous variations of parameters. Consequently, local OAT approaches cannot detect interactions between parameters. Moreover, the linear regression analysis mentioned above supposes a linearity of the relation between the parameters and the outputs, which will fail to identify nonlinear relationships as illustrated in fig. 4.12.

4.2.2 Global sensitivity analysis

In contrast with local methods, global sensitivity analysis focuses on the study of the effect of the parameters but it does not constrain their values to the small region around a working point. Instead, it permits the parameters to take any value in a large region of interest. A simple approach consists in the evaluation of the output value at random points, or at points defined from existing experimental data, and observe the trend in a scatterplot of parameters versus an output, as shown in fig. 4.13. This visual analysis can be quantified with a linear regression of these data, or with the calculation of the mean and variance of the outputs. However, these simple methods do not account for the joint effect of several parameters.

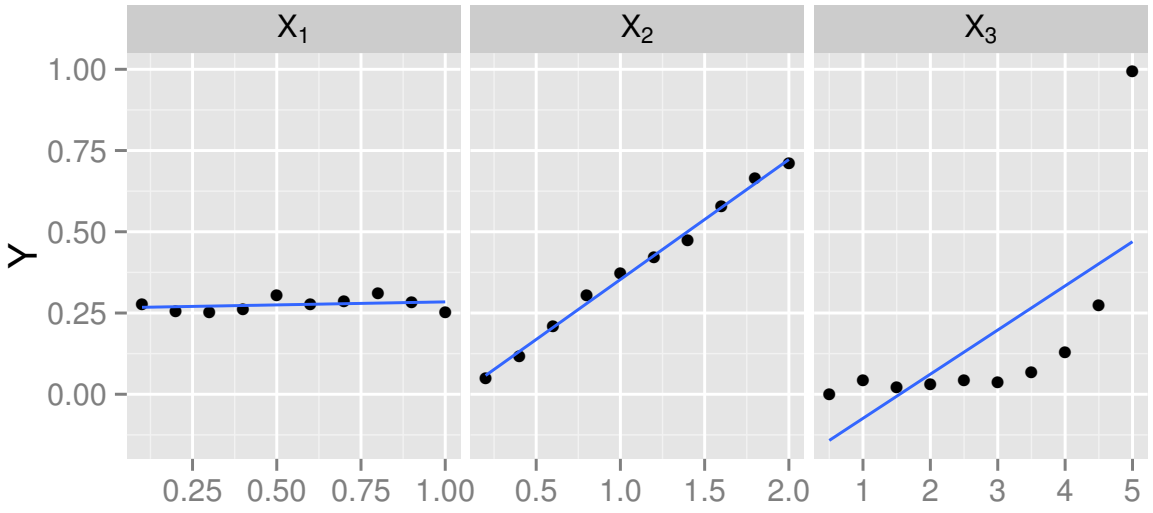

FIGURE 4.12– An example of one-at-time sensitivity analysis for three parameters X_1, X_2 and X_3 over an output $Y = f(X)$. The right plot shows little effect of X_1 over the output, the middle plot shows a linear effect of X_2, and the right plot shows a non-linear effect of X_3.

The most popular family of global sensitivity analysis methods is the variance-based approach. This approach tries to identify what part of the variability of Y can be attributed to the variability of each parameter X_i (or groups of parameters). Its starting point is the following question: Does Y vary more or less when one fixes one (or many) of its parameters? A detailed explanation of how this question is mathematically addressed is presented in (SALTELLI et al., 2008; SOBOL, 1993, 2001). Briefly, SOBOL introduced the notion of *first-order effect* as:

$$S_i = \frac{\mathrm{Var}[\mathbb{E}[Y|X_i]]}{\mathrm{Var}[Y]}\,, \tag{4.11}$$

which defines the effect of the variation of X_i over the output Y. A *second-order effect* measures the effect of variations of two parameters X_i and X_j:

$$S_{ij} = \frac{\mathrm{Var}[\mathbb{E}[Y|X_i, X_j]] - \mathrm{Var}[\mathbb{E}[Y|X_i]] - \mathrm{Var}[\mathbb{E}[Y|X_j]]}{\mathrm{Var}[Y]}, \qquad \forall i \neq j\,. \tag{4.12}$$

The definition of higher-order effects is possible, but the number of parameter combinations increases quickly. Nevertheless, it is important to note that, due to variance decomposition, all effects are strictly positive and the sum of all effects is equal to one:

$$\sum_i S_i + \sum_i \sum_{i<j} S_{ij} + \sum_i \sum_{i<j} \sum_{j<l} S_{ijl} + \ldots S_{123\ldots k} = 1\,, \tag{4.13}$$

which effectively quantifies each effect to a value in $[0, 1]$.

Considering the great number of possible combinations introduced by higher-order effects, SALTELLI et al. introduced a simpler approach, where only the first-order indices are calculated

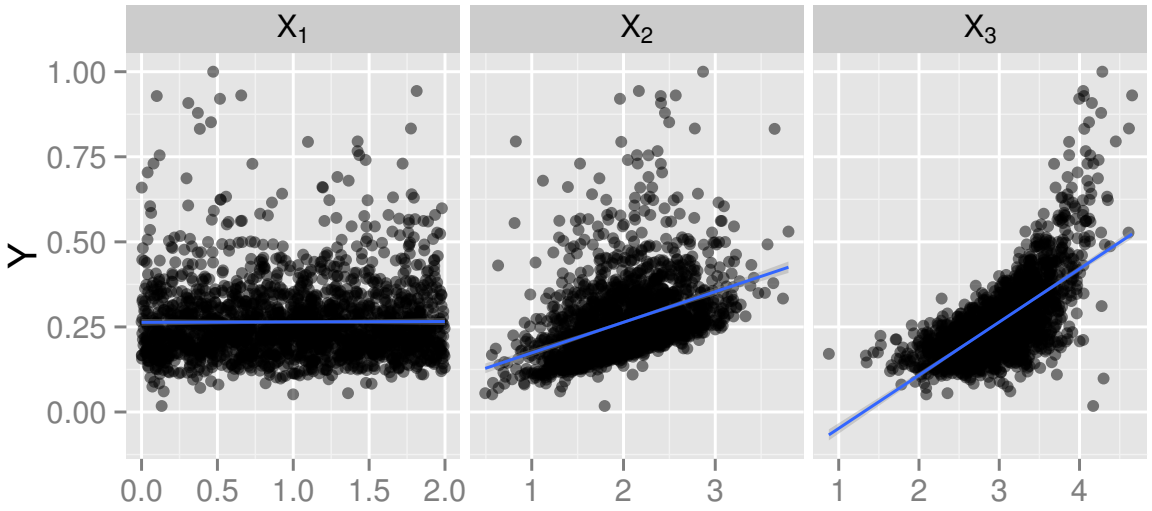

FIGURE 4.13– An example of a scatterplot analysis to evaluate the effect of three parameters X_1, X_2 and X_3 over an output $Y = f(X)$. The corresponding linear regression is shown in blue. The left plot (X_1) does not show any effect, the middle plot (X_2) shows a linear effect, and the right plot (X_3) shows a variability that may be due to interactions or non-linearities.

with eq. (4.11), while all higher-order effects are grouped in the *total-order effect*:

$$S_{Ti} = S_i + \sum_{i \neq j} S_{ij} + \sum_{i \neq j \neq l} S_{ijl} + \cdots + S_{123\ldots k} \,. \tag{4.14}$$

With Sobol's first-order and total-order effects, one can respectively identify and quantify the amount of variability that can be attributed to a sole parameter (S_i) and to the interaction of such parameter with the other parameters (S_{Ti}).

Although highly descriptive, the first- and total-order effects are difficult and computationally expensive to calculate, namely because the conditional variances of continuous variables are defined by multidimensional integrals. Two main approaches tackle this problem: *i)* the design of estimators for the sensitivity indices based on Monte Carlo solutions to eqs. (4.11) and (4.14) (SALTELLI et al., 2010), or *ii)* the Fourier Amplitude Sensitivity Test (FAST) which explores the parameter space $\mathbb{P}$ in a particular fashion that associates frequencies to each parameter (CUKIER et al., 1978). In both cases, the amount of evaluations, or model simulations, necessary to calculate the sensitivity indices is very high, which limits the application of global sensitivity analysis to models where the number of parameter is reduced and when one counts with a significant computational budget. This is the main reason that drives another type of global sensitivity analysis that permits to cheaply identify and exclude unimportant parameters: screening methods.

4.2.3 Screening methods

In contrast to previous global sensitivity methods, screening methods do not quantify the sensitivity of a parameter, in the sense of Sobol. Instead, they permit to identify qualitatively which parameters of a function are relatively influent on the function's output and which parameters can be ignored. This information can help reduce the dimensionality of future analysis or estimation phases. The most common screening method is the Morris elementary effects method (Morris, 1991).

Morris' method explores a subspace of the parameter space $\Omega \in \mathbb{P}$: a k-dimensional unit cube regularly divided as a grid of p levels [23]. In this space, it calculates an *elementary effect*, defined as:

$$EE_i = \frac{f(x_1, \ldots, x_i, \ldots, x_k) - f(x_1, \ldots, x_i + \Delta, \ldots, x_k)}{\Delta}, \tag{4.15}$$

where Δ is a predefined multiple of $1/k-1$, and $(x_1, x_2, \ldots, x_k)$ is a randomly selected point, such that each x_i takes a value in $\{0, 1/(k-1), 2/(k-1), \ldots, 1-\Delta\}$. The method starts with the calculation of r different elementary effects for all parameters, calculated with a clever experimental plan that uses $r(k-1)$ simulations (Morris, 1991). For each parameter X_i, the mean and standard deviation $(\mu_i \pm \sigma_i)$ of the elementary effects are computed and these two values are then studied in the μ vs. σ plane. In order to avoid the mutual cancellation of symmetrical elementary effects, more recent works (Campolongo et al., 2004) enhanced the method of Morris by using the mean over the absolute value of eq. (4.15), denoted μ_i^*.

The analysis of the elementary effects results in the μ^* vs. σ plane, illustrated in fig. 4.14, derives the following information:

- Parameters with low μ_i^* and σ_i can be considered as negligible parameters; a perturbation of this parameter does not cause a significant effect on the output.
- Parameters with large μ_i^* but low σ_i reveal a linear effect of parameter X_i over the output; a perturbation of this parameter cause a constant, non negligible effect over the output.
- Parameter with large μ_i^* and large σ_i can be caused by a nonlinear effect of parameter X_i or by an important interaction with other parameters; a perturbation of this parameter causes a non negligible effect, but this effect varies for different X_i.

The Morris elementary method is an advantageous tool to examine and identify important parameters of a function or model. Due to its relative low computational requirements, it can be used prior to any heavy sensitivity analysis or extensive parameter exploration such as during a parameter estimation method. This method can quickly point out linear relations between parameters and outputs. On the other hand, the elementary effect method presents two specific disadvantages: it does not quantify the effect of a parameter, and it cannot discern between nonlinear relations and parameter interactions. For this kind of analysis, one must turn to global sensitivity analysis using Sobol indices, as presented previously in section 4.2.2.

23. The original definition is constrained to a unit cube for simplicity, but it can be easily transformed to any uniform range.

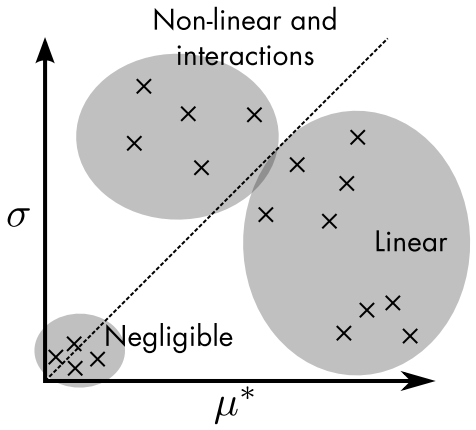

FIGURE 4.14– Example of the results of the Morris elementary effects method. The elementary effects of all parameters are analyzed in the $\mu^* - \sigma$ plane, identifying negligible effects, parameters with a linear effects and parameters that have a non-linear or interaction-related effect.

4.2.4 Proposed approach

For the modeling framework and the clinical applications presented in this manuscript, sensitivity analyses played an important role for the understanding of the underlying mechanisms of the modeled systems. The utilization of any sensitivity analysis for our modeling applications is straightforward: the function $y = f(X)$ used in the formalization of all sensitivity analyses can be easily adapted, according to our previous definition of a simulator output, $y = S^h(M^h, P_S, F)$, where S^h is the simulation process applied to a model $M^h\,(F, \mathbf{I}, \mathbf{O}, \mathbf{E}, \mathbf{P})$, using model parameter values $\mathbf{P}$ and inputs $\mathbf{I}$, as denoted in definitions 2.1 and 2.3, and y is an output of the model. Our problem becomes, thus, to analyze how the variations on y can be apportioned to changes in $\mathbf{P}$ and $\mathbf{I}$, which are particularly difficult to define and measure on real physiological applications.

In chapter 3, the importance of sensitivity analysis was emphasized since they help identify the most important variables that need to be considered for a successful multi-formalism and multi-scale integration. For this identification, the screening method of Morris was favored for its useful compromise between parameter space exploration and computational requirements. Moreover, in order to complement the qualitative identification of the nature of the parameter effects provided by Morris' method, the following sensitivity index was used:

$$S_{Mi} = \sqrt{(\mu_i^*)^2 + (\sigma_i)^2}\,, \tag{4.16}$$

applied to all parameters X_i. Then, parameters are sorted according to their S_{Mi}, as illustrated in fig. 4.15. This index, which has been used in other modeling applications (DUARTE et al., 2003; SCHREIDER et al., 2011) provides a rank of the parameter effects; parameters with a high sensitivity or strong interactions will have a high S_{Mi}, while unimportant ones are associated with a low S_{Mi}.

Since the employment of the Morris elementary effects method was ubiquitous in the applications of this thesis, it was directly implemented and embedded in M2SL. The class `sa::Morris`

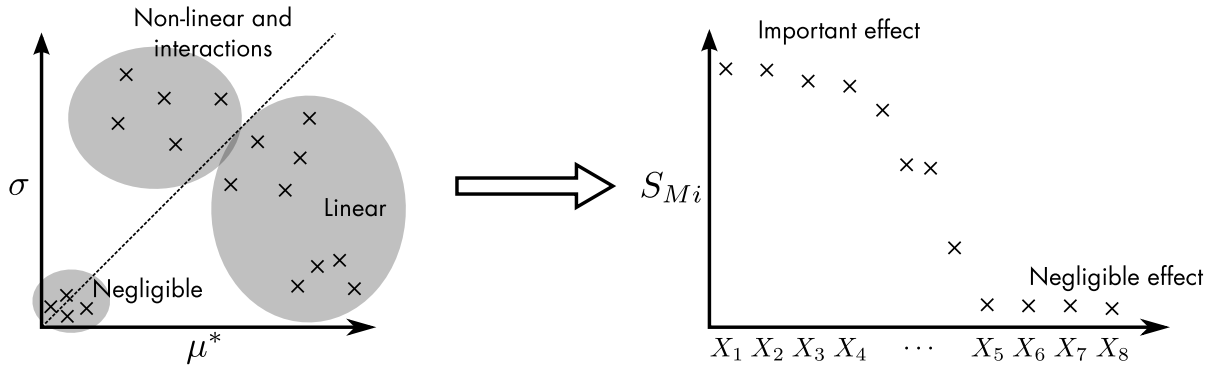

FIGURE 4.15– Identification of important and negligible parameters from the elementary effects. The right plot shows the same results of a Morris analysis, but ranked according to the S_{Mi} index (cf. eq. (4.16)).

contains this implementation, and it provides an simple API to define the necessary information for the application of the method, which are: *i)* the definition of which model parameters will be analyzed, including their respective value ranges, and *ii)* the definition of the parameters of Morris' method: the number of levels p, the value of the default perturbation Δ, and the number of repetitions r.

All other sensitivity analysis methods, in particular for chapter 7, were used as an external tool of M2SL (cf. fig. 4.8), using the `sensitivity` package of the statistical framework R [24].

4.3 Parameter identification

As explained in chapter 2, the parameter estimation of a model can be considered as an optimization problem, where the objective is to find the parameter values P_{opt} that minimizes an error function g_ϵ between the experimental and the simulated data:

$$\begin{aligned} \mathbf{P}_{\text{opt}} = & \underset{\mathbf{P}\in\mathbb{P}}{\operatorname{argmin}}\ g_\epsilon(O_{\text{sim}}(\mathbf{P}), O_{\text{obs}}) \\ & \text{subject to } h(O_{\text{sim}}(\mathbf{P}))\,, \end{aligned} \tag{4.17}$$

where $O_{\text{sim}}(\mathbf{P}) = S^h(M^h, P_S, F)$, with $M^h\,(F, \mathbf{I}, \mathbf{O}, \mathbf{E}, \mathbf{P})$.

The field of mathematical optimization offers a vast choice of methods and algorithms that solve this kind of problems: analytic approaches, iterative methods, gradient-based methods, deterministic and stochastic approaches, among others (NEMHAUSER et al., 1989). However, not all of these methods are appropriate for the problem of parameter identification because *i)* for the clinical applications of this manuscript, the dimensionality of the problem is high enough to forbid the employment of methods whose computational complexity is exponential with respect to the number of parameters, *ii)* the nature of the underlying equations are either non-linear or not well understood, and *iii)* the objective functions and constraints are the result of complex model equations which complicate the calculation of their derivatives or partial derivatives. These

24. `http://www.r-project.org`

limitations quickly discard classical optimization methods, such as Newton's method, or Lagrange multipliers; linear programming approaches, such as the simplex algorithm (DANTZIG, 1998); and exhaustive exploration approaches, such as branch-and-bound methods (LAND et al., 1960). The remaining methods include approaches that approximate numerically the derivatives of the objective function, methods that use an heuristic to select interesting points in the parameter space, and methods based on a stochastic process.

4.3.1 Deterministic approaches

In this categorization of optimization techniques, deterministic approaches are defined to provide a contrast to stochastic approaches: these methods find the optimal or a sub-optimal solution to eq. (2.1) with a process that does not rely on a random behavior. Algorithms that calculate or approximate derivatives and gradients fall into this category. Among them, a popular method is the gradient descent method; an iterative process that starts from an initial point x_0 and then repeatedly moves the point with the following rule:

$$x_{k+1} = x_k - \lambda \nabla g_\epsilon \,, \tag{4.18}$$

where ∇g_ϵ is the (approximated) gradient of the objective function with respect to its parameters, and λ is a configurable step size, which is usually defined as a small value.

An example of a deterministic approach that does not need the calculation of gradients is the popular hill-climbing algorithm (MINSKY, 1961). This algorithm only requires the definition of a neighborhood function to obtain a list of interesting points around a sub-optimal solution, and then moves to the neighbor that provides the best improvement. Although very simple, hill-climbing depends on the quality of its neighborhood function and the initial point. In many cases, this algorithm finds a local minimum and stays stuck in this point.

Another widely popular technique is the Nelder-Mead algorithm (NELDER et al., 1965); a method that maintains a set of multidimensional simplex [25], whose vertices represent a possible solution to the minimization function. This list of solutions is iteratively modified, moving the point that represents the worst solution using different heuristics, illustrated in fig. 4.16. The predefined contraction and expansion heuristics of the Nelder-Mead algorithm can avoid some cases of local minima, but convergence to a global minimum is not guaranteed. However, this method remains extremely practical because it does not introduce any assumptions on the parameter space and it does not necessitate the definition of derivatives or neighborhood functions.

In general, deterministic methods are interesting because they eventually converge to a solution and do not need much information regarding the objective functions. However, the main disadvantages of these methods are *i)* the gradient estimations and the heuristics used require several evaluations of the objective function, which becomes problematic when the dimensionality of the parameter space is considerable, and *ii)* the convergence of these methods is not guaranteed:

25. Here, the term `simplex` refers to a n-dimensional polytope.

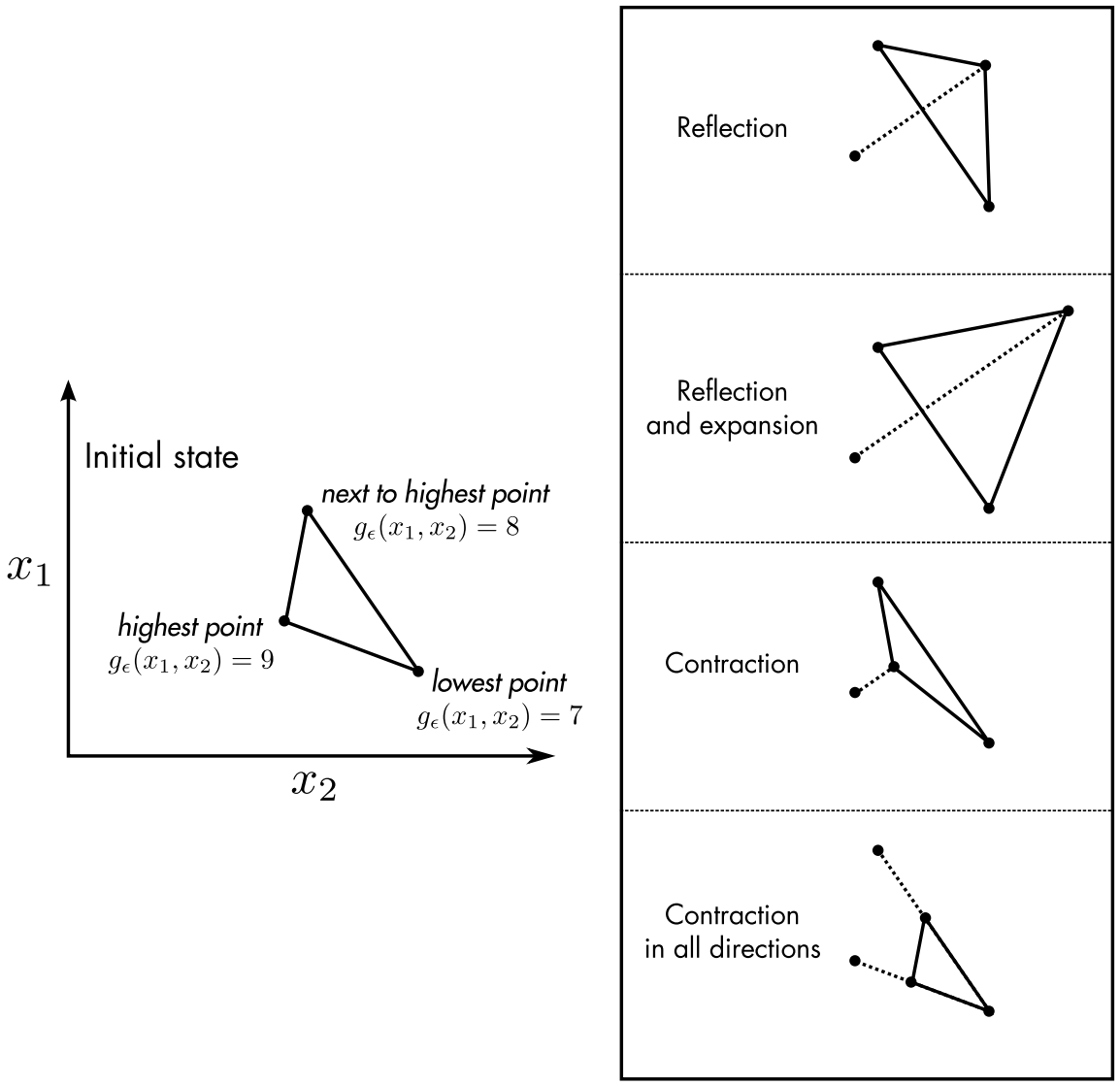

FIGURE 4.16– Example of the different strategies adopted on the Nelder-Mead algorithm, for a minimization problem on two parameters x_1 and x_2.

it depends on the initial point, which yields a convergence towards a local minimum, where the algorithm remains stuck. The former point, unfortunately, cannot be avoided. On the other hand, the latter can be alleviated by restarting the algorithms with different initial conditions, by introducing of stochastic perturbations, or by maintaining a list of visited solutions which are to be avoided in order to find new solutions (this last approach is the base of tabu search, GLOVER, 1986).

4.3.2 Stochastic approaches

Stochastic search approaches are interesting when the parameter space and objective function are not well understood, or when the parameter exploration requires random perturbations in order to avoid local minima. For example, since the hill-climbing algorithm can get "stuck" on a

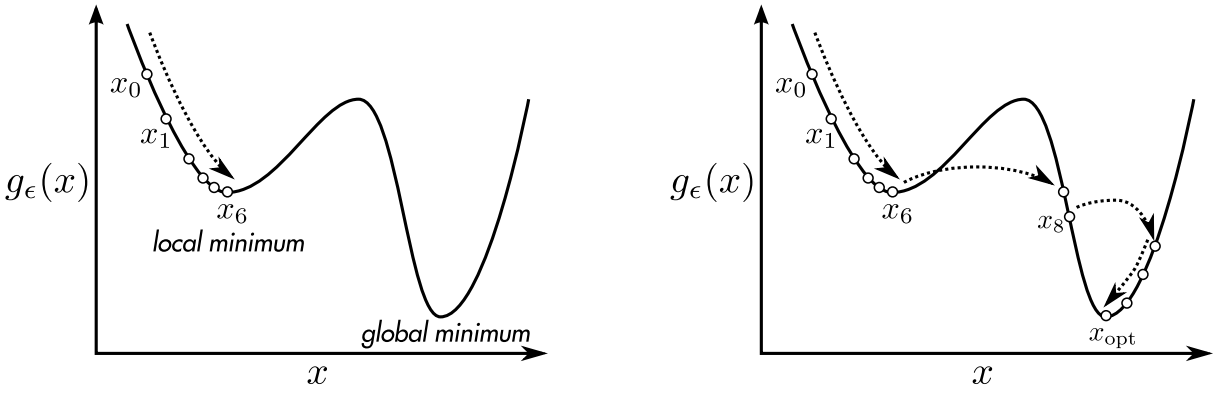

(a) Hill-climbing

(b) Simulated annealing

FIGURE 4.17– Illustrative example of hill-climbing and simulated annealing minimization on a single parameter objective function. Using the same starting point x_0, hill-climbing finds a local minimum, while simulated annealing shows random "jumps" and finds the optimal solution x_{opt}.

local minimum, the introduction of random "jumps" can move the current solution out of the region and into a more interesting space, as shown in fig. 4.17. This technique is also known as *simulated annealing* (KIRKPATRICK, 1984).

A notable and popular stochastic approach is the particle swarm optimization (EBERHART et al., 1995): an iterative procedure where a list of solutions is maintained and each candidate solution *wanders* the parameter space with a behavior that mixes exploration and attraction to good solutions. The converge of approaches that constantly evolve a list of candidate solutions is not guaranteed either; it mostly depends on a good choice of the algorithm parameters, principally the size of the candidate solution list and the number of iterations. However, stochastic approaches are praised for their ability to constantly explore the parameter space and avoid local minima.

4.3.2.1 Evolutionary algorithms

Within the stochastic approaches, evolutionary algorithms stand out for their original foundations. Evolutionary algorithms (EA) follow the approach of maintaining a set of candidate solutions, termed *population*, and repeatedly evolving this population with processes inspired by biological evolution: selection of the fittest, reproduction, recombination and mutation. Among the wide range of algorithms classified as EA, the most popular group used in optimization is the genetic algoritms (GA), initially conceived in (HOLLAND, 1975) and thoroughly formalized in (GOLDBERG, 1989). In this kind of algorithms, the following notation is used: a candidate solution is called an *individual*. An individual represents a solution by encoding it in the form of genetic information, or *alleles*. For example, in the case of parameter estimation, each allele can be a binary representation of the value of a parameter. The population evolves as a result of the following procedure, illustrated in fig. 4.18:

1. An initial population with N individuals is initialized, where each individual contains a random value for each one of its alleles. This generates a first generation of possible

solutions.

2. Each individual of the population is assigned with a value that measures its *fitness*, a quantification of how good the individual is. The fitness value of an individual directly affects its chances to survive and reproduce. The calculation of the fitness requires the evaluation of the target function g_ϵ, but it can also be affected by other variables.
3. An internal variable that counts the number of generation is incremented. This variable can be useful for the stopping criteria.
4. According to their fitness and a stochastic process, a selection of individuals is performed. This phase designates pairs of individuals that will reproduce.
5. For each pair of selected individuals a reproduction operation generates two new individuals whose alleles are a combination of the two progenitors. This reproductive process occurs with a predefined probability p_c for each pair of individuals. Newly generated individuals may go through a mutation process, with another predefined probability p_m, which slightly modifies one or more of its alleles. The probabilities p_c and p_m directly control the exploration of new solutions. At the end of this stage, $2N$ individuals exist: the parent population of size N and a new offspring population of the same size.
6. All new generated individuals are evaluated; their fitness is determined as well.
7. At this point, different strategies are possible: either the new population completely replaces the old population, or a replacement procedure that accounts for each individual fitness selects and discards all individuals to produce the next generation, a population of size N.
8. Finally, if a stopping criteria is met, the algorithm stops or, in the contrary, the algorithm restarts from step 3. Possible stopping criteria include a maximum number of generations (i.e. iterations) or when the individuals of the population have reached a certain fitness value.

As other stochastic approaches, EAs cannot assure convergence toward the optimal solution and their performance depend on a good choice of the EA parameters, Nevertheless, they present an interesting compromise of space exploration, number of evaluations and quality of the solutions found, and they has been successfully used for parameter identification in other applications (Fleureau, 2008).

4.3.3 Multiobjective optimization

Until this point, the discussion of parameter estimation as optimization problem has been based on the minimization of a single function g_ϵ; a single-objective optimization. However, in the clinical applications presented in this work, we found that the parameter estimation should take into account not one, but several objective functions. The family of algorithms designed for the collective minimization of two or more target functions is called multi-objective optimization methods. Formally, they solve the problem:

$$\begin{aligned} &\underset{P\in\mathbb{P}}{\operatorname{argmin}} \left(g_\epsilon^{(1)}, g_\epsilon^{(2)}, \ldots, g_\epsilon^{(k)}\right) \\ &\text{subject to } h(O_{\text{sim}}(P))\,, \end{aligned} \tag{4.19}$$

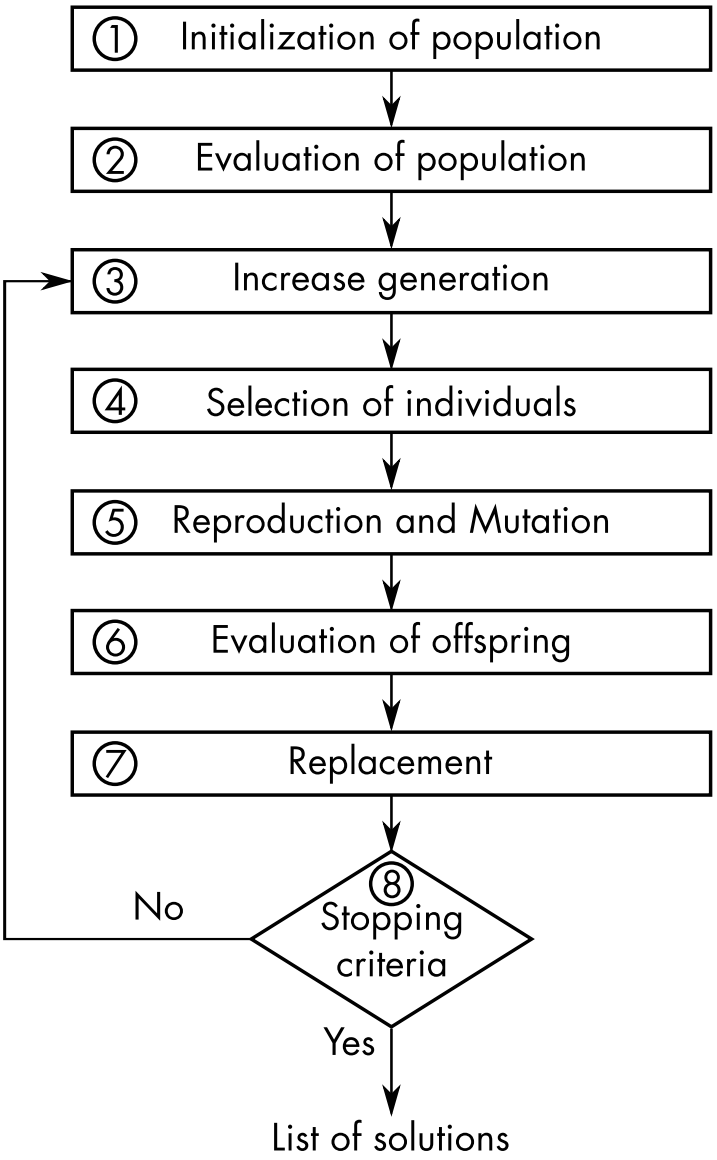

FIGURE 4.18– General scheme of genetic algorithms.

where $k \geq 2$ and each $g_\epsilon^{(i)} \equiv g_\epsilon^{(i)}(O_{\text{sim}}(P), O_{\text{obs}}(P))$ is an error function as defined for the single-objective case in eq. (2.1).

The main problem of multiobjective optimization is the lack of total order in the solution space. In other words, since there is an infinite number of solutions that cannot be compared between each other, it is impossible to find a single optimal solution for eq. (4.19). For example, assuming a multiobjective problem with two target functions [26], one cannot compare a candidate solution $s_1 = (2, 3)$ with $s_2 = (3, 2)$ because, in one case a function is lower while the other one is higher. However, if a solution $s_3 = (1, 1)$ exists, it is certain that $s_3 < s_1$ and $s_3 < s_2$ because

26. In this example, a solution $s = (x_1, x_2)$ denotes a set of values that evaluate the two target functions as $g_\epsilon^{(1)}(s) = x_1$ and $g_\epsilon^{(2)}(s) = x_2$.

this solution presents a better minimization of both target functions. Due to this particularity of collective optimization, many multiobjective minimization efforts are focused on the identification of these *incomparable* points as long as they minimize each objective function as much as possible.

In general, multiobjective problems are solved using one of the following techniques (or a combination of them):

Pareto region estimation: the approach that consists in finding the Pareto region (illustrated in fig. 4.19), a set of solutions whose objective functions cannot be improved without a deterioration in another objective function. Consequently, a multiobjective optimization does not find the optimal parameter values P_{opt}, but a set of Pareto-efficient parameter values $\mathbb{P}_{\text{Pareto}}$.

Scalarization: a straightforward approach where the original multiobjective problem is converted to a single-objective optimization. An example of such transformation can be linear combination of all target functions with a weight vector $W = [w_1, \ldots, w_k]$, which becomes:

$$\begin{aligned} P_{\text{opt}} = \underset{P \in \mathbb{P}}{\operatorname{argmin}} & \sum_{i=1}^{k} w_i g_\epsilon^{(i)} \\ & \text{subject to } h(O_{\text{sim}}(P)) \,. \end{aligned} \tag{4.20}$$

However, this scalarization is not applicable when the target functions do not share the same units.

Interaction: when a total order of the solution space is formalized with an utility function, which is defined by the interests of an expert, or when the Pareto region is estimated and then the expert decides which solutions are more interesting.

Currently, the most popular approach is the Pareto estimation using evolutionary algorithms (Coello et al., 2007), a field named multiobjective evolutionary algorithms (MOEA). Using the approach presented in section 4.3.2.1 and some modifications that will be explained later, these algorithms can obtain a set of solutions that estimate the Pareto region. Among this family of methods, the most popular ones are the Strength Pareto Evolutionary Algorithm (SPEA) (Zitzler, 1999; Zitzler et al., 2004) and the Non-dominated Sorting Generic Algorithm (NSGA) (Deb et al., 2001). The latter will be detailed in our proposed approach, since it was used for two multiobjective estimations in the clinical applications of this work.

4.3.4 Proposed approach

During the initial parameter identifications of the modeling applications of this thesis, mono-objective and deterministic approaches were used to perform an initial exploration of parameter spaces. In particular, the Nelder-Mead method was implemented and included in the M2SL library as the `id::SimplexOptimizator` class. Shortly after some initial identifications, it became evident that this algorithm does not handle local minima well, which justified further the use of EA. Further, clinical applications were associated with different sources of observable data.

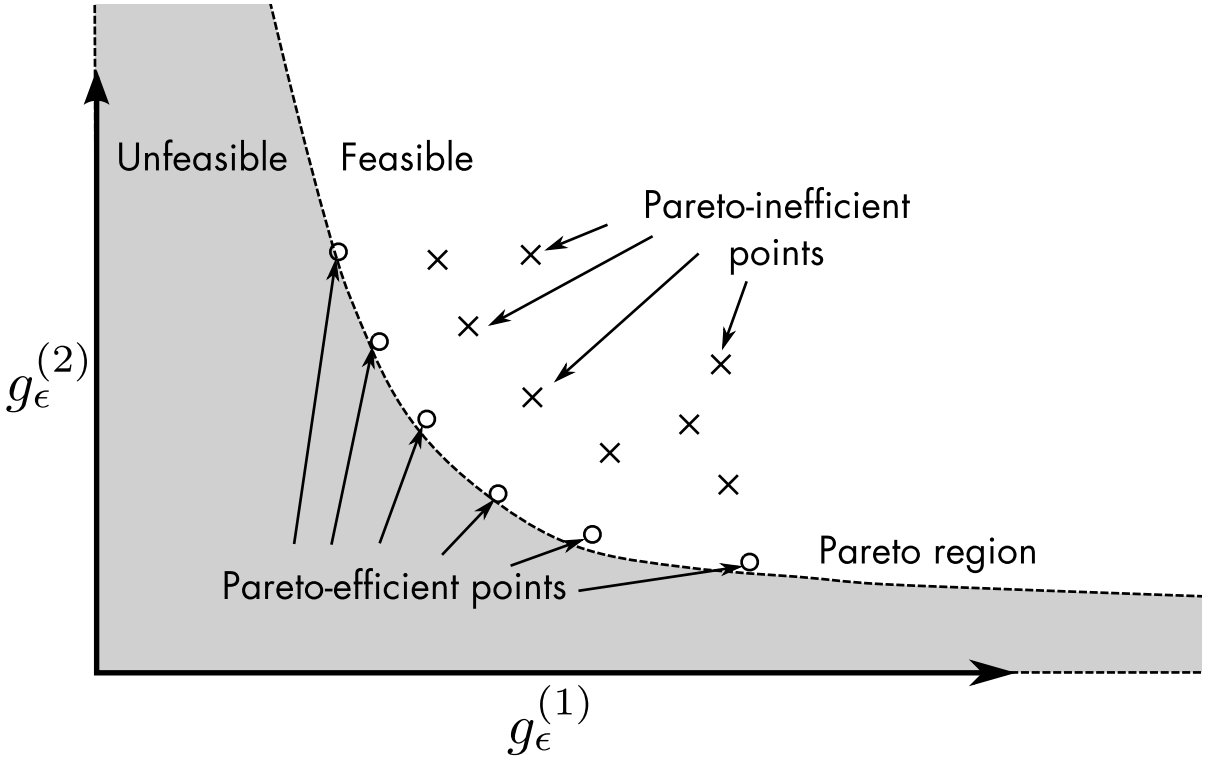

FIGURE 4.19– An example of a Pareto region for two minimization functions. Circles and crosses denote feasible points in the solution space. Among circled points, it is not possible to minimize one of the objective functions without increasing the other function. However, circled points are always better than crossed points because they decrease both target functions.

This events directed all estimation efforts towards evolutionary algorithms and multi-objective evolutionary algorithms.

Among the available MOEA in the literature, the Non-dominated Sorting Genetic Algorithm (NSGA) was selected, since it reportedly provides a better estimation of the Pareto region (TAN et al., 2002). This multi-objective optimization algorithm follows the general guidelines of any EA, illustrated in fig. 4.18, with some modifications for the evaluation and replacement procedures, which will explained in section 4.3.4.6. But first, the following considerations were introduced to apply EAs as a parameter estimation tool.

4.3.4.1 Objective functions

The objective functions were defined exactly as eq. (4.19), where each $g_\epsilon^{(i)}$ represents an error function that compares the ith observable output of the real clinical system with its corresponding output variable of the simulated data.

For cases when the clinical and simulated data consists of a single value, $g_\epsilon^{(i)}$ is defined as:

$$g_\epsilon^{(i)}(O_{\text{sim}}(P), O_{\text{obs}}(P)) = \left| O_{\text{sim}}^{(i)}(P) - O_{\text{obs}}^{(i)}(P) \right| , \tag{4.21}$$

where P represents a set of parameter values, $O_{\text{sim}}^{(i)}(P)$ is the ith simulated output of a model

with parameters P, and $O^{(i)}_{\text{obs}}(P)$ is the observed (clinical) datum that correspond to the system under the same parameters P.

When clinical and simulated data consist of a time series, one of the following functions can be used:

1. The sum of the error between clinical and simulated signals within a window between $[t_0, t_f]$:

$$g^{(i)}_{\epsilon}(O_{\text{sim}}(P), O_{\text{obs}}(P)) = \sum_{t=t_0}^{t_f} \left| O^{(i)}_{\text{sim}}(P,t) - O^{(i)}_{\text{obs}}(P,t) \right| . \tag{4.22}$$

2. The relative mean squared error ($rMSE$) between the clinical and simulated signals within a window $[t_0, t_f]$:

$$g^{(i)}_{\epsilon}(O_{\text{sim}}(P), O_{\text{obs}}(P)) = \frac{\sum_{t=t_0}^{t_f} \left(O^{(i)}_{\text{sim}}(P,t) - O^{(i)}_{\text{obs}}(P,t) \right)^2}{\sum_{t=t_0}^{t_f} \left(O^{(i)}_{\text{obs}}(P,t) \right)^2} . \tag{4.23}$$

4.3.4.2 Individual representation

An individual P_j is defined as a set of values for each parameter $[p_{j0}, p_{j1}, \ldots, p_{jn}]$. Each allele of the individual corresponds to a parameter value, and it is internally represented as a floating-point value. For example, in fig. 4.20(b), the leftmost individual represents the parameter values $[p_0 = 64.0, p_1 = 120.0, \ldots, p_n = 543.0]$.

4.3.4.3 Population initialization

The first population of the EA is generated randomly, within the bounds of the parameter space $\mathbb{P}$. For each parameter p_l, a range $[p_{\min,l}, p_{\max,l}]$ is defined to designate its minimum and maximum value. Every individual $P_j = [p_{j0}, \ldots, p_{jl}, \ldots, p_{jn}]$ is initialized with random alleles: $p_{jl} \sim \mathcal{U}(p_{\min,l}, p_{\max,l})$.

4.3.4.4 Selection algorithm

The strategy that selects pair of parents that will reproduce was the *tournament* selection: From a population of size N, four individuals P_1, P_2, P_3, P_4 are picked randomly with equal probability. Then, P_1 and P_2 are compared (this is the aforementioned *tournament*), the individual with best fitness is selected as the first parent P_{p1}. Similarly, the best among P_3 and P_4 determines the second parent P_{p2}. This pair of parents will then be subject to crossover. The tournament process is then repeated until N parents have been selected.

This method represents a well-known selection algorithm (Goldberg, 1989; Michalewicz, 1996): it prefers the selection of the best individuals, but inferior individuals still have a chance to reproduce as well, provided that they are confronted with a worse individual during the tournament.

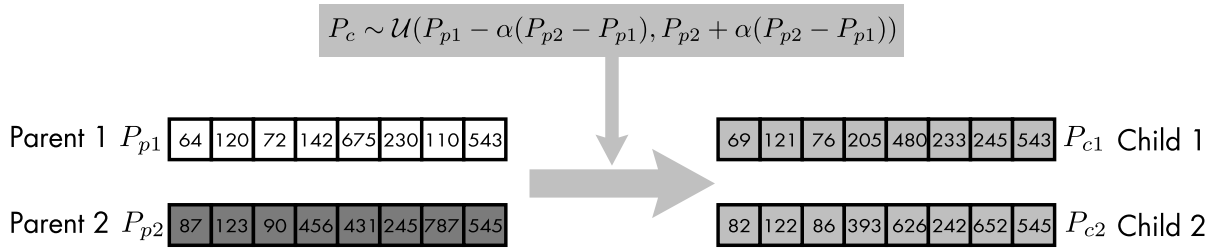

(a) α-blending crossover.

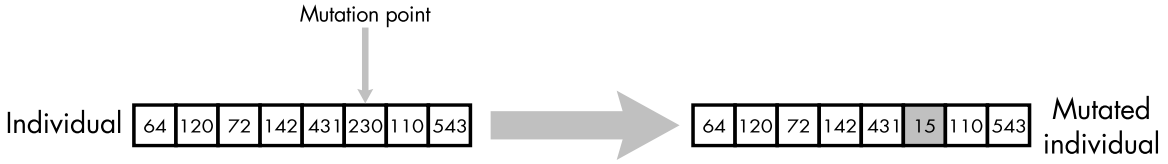

(b) Single point mutation.

FIGURE 4.20– Illustrative example of the crossover and mutation procedures for the evolutionary algorithm.

4.3.4.5 Reproduction: crossover and mutation algorithms

For each pair of individuals P_{p1} and P_{p2} from the selection algorithm, a crossover of their generic information may occur with a probability of p_c. The combination of the alleles of each individuals is performed using the α-blending approach (GOLDBERG, 1989), illustrated in fig. 4.20(a): for each parameter p_l, a random value is generated from an uniform distribution in the range $[p_{p1,l} - \alpha(p_{p2,l} - p_{p1,l}), p_{p2,l} + \alpha(p_{p2,l} - p_{p1,l})]$. This strategy generates random points that are over a line that traverses the parent individuals, potentially improving the solutions provided by the two progenitors.

After the crossover process has generated two new child individuals P_{c1} and P_{c2}, each allele may be modified with probability p_m by a mutation operator, using a random uniform mutation (GOLDBERG, 1989), illustrated in fig. 4.20(b): an allele is mutated by selecting a random uniform value between the limits of the corresponding parameter. The application of the mutation operator is very important for the exploration of the parameter space; it yields new individuals that are difficult to obtain with a crossover operator alone.

4.3.4.6 Non-dominated Sorting Genetic Algorithm (NSGA-II)

The Non-dominated Sorting Genetic Algorithm is a MOEA that introduces two elements: a domination function that presents a partial order of the individuals, and a diversity function designed to avoid similar individuals. These two ideas are put together with a modification to the underlying procedures of the genetic algorithm, which conforms the NSGA approach. More recently, its original author further improved NSGA to speed up the computational performance of the algorithm and the diversity function. This improvement was named NSGA-II (DEB et al., 2002).

The element related to domination states that, given a pair of individuals P_i and P_j, it is possible to determine which solution is more efficient:

$$(P_i \text{ dominates } P_j) \equiv (\forall_k : g_\epsilon^{(k)}(P_i) \leq g_\epsilon^{(k)}(P_j)) \,. \tag{4.24}$$

In other words, P_i dominates P_j when not one objective function is further reduced by P_j. This relation between individuals permits to define a *rank* attribute for each individual: an individual has rank 0 when it is not dominated by any other individual, rank 1 when it is dominated by one individual, and so on. A group of individuals with the same rank are incomparable, otherwise they would be in a higher or lower rank. The set of all individuals with rank m is called the m-front (F_m). The main objective of the NSGA-II algorithm is to iteratively evolve a population whose individuals in F_0 are the estimation of the Pareto region.

The diversity function of NSGA-II arises from the partial order established by the domination function: it complements comparison of individuals that have the same rank. This function assigns an utility to each individual as a value in $[0, \infty)$ that measures a distance function between an individual $P_i \in F_m$ and all other individuals in F_m. Thus, an individual with a high crowding value is a solution that is very different from all other solutions, while an individual with zero crowding value is a repeated individual. The secondary objective of the NSGA-II algorithm is to have a population whose individuals in F_0 are as diverse as possible.

The combination of the domination and the crowding relation can be summarized in a comparison operator $\prec_n$, defined as:

$$\begin{aligned} P_i \prec_n P_j \text{ if } &(\text{rank}(P_i) < \text{rank}(P_j)) \\ &\text{or } (\text{rank}(P_i) = \text{rank}(P_j)) \text{ and } (\text{crowd}(P_i) > \text{crowd}(P_j)) \,, \end{aligned} \tag{4.25}$$

where crowd denotes the diversity function. This comparison is embedded in the main genetic algorithm of NSGA-II, following the approach explained before in fig. 4.18, with a customized replacement procedure, illustrated in fig. 4.21.

The replacement procedure of NSGA-II starts after the population of generation n has generated a child population, which has been evaluated. First, the parent and child population are merged and the rank of each individual is calculated. This step permits to identify all the fronts of the merged population. Then, each front is directly selected, starting with F_0, until the new population is full. At one point, one of the fronts will have too many individuals to fit in the remaining space of the new population, such as F_2 in the example of fig. 4.21. In this case, the front will be sorted according to the $\prec_n$ order (see eq. (4.25)), i.e. according to their diversity function, since all these individuals will have the same rank. Once the individuals are sorted, only the best ones pass to the new population, which constitutes the population of generation $(n + 1)$.

4.4 Conclusion

This chapter presented three specific contributions to the modeling and simulation framework that represents the base methodology used throughout the rest of this work: a contribution to

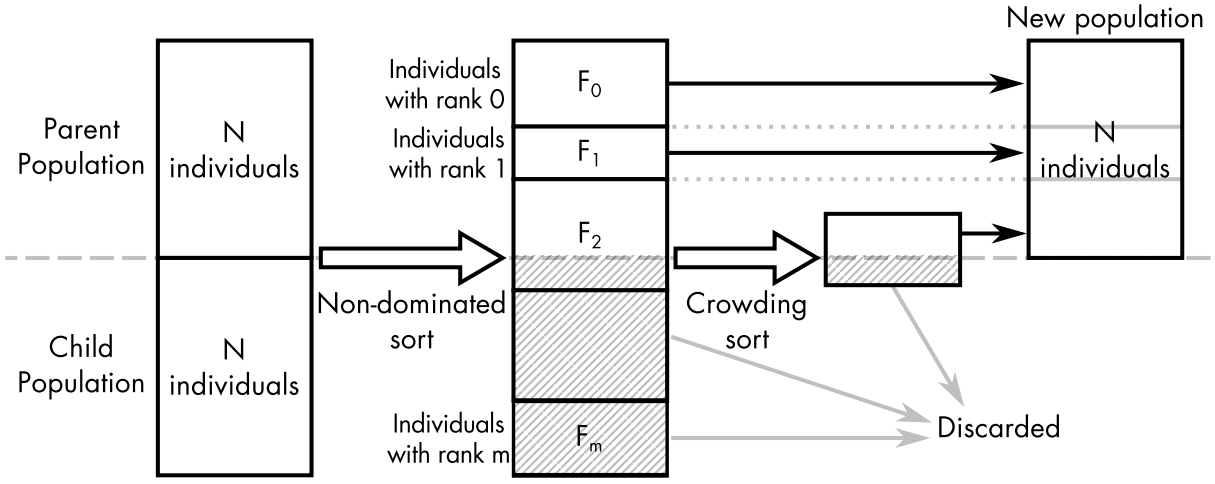

FIGURE 4.21– Diagram of the NSGA-II approach to the replacement procedure.

multi-formalism modeling using a custom simulation library, the adaptation and integration of sensitivity analysis methods applicable to multi-formalism models and the application of a novel parameter identification approach based on multi-objective evolutionary optimization.

For the first contribution, a synthesis of the current modeling and simulation tools was first presented. These tools provide an extremely helpful support for various scientific domains. Even though many of them provide means to define hybrid systems, only a few tackle the simulation of multi-formalism systems. Furthermore, multi-formalism simulation is still a field in research and current solutions do not provide the ability to simultaneously use formalism-specific simulators that solve the temporal synchronization and input/output coupling. For these reasons, our first contribution consisted in the development of the multi-formalism modeling and simulation library (M2SL). This chapter presented the detailed description of M2SL, which provides an implementation to temporal synchronization strategies and variable coupling implementation as presented in chapter 3. During this work, the development of M2SL was crucial, resulting in the creation of additional tools designed to ease the model development phase. These tools are registered and published in a website; they have been listed as part of the tools of the Virtual Physiological Human Network of Excellence, and they are currently used by several laboratories.

The second contribution included in this chapter presented a concise portrayal of the current techniques of sensitivity analysis, which can be easily adapted for the analysis of model parameters. Three categories among these methods were identified, providing different knowledge about the relation between model parameters and simulation outputs. Since the application of sensitivity analysis is critical for a successful multi-resolution integration, as explained in chapter 3, this chapter shows how these sensitivity analysis methods can be applied to the simulation notation used in this work.

Finally, the third contribution was dedicated to the subject of parameter identification. In this chapter, this problem was formulated as a mathematical optimization problem. The complex nature of the parameter identifications performed in this thesis suggests the selection of evolutionary algorithms (EA) and multi-objective evolutionary algorithms (MOEA). Therefore, amid the existing MOEAs, the Non-dominated Sorting Genetic Algorithm was presented along the general schema and concepts of EA. Finally, the adaptation of evolutionary algorithms to our modeling application was formalized, providing a common base for all parameter identifications in the following chapters.

References

Britten, R. D., G. R. Christie, C. Little, A. K. Miller, C. Bradley, A. Wu, T. Yu, P. Hunter, and P. Nielsen (2013). "FieldML, a proposed open standard for the physiome project for mathematical model representation". In: *Medical & biological engineering & computing*, pp. 1–17.

Campolongo, F., J. Cariboni, A. Saltelli, and W. Schoutens (2004). "Enhancing the Morris method". In: *Proceedings of SAMO 2004, 4th Int. Conf. on Sensitivity Analysis of Model Output*.

Christie, G. R., P. M. Nielsen, S. A. Blackett, C. P. Bradley, and P. J. Hunter (2009). "FieldML: concepts and implementation". In: *Philosophical Transactions of the Royal Society A: Mathematical, Physical and Engineering Sciences* 367.1895, pp. 1869–1884.

Coello, C. A. C., G. B. Lamont, and D. A. V. Veldhuizen (2007). *Evolutionary algorithms for solving multi-objective problems*. 2nd ed. Springer.

Cukier, R., H. Levine, and K. Shuler (1978). "Nonlinear sensitivity analysis of multiparameter model systems". In: *Journal of computational physics* 26.1, pp. 1–42.

Dantzig, G. B. (1998). *Linear programming and extensions*. Princeton university press.

De Lara, J. and H. Vangheluwe (2002). "AToM3: A Tool for Multi-formalism and Meta-modelling". In: *Fundamental approaches to software engineering*. Springer, pp. 174–188.

Deb, K., A. Pratap, S. Agarwal, and T. Meyarivan (2002). "A fast and elitist multiobjective genetic algorithm: NSGA-II". In: *Evolutionary Computation, IEEE Transactions on* 6.2, pp. 182–197.

Deb, K. and D. Kalyanmoy (2001). *Multi-Objective Optimization Using Evolutionary Algorithms*. New York, NY, USA: John Wiley & Sons, Inc. ISBN: 047187339X.

Defontaine, A. (2006). "Modélisation multirésolution et multiformalisme de l'activité électrique cardiaque". PhD thesis. Université de Rennes 1.

Duarte, J., M. Vélez-Reyes, S. Tarantola, F. Gilbes, and R. Armstrong (2003). "A probabilistic sensitivity analysis of water-leaving radiance to water constituents in coastal shallow waters". In: *Proceedings of SPIE*. Vol. 5155, p. 162.

Eberhart, R. and J. Kennedy (1995). "A new optimizer using particle swarm theory". In: *Micro Machine and Human Science, 1995. MHS'95., Proceedings of the Sixth International Symposium on*. IEEE, pp. 39–43.

EPA (2009). *Guidance on the Development, Evaluation, and Application of Environmental Models*. Tech. rep. U.S. Environmental Protection Agency.

Fleureau, J. (2008). "Intégration de données anatomiques issues d'images MSCT et de modéles électrophysiologique et mécanique du coeur". PhD thesis. Universite de Rennes 1.

Galassi, M. and B. Gough (2006). *GNU scientific library: reference manual*.

Garny, A., D. P. Nickerson, J. Cooper, R. W. dos Santos, A. K. Miller, S. McKeever, P. M. Nielsen, and P. J. Hunter (2008). "CellML and associated tools and techniques". In: *Philosophical Transactions of the Royal Society A: Mathematical, Physical and Engineering Sciences* 366.1878, pp. 3017–3043.

Glover, F. (1986). "Future paths for integer programming and links to artificial intelligence". In: *Computers & Operations Research* 13.5, pp. 533–549.

GOLDBERG, D. E. (1989). *Genetic algorithms in search, optimization, and machine learning*. 1st. Addison-Wesley Longman Publishing Co., Inc.

HERNÁNDEZ, A. I., V. LE ROLLE, A. DEFONTAINE, and G. CARRAULT (2009). "A multiformalism and multiresolution modelling environment: application to the cardiovascular system and its regulation". In: *Philos Transact A Math Phys Eng Sci* 367.1908. PTRSA, pp. 4923–4940. DOI: 10.1098/rsta.2009.0163.

HERNÁNDEZ, A. I., V. LE ROLLE, D. OJEDA, P. BACONNIER, J. FONTECAVE-JALLON, F. GUILLAUD, T. GROSSE, R. G. MOSS, P. HANNAERT, and S. R. THOMAS (2011). "Integration of detailed modules in a core model of body fluid homeostasis and blood pressure regulation". In: *Progress in Biophysics and Molecular Biology* 107, pp. 169–182. DOI: 10.1016/j.pbiomolbio.2011.06.008.

HOLLAND, J. (1975). *Adaptation in Natural and Artificial Systems*. Michigan Press. Re-issued by MIT Press (1992).

HUCKA, M., A. FINNEY, H. SAURO, H. BOLOURI, J. DOYLE, H. KITANO, A. ARKIN, B. BORNSTEIN, D. BRAY, A. CORNISH-BOWDEN, et al. (2003). "The systems biology markup language (SBML): a medium for representation and exchange of biochemical network models". In: *Bioinformatics* 19.4, pp. 524–531.

KIRKPATRICK, S. (1984). "Optimization by simulated annealing: Quantitative studies". In: *Journal of statistical physics* 34.5-6, pp. 975–986.

KOHL, P. and D. NOBLE (2009). "Systems biology and the virtual physiological human". In: *Molecular Systems Biology* 5.1.

LAND, A. H. and A. G. DOIG (1960). "An automatic method of solving discrete programming problems". In: *Econometrica: Journal of the Econometric Society*, pp. 497–520.

LE ROLLE, V. (2006). "Modélisation Multiformalisme du Système Cardiovasculaire associant Bond Graph, Equations Différentielles et Modèles Discrets". PhD thesis. Rennes: Université de Rennes 1.

MICHALEWICZ, Z. (1996). *Genetic algorithms+ data structures= evolution programs*. springer.

MILLER, K. (2010). "Physiome THE". In: *A mission imperative. Biomedical Computation Review*, pp. 8–15.

MINSKY, M. (1961). "Steps toward artificial intelligence". In: *Proceedings of the IRE* 49.1, pp. 8–30.

MIRAMS, G. R., C. J. ARTHURS, M. O. BERNABEU, R. BORDAS, J. COOPER, A. CORRIAS, Y. DAVIT, S.-J. DUNN, A. G. FLETCHER, D. G. HARVEY, et al. (2013). "Chaste: An Open Source C++ Library for Computational Physiology and Biology". In: *PLoS computational biology* 9.3, e1002970.

MORRIS, M. (1991). "Factorial sampling plans for preliminary computational experiments". In: *Technometrics* 33.2, pp. 161–174.

NELDER, J. and R. MEAD (1965). "A simplex method for function minimization". In: *The computer journal* 7.4, p. 308.

NEMHAUSER, G. L., A. R. KAN, and M. TODD (1989). *Optimization, volume 1 of Handbooks in operations research and management science*. North-Holland, Amsterdam.

QUESNEL, G., R. DUBOZ, and E. RAMAT (2009). "The Virtual Laboratory Environment – An operational framework for multi-modelling, simulation and analysis of complex dynamical systems". In: *Simulation Modelling Practice and Theory* 17, pp. 641–653.

SALTELLI, A., K. CHAN, E. M. SCOTT, et al. (2000). *Sensitivity analysis*. Wiley New York.

SALTELLI, A., M. RATTO, T. ANDRES, F. CAMPOLONGO, J. CARIBONI, D. GATELLI, M. SAISANA, and S. TARANTOLA (2008). *Global sensitivity analysis: the primer*. Wiley-Interscience.

SALTELLI, A., P. ANNONI, I. AZZINI, F. CAMPOLONGO, M. RATTO, and S. TARANTOLA (2010). "Variance based sensitivity analysis of model output. Design and estimator for the total sensitivity index". In: *Computer Physics Communications* 181.2, pp. 259 –270. ISSN: 0010-4655. DOI: http://dx.doi.org/10.1016/j.cpc.2009.09.018.

SCHREIDER, S. and R. BRADDOCK (2011). "Application of the Morris algorithm for sensitivity analysis if the REALM model for the Goulburn Irrigation System". In: *Environmental Modeling and Assessment* 11.4, pp. 297–313.

SOBOL, I. M. (1993). "Sensitivity estimates for nonlinear mathematical models". In: *Mathematical Modelling and Computational Experiments* 1.4, pp. 407–414.

— (2001). "Global sensitivity indices for nonlinear mathematical models and their Monte Carlo estimates". In: *Mathematics and computers in simulation* 55.1-3, pp. 271–280.

Tan, K. C., T. H. Lee, and E. F. Khor (2002). "Evolutionary algorithms for multi-objective optimization: performance assessments and comparisons". In: *Artificial intelligence review* 17.4, pp. 251–290.

Vangheluwe, H. (2001). "Multi-formalism modelling and simulation". PhD thesis. Universiteit Gent.

Vittorini, V., M. Iacono, N. Mazzocca, and G. Franceschinis (2004). "The OsMoSys approach to multi-formalism modeling of systems". English. In: *Software and Systems Modeling* 3.1, pp. 68–81. issn: 1619-1366. doi: 10.1007/s10270-003-0039-5.

Zeigler, B. P., H. Praehofer, and T. G. Kim (2000). *Theory of modeling and simulation: Integrating discrete event and continuous complex dynamic systems*. 2nd ed. Academic Press.

Zitzler, E. (1999). "Evolutionary algorithms for multiobjective optimization: Methods and applications". PhD thesis. Swiss Federal Institute of Technology Zurich.

Zitzler, E., M. Laumanns, and S. Bleuler (2004). "A tutorial on evolutionary multiobjective optimization". In: *Metaheuristics for Multiobjective Optimisation*, pp. 3–37.

CHAPTER 5

An example of multi-resolution integration: The Guyton model

Résumé

Ce chapitre est une application directe de l'approche de modélisation multi-résolution proposée dans cette thèse. L'objectif est d'étudier les conséquences court et moyen terme de l'insuffisance cardiaque qui est une pathologie hautement multi-factorielle. Dans cette application, un exemple typique d'intégration horizontal, représenté par le modèle de Guyton, a été couplé avec une description plus détaillée et pulsatile des ventricules. L'influence de cette intégration a pu être étudiée en appliquant des méthodes d'analyse de sensibilité adaptées. Les simulations, obtenues avec le modèle couplé, reproduisent les réponses observées à court et moyen terme lors d'un épisode aiguë d'insuffisance cardiaque.

This chapter presents an example of the application of the methods and tools presented in chapters 3 and 4 to the analysis of the dynamic and integrated behavior of the cardiovascular and renal systems (CVR). The first section presents the pathology that will be addressed in this chapter (heart failure) and the reasons why a model-based analysis may be of interest in this kind of multi-factorial pathology.

The proposed model-based approach is presented in section 5.1. It is directly based on the multi-resolution paradigm introduced in chapter 3, that couples a horizontally-integrated model of the CVR and their regulation, with more detailed sub-modules of the cardiac function. The following sections are dedicated to the resolution of the main problems related to this multi-resolution developments:

Core-model development: The modular, object-oriented implementation of an horizontally-integrated model of the CVR (the Guyton model) into our multi-formalism modeling and simulation framework (M2SL) is described in section 5.3. Simulation results are verified with respect to benchmark data available for this model.

Optimization of the temporal coupling: Each module of Guyton model presents its own temporal dynamics, which can vary significantly between the different physiological processes that are implemented. Section 5.4 describes how the proposed temporal synchronization methods (cf. chapter 3) are able to significantly improve simulation performance.

Multi-resolution model integration: The original Guyton model does not include a pulsatile representation of the ventricles. The global methodology proposed in chapter 3 for coupling heterogeneous sub-models into a multi-resolution model is applied in section 5.5 to integrate a model of pulsatile ventricles into the Guyton model, while preserving the stability and physiological properties of the original model.

Once these steps are completed, the integrated, multi-resolution model is able to reproduce pathological conditions which were impossible to simulate with the original model. An example of a paroxysmal by-ventricular desynchronization on a virtual heart failure patient is presented, as an example of the usefulness of the proposed approach.

5.1 Heart failure

Heart failure (HF) is a pathological state characterized by the inability for the heart to provide a sufficient pump action to maintain the blood flow necessary for the needs of the body. According the European society of cardiology (Remme et al., 2002), HF could be characterized by systolic and/or diastolic dysfunctions. The most common cause of heart failure is left ventricular systolic dysfunction. Most cases are a result of end-stage coronary artery disease (CAD), either with a history of myocardial infarction or with a chronically underperfused myocardium. Both processes are present simultaneously in many patients. Other common causes of systolic dysfunction include dilated cardiomyopathy, valvular heart disease, hypertensive heart disease, toxin-induced cardiomyopathies (e.g. alcohol), and congenital heart disease. The majority of systolic dysfunctions is coupled to diastolic dysfunctions. However, a diastolic HF could be suspected when symptoms occur with a preserved ejection fraction. Diastolic dysfunctions are relatively unusual in younger patients, but their prevalence rises in older patients. In fact, systolic hypertension and myocardial hypertrophy directly influence the cardiac function.

Although the heart is the main organ involved in HF, a variety of neurohumoral regulatory mechanisms are triggered during the early stages of HF, covering a wide range of time scales (from seconds to weeks). Although these mechanisms can compensate for the consequences of HF in the short term, they become deleterious in the mid to long terms and may accentuate ventricular dysfunction and cause a permanent increase in preload and afterload, a structural remodeling of the heart, pulmonary or peripheral edema, decreased renal output and dyspnea on exertion. Therefore, the study of the mechanism underlying HF requires the analysis of the complex interactions between the different physiological functions involved in this multifactorial pathology : cardiac function, circulatory system, autonomic nervous system, renin-angiotensin-aldosterone system and respiratory system. In order to realize such systemic analysis, the

proposed model-based aproach should take into account the influence of these physiological functions while providing a detailed description of the cardiac activity.

5.2 Problem statement

The analysis of the mechanisms involved in HF is complicated because it should include physiological a priori knowledge on the interactions between different physiological functions. The approach proposed in this chapter is based on the definition of an appropriate model including a multi-organ representation of the cardiovascular system and its regulation, while taking into account the systolic and diastolic properties of the ventricles.

The application of such a multi-resolution approach requires the definition of a global physiological model, horizontally integrated, that can be used as the “core model” for vertical integration of higher resolution sub-models. The basic "core model" must include descriptions of the heart, lungs, kidneys, muscles, blood vessels, and major fluid compartments. The first example of a physiological model with such a horizontal integration goal was the pioneering work of Guyton, Coleman, and Granger (Guyton et al., 1972, henceforth referred to as G72) which provided a multi-organ analysis of the regulation of the general cardiovascular system capable of exploring events over times ranging from seconds to weeks or months. This model was extended by (Ikeda et al., 1979) to include a representation of acid-base regulation involving a greatly expanded list of solutes. A later version of G72 was stabilized dating from 1992, and though this model was never published it became the working version for Guyton and colleagues and has survived in Fortran and C within their group, along with a rather sophisticated command-line user interface in MS-DOS® (MODSIM Montani et al., 1989).

In the context of the present chapter, G72 model has the advantage of having a formal description and includes the adequate documentation for the various components. However, the Guyton models, as well as their more recent versions (Montani et al., 2009), do not include a pulsatile cardiac function. This is a major limitation when studying HF, since *i)* the model cannot represent the systolic and diastolic characteristics of HF, or a biventricular desynchronization, *ii)* some useful clinical variables, such as the maximum of the arterial pressure derivative cannot be simulated, and *iii)* a more realistic representation of short-term regulatory loops (such as the baroreflex) requires these pulsatile variables. The model-based analysis presented in this chapter is an example of integration at different time scales in which the non-pulsatile ventricles of the original Guyton model are replaced by a pulsatile, elastance-based model of the heart, including inter-ventricular interaction through the septum.

5.3 Implementation of the Guyton model in M2SL

Before presenting the integration of models at different time scales, the first milestone of this modeling application was the implementation and analysis of the Guyton model in M2SL.

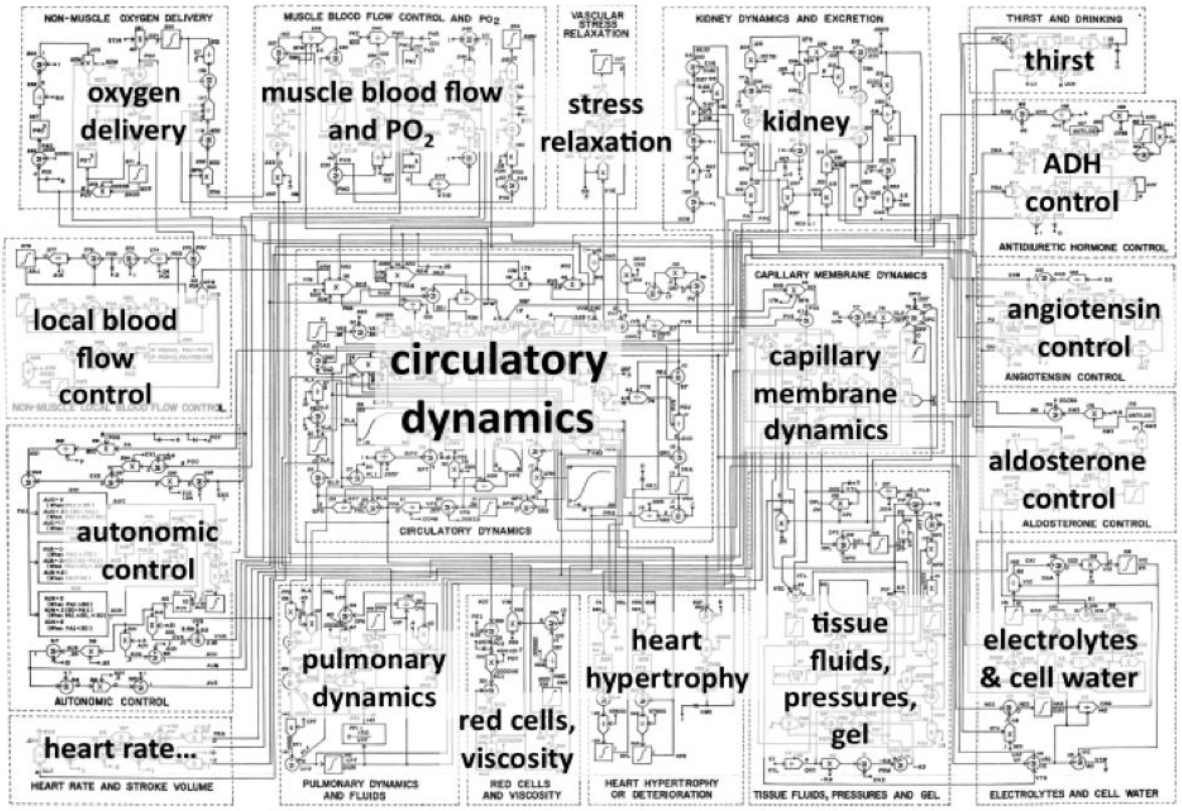

Figure 5.1– Schema of the classic Guyton model. Reproduction of the whole model (with permission from Guyton et al., 1972), overlaid with names of the various submodules.

5.3.1 The Guyton models

The original model of Guyton was the first "whole-body", integrated mathematical model of a physiological system. It allows for the dynamic simulation of systemic circulation, arterial pressure and body fluid regulation, including short and long-term regulations. From a modeling standpoint, it is actually a composite approach, since the model uses both exact physical and physiological laws (explicit and validated) and curve fits of experimental data or simply tabulated data, e.g. left ventricular output as a function of systemic arterial pressure is given as a piecewise linear graph. The G72 model consists of 18 modules (350+ elementary blocks), containing approximately 160 variables, including more than 40 state variables (cf. fig. 5.1). The model contains a total of approximately 500 numerical entities (model variables, parameters and constants).

In essence, Guyton's original model is constructed around a "central" circulatory dynamics module in interaction with 17 "peripheral" modules corresponding to physiological functions (such as pulmonary dynamics and fluids or non-muscle oxygen delivery; see (Guyton et al., 1972)). An examination of the original code or published diagram reveals that, in addition to its interconnected module structure, the model is characterized by a wide range of time scales in the different modules, ranging from 5×10^{-4} min (autonomic control) to 10^4 min (heart hypertrophy

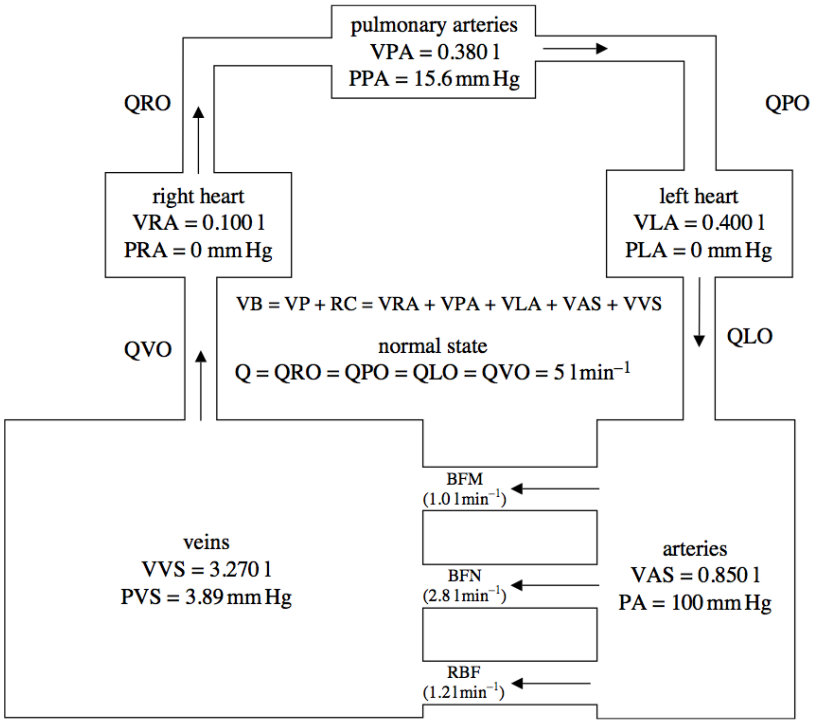

FIGURE 5.2– Distribution of blood flow through the general circulation. Volume (V), flow (Q) and pressure (P) are defined in different compartments: right atrium (VRA, PRA), left atrium volume (VLA, PLA), systemic arteries (VAS, PA), veins (VVS, PVS), pulmonary arteries (VPA, PPA), muscle and non-muscle blood flow (BFM and BFN), renal blood flow (RBF), left output (QLO), right output (QRO), venous output (QRO), pulmonary output (QRO). Baseline values for certain variables are shown.

or deterioration).

Figure 5.2 shows the distribution of blood as it flows through the main compartments of the general circulation, namely right atrium (VRA), left atrium (VLA), systemic arteries (VAS) and veins (VVS), and pulmonary arteries (VPA). The variables QVO, QRO, QPO, and QLO represent blood flow at various points along the circulation. VB is the total blood volume. BFM and BFN are the muscle and non-muscle blood flow, respectively, and RBF is the renal blood flow. The terms PLA, PPA, PRA, PA and PVS represent the five compartmental pressures, relative to atmospheric pressure. In the model, the volume of these main compartments are given by:

$$\mathrm{VAS} = \int (\mathrm{QLO} - \mathrm{QAO})\, dt + 0.2610 \cdot \mathrm{VB}\,, \tag{5.1}$$

$$\mathrm{VVS} = \int (\mathrm{QAO} - \mathrm{QVO})\, dt + 0.3986 \cdot \mathrm{VB}\,, \tag{5.2}$$

$$\mathrm{VRA} = \int (\mathrm{QVO} - \mathrm{QRO})\, dt + 0.0574 \cdot \mathrm{VB}\,, \tag{5.3}$$

$$\mathrm{VPA} = \int (\mathrm{QRO} - \mathrm{QPO})\, dt + 0.1550 \cdot \mathrm{VB}\,, \tag{5.4}$$

$$\mathrm{VLA} = \int (\mathrm{QPO} - \mathrm{QLO})\, dt + 0.1280 \cdot \mathrm{VB}\,, \tag{5.5}$$

where the last term in each equation represents the redistribution of changes of total blood volume (VB; due to, for example, haemorrage or, on the contrary, haematopoiesis) among the various compartments (the fractions sum to 1.0). Ventricular function is represented by a static algebraic equation, providing mean ventricular outputs (QLO and QRO for the left and right ventricles, respectively), which are computed as the product of the baseline ventricular outflow and various other parameters, including the mean arterial pressure (PA), pulmonary pressure (PPA) and the autonomic effect on cardiac contractility (AUH).

The original implementation of G72, based on fortran, is not adapted for the objective of the work. In fact, we feel that this was an obligatory step, preliminary to replacement of the original modules by updated or more detailed versions, to implement the corresponding modules of the Guyton model as different physiological and functional blocks, each with specified inputs and outputs, and without manually specifying integration step-sizes (as was the case in the original code).

5.3.2 Guyton Model implementation

The Guyton model has been implemented using M2SL (M_{G72}) as a coupled model (M^{coup}) that consists of a set of N interconnected atomic models ($M_i^a \quad i = 1, \ldots, N$, cf. chapter 3). Each atomic model corresponds to the "blocks" described in the original paper. Additionally, one coupled model class (the `Guyton72` class) was defined, to create instances of all other classes, as sub-model components, and to perform input-output couplings between these components. A class diagram of the implementation is presented in fig. 5.3. Two continuous formalisms are used in the description of this model: ordinary differential equations (ODE) and algebraic equations (AE). The preferred continuous simulator defined for the 18 atomic models with F = ODE is the fourth-order Runge-Kutta method.

5.3.3 Verification

In order to verify the M2SL C++ version of the model, we simulated three *in silico* experiments described in the 1972 Guyton et al. paper and compared the results with the output from the original FORTRAN program in Guyton's laboratory (provided by R.J. White, who worked in Guyton's laboratory at the time). The comparison results are published in (Hernández et al., 2011; Thomas et al., 2008). This section presents an example of one of these benchmarks (BM1). This experiment is the simulation of hypertension in a salt-loaded, renal-deficient patient by first reducing the renal mass by 70 % and later increasing the salt intake five-fold at, respectively, 2 hours and 4 days after the beginning of the simulation. The simulations correctly predict that the reduction in renal mass induces a decrease in cardiac output and an increase in peripheral resistance and arterial pressure. In response to the increased salt load, the extracellular volume, blood volume and cardiac output rise while the total peripheral resistance falls (fig. 5.4).

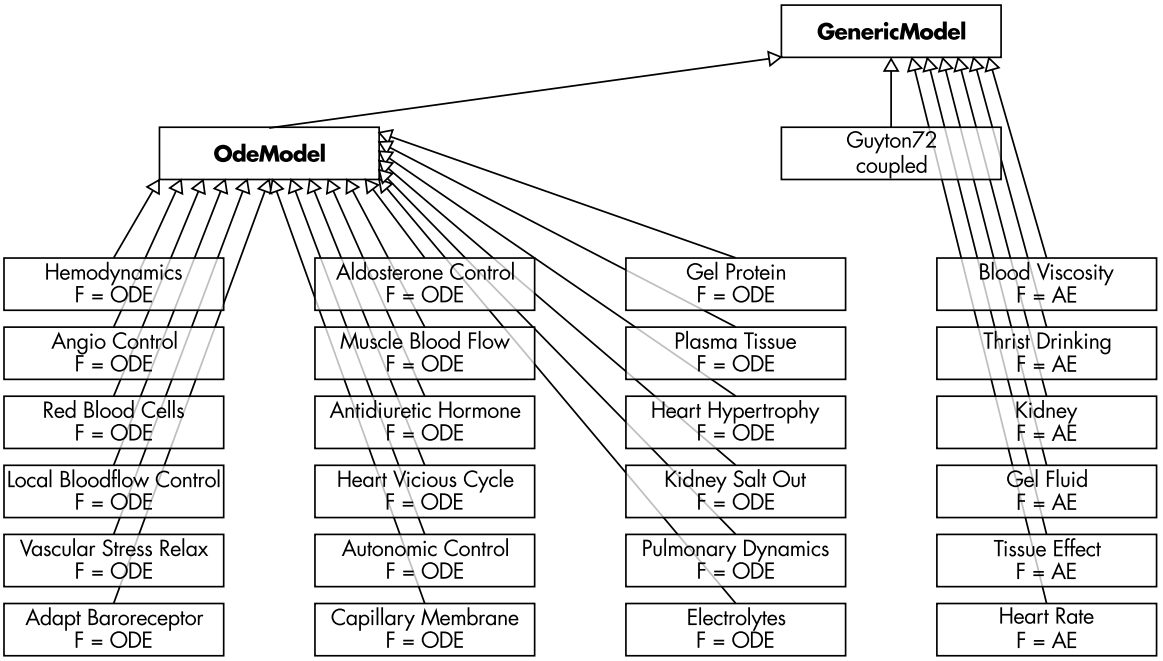

FIGURE 5.3– Simplified class diagram of the M2SL implementation for the M_{G72} model. The class `Guyton72` is the coupled model that links all other atomic models as components. The description formalism F of each component is also displayed: algebraic equations (AE) and ordinary differential equations (ODE).

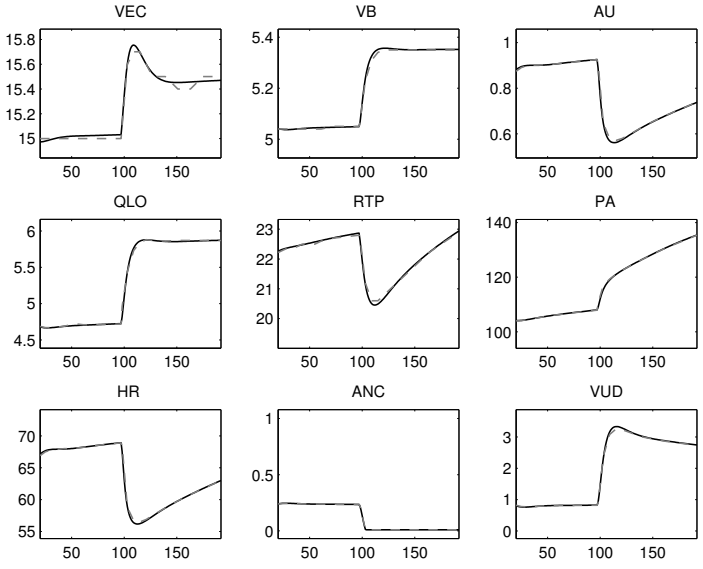

FIGURE 5.4– Comparison of M2SL simulations (black curves) with the original Guyton model (dotted curves). Benchmark experiment 1. Salt-loaded, renal-deficient patient: VEC (extracellular fluid volume in litres), VB (blood volume in litres), AU (ratio to normal sympathetic stimulation), QLO (cardiac output in L/min), RTP (total peripheral resistance in mmHg min/L), PA (mean arterial pressure in mmHg), HR (heart rate in bpm), ANC (ratio to normal angiotensin concentration), and VUD (urinary output in mL/min). Total experiment time (x-axis, in hours) was 192 h (8 days).

5.4 Optimization of the temporal coupling

In this section, we will use simulations of the M_{G72} implementation to compare the evolution of $\delta t_{a,i}$ for all atomic models, using the three different strategies for temporal synchronization (ST1–ST3). Additionally, the advantage of the M2SL implementation with respect to a Simulink®implementation of the Guyton model (published by Kofránek et al., 2010) will be shown. ST1 will be used as a reference for the comparison of the computation time to perform the whole simulation and to estimate the mean-squared error (MSE) of all the output variables of the simulation, after re-sampling outputs from ST2 and ST3 with a spline interpolation to the same time scale on ST1. A MSE of 10^{-3} was considered satisfactory. ST1 was performed with $\delta t_c = \delta t_{a,i} = 10^{-4}$ min, which was the highest value presenting a stable output. As a sub-sampling period is applied to obtain each sample of the model's output, the mean value of each $\delta t_{a,i}(t)$ on these sub-sampling periods has been calculated. Figures 5.5 and 5.6 show these $\delta t_{a,i}(t)$, for the benchmark presented in section 5.3.3, with time-synchronisation strategies ST2 and ST3, respectively. Figure 5.7 shows the computation time for 25 simulations for each strategy, including a simulation of a Simulink version configured at the same fixed step of ST1.

For ST2, although the values of $\delta t_c(t) = \delta t_{a,i}, \forall i$ are always slightly higher than in strategy ST1, computation times are similar to those obtained with that method (ratio of the simulation time with ST1/ST2 = 1.25). This is mainly due to the fact that for ST2, computation time is consumed to estimate the smallest $\delta t_{a,i}$ at each coupling instant, while ST1 does not need to apply multiple integration steps to determine the optimal simulation step. The mean-squared error obtained with this strategy, when compared to ST1 is 2.5285×10^{-5}.

Concerning ST3, the value of δt_c was fixed experimentally to 2.5×10^{-3} min. The heterogeneous dynamics of each atomic model can be appreciated in figure 5.6. Simulation under this configuration was $\sim$4 times faster than those observed with ST1 and the relative mean-squared error was 5.9385×10^{-4}.

Finally, a global outline of the advantages of the M2SL implementation of the Guyton model, from a computational point of view is shown in fig. 5.7. While Simulink is highly appreciated in the community for its graphical programming capabilities and a large toolbox of modules, this result demonstrates that M2SL outperforms Simulink by one order of magnitude. This important difference demonstrates the capabilities of the optimized implementation of M2SL.

5.5 Integration of pulsatile ventricles: a multi-resolution approach

Our core model implementation has the advantage to be sufficiently robust to handle the wide range of spatial and temporal scales, and flexible enough to accept sub-modules in a variety of formalisms. The M_{G72} implementation is the first step of the multiresolution integration of a detailed cardiac module. In order to couple a pulsatile heart, the left (LV) and right (RV) ventricles of the Guyton model were substituted with pulsatile ventricular models. To our

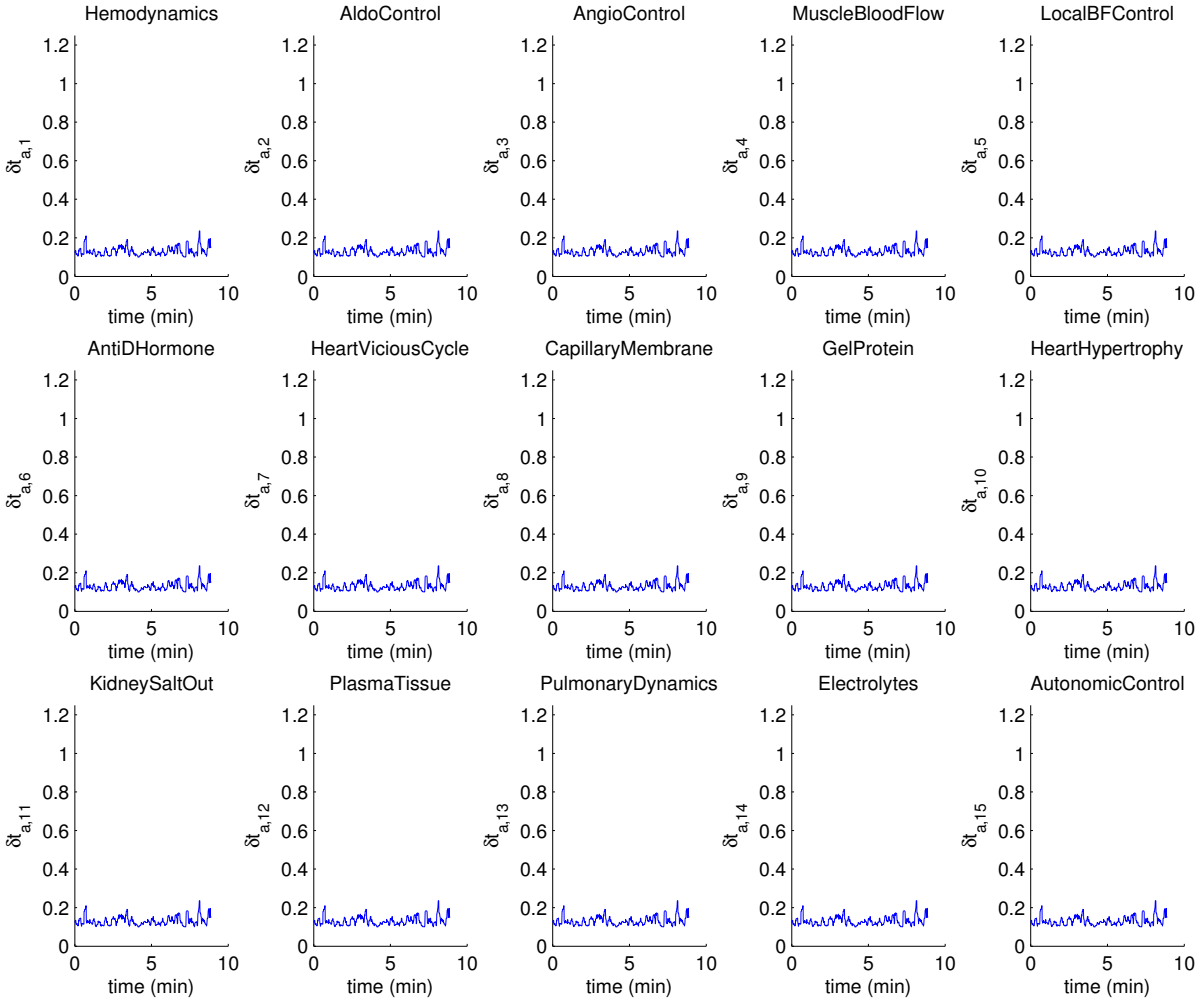

FIGURE 5.5– Evolution of $\delta t_{a,i}$ (in $\min \times 10^3$) for the main atomic models of the M2SL G72 implementation during the simulation of BM1, using time-synchronization strategy ST2.

knowledge, the first attempt to integrate a pulsatile heart into the Guyton model was proposed by (WERNER et al., 2002). However, their work focused on analysing the short-term response of the system, and no details on coupling with all the Guyton components were given. In addition, simulation results were not compared to Guyton's results.

Following the methodology proposed in chapter 3, this substitution process requires *i)* the definition of coupling transformations in order to preserve the numerical and physiological properties of the original model, *ii)* parameter identification for the proposed coupling transformations, and *iii)* a sensitivity analysis providing information on the impact of integrating the new pulsatile model.

5.5.1 Coupling the Guyton and the pulsatile models

The general method proposed in chapter 3 will be applied here to replace the original, non-pulsatile cardiac sub-model of M_{G72} with an elastance-based pulsatile model of the heart,

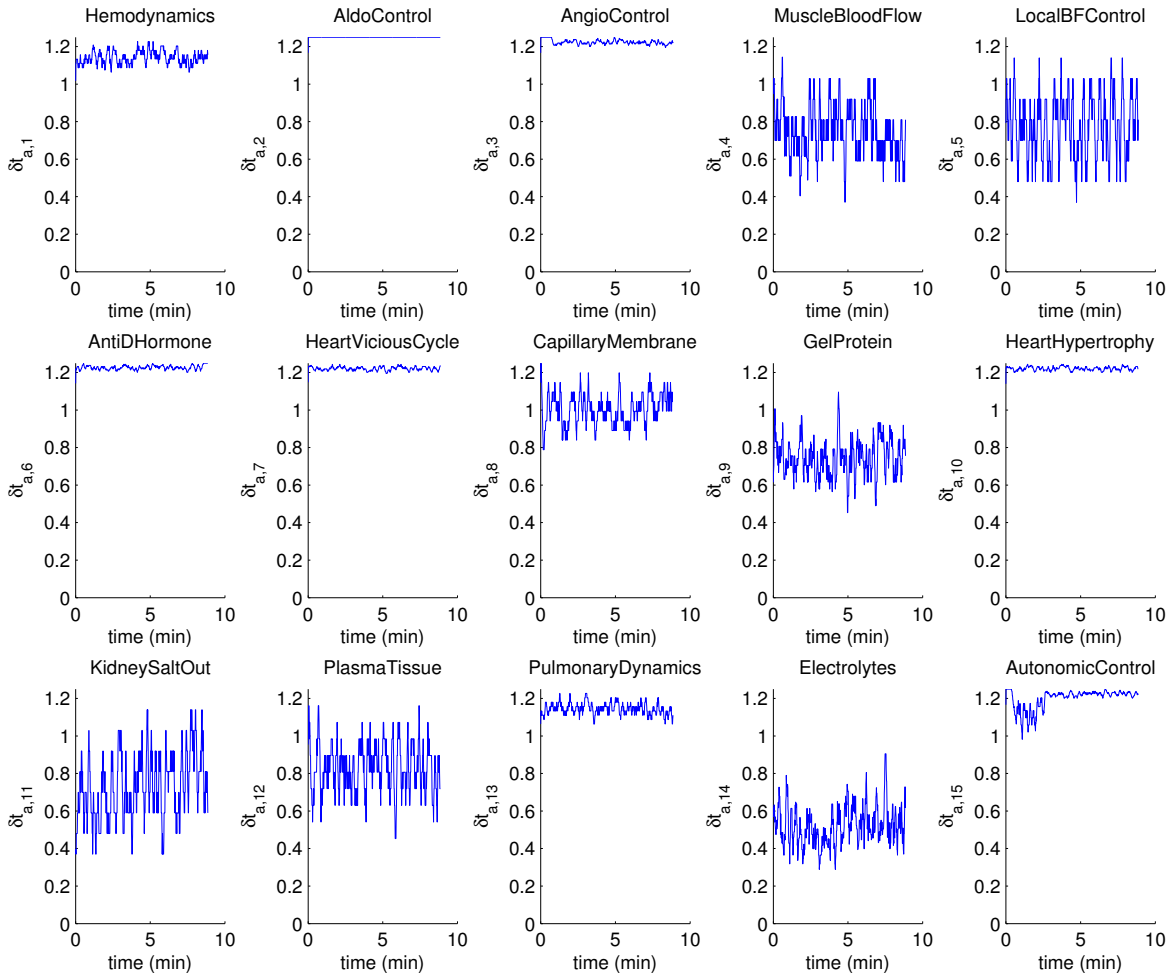

Figure 5.6– Evolution of $\delta t_{a,i}$ (in min$\times 10^3$) for the main atomic models of the M2SL G72 implementation during the simulation of BM1, using time-synchronization strategy ST3.

including interventricular interaction through the septum ($M_{G72\text{-}P}$). In this case, the set M_R is the Heart sub-module, located within the Circulatory Dynamics coupled module.

$\mathcal{O}_c$ = PLA (left atrial pressure), PA (arterial pressure), PRA (right atrial pressure), PPA (pulmonary arterial pressure), AUR (autonomic effect on heart rate) and AUH (autonomic effect on heart strength)

$\mathcal{I}_c$ = QMI (mitral flow), QLO (left ventricular outflow), QTR (triscupid flow), QRO (right ventricular outflow).

Figure 5.8 depicts the integration of the new models within the Circulatory Dynamics coupled module and within $M_{G72\text{-}P}$. In order to integrate a pulsatile heart, the Guyton left heart model was substituted with a coupled model that includes two valves and a ventricle. The heart valves are represented by modulated resistances that depend on the pressure gradient across the wall. The first coupling interface concerns the hemodynamic variables. Atrial and arterial pressures of the Guyton model are connected as inputs to the pulsatile models and trans-valvular flows obtained from the pulsatile model are connected to the Guyton model.

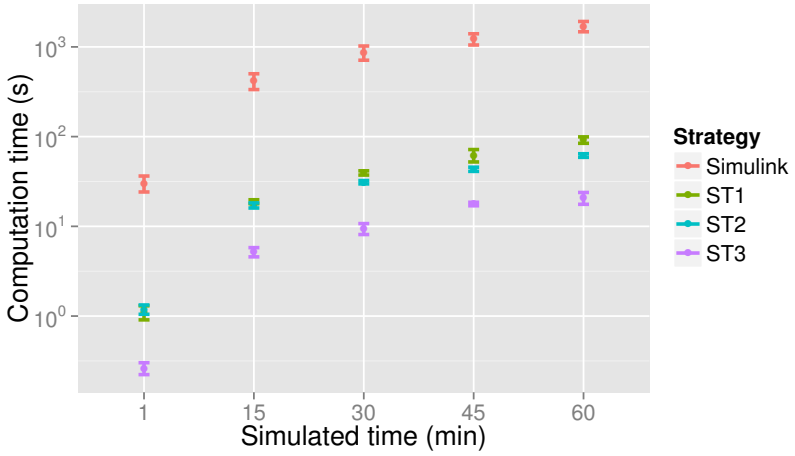

FIGURE 5.7– Computation times for the simulation of the Guyton model for each time synchronization strategy in M2SL (ST1, ST2, ST3) and an implementation in Simulink®.

The inputs of the pulsatile model are $I_D = t_e$, PA (arterial pressure), PLA (left atrial pressure), PRA (right atrial pressure) and PPA (pulmonary arterial pressure) and its outputs O_D = QMI (flow through the mitral valve), QLO (flow through the aortic valve), QTR (flow through the tricuspid valve), QRO (flow through the pulmonary valve). In order to couple this model with elements in M_C, these I_D and O_D should be connected to the corresponding elements in I_C and O_C, defined previously, through coupling objects integrating appropriate transformations $T_{D,C}$ and $T_{C,D}$. The coupling of hemodynamic variables (pressures and flows) is relatively simple in this case, since they are represented with the same physical units in I_D, O_D, I_C and O_C. However, the temporal resolution of these variables in I_D and O_D is significantly different. A first approach, based on the application of a filter for the transformation of these variables has been presented in a previous work (HERNÁNDEZ et al., 2009).

In order to obtain pulsatile variables, a time-varying elastance formalism, including ventricular interaction as proposed by (SMITH et al., 2007) was used. Ventricular elastances vary between values obtained from the End Systolic Pressure-Volume Relationship and the End Diastolic Pressure-Volume Relationship (EDPVR). End systolic (P_{es}) and end diastolic (P_{ed}) pressures are defined as:

$$P_{\text{es}}(V) = E_{\text{es}}(V - V_d)\,, \tag{5.6}$$

$$P_{\text{ed}}(V) = P_{\text{o}}(e^{\lambda(V-V_{\text{o}})} - 1)\,, \tag{5.7}$$

where E_{es} is the end systolic elastance; V_d is the volume at zero pressure; P_0, λ, and V_0 are the parameters defining the EDPVR. The pressure-volume relationship of each ventricle is calculated by:

$$P(V) = e(t)P_{\text{es}}(V) + (1 - e(t))P_{\text{ed}}(V)\,, \tag{5.8}$$

where $e(t)$ represents the elastance function that will be defined later on. The septum is represented by a flexible common wall between the LV and the RV. The LV free wall volume

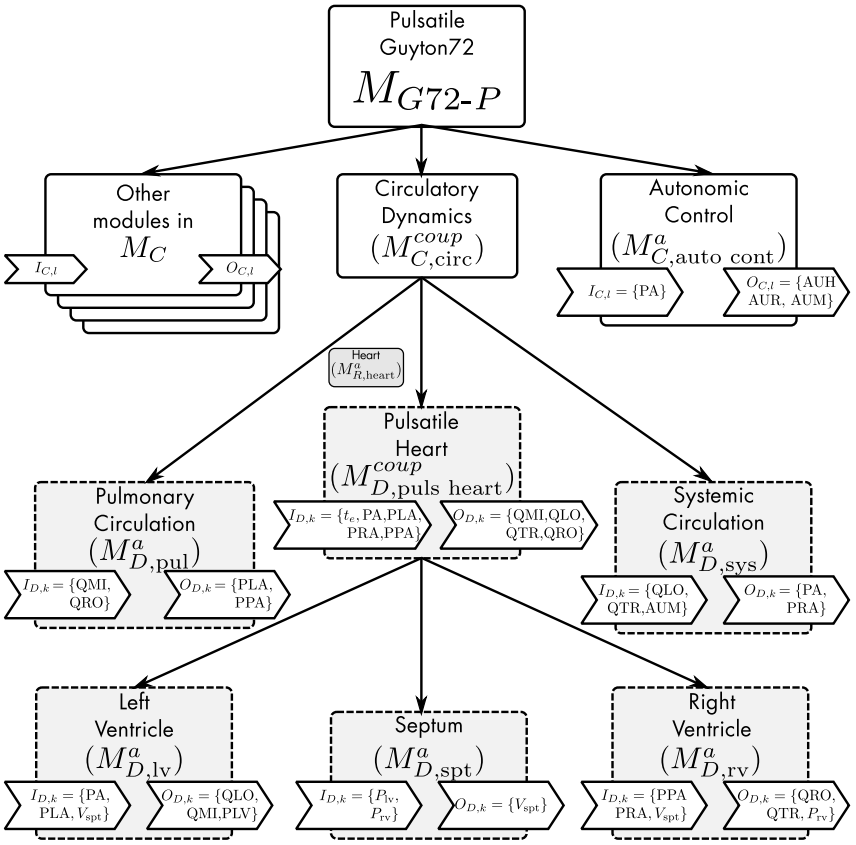

FIGURE 5.8– Integration of a pulsatile ventricular model into the original M_{G72}. White boxes represent models in M_C, gray boxes with continuous lines represent models in M_R, gray boxes with segmented lines represent models in M_D. Input and output variables of each model are shown as arrow-shaped boxes at the left and right sides of each box, respectively.

(V_{lvf}) and the RV free wall volume (V_{rvf}) are defined as:

$$V_{\mathrm{lvf}} = V_{\mathrm{lv}} + V_{\mathrm{spt}}\,, \tag{5.9}$$

$$V_{\mathrm{rvf}} = V_{\mathrm{rv}} - V_{\mathrm{spt}}\,, \tag{5.10}$$

where V_{spt}, V_{lv} and V_{rv} are respectively the septum, LV and RV volumes. The computation of the septum volume is the solution of the equation linking the septum pressure to the difference between left and right ventricular pressures:

$$P_{\mathrm{spt}} = P_{\mathrm{lv}} - P_{\mathrm{rv}}\,, \tag{5.11}$$

$$\begin{aligned} P_{\mathrm{spt}} = {} & e(t)E_{\mathrm{es,spt}}(V_{\mathrm{spt}} - V_{\mathrm{d,spt}}) \\ & + (1 - e(t))P_{0,\mathrm{spt}}(e^{\lambda(V - V_{\mathrm{o}})} - 1)\,, \end{aligned} \tag{5.12}$$

A second coupling interface deals with the modulation of the cardiac activity through continuous variables of the Guyton model representing the autonomic control of the chronotropic and inotropic effects (AUR_0, and AUH_0 respectively). Since AUR_0 and AUH_0 are dimensionless

variables, the following linear transformations are applied:

$$\mathrm{AUR} = S_{\mathrm{AUR}}(\mathrm{AUR}_0 - 1) + B_{\mathrm{AUR}}\,, \tag{5.13}$$

$$\mathrm{AUH} = S_{\mathrm{AUH}}(\mathrm{AUH}_0 - 1) + B_{\mathrm{AUH}}\,, \tag{5.14}$$

where S_{AUR} and S_{AUH} are sensitivity controllers and B_{AUR} and B_{AUH} are baseline controllers. These controller parameters have to be tuned to adjust the level of autonomic regulation. A transformation based on an Integral Pulse Frequency Modulation (IPFM) model (Rompelman et al., 1977) has been further defined to convert AUR into a series of pulses that will activate ventricular elastances. Each emitted pulse of the IPFM generates a variation of the ventricular elastance, which depends on AUR as follows:

$$e(t) = Ae^{-B(t_e \cdot \mathrm{AUR} - C)^2}\,, \tag{5.15}$$

where t_e is the time elapsed since the last activation pulse and $A = 1$; $B = 80\,\mathrm{s}^{-2}$ and $C = 0.27\,\mathrm{s}$ are the elastance parameters proposed in (Smith et al., 2007). Finally, the end-systolic elastance E_{es} is modulated by:

$$E_{\mathrm{es}} = \mathrm{AUH} \cdot E_{\mathrm{es0}}\,, \tag{5.16}$$

where E_{es0} is the basal value for the end-systolic elastance.

5.5.2 Identification of the controller parameters

Controller parameters P=[S_{AUR}, B_{AUR}, S_{AUH}, B_{AUH}] were identified by comparing the simulations obtained from the original Guyton model with those obtained from the proposed integrated, pulsatile model, during the 5 minute-simulation of a sudden severe muscle exercise, which is an original experiment described in the 1972 Guyton et al. paper (Guyton et al., 1972).

The error function g_ϵ, which is minimized during the identification process, is computed as:

$$g_\epsilon = \sum_{i=1}^{6} \sum_{n=1}^{N} \left| Y_j^{\mathrm{pulsatile}}(n) - Y_j^{\mathrm{original}}(n) \right| \tag{5.17}$$

where n is the sample index, N is the number of simulated samples (equivalent to 5 min at a sampling period of 10^{-2} min) and variables Y_j^{original} and $Y_j^{\mathrm{pulsatile}}$ correspond to detrended and scaled versions of the j-th output variable, obtained from the original and pulsatile versions of the model, respectively. The six output variables presented in fig. 5.9, which were validated against published data in (Hernández et al., 2009), have been selected to calculate g_ϵ. In order to identify P, an evolutionary algorithm (EA) has been applied, as explained in chapter 4. The repeatability of the obtained optimal parameters was assessed applying the identification method four times, with different initial populations.

5.5.3 Sensitivity Analysis

In order to assess the impact of integrating pulsatile ventricles, an input/output sensitivity analysis of the "Circulatory Dynamics" module was performed. A screening method, in particular

Table 5.1– Identified values for the sensitivity (S) and baseline (B) controllers for four realizations of the identification algorithm.

Parameter	Value	Parameter	Value
S_{AUR}	0.710 ± 0.017	B_{AUR}	0.870 ± 0.009
S_{AUH}	0.330 ± 0.028	B_{AUH}	0.290 ± 0.006

the Morris elementary effects method, was chosen because it provides information on nonlinearities and interactions between variables, with limited computational costs. Further details of these methods were presented in chapter 4.

5.5.4 Parameter identification and sensitivity analysis results

Table 5.1 shows the mean values and the standard deviations of the identified parameters obtained with the EA. Using these mean parameter values, fig. 5.9 shows the comparison of the output of the pulsatile and original models for the simulation of a sudden severe muscle exercise, used during the identification process. In order to facilitate the comparison between both model outputs, pulsatile variables have been low-pass filtered. A close match is observed between both simulations. The mean relative root mean squared error (rRMSE) equals 0.0025.

The proposed model provides simulations of pulsatile pressures and volumes for RV and LV. These variables do not exist in the original model. An example of these pulsatile variables is presented in fig. 5.10, with the simulation of ventricular Pressure-Volume (PV) loops, obtained by changing systemic resistance. The end-systolic PV relation has been found to be linear. These

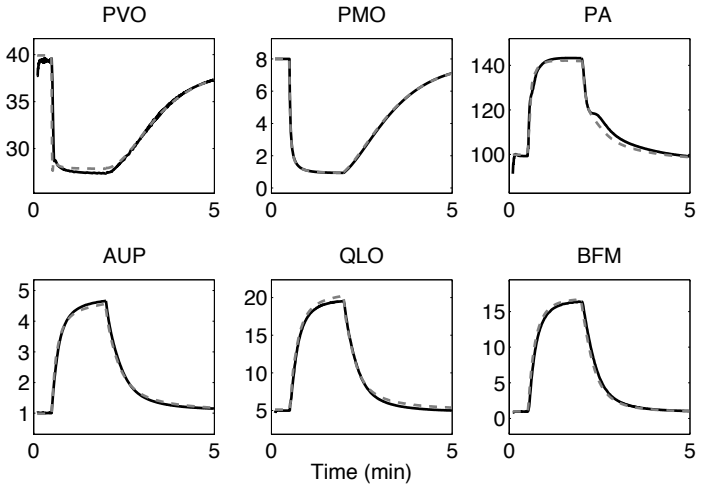

Figure 5.9– Comparison of the output of the pulsatile model (black curves) with the original Guyton model (dashed curves) during a 5 minute simulation of sudden severe muscle exercise. PVO (muscle venous oxygen pressure in mmHg), PMO (muscle cell oxygen pressure in mmHg), PA (mean arterial pressure in mmHg), AUP (sympathetic stimulation, ratio to normal), QLO (cardiac output in L/min) and BFM (muscle blood flow in L/min). Black lines are filtered versions of the pulsatile signals, obtained by integrating these signals on each cardiac cycle and dividing by the cardiac period.

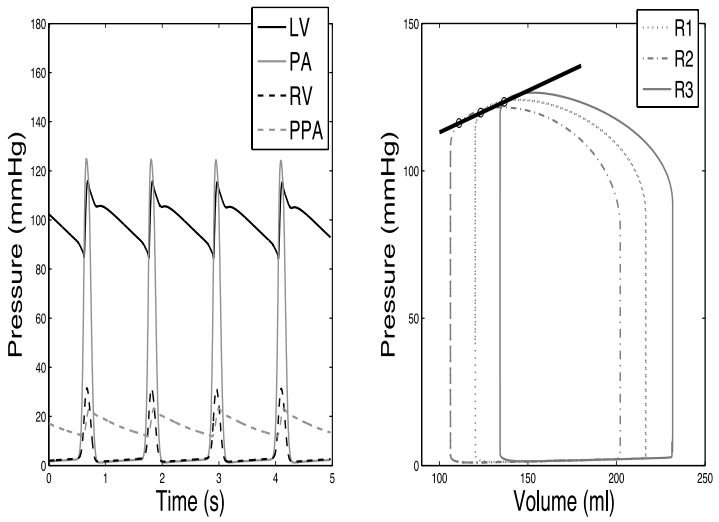

FIGURE 5.10– Simulations results obtained from the pulsatile model on LV and RV pressures, systemic (PA) and pulmonary (PPA) arterial pressures. PV loops are simulated using different values for the systemic resistance of the Guyton model (R1 = 11, R2 = 23 and R3 =46 mmHg min L^{-1}).

simulations are consistent with clinical observations (ARONEY et al., 1989).

Figure 5.11 shows the Morris input/output sensitivity results on the mean PA with $p = 20$ levels and $r = 5k$ realizations ($k = 16$ and $k = 17$ respectively for the original and pulsatile models). In both cases, the most influential inputs are the plasma volume (VP), the autonomic regulation of vasoconstriction on arteries (AUM) and the vascular volume caused by relaxation (VVR). A slightly higher sensitivity to inputs that modulate the systemic resistance (ANM, ARM and AMM) is observed on the pulsatile model. These factors are more influential than AUH_0, which is on the same sensitivity level in both models. This is mainly due to the more realistic response of the pulsatile model to changes in afterload.

5.6 Simulation of an acute decompensated heart failure (ADHF)

Figure 5.12 presents the main hemodynamic and regulatory variables represented in the proposed pulsatile model for the simulation of a stable HF state. At t =24 h of simulated time, parameter values E_{es0} and V_d were reduced ($E_{es0,lv}$ =0.7 mmHg mL^{-1}, $E_{es0,rv}$ =0.5 mmHg mL^{-1} and $V_{d,lv}$ =20 mL) to correspond to those observed from HF patients (ARONEY et al., 1989). This reduced ventricular function causes a sudden decrease of PA and cardiac output and a significant increase in atrial pressures and ventricular preload, leading to an accumulation of fluid on the systemic and pulmonary spaces. In order to compensate for this hemodynamic response, neurohumoral regulations are initiated with a fast autonomic modulation (AU), combined with the slower response of the renin-angiotensin system (ANM). A stable HF state is reached, with

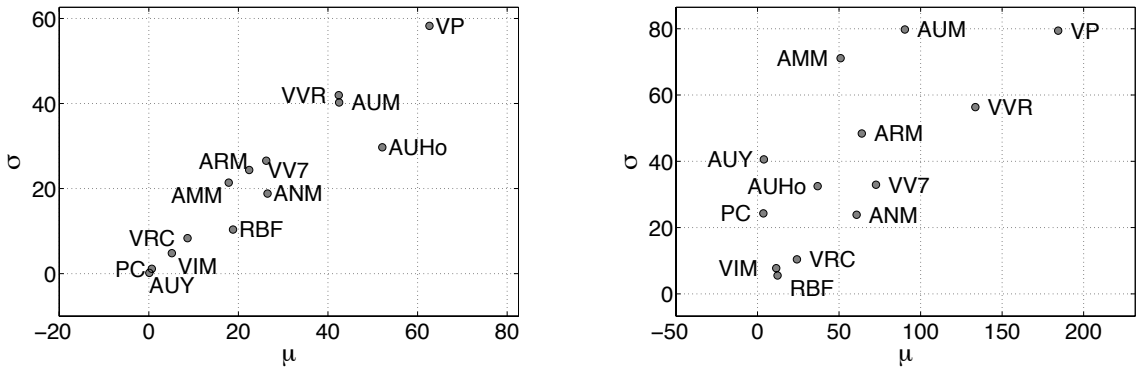

(a) Original Guyton model

(b) Pulsatile Guyton model

Figure 5.11– Morris sensitivity results for the arterial pressure obtained by the original and pulsatile models. The parameters included in the analysis were: HPL (hypertrophy effect on LV), HPR (hypertrophy effect on RV), VP (plasma volume), VVR (basic venous volume), AUH0 (autonomic effect on heart strength), AUM (sympathetic vasoconstrictor effect on arteries), ARM (non-muscle global autoregulation multiplier), AMM (muscle autoregulation multiplier), RBF (renal blood flow), VRC (volume of red blood cells), VV7 (vascular volume due to short-term stress relaxation), ANM (general angiotensin multiplier effect), PC (capillary pressure), AUY (sensitivity of sympathetic control of veins), VIM (blood viscosity effect on resistance), HMD (cardiac depressant effect of hypoxia).

an increased sympathetic tone, fluid retention and reduced PA and cardiac output.

Finally, the simulation of an ADHF event is shown in fig. 5.13. The simulation starts from a stable HF state obtained, for example, after implanting a CRT device. A sudden desynchronization of both ventricles (inter-ventricular delay = 200 ms) is simulated at time $t = 5$ min. This event reproduces a sudden loss of capture of the LV lead that can be observed on CRT patients due to lead displacement. The model response presents a decreased PA and a regulatory response which are in accordance with clinical observations (Whinnett et al., 2006).

5.7 Conclusion

This chapter presents an example of temporal multiscale integration in which the non-pulsatile ventricles of the original Guyton model are replaced by a pulsatile, elastance-based model of the cardiac function. In order to perform this integration, the interfacing method, proposed in chapter 3, is applied to couple these heterogeneous models. Although the proposed model is already useful for analyzing the main interaction effects that may be considered for the development of new ADHF detection methods, it still has to be improved and validated. To that end, an initial validation of some model components, such as the reproduction of patient-specific trans-valvular flows for different cardiac resynchronization therapy (CRT) pacing configurations using the time-varying elastance model with pulsatile atria and ventricles has been undertaken in chapter 7 (Ojeda et al., 2013). Moreover, the proposed interfacing approach has been applied to integrate improved versions of other important components of the model, such as the renin angiotensin system (Guillaud et al., 2010). The validation of the global, interconnected model

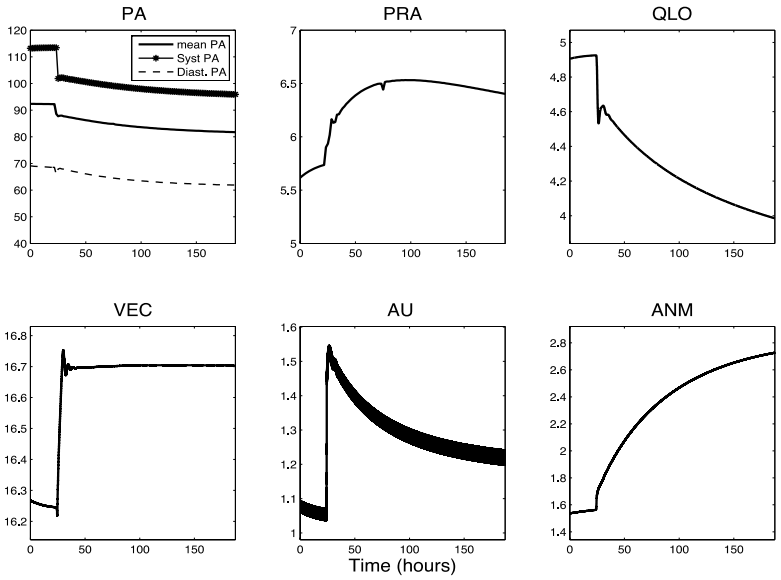

FIGURE 5.12– Simulation of a heart failure state. PA (arterial pressure in mmHg), PRA (mean right atrial pressure in mmHg), QLO (cardiac output in L/min), VEC (extracellular fluid volume in L), AU (autonomic activity, ratio to normal), ANM (angiotensin multiplier effect, ratio to normal).

is a challenging task, mainly because of observability limitations in long-term monitoring. The data captured from new-generation CRT devices will be useful to tackle this issue.

References

ARONEY, C. N., H. C. HERRMANN, M. J. SEMIGRAN, G WILLIAM, C. A. BOUCHER, and M. A. FIFER (1989). "Linearity of the left ventricular end-systolic pressure-volume relation in patients with severe heart failure". In: *Journal of the American College of Cardiology* 14.1, pp. 127–134.

GUILLAUD, F. and P. HANNAERT (2010). "A computational model of the circulating renin-angiotensin system and blood pressure regulation". In: *Acta biotheoretica* 58.2-3, pp. 143–170.

GUYTON, A., T. COLEMAN, and H. GRANGER (1972). "Circulation: overall regulation". In: *Annual review of physiology* 34.1, pp. 13–44.

HERNÁNDEZ, A. I., V. LE ROLLE, A. DEFONTAINE, and G. CARRAULT (2009). "A multiformalism and multiresolution modelling environment: application to the cardiovascular system and its regulation". In: *Philos Transact A Math Phys Eng Sci* 367.1908. PTRSA, pp. 4923–4940. DOI: 10.1098/rsta.2009.0163.

HERNÁNDEZ, A. I., V. LE ROLLE, D. OJEDA, P. BACONNIER, J. FONTECAVE-JALLON, F. GUILLAUD, T. GROSSE, R. G. MOSS, P. HANNAERT, and S. R. THOMAS (2011). "Integration of detailed modules in a core model of body fluid homeostasis and blood pressure regulation". In: *Progress in Biophysics and Molecular Biology* 107, pp. 169–182. DOI: 10.1016/j.pbiomolbio.2011.06.008.

IKEDA, N., F. MARUMO, M. SHIRATAKA, and T. SATO (1979). "A model of overall regulation of body fluids". In: *Annals of biomedical engineering* 7.2, pp. 135–166.

KOFRÁNEK, J and J RUSZ (2010). "Restoration of Guyton s diagram for regulation of the circulation as a basis for quantitative physiological model development". In: *Physiological Research* 59.6, pp. 897–908.

MONTANI, J. P. and B. N. VAN VLIET (2009). "Understanding the contribution of Guyton's large circulatory model to long-term control of arterial pressure". In: *Exp. Physiol.* 94, pp. 382–388.

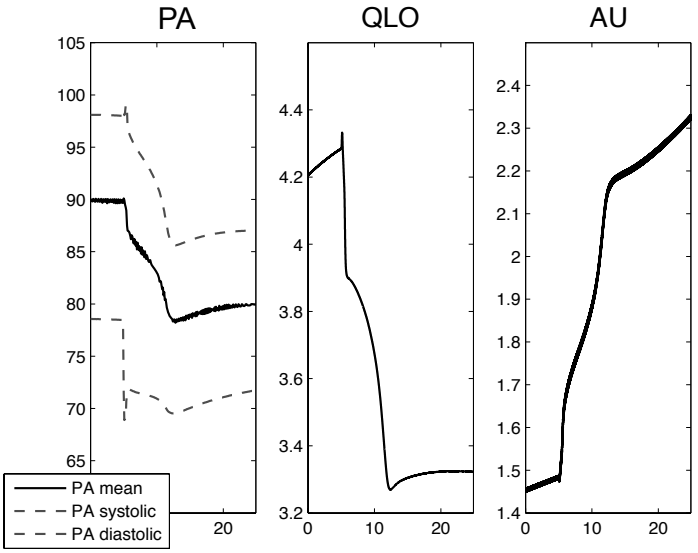

Figure 5.13– Simulation of a heart failure state. PA (arterial pressure in mmHg), PRA (mean right atrial pressure in mmHg), QLO (cardiac output in L/min), VEC (extracellular fluid volume in L), AU (autonomic activity, ratio to normal), ANM (angiotensin multiplier effect, ratio to normal).

Montani, J., T. Adair, R. Summers, T. Coleman, and A. Guyton (1989). "A simulation support system for solving large physiological models on microcomputers". In: *International journal of bio-medical computing* 24.1, pp. 41–54.

Ojeda, D., V. Le Rolle, K. Tse Ve Koon, C. Thebault, E. Donal, and A. I. Hernández (2013). "Towards an atrio-ventricular delay optimization assessed by a computer model for cardiac resynchronization therapy". In: *Proceedings of the 9th International Seminar on Medical Information Processing and Analysis*. Ed. by S. D. Library.

Remme, W and K Swedberg (2002). *Recommandations pour le diagnostic et le traitement de l'insuffisance cardiaque chronique, société européenne de cardiologie*. 95. Archives des Maladies du coeur et des vaisseaux, pp. 5–53.

Rompelman, O, A. Coenen, and R. Kitney (1977). "Measurement of heart-rate variability—part 1: comparative study of heart-rate variability analysis methods". In: *Medical and Biological Engineering and Computing* 15.3, pp. 233–239.

Smith, B., S. Andreassen, G. Shaw, P. Jensen, S. Rees, and J. Chase (2007). "Simulation of cardiovascular system diseases by including the autonomic nervous system into a minimal model". In: *Computer methods and programs in biomedicine* 86.2, pp. 153–160.

Thomas, S. R., P. Baconnier, J. Fontecave, J.-P. Françoise, F. Guillaud, P. Hannaert, A. Hernández, V. Le Rolle, P. Mazière, F. Tahi, et al. (2008). "SAPHIR: a physiome core model of body fluid homeostasis and blood pressure regulation". In: *Philosophical Transactions of the Royal Society A: Mathematical, Physical and Engineering Sciences* 366.1878, pp. 3175–3197.

Werner, J, D Böhringer, and M Hexamer (2002). "Simulation and prediction of cardiotherapeutical phenomena from a pulsatile model coupled to the Guyton circulatory model". In: *IEEE Trans Biomed Eng* 49.5, pp. 430–439. doi: 10.1109/10.995681.

Whinnett, Z. I., J. E. Davies, K Willson, C. H. Manisty, A. W. Chow, R. A. Foale, D. W. Davies, A. D. Hughes, J Mayet, and D. P. Francis (2006). "Haemodynamic effects of changes in atrioventricular and interventricular delay in cardiac resynchronisation therapy show a consistent pattern: analysis of shape,

magnitude and relative importance of atrioventricular and interventricular delay". In: *Heart* 92.11, pp. 1628–1634. DOI: 10.1136/hrt.2005.080721.

CHAPTER 6

Patient-specific modeling and parameter analysis of the coronary circulation

Résumé

Ce chapitre présente la deuxième application clinique de cette thèse qui est l'analyse à base de modèles de la circulation coronarienne lors d'atteintes tritronculaires. L'objectif est notamment d'étudier l'importance de l'hétérogénéité de la circulation collatérale dans cette pathologie. Les analyses de sensibilités réalisées sur les paramètres du modèle ont mis en évidence l'importance de ces vaisseaux collatéraux ainsi que certains paramètres hémodynamiques. Par ailleurs, la méthode d'identification spécifique-patient a pu être appliquée à l'analyse des données obtenues lors de procédures de pontages coronariens. Les résultats présentés reproduisent de manière satisfaisante les données mesurées pendant la chirurgie et le développement de la circulation collatérale a pu être évalué pour chaque patient.

In this chapter, we will present an example of a modeling application and model-based analysis of an impaired coronary circulation due to coronary artery disease (CAD). This study is the one of the three applications of this thesis based on patient-specific modeling, using the methods presented in chapter 2 and taking advantage of the parameter analysis tools provided by M2SL, as explained in chapters 3 and 4. The content of this chapter is based on the related publication (Ojeda et al., 2013).

6.1 Coronary circulation

6.1.1 Physiopathological aspects

The coronary circulation is the part of the systemic circulation that provides blood to the cardiac muscle, supplying the heart the necessary oxygen and nutrients to guarantee its

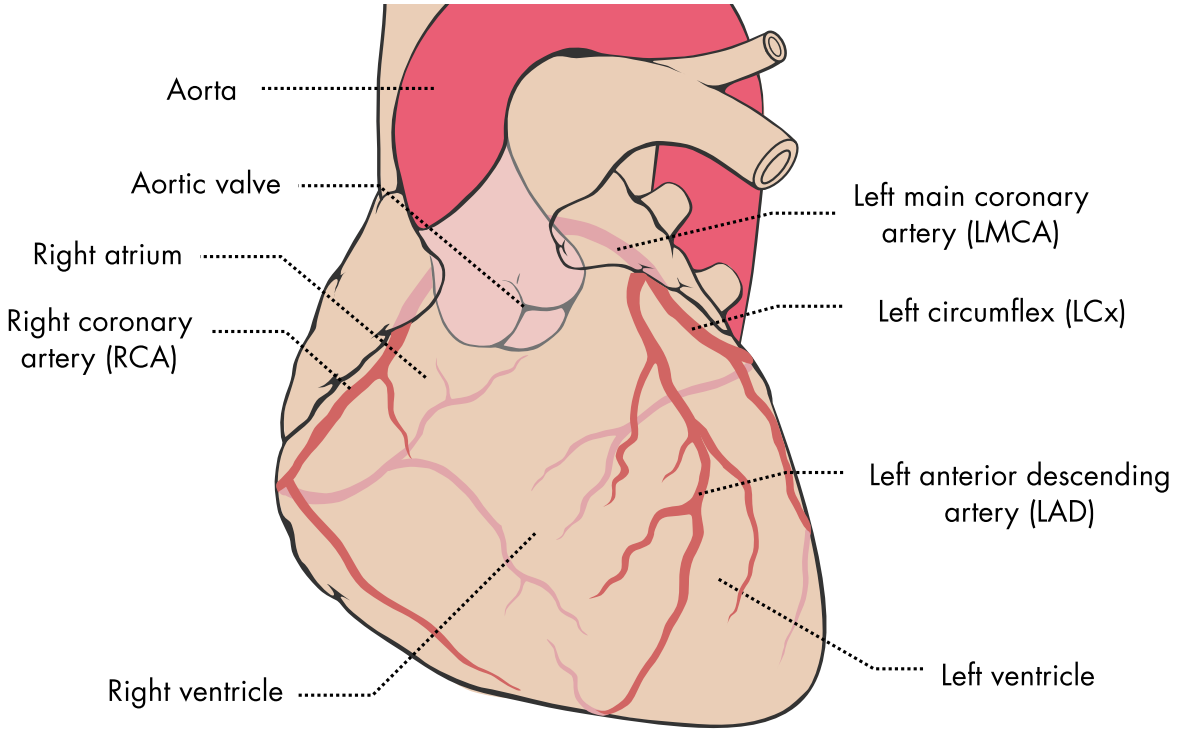

FIGURE 6.1– The heart and its coronary circulation, including the main coronary arteries. Based and modified from Patrick J. Lynch, Wikimedia Commons.

continuous contraction cycle. The human coronary circulation, illustrated in fig. 6.1, starts from two arteries originating early in the aorta, above the semilunar valve. The right coronary artery (RCA) descends through the coronary sulcus, supplying most of the right ventricle and the posterior part of the left ventricle in most cases; the structure of the coronary circulation tree can vary among individuals. The left main coronary artery (LMCA) also arises next to the aortic valve and it quickly bifurcates into the left anterior descending artery (LAD, also called anterior intraventricular artery) and the left circumflex artery (LCx). These arteries continue to branch further and, in most people, supply the anterior and left lateral portions of the left ventricle. From the main arteries, which lie on the surface of the heart, smaller intramuscular arteries penetrate the muscle, dividing further into arterioles and capillaries, supplying most of the myocardial muscle. Finally, these vessels pour into venules and the into larger veins, joined together at the coronary sinus and lastly opening directly into the right atrium.

This coronary circulation is a unique system of the cardiovascular, not only because its efficiency directly affects the cardiac activity, but also because the blood flow is in turn affected by cardiac contraction. In fact, the coronary circulation presents a particular phasic flow profile: during systole, the coronary blood flow experiences a sudden drop caused by the strong compression of the ventricles and the collapse of intramuscular vessels (SABISTON et al., 1957). When the myocardium relaxes, the forward coronary flow is reestablished and increases quickly; most of the coronary flow occurs during diastole, as illustrated in fig. 6.2. However, the amplitude of the left and right coronary phasic profiles are not equivalent, mostly because the left coronary

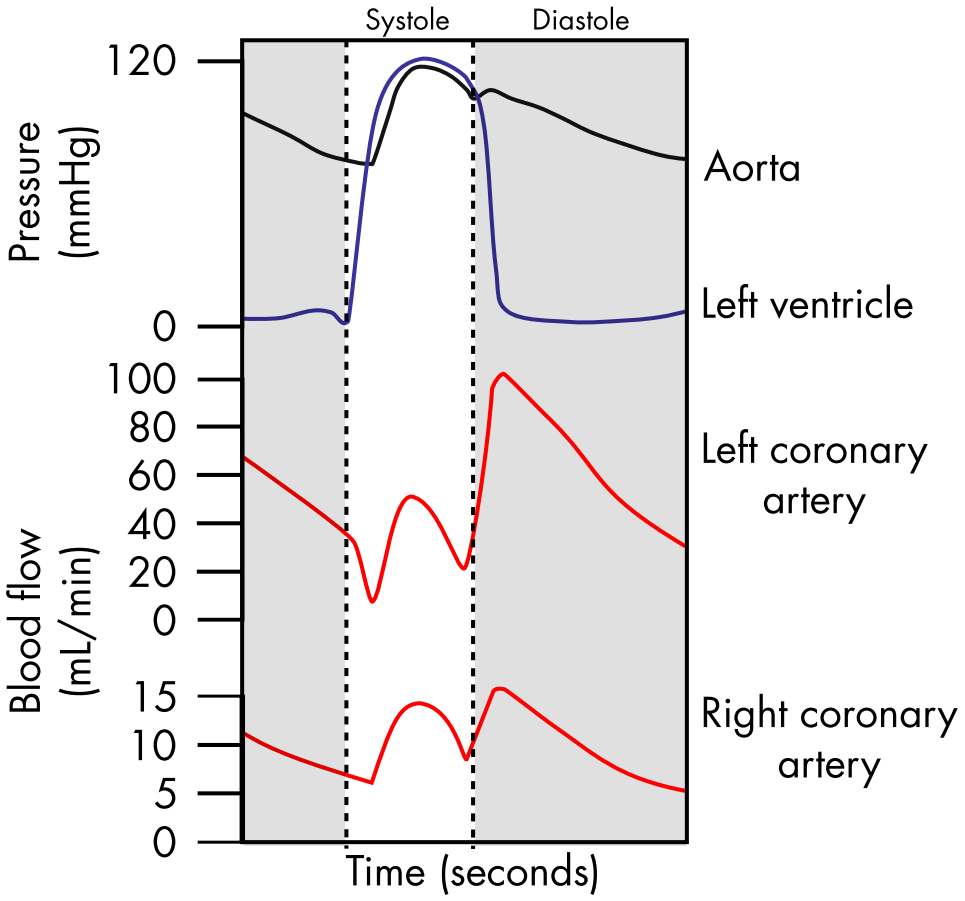

FIGURE 6.2– Typical coronary artery flow, with corresponding aortic and ventricular pressure. During systole, coronary flow drops. Then, it increases rapidly in diastole.

arteries supply the much stronger left ventricle (GUYTON et al., 2005).

The accumulation of plaque in the coronary arteries, i.e. coronary artery disease, represents one of the leading causes of morbidity and mortality worldwide (FINEGOLD et al., 2012; WHO, 2008). Intra-coronary plaque accumulation leads to protrusions inside the arteries, producing a pathological narrowing of the coronary arteries (stenoses) and therefore reducing or completely interrupting blood flow. The myocardial tissue irrigated downstream from stenotic lesions will receive an insufficient blood supply, leading to myocardial ischemia (with possible myocardial hibernation and contractile dysfunction (HEUSCH et al., 2005)) or even an infarction.

In the case of triple-vessel disease, the right coronary artery is completely occluded, while the left arteries present partial stenoses. Even thought there are several therapeutic treatments, the recommended guidelines for patients with complete stenoses suggest a treatment based either on coronary angioplasty or coronary artery bypass graft (CABG) surgery (MOHR et al., 2013). However, triple-vessel disease patients often present a developed network of alternative vessels

that perfuse the myocardial regions that have been affected for a considerable time (ABOULIATIM, 2011). While the benefit of the consideration of these collateral vessels is still controversial (STEG et al., 2010), they can be useful in delicate patients, where the number of bypasses should be limited.

6.1.1.1 Collateral circulation

The emergence of the collateral circulation to perfuse areas affected by occlusions is a very debated topic. On one hand, when an occlusion of a large coronary artery occurs rapidly, an autoregulatory mechanism dilates small anastomoses within seconds and a relatively low flow is maintained up to 24 hours. After approximately a month, collateral flow attains a normal coronary flow. On the other hand, when the narrowing of the artery occurs slowly over some years, the collateral vessels show a development in parallel to the gradual decline of the arterial occlusion (GUYTON et al., 2005). Moreover, the presence of small collaterals from birth has been observed in the normal human heart (KOERSELMAN et al., 2003).

The origin and development of collateral vessels depends on different trigger factors such as increase of pressure gradient, ischemia, wall shear stress, and complex endothelial mechanisms thoroughly explained in (SCHAPER, 2009). Although their impact on CAD is still controversial, clinical studies have shown a correlation between collateral circulation and myocardial sensitivity to ischemia (SCHAPER, 2009; SEILER, 2003). In fact, the collateral development has been shown to be an relevant factor on the recovery of the infarcted left ventricle after reperfusion (LEE et al., 2000) and it helps prevent left ventricular aneurysms (HIRAI et al., 1989). Unfortunately, the collateral perfusion is difficult to assess directly (BERRY et al., 2007; WERNER et al., 2003) and, consequently, collateral perfusion is still poorly understood (WATERS et al., 2011).

6.1.2 Modeling coronary vascular dynamics: state of the art

Motivated by the worldwide impact of heart disease, and admitting that the coronary circulation is a complex system, in silico modeling has been consistently used with the clinical goal of developing patient-specific models to improve the diagnosis, therapy and treatment of these pathologies (SIEBES et al., 2010). To achieve this goal, as in every physiological modeling application, one needs to characterize the coronary circulation and examine the underlying mechanisms that occur in different physical and temporal references (WATERS et al., 2011). Indeed, the phenomena associated with coronary circulation can be situated from a cellular, up to a organ scale, while the temporal scales of its underlying processes can vary from seconds (e.g. a cardiac cycle) to years (e.g. plaque formation or vascular remodeling).

A comprehensive description of the current state of coronary vascular modeling can be found in (LEE et al., 2012; WATERS et al., 2011). These authors summarize current coronary modeling efforts in various sub-disciplines whose objectives are the description of: *1)* coronary vascular structure, the characterization of the structure of the vessels, *2)* mechanical properties of the coronary vasculature and its surrounding tissues, including the myocardium, large coronary

arteries and venous system, *3)* blood flow, whose characteristics vary from large coronary arteries to the microcirculation, *4)* oxygen transport and diffusion processes, *5)* regulation mechanisms that assure a blood flow that meets the metabolic requirements of the cardiac muscle, *6)* angiogenesis, the gradual development and remodeling of the coronary vessels, *7)* vascular cellular mechanics, the process where endotelial cells react to local fluid dynamics (e.g. shear stress) and respond with lumen diameter modifications and the emission of biochemical signals that have an important effect on other phenomena. The variety and interaction of different mechanisms make the coronary circulation a suitable field for model integration efforts, such as the cardiac Physiome project (Bassingthwaighte et al., 2009).

For the clinical application of this chapter, we will focus on the blood flow dynamics of various vessels. A wide range of computational models of blood flow dynamics has been proposed in the literature, at different levels of detail (Lee et al., 2012), from lumped-parameter (0D) representations, through pulse-wave propagation (1D) dynamics and full detailed, anatomically-based 3D computational fluid dynamics models. Although most recent coronary blood flow modeling efforts have been directed towards the more detailed models (Waters et al., 2011), the lumped-parameter approach remains a useful element in the multiscale vascular modelling for retaining the computational tractability, as demonstrated by a number of recent works (Lee et al., 2012). Lumped-parameter representations of blood flow and pressure dynamics, such as Windkessel models, capture the main characteristics based on an electrical circuit analogy (Sagawa et al., 1990), while providing an abstraction that is easy to understand, uses few parameters, and provides a good compromise between computational cost and accuracy (Olufsen et al., 2004).

Among the publications that use Windkessel models of the coronary circulation, Wang et al. proposed a representation of the left coronary tree and its branches, while integrating the effect of stenoses on blood flow and the systolic flow drop that characterizes the coronary blood flow (Wang et al., 1989). Later, (Pietrabissa et al., 1996) extended this approach with revascularisations through coronary bypass grafts and applying an intra-myocardial pump model (Spaan et al., 1981) to explain the systolic flow. However, none of these models consider the blood supply through collateral circulation, which is often present in patients with CAD.

6.2 Problem statement

Computational models willing to represent CAD should include the collateral vessels. Previous works have proposed an extension of the model in (Pietrabissa et al., 1996), by integrating collateral circulation and the right coronary artery (Maasrani et al., 2008). Also, an initial validation of the proposed model in the CAD context has been performed, by reproducing the mean blood flows and pressures obtained from clinical data (Maasrani et al., 2011). However, this validation was based on the unrealistic assumption that all collateral vessels presented the same characteristics (i.e. with the same model parameters), independently of the myocardial region they irrigate. In fact, clinical trials suggest that CAD patients can develop collaterals with different structures and development (Werner et al., 2003), depending on factors such as

stenosis severity, ischemic episodes, etc.

The objective of the modeling application presented in this chapter is to extend the model mentioned above by integrating collateral vessels (MAASRANI et al., 2011), with an emphasis on the analysis of the effect of heterogeneous parameters on the collateral network. This extension was based on an exhaustive sensitivity analysis of the model, followed by an advanced parameter-estimation method designed to provide a model-based, patient-specific estimation of the collateral development for patients suffering triple-vessel disease. The clinical objective of the proposed approach is to help with the assessment of the development and influence of the coronary collateral circulation, which may be useful for the clinicians for the followup and post-operatory treatment choices. In the long-term, this work intends to provide new elements and insight towards a pre- and per-operatory assistance to CABG.

6.3 Materials and methods

6.3.1 Clinical measurements

The clinical data used in this study was obtained during an off-pump coronary surgical procedure, thoroughly described in previous publications of our team (CORBINEAU et al., 2001). Pre-operative data, presented in previous publications (ABOULIATIM et al., 2011; MAASRANI et al., 2011) and summarized in table 6.1, consist of artery diameter reductions due to stenoses, estimated with bi-plane angiographies. Additionally, a visual estimation of collateral filling, shows the Rentrop classification (RENTROP et al., 1985) of each patient (0: no observable filling due to collaterals, 1: observable filling of the distal branches without filling on the epicardial segment, 2: partial filling on the epicardial segment, and 3: complete filling due to collaterals). Intra-operative data consist of pressure and flow measurements, acquired at different places of the coronary tree during the revascularization surgery on ten patients with a chronic occlusion of the right coronary artery (RCA) and stenoses on the left main coronary artery (LMCA), left anterior descending (LAD) and left circumflex (LCx) (fig. 6.3).

During the CABG surgery, patients are artificially ventilated, anesthetized and under the effect of glyceryl trinitrate, a potent vasodilator. Mean arterial pressure is measured with a radial catheter, and mean blood flows are measured using a transit time ultrasonic flow meter (Medistim Butterfly Flowmeter 2001) under different graft configurations (from here on denoted *cases*) explained next. First, the perfusion of RCA is reestablished with a saphenous vein graft (RCAg) from the aorta. At this moment, the graft is clamped while the aortic pressure (P_{ao}), central venous pressure (P_{v}) and pressure distal to the RCA occlusion (P_{w}) are measured simultaneously (case 0G). Then, the graft is opened (case 1G) to measure P_{ao}, P_{v}, and the blood flow across the graft (Q_{RCAg}). Afterwards, the left coronary arteries are revascularized with two internal thoracic artery grafts (LADg and LCxg) from the aorta to the LAD and LCx. The same variables are measured with the right graft clamped (case 2G), but including also the blood flow across the left grafts (Q_{LCxg} and Q_{LADg}). Finally, when all the grafts are in place and

TABLE 6.1– Pre-operative data obtained for ten patients with triple vessel disease: percentage of area reduction of stenosed arteries and Rentrop grade (0–3) of the right coronary artery. Stenosis data extracted from (MAASRANI et al., 2011). Rentrop evaluation extracted from (ABOULIATIM et al., 2011).

Patient	**LMCA (%)**	**LAD (%)**	**LCx (%)**	**Rentrop grade**
1	26	99	90	3
2	46	89	95	2
3	92	85	96	3
4	19	86	97	3
5	20	88	92	3
6	85	94	82	2
7	80	0	85	3
8	87	70	90	1
9	83	78	0	1
10	75	93	0	2

opened, all pressure and blood flow measurements are repeated (case 3G). All intra-operative data are the mean value after hemodynamic stabilization, summarized in table 6.2.

6.3.2 Model description

As mentioned before, the model used in this application is directly based on the publication by Maasrani et al. (MAASRANI et al., 2011), represented in fig. 6.5 and implemented using the M2SL simulation library described in chapter 4. In this model, each coronary artery is associated with an RLC circuit as shown in fig. 6.4. The flow dynamics of an artery are described by the following differential equations:

$$L\frac{dQ_1}{dt} = P_1 - P_2 - Q_1 R\,, \tag{6.1}$$

$$C\frac{dP_2}{dt} = Q_1 - Q_2\,, \tag{6.2}$$

a description that takes into account the resistance to the flow due to friction, the inertia of the flow and volume changes explained by the elasticity of the vessel walls.

Coronary arterioles and capillaries (LADc, RCAc, LCxc) and collateral vessels (col1 to col5) are represented by a lumped resistance [1], since resistive effects for these small diameters overwhelm the inertia and elasticity dynamics (OLUFSEN et al., 2004). Collateral vessels are expected to exist in the five locations shown in fig. 6.3, a configuration that resembles a similar study in (ROCKSTROH et al., 2002). However, they can also be undeveloped, which would be represented by a very high value of the collateral resistance.

Parameter values related to arteries and grafts (R, L and C) are extracted from previous works by (PIETRABISSA et al., 1996). These values are calculated from the vessel length (L) and

1. Note that for this application, the term *capillary resistances* is used to refer to the lumped resistance of the coronary arteriolar networks.

TABLE 6.2– Intra-operative data of ten patients with triple vessel disease. Mean aortic pressure (P_{ao}), venous pressure (P_v) and coronary wedge pressure (P_w) are expressed in mmHg. Mean graft flows in the right graft (Q_{RCAg}), left graft to anterior descending (Q_{LADg}) and left graft to circumflex (Q_{LCxg}) are measured in mL/min.

Patient	**Case**	P_{ao}	P_v	P_w	Q_{RCAg}	Q_{LADg}	Q_{LCx}
1	0G	60	3	35	—	—	—
	1G	66	2	—	35	—	—
	2G	51	0	31	—	34	27
	3G	61	1	—	66	40	14
2	0G	85	9	49	—	—	—
	1G	85	8	—	45	—	—
	2G	82	13	49	—	23	32
	3G	86	13	—	45	21	19
3	0G	85	6	40	—	—	—
	1G	85	7	—	28	—	—
	2G	80	7	40	—	22	48
	3G	85	7	—	74	19	45
4	0G	75	9	43	—	—	—
	1G	79	10	—	11	—	—
	2G	69	10	42	—	59	40
	3G	75	11	—	26	57	30
5	0G	77	5	53	—	—	—
	1G	76	5	—	63	—	—
	2G	61	3	36	—	24	56
	3G	67	2	—	69	18	46
6	0G	78	6	35	—	—	—
	1G	65	6	—	18	—	—
	2G	70	6	28	—	11	12
	3G	64	5	—	30	14	18
7	0G	83	14	29	—	—	—
	1G	82	14	—	53	—	—
	2G	88	14	40	—	28	43
	3G	78	13	—	51	28	29
8	0G	76	6	46	—	—	—
	1G	76	6	—	9	—	—
	2G	68	6	43	—	38	16
	3G	64	6	—	10	28	17
9	0G	70	14	37	—	—	—
	1G	70	14	—	60	—	—
	2G	70	14	40	—	24	60
	3G	82	13	—	51	23	45
10	0G	64	10	47	—	—	—
	1G	64	10	—	11	—	—
	2G	64	10	48	—	20	7
	3G	60	10	—	14	18	13

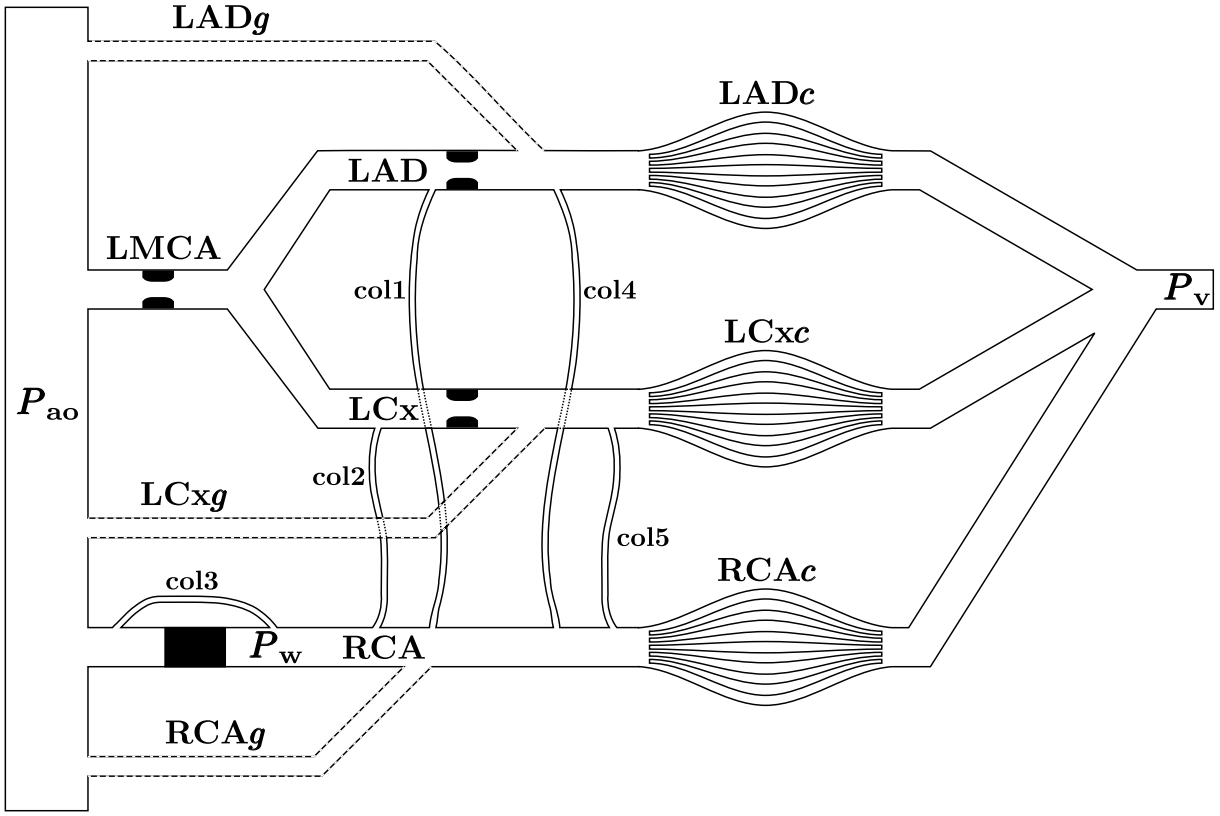

FIGURE 6.3– Hemodynamic diagram of the coronary circulation of a patient with triple-vessel disease. A complete occlusion of the RCA is represented with a filled black box. Stenoses, represented with rounded black boxes, are present in the LMCA, LAD and LCx. Grafts implanted during the CABG surgery are represented with segmented lines.

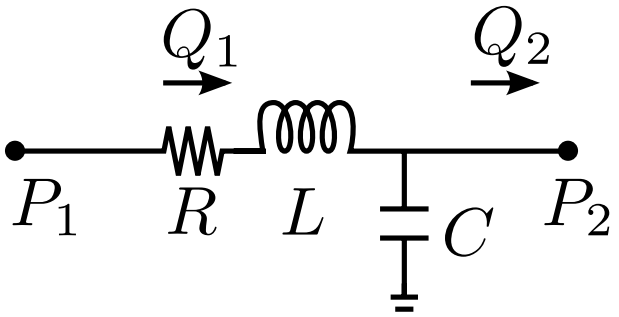

FIGURE 6.4– Lumped parameter model of an artery. The input pressure P_1 and outflow Q_2 are known.

diameter (D) using the Hagen–Poiseuille law, which assumes a laminar flow:

$$\begin{aligned} R &= \frac{128\mu L}{\pi D^4}\,, \\ L &= \frac{4\rho L}{\pi D^2}\,, \\ C &= \frac{\pi D^3 L}{4Eh}\,, \end{aligned} \tag{6.3}$$

where μ ($4 \times 10^{-3}\,\mathrm{kg\,m\,s}$) stands for blood viscosity, E ($2 \times 10^5\,\mathrm{Pa}$) is the elastic modulus of the

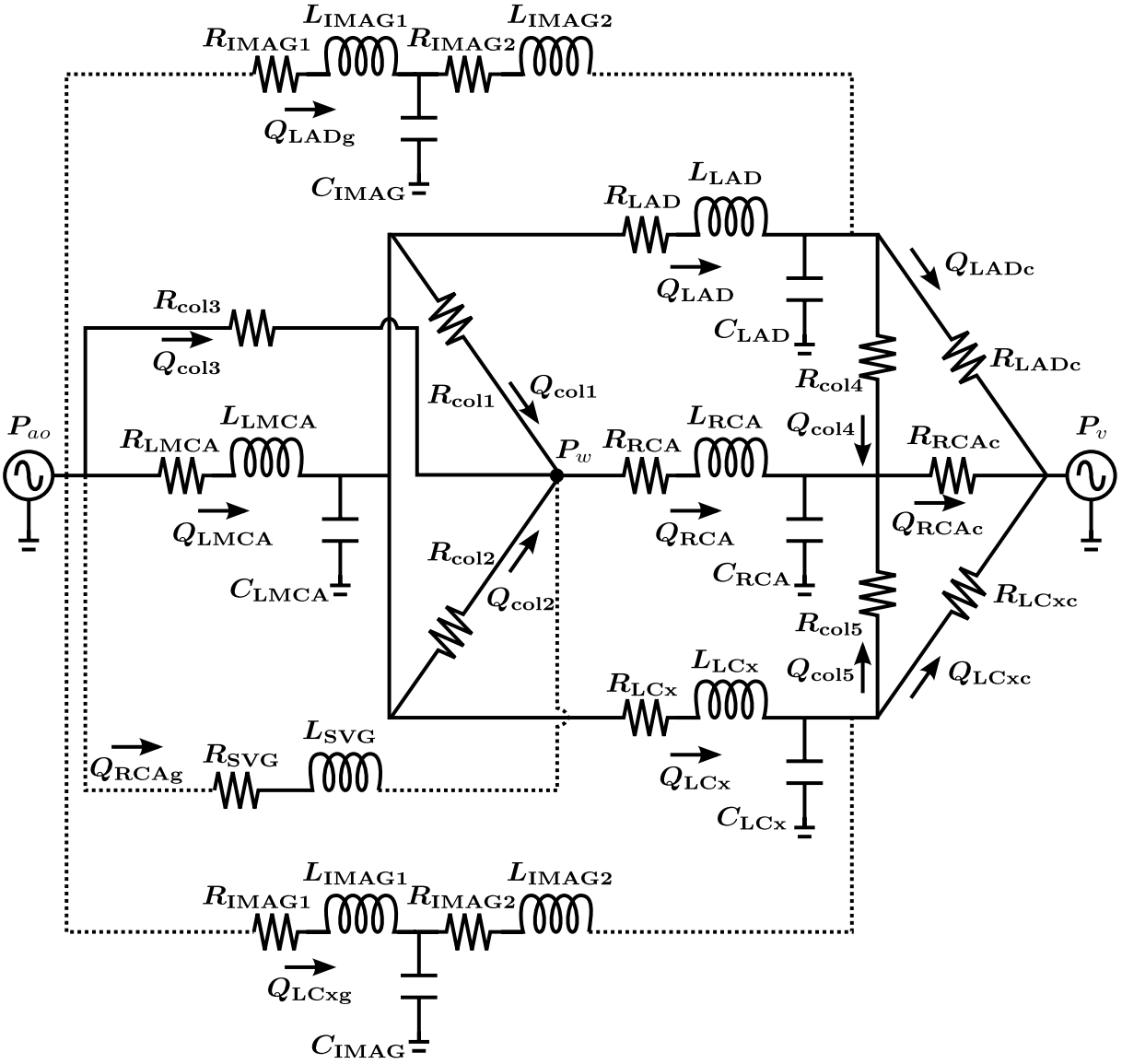

FIGURE 6.5– Model of the coronary circulation.

vessel wall, ρ ($1 \times 10^3\,\mathrm{kg\,m^{-3}}$) is the blood density, and h is vessel wall thickness. Although patient-specific values for these parameters can be estimated with a pre-operatory angiography, these measurements were not available for the ten patients considered here. In exchange, values from (PIETRABISSA et al., 1996) were used directly, summarized in table 6.3. Nevertheless, patient-specific area reductions due to stenoses were used to adjust the RLC parameters, following the transformation proposed in (WANG et al., 1989):

$$\begin{aligned} R_{\mathrm{stenosis}} &= R\alpha^{-2}\,, \\ L_{\mathrm{stenosis}} &= L\alpha^{-1}\,, \\ C_{\mathrm{stenosis}} &= C\alpha^{3/2}\,. \end{aligned} \tag{6.4}$$

with $\alpha = 1 - p_{\mathrm{stenosis}}$, where p_{stenosis} is the percentage of area reduction due to stenosis (scaled

to one), available in table 6.1. Lastly, parameters associated with small arteries will be identified from clinical data.

Knowing the values of the parameters described below, and using the aortic (P_{ao}) and venous (P_v) pressure inputs, blood flows and pressures can be simulated across all arteries, capillaries, collaterals and grafts, including the total coronary flow (Q_t) as the sum of blood flows through all capillaries.

TABLE 6.3– Parameter values for vessels of the coronary model.

Vessel	**Resistance** mmHg s/mL	**Inductance** mmHg s^2/mL	**Capacitance** mL/mmHg
LMCA	0.1	0.02	0.002
LAD	0.5	0.03	0.0015
LCx	0.3	0.02	0.0011
RCA	0.3	0.02	0.0008
IMAGI	1.4	0.08	0.0054
IMAGII	5.3	0.17	
SVG	0.2	0.04	

One of the most important features of this model is the integration of the collateral vessels as resistances (R_{col}). Previous works were based on the assumption that all R_{col} are equal (homogeneous collateral development). However, recent clinical trials have shown that CAD patients present an heterogeneous collateral development (WERNER et al., 2003), which depend on several factors, such as the vascularisation of the coronary circulation, development and severity of stenoses, duration of ischemic episodes, metabolic disorders, among others (SEILER, 2003). For this application, a study the effect of this heterogeneous collateral development is presented through a sensitivity analysis of the model. Moreover, a more flexible model-based method is used to estimate patient-specific collateral developments, eliminating the constraint of the equality of all R_{col}.

6.3.3 Sensitivity analysis

A parameter sensitivity analysis was performed on the coronary circulation model in order to study, in particular, the relative sensitivity of the parameters on the main outputs of the model. Until today, sensitivity analyses have been applied locally only to a limited number of parameters, using an informal local sensitivity approach and under the hypothesis of an equal collateral development (HARMOUCHE et al., 2012; MAASRANI et al., 2013).

Morris' elementary effects method (MORRIS, 1991) was used to define a rank of the importance of each parameters. Recall from chapter 4 that the elementary effects method explores a hypercube divided in p levels by calculating r elementary effects. From these elementary effects, two measures are calculated, μ^* and σ, representing the mean and standard deviation of the r samples for the effects. With these values, a sensitivity index is calculated for each parameter X_i as:

$$S_{Mi} = \sqrt{(\mu_i^*)^2 + (\sigma_i)^2}\,. \qquad \text{(4.16, revisited)}$$

In the interest of using physiologically relevant parameter values during the sensitivity analysis, the ranges for each parameter were defined as follows. Aortic and venous input pressures are simulated as pulsatile signals, adjusted to have a mean value between 60 to 120 mmHg for P_{ao}, and 3 to 14 mmHg for P_{v}. Capillary resistances were limited to the range defined from 27 to 525 mmHg s/mL, while collateral resistances were limited from 104 to 2000 mmHg s/mL. These ranges were arbitrarily defined by taking the mean values published by Maasrani et al. (MAASRANI et al., 2011), which were estimated from patient data, and multiplying it by 0.2 and 3.85 in order to create a range that is large enough to contain all patient-specific values used for this model until today in (MAASRANI et al., 2008, 2011; MAASRANI et al., 2013). Parameters related to arteries and grafts (R, L and C) were defined similarly, taking the baseline values shown in table 6.3, which were estimated from angiographic measurements in (PIETRABISSA et al., 1996; WANG et al., 1989), and multiplying by the same factors. The observed outputs were the mean values of blood flows and pressures during six cardiac cycles.

6.3.4 Parameter identification

6.3.4.1 Previous approaches

The determination of important parameters with the sensitivity analysis provides key information towards accurate simulations and patient-specific parameters. Previous works attempting the creation of personalized models of the coronary circulation in CAD focus on the calculation of capillary and collateral resistances, assuming that collateral resistances are represented by a common parameter for each patient. This approach, presented in (MAASRANI et al., 2008), can be summarized as follows:

– First, the 3G case is considered, where the left graft flows are known (Q_{RCAg}, Q_{LADg} and Q_{LCxg}), and collateral flows are assumed minimal. Under this case, when only the resistive effects of the coronary circuit (fig. 6.5) are considered, the capillary resistance can be calculated analytically as:

$$R_{\mathrm{LADc}} = \frac{(P_{\mathrm{ao}} - P_{\mathrm{v}}) - Q_{\mathrm{LADg}} R_{\mathrm{LADg}}}{\left(1 + \frac{R_{\mathrm{LADg}}}{R_{\mathrm{LAD}}}\right) Q_{\mathrm{LADg}}}\,, \tag{6.5}$$

$$R_{\mathrm{LCxc}} = \frac{(P_{\mathrm{ao}} - P_{\mathrm{v}}) - Q_{\mathrm{LCxg}} R_{\mathrm{LCxg}}}{\left(1 + \frac{R_{\mathrm{LCxg}}}{R_{\mathrm{LCx}}}\right) Q_{\mathrm{LCxg}}}\,, \tag{6.6}$$

$$R_{\mathrm{RCAc}} = \frac{(P_{\mathrm{ao}} - P_{\mathrm{v}}) - (R_{\mathrm{RCAg}} - R_{\mathrm{RCA}}) Q_{\mathrm{RCAg}}}{Q_{\mathrm{RCAg}}}\,. \tag{6.7}$$

– Once the capillary resistances are calculated, they are assumed equal for all cases. Then, the 2G case is considered, where the coronary wedge pressure is known (P_{w}) and the pressure difference between the left and right coronary trees drives a non negligible collateral flow. It is at this point that all collateral resistances are assumed equal ($R_{\mathrm{col1}} = R_{\mathrm{col2}} = R_{\mathrm{col3}} = R_{\mathrm{col4}} = R_{\mathrm{col5}}$) and a single value R_{col} is changed until the simulated P_{w} converges to the clinical measured counterpart.

The parameter values calculated with this approach are shown in table 6.4.

TABLE 6.4– Estimated parameters according to the analytical approach of (MAASRANI et al., 2011).

Patient	R_{LADc}	R_{RCAc}	R_{LCxc}	R^*_{col}
1	83.3	54.1	207.9	160
2	174.6	96.9	210.9	430
3	213.0	62.8	94.2	350
4	47.5	147.2	119.1	565
5	175.3	56.1	68.7	205
6	240.4	117.6	135.5	1055
7	50.2	76.0	118.4	650
8	77.6	347.6	196.0	970
9	374.8	80.7	33.7	420
10	155.9	213.8	62.1	405

6.3.4.2 A multiobjective optimization approach

We propose a parameter identification procedure that, in contrast to the previous approach mentioned before, seeks to estimate these collateral resistances individually, in a patient-specific manner. The proposed parameter estimation method will focus on the most sensitive parameters of the model, which have been determined by the rank of importance calculated during the sensitivity analysis phase.

In order to obtain an estimation that is as close as possible to real data, all the clinical measurements, under all graft scenarios, are compared to simulated data. The estimation is defined as the joint minimization of the following functions:

$$\begin{aligned} & f_V(\mathbf{p}) = \left| V^{\text{cli}} - V^{\text{S}} \right| \\ & \text{for all } V \in \{P_{w,0G}, Q_{\text{RCAg},1G}, P_{w,2G}, Q_{\text{LADg},2G}, \\ & \qquad Q_{\text{LCxg},2G}, Q_{\text{RCAg},3G}, Q_{\text{LADg},3G}, Q_{\text{LCxg},3G}\}, \end{aligned} \tag{6.8}$$

where $^{\text{cli}}$ denotes variables observed during the CABG procedure for a particular patient and $^{\text{S}}$ denotes the corresponding variables simulated by the model using the parameter vector $\mathbf{p}$. Here, both simulated and observed variables are the average value after hemodynamic stabilization and not their continuous, pulsatile values.

Since the error functions defined in eq. (6.8) are not differentiable with respect to the model parameters, and considering that we have formulated the estimation as the combined minimization of eight functions, a multi-objective evolutionary algorithm was used to estimate the model parameters: the Non-dominated Sorting Generic Algorithm (NSGA-II) (DEB et al., 2001), presented in chapter 2.

In order to avoid populations with dominant individuals [2] that have nonetheless high error values for some of their objective functions, an additional consideration was included: Whenever the population contains 95% of dominant individuals, the mean of the sum of all objective

2. Note that, in this work, we use the term *individual* only to refer to the EA representation of a solution, and not to a *patient*.

functions of eq. (6.8) is calculated. Then, the evolutive algorithm is resumed with an additional constraint that penalizes any individual whose sum of objectives is greater than the mean. With this modification, individuals with high global error are systematically replaced with others that minimize the sum of objectives.

6.4 Results and discussion

6.4.1 Sensitivity analysis

The sensitivity analysis was performed with different levels $p = 10$ and 20, and number of repetitions r =100, 200, 500 and 1000, all which produced similar results. In this section, the results for $p = 20$, $r = 1000$ and $\Delta = 0.526$ are presented. Results are organized by output and graft scenario, sorted by their S_{Mi} as defined in eq. (4.16). Figure 6.6 shows coronary blood flow through all arteries and total coronary flow, fig. 6.7 shows flows through collateral vessels, and fig. 6.8 shows flows through graft vessels and blood pressure distal to the RCA occlusion.

6.4.1.1 Common sensitivity patterns and most sensitive parameters

Regarding the identification of the most sensitive parameters of the model, the results reveal some common patterns for all outputs. There is a significant sensitivity to the resistive effects of the vessels, and a very low effect from inertances and capacitances. This is caused by the use of averaged output variables throughout several cardiac cycles, even though the simulation uses pulsatile signals for P_{ao} and P_{v}. When averaging output variables, phase dynamics are filtered out. Considering that all clinical data related to this study are average values after hemodynamic stabilization, all previous studies, including this work, continue to use mean values of the model output.

Another pattern of the results is that capillary resistances present the most important effect. As shown in figs. 6.6 and 6.8, all arterial and graft flows exhibit this behavior. Artery flows present an outstanding effect from capillaries, with a sensitivity at least ten times higher than the next parameter in the rank. The collateral flows results in fig. 6.7 are the only outputs where this pattern is less pronounced, since the sensitivity of the capillaries is similar to that of the resistance of the associated collateral vessel. These observations show that capillary resistances are an important regulator of coronary blood flow, which is a known fact, supported by clinical studies that acknowledge the importance of arterioles and capillaries on the regulation of myocardial perfusion (KAUL et al., 2008). Moreover, it has also been identified that collateral resistances influence the myocardial blood flow (BILLINGER et al., 2001). Results of the sensitivity analysis also agree with this clinical observation, considering that myocardial blood flow is related to the variable Q_t of the model. Furthermore, it is possible with the model to compare the effect of both mechanisms: a perturbation of capillary resistances provokes a more important change in Q_t than a similar perturbation of any collateral resistance.

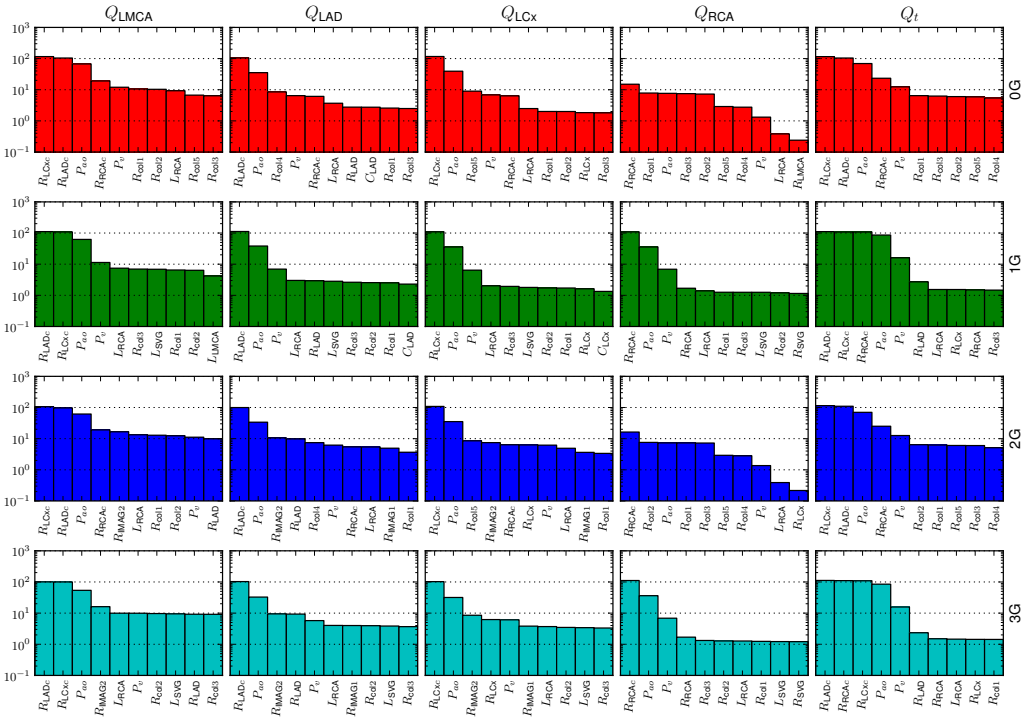

FIGURE 6.6– Morris sensitivity results for arterial flows (Q_{LMCA}, Q_{LAD}, Q_{LCx}, Q_{RCA}) and total coronary flow (Q_t). The Morris parameters used were $p = 20$, $\Delta = {}^{r}/_{2(p-1)} = 0.526$ and $r = 1000$ repetitions. Graphs are organized by graft cases (rows) and output variable (columns). Each graph contains only the ten most important parameters, where a bar represents the value S_{Mi} as defined in eq. (4.16) (the higher the bar, the higher the influence of the parameter).

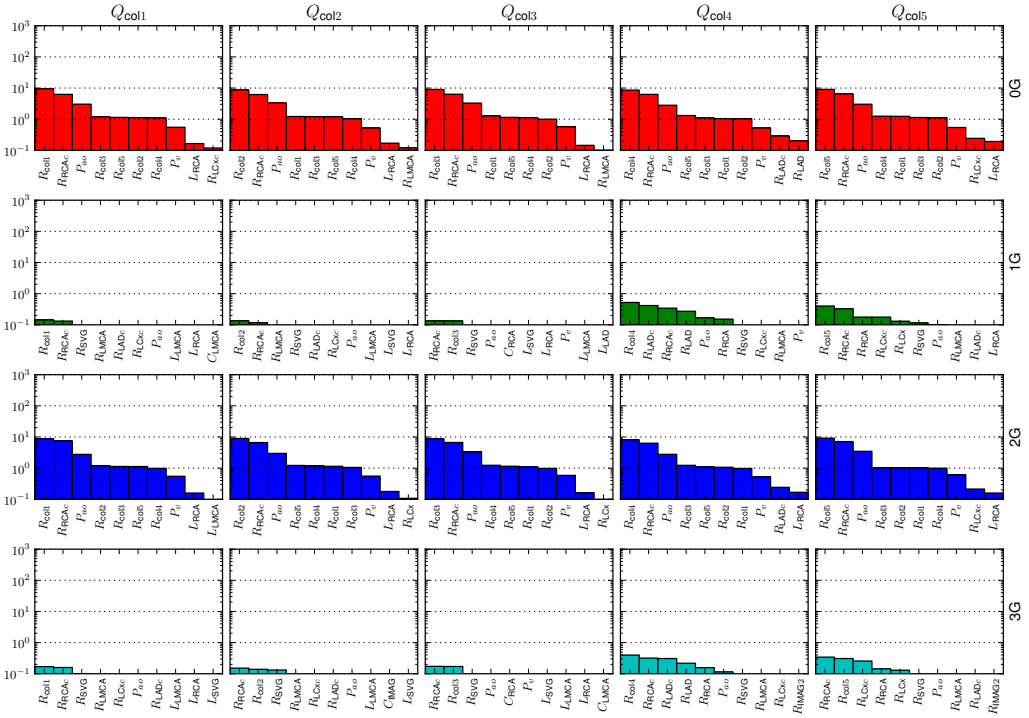

FIGURE 6.7– Morris sensitivity results for collateral flows (Q_{col1}, Q_{col2}, Q_{col3}, Q_{col4}, Q_{col5}). The Morris parameters used were $p = 20$, $\Delta = p/2(p-1) = 0.526$ and $r = 1000$ repetitions. Graphs are organized by graft cases (rows) and output variable (columns). Each graph contains only the ten most important parameters, where a bar represents the value S_{Mi} as defined in eq. (4.16) (the higher the bar, the higher the influence of the parameter).

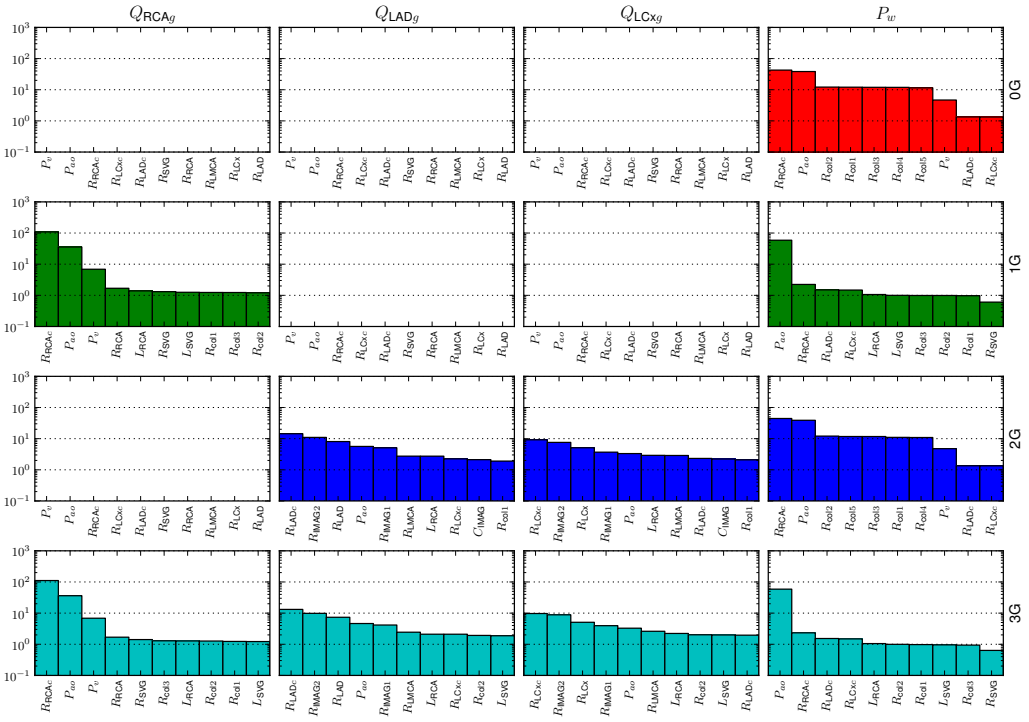

FIGURE 6.8– Morris sensitivity results for the coronary graft flows (Q_{RCAg}, Q_{LADg}, Q_{LCxg}) and coronary wedge pressure (P_{w}). The Morris parameters used were $p = 20$, $\Delta = p/2(p-1) = 0.526$ and $r = 1000$ repetitions. Graphs are organized by graft cases (rows) and output variable (columns). Each graph contains only the ten most important parameters, where a bar represents the value S_{Mi} as defined in eq. (4.16) (the higher the bar, the higher the influence of the parameter).

6.4.1.2 Role of the right capillary bed

The presence of capillary resistances as important parameters for each output is consistent with the analog electrical network of fig. 6.5; each arterial and graft flow depends on the most distal resistance of the respective branch. However, the capillary for the right circulation R_{RCAc} presents systematically a high sensitivity rank, even for blood flows of the left circulation, such as Q_{LMCA}, Q_{LAD} and Q_{LCx}, under the 0G and 2G cases. This effect of R_{RCAc} on the left circulation is only possible through the collateral flow between right and left coronary branches.

The right capillary bed is also a major determinant of all collateral flows, as shown in fig. 6.7. No other capillary resistance seems to have an important effect for the hemodynamics of the collateral network. This result is closely related to the the sensitivity results for P_{w} in fig. 6.8. In this coronary model, collateral flows are directly proportional to the pressure difference between the left and right coronary branches (i.e. the pressure gradient between P_{LMCA}, P_{LAD} or P_{LCx}, and P_{w}). Consequently, any modification of P_{w} should have a similar effect on collateral flows.

The sensitivity analysis suggest that there is a different role of the right and left capillary beds on the coronary circulation due to collateral flow. To our knowledge, there is no clinical study that addresses this observation. However, this is coherent in triple-vessel disease, where the left beds are affected by partial stenosis, while the right bed could be damaged by the RCA thrombosis. It is worth mentioning that the model does not consider distal collaterals between LCx and LAD, which could result in a more significant contribution of the left capillaries.

6.4.1.3 Uneven effect of collateral resistances

Since one of the objectives of this work is to revise the hypothesis of the equality of collateral resistances, we examined closely the effect of these parameters on all model outputs. First, it is clear from fig. 6.7 that collateral resistances are the most important parameters for the collateral blood flow. Each Q_{col} depends primarily on their respective R_{col}, yet the other resistances seem to have an effect as well, since they have an effect on P_{w}. This observation implies that incorrectly estimating any one collateral resistance will have a major effect on the corresponding vessel, and a non-negligible effect in the whole assessment of the collateral situation of the patient.

Regarding the effect on other model outputs, for cases 0G and 2G it seems that collaterals are also important parameters, but for Q_t and Q_{LMCA} there is no clear distinction between them. On the other hand, Q_{RCA} seems to be more affected by collaterals that originate in the proximal part of the circulation (R_{col1}, R_{col2} and R_{col3}) with respect to collaterals from more distal parts (R_{col4} and R_{col5}). The former collaterals have a flow directly proportional to P_{ao} or P_{LMCA}, while the latter are proportional to P_{LAD} and P_{LCx}. Due to the coronary tree structure, and particularly to the presence of partial stenoses in the left branches, flows Q_{col1}, Q_{col2} and Q_{col3} will have a higher driving pressure than Q_{col4} and Q_{col5}. The inequality of the sensitivities to collateral resistances could thus be caused by these differences of driving pressures.

A similar uneven effect of collaterals is also noticeable for Q_{LAD} and Q_{LCx} flows. Here, a modification of R_{col4} and R_{col5} provokes a more important modification of these flows since these

collaterals directly steal blood flow from the LAD and LCx arteries in order to reperfuse the occluded RCA. As with Q_{col} flows, imprecise estimation of R_{col} will then have a perceptible effect on the mean blood flow of the coronary arteries. Proximal collaterals will affect the right coronary hemodynamics, while distal will mostly affect the left counterpart.

6.4.1.4 Effect of graft configuration

The graft configuration deeply affects the sensitivity of the model parameters on all levels. Collateral resistances, which are usually among the most important parameters for arterial and collateral flows, become almost negligible under the 1G and 3G cases. As previously observed by (Maasrani et al., 2008), revascularization through the right graft reduces the pressure difference between the right and left branches of the coronary tree, hence the reperfusion through collateral vessels is reduced. Although significantly diminished, collateral flow is still present, since P_{w} results in fig. 6.8 show that this right territory pressure is still slightly sensitive to changes in the capillaries of the left territory and proximal collaterals.

In addition to the modification of the collateral dynamics, the presence of the right graft also increases the sensitivity of the right capillary, as shown for the results of Q_t, when comparing cases 0G and 2G with cases 1G and 3G. Since the right circulation is so poorly perfused due to the RCA occlusion (cases 0G and 2G), changes in R_{RCAc} do not produce an absolute effect as high as the changes in R_{LADc} or R_{LCxc}. With the presence of the right graft (cases 1G and 3G), the effective flow through RCA is higher, which re-enables the effect of the RCA capillary.

On the other hand, the presence of the LADg and LCXg (case 2G) does not have a major impact on the model outputs: collateral vessels have the same effect as in the 0G case, and the right capillary sensitivity does not change for any variable. While these two grafts reperfuse the left territory, RCA is still poorly perfused due to its occlusion. Therefore, under this graft configuration, the right territory can only be reperfused through the collateral vessels, which explains why the R_{col} parameters are still observed as highly sensitive parameters.

6.4.1.5 Effect of input variables

Aortic pressure is consistently present in all arterial, collateral and graft flows. With respect to the model parameters, results show that, in general, P_{ao} is slightly less influent than capillary resistances, but more important than collateral resistances. On the other hand, P_{v} presents an effect that is comparable to the effect of collateral resistances. For all flows, with the exception of RCA, the effect P_{ao} and P_{v} does not show any significant variation among different graft cases. However, the presence of the right graft (cases 1G and 3G) increases the importance of P_{ao} and P_{v} on the Q_{RCA}, since the new graft flow directly depends on the pressure gradient between P_{w} and P_{ao}.

Although the sensitivity analysis showed that the effect of aortic pressure is important on all coronary flows, this result challenges clinical observations: constant perfusion has been observed for variations of arterial pressures within 60 to 140 mmHg (Johnson, 1991). Such constant

perfusion is explained by autoregulatory mechanisms that modulate the vasodilation of large vessels in order to supply the cardiac muscle according to the metabolic demands. Since our model does not account for these mechanisms, this confrontation will be listed as one of the model limitations.

6.4.2 Parameter identification

Based on the sensitivity analysis results, which indicated that the most sensitive parameters for the coronary circulation model in a non-pulsatile configuration are the capillary and collateral resistances, the identification method was focused on estimating the optimal values for $\mathbf{P} = [R_{\text{LADc}}, R_{\text{RCAc}}, R_{\text{RCAc-1G}}, R_{\text{LCxc}}, R_{\text{col1}}, R_{\text{col3}}, R_{\text{col4}}, R_{\text{col5}}]$, where $R_{\text{RCAc-1G}}$ is the right capillary resistance for the 1G case. R_{col2} was not included in $\mathbf{P}$, but considered to be equal to R_{col1}. This is because these two resistances are in parallel (see fig. 6.5); several configurations of these resistances are equivalent, which would cause a high variability in the results. Each parameter was limited to the same physiologically plausible ranges used in the sensitivity analysis.

The MOEA optimization was run for each of the ten patients presented in (MAASRANI et al., 2011), with a population for the evolutionary algorithm of 10000 individuals, during 500 generations, with a probability of crossover and mutation of $p_m = 0.8$ and $p_c = 0.25$, respectively. Results of the parameter estimation for each patient are shown in table 6.5. Different configurations with larger population sizes, more generations and different probabilities were also tested, generating similar results. Since the final population contains 10000 individuals, this table shows the mean value and the variability of the parameter values found in the 10% of the population with the lowest sum of the functions defined in eq. (6.8). Detailed information regarding the error for each objective function is shown in table 6.6, as well as a comparison of the parameters found with the estimation procedure in (MAASRANI et al., 2011).

6.4.2.1 Evaluation of the estimation procedure

The capillary resistances values found by the multiobjective estimation, shown in table 6.5, have a good consistency with the values of previous estimation by Maasrani et al. (table 6.4). There are some exceptions: *i)* patients 6, 8 and 9, with a difference in the R_{LADc} parameter of 128, 18.7 and 37.8 mmHg s/mL, respectively, and *ii)* patients 6, 8 and 10, with a difference in the R_{LCxc} parameter of 100, 53.3 and 45.2 mmHg s/mL, respectively. These differences are accounted by the fact that the two estimation procedures are fundamentally different. Maasrani's estimation procedure, explained in (MAASRANI et al., 2008) calculates R_{LADc} and R_{LCxc} by using the measured graft flow in the case 3G, while assuming a negligible collateral flow and constant collateral resistances. The sensitivity analysis results showed that these assumptions are not necessarily true.

Clinical data along with the estimated variables of the proposed method and previous publications are shown in table 6.5; these tables also show the estimation error calculated with eq. (6.8). This evaluation measure shows a significant decrease in the total error for all patients.

TABLE 6.5– Values identified for ten patients using the multiobjective optimization method. Each row represents the $\mu \pm \sigma$ of the best 10% individuals in the final population. The final row shows the mean difference across all patients between parameter values in (MAASRANI et al., 2011) (M1†, cf. table 6.4) and the values found by the multiobjective estimation. All resistances values are given in mmHg s/mL.

(a) Capillary resistances (R_{LADc}, R_{RCAc}, R_{LCxc}), the right coronary capillary for the 1G revascularization case ($R_{\text{RCAc-1G}}$).

Patient	R_{LADc}	R_{RCAc}	$R_{\text{RCAc-1G}}$	R_{LCxc}
1	83.0±0.1	54.4±0.0	129.7±0.1	197.8±0.4
2	171.7±0.1	99.6±0.0	137.9±0.0	201.9±0.1
3	205.8±0.1	63.5±0.0	256.1±0.4	92.5±0.0
4	47.8±0.0	150.0±0.0	522.6±1.3	118.4±0.2
5	169.8±0.1	58.7±0.0	95.0±0.0	65.1±0.0
6	368.1±1.0	117.7±0.0	203.8±0.1	234.6±0.8
7	53.8±0.1	77.6±0.0	82.0±0.0	106.6±0.0
8	58.8±0.2	357.1±0.1	523.9±0.1	248.7±0.6
9	337.4±0.4	84.9±0.0	59.9±0.0	27.8±0.0
10	152.6±0.2	215.5±0.1	324.0±0.5	106.7±0.9
Difference with M1†	20.7	2.6	—	23.9

(b) Collateral resistances ($R_{\text{col1}} = R_{\text{col2}}$, R_{col3}, R_{col4}, R_{col5}). Rentrop score grades (RS) are also included from table 6.1 for discussion in text.

Patient	RS	R_{col1}	R_{col3}	R_{col4}	R_{col5}
1	3	109.8± 0.2	1863.5±108.8	1974.8±24.8	104.0± 0.0
2	2	256.5± 6.8	1393.8±283.2	377.9± 1.7	104.1± 0.1
3	3	935.6± 25.5	104.2± 0.3	637.9± 8.3	344.6± 1.6
4	3	341.2±124.1	1212.9±442.4	897.8±11.1	1994.6± 7.3
5	3	104.8± 1.4	283.1± 15.8	104.1± 0.1	104.0± 0.0
6	2	1993.7± 7.1	245.6± 0.4	1998.3± 2.1	1995.8± 5.2
7	3	1989.6± 14.8	1218.7± 30.4	1986.7±18.8	192.0± 0.3
8	1	1994.4± 8.3	415.4± 1.0	1990.9±10.7	1998.8± 1.8
9	1	1940.1± 57.5	1993.0± 9.1	286.7± 0.6	150.7± 0.8
10	2	1957.6± 40.1	112.5± 0.3	1364.8±24.5	1943.8±54.8
Difference with M1†		750.9	743.7	698.3	615.4

Patients 1 and 3 present the best improvements, with an error that is ten and twenty times lower. This major decrease is mostly due to the large difference with clinical data for the 1G case in previous identifications. In general, Maasrani's estimations have a significant error for this graft case. Since the Maasrani's estimation used only clinical data from cases 2G and 3G, it is not a surprise that simulations for cases 0G and 1G present a higher errors, while 2G and 3G variables are estimated more accurately. The proposed estimation method presents an improvement for almost all variables in all graft cases, because it exploits all available data for all cases. In

TABLE 6.6– Simulation results for the coronary circulation model: cli* variables are from clinical data, M1† are from simulations of Maasrani et al. (MAASRANI et al., 2011), M2‡ are from the best solution found by the multiobjective estimation. Total error was calculated as the cumulative sum of functions in eq. (6.8) for pressure or flow variables. Error for M2‡ is the mean and standard deviation of the best 10% individuals of the final population.

(a) Results for patients 1 to 5.

Case	Variable	Source	Patient				
			1	2	3	4	5
0G	P_{w}	cli*	35.0	49.0	40.0	43.0	53.0
		M1†	31.6	44.5	33.1	38.3	41.4
		M2‡	35.0	48.9	39.8	43.0	48.6
1G	Q_{RCAg}	cli*	35.0	45.0	28.0	11.0	63.0
		M1†	88.2	52.4	86.6	35.1	85.4
		M2‡	35.1	45.3	28.1	11.0	63.5
2G	P_{w}	cli*	31.0	49.0	40.0	42.0	36.0
		M1†	31.3	49.0	40.1	42.3	35.7
		M2‡	30.7	58.3	43.2	42.8	42.8
	Q_{LADg}	cli*	34.0	23.0	22.0	59.0	24.0
		M1†	39.6	24.0	28.5	54.3	22.3
		M2‡	34.9	23.1	22.1	54.7	24.1
	Q_{LCxg}	cli*	27.0	32.0	48.0	40.0	56.0
		M1†	17.6	22.4	49.2	30.2	46.6
		M2‡	20.8	29.8	48.2	28.5	49.0
3G	Q_{RCAg}	cli*	66.0	45.0	74.0	26.0	69.0
		M1†	67.6	45.4	75.3	27.0	70.5
		M2‡	66.5	45.3	74.6	26.0	69.8
	Q_{LADg}	cli*	40.0	21.0	19.0	57.0	18.0
		M1†	38.9	21.1	19.0	56.8	18.3
		M2‡	40.4	21.1	19.1	57.9	18.1
	Q_{LCxg}	cli*	14.0	19.0	45.0	30.0	46.0
		M1†	13.9	19.2	44.7	30.1	45.6
		M2‡	14.1	19.1	45.2	30.1	46.1
Variables		**Source**	**Total error**				
Pressures (mmHg)		M1†	3.6	4.7	6.0	5.0	11.9
		M2‡	0.5±0.0	0.3±0.1	0.2±0.1	5.4±0.0	0.8±0.3
Flows (mL/min)		M1†	71.1	18.7	64.6	39.9	37.6
		M2‡	1.3±0.0	11.2±0.1	3.4±0.1	12.2±0.0	12.7±0.3

particular, the Q_{RCAg} for case 1G always presents a lower estimation error. This improvement, as well as the close consistency with clinical data for Q_{RCAg} in the 3G case, is certainly due to the addition of a different R_{RCAc} for the 1G case. Finally, the low error on P_{w} variables for cases 0G and 2G improve the calculation of clinical indices based on this pressures, such as the pressure-based collateral flow index (PIJLS et al., 1995).

Patients 4, 5, 6 and 9 represent the estimation results with the highest total error. However,

TABLE 6.6– Simulation results for the coronary circulation model: cli* variables are from clinical data, M1† are from simulations of Maasrani et al. (MAASRANI et al., 2011), M2‡ are from the best solution found by the multiobjective estimation. Total error was calculated as the cumulative sum of functions in eq. (6.8) for pressure or flow variables. Error for M2‡ is the mean and standard deviation of the best 10% individuals of the final population.

(b) Results for patients 6 to 10.

Case	Variable	Source	Patient 6	7	8	9	10
0G	P_{w}	cli*	35.0	29.0	46.0	37.0	47.0
		M1†	28.2	37.0	45.1	37.9	44.9
		M2‡	34.9	35.4	45.9	37.7	47.0
1G	Q_{RCAg}	cli*	18.0	53.0	9.0	60.0	11.0
		M1†	31.9	55.9	14.6	45.6	18.9
		M2‡	18.1	53.6	9.2	61.0	11.0
2G	P_{w}	cli*	28.0	40.0	43.0	40.0	48.0
		M1†	28.4	40.2	44.5	40.0	48.2
		M2‡	32.6	39.8	43.2	39.9	48.0
	Q_{LADg}	cli*	11.0	28.0	38.0	24.0	20.0
		M1†	17.9	36.3	31.8	23.1	21.7
		M2‡	11.0	28.4	38.3	24.4	20.1
	Q_{LCxg}	cli*	12.0	43.0	16.0	60.0	7.0
		M1†	22.6	37.5	19.9	41.1	15.9
		M2‡	12.0	43.2	16.1	42.2	7.0
3G	Q_{RCAg}	cli*	30.0	51.0	10.0	51.0	14.0
		M1†	30.3	52.0	10.5	53.2	14.8
		M2‡	30.2	51.4	10.0	51.6	14.0
	Q_{LADg}	cli*	14.0	28.0	28.0	23.0	18.0
		M1†	14.3	28.2	28.1	22.9	18.0
		M2‡	9.2	23.1	35.0	23.4	18.0
	Q_{LCxg}	cli*	18.0	29.0	17.0	45.0	13.0
		M1†	18.1	29.2	17.2	44.6	13.0
		M2‡	10.0	29.2	14.3	46.2	6.3
Variables		**Source**	**Total error**				
Pressures (mmHg)		M1†	6.9	8.8	1.8	2.0	2.1
		M2‡	0.0±0.0	6.6±0.0	0.0±0.0	0.9±0.0	0.0±0.0
Flows (mL/min)		M1†	30.3	19.4	18.1	56.8	18.1
		M2‡	17.5±0.0	5.3±0.0	10.3±0.0	19.0±0.0	6.9±0.0

they still improve the previous estimation by a significant difference. The source of the estimation error for these patients come mostly from the left graft flows and P_{w}. It can be noted in table 6.6 that whenever there is an important error in Q_{LADg} or Q_{LCxg} in the 2G case, there is no significant error in the 3G case. As with Q_{RCAg}, careful examination of the final population shows that individuals can either minimize $Q_{\mathrm{LADg},2G}$ or $Q_{\mathrm{LADg},3G}$, but not both at the same time, and similarly for Q_{LCxg}. Once again, introducing new R_{LADc} or R_{LCxc} for the particular

case of 2G may improve the estimation error. Nevertheless, we decided not to include these additional parameters in order to keep the number of estimated parameters to a minimum.

6.4.2.2 Modification of the right capillary resistance

Concerning the right capillary resistance for the 1G case, table 6.5 shows that there is an important modification of this part of the coronary circulation under that particular graft case. Excluding patient 9, the $R_{\text{RCAc-1G}}$ parameter shows a significant increase with respect to R_{RCAc}.

A possible scenario that could explain this increase of the right capillary resistance is the modification on the myocardial contractility of the right territory as a consequence of the reperfusion of this region. An improved contractility due to better oxygenation of the muscle would cause an augmented collapse of the capillaries. However, since the 3G case reperfuses in the same way the right territory, a similar effect was expected. This was not the case, since the estimation procedure showed that there is a strong relationship between the right capillary for the 1G and 3G cases.

6.4.2.3 A new assessment of patient-specific collateral development

Since the estimation procedure is not based on the equality of the collateral resistances, the results of table 6.5 show an interesting way to estimate the collateral development in a patient-specific manner. These results can be compared with the Rentrop grade.

All ten patients included in this application show some collateral development (Rentrop grade higher than 0). This is consistent with the results obtained from the parameter identification phase, since all patients have at least one significantly low collateral resistance. In particular, patients 8 and 9, the only cases with a Rentrop grade of 1, present consistent results since they show relatively high values for proximal collateral resistances. Patients 1, 3, 4, 5 and 7, whose Rentrop grade is 3, should show low resistances for one of the proximal collaterals and probably one of the distal resistances as well. Indeed, this pattern is true, except for patient 7, whose identified parameters show very high resistances for all collaterals but R_{col5}. The estimation error for this patient could be explained by the high error for P_{w} under the 0G case (table 6.6) or by a misinterpretation during the evaluation of the Rentrop grade.

It should be noted that there is not always an agreement between the Rentrop grade and the parameter estimation results; the collateral assessment provided by this estimation cannot currently replace the Rentrop scoring system, but can be used as a complementary information that is not affected by intra or inter-observer errors. For instance, low values for collaterals R_{col4} and R_{col5} were obtained for Patient 9, which can explain its Rentrop grade since these vessels reperfuse the RCA at the distal area. On the other hand, patient 8 showed high values for these collaterals, which would not justify the distal collateral filling. Considering that the estimation results have a relatively low error for this patient, it is possible that this specific coronary circulation model is not appropriate for some patients. In particular, this model does

not account for extracardiac collateral vessels, which can be found, although very rarely, on patients with triple-vessel disease (Lee et al., 2008).

Finally, identified parameters should be treated with care when the variability of the results is significant. As shown in table 6.5, the top 10% individuals of the final population for patients 1, 2 and 4 present a significant variability for R_{col3}. Patient 4 also shows this variation for R_{col1}. In consequence, it cannot be affirmed that R_{col3} (or R_{col1}) for these patients was successfully identified with the available data and the multiobjective procedure. Moreover, this significant variability has a small effect on the total error of the final population (table 6.6), which indicates that these collaterals have a small sensitivity to the sum of functions in eq. (6.8). Although this seems to contradict the results of the sensitivity analysis, it only presents an interpretation of 1000 individuals with parameters in the restricted space defined around the mean and standard deviation shown in table 6.5; while the sensitivity analysis provided results on a much larger parameter space.

6.4.3 Limitations and further work

The model and analyses presented in this chapter present some limitations enumerated below. Some of these limitations have already been addressed, yet the current state of these new developments are still a work in progress.

6.4.3.1 Effect of vasodilators

The model presented in this chapter represents the coronary circulation under the assumption that this circulation is under the effect of vasodilators (glyceryl trinitrate) and anesthetics (propofol). In addition to partial vasodilation, particularly in larger arteries and arterioles with diameter $> 100\,\mu\text{m}$ (Jones et al., 1996), this attenuates coronary blood flow autoregulation mechanisms of small arteries and arterioles, and the response of the autonomic nervous system. In consequence, parameter estimation results should be handled with care, since the resistances of coronary arteries and arterioles will increase under awake conditions. However, even in these conditions, the estimation of collateral development may not change significantly, since these vessels do not necessarily present smooth muscle.

6.4.3.2 Flow-independent resistance of stenoses

As in our previous publications (Abouliatim et al., 2011; Maasrani et al., 2008, 2011), we have represented the pressure loss across stenoses with a resistance adjusted with respect to area reduction, following eq. (6.4). This is a strong hypothesis that simplifies the simulation and identification phases and allows us to compare the results with our previous works. However, this hypothesis is known to be unrealistic, since the stenosis resistance is dependent on flow (Gould, 1985; Manor et al., 1994; Siebes et al., 2002).

Following (SIEBES et al., 2002), it is possible to use a flow-dependent resistance on stenotic arteries:

$$R_{\text{stenosis}} = A_v + BQ^2 \,, \tag{6.9}$$

where A_v is a coefficient for viscous pressure losses and B is a coefficient for inertial pressure losses at the exit of the stenotic region. The values of these coefficients account for the stenosis when calculated from the cross-sectional areas of the stenotic lumen and of the normal arterial segment (A_s and A_n, respectively), as suggested by (MANOR et al., 1994):

$$A_v = \frac{8\pi L_s}{A_s^2} \,, \tag{6.10}$$

$$B = \frac{\rho}{2}\left(\frac{1}{A_s} - \frac{1}{A_n}\right) \,, \tag{6.11}$$

where L_s is the length of the stenosis and ρ stands for blood viscosity.

The same methodology presented in this chapter can be applied to the model modified to include the flow-dependent resistance at the stenosed arteries. For the sensitivity analysis, two choices are possible: either all A_v and B for LMCA, LAD and LCx are included directly, or the stenosis reduction of each artery is included in the analysis, which yields the coefficients using eqs. (6.10) and (6.11). Using the latter, an additional sensitivity analysis was performed with the same configuration mentioned in section 6.4.1.

The results of this preliminary analysis are included in appendix B. However, a direct comparison with figs. 6.6 to 6.8 is not fair, since the initial sensitivity analysis did not account for the stenotic area reductions (these parameters were not considered because they are part of the pre-operative data). Therefore, appendix B also includes the results of an additional sensitivity analysis with the parameter adjustments of eq. (6.4). Fortunately, the main behaviors and tendencies identified in this chapters still hold for a model that uses a flow-dependent stenosis resistance, even if the sensitivity of arterial flows is reduced due to the fact that flow-dependent formulation results in a reduction of all coronary flows.

On the other hand, the parameter estimation results using a flow-dependent stenosis model can change significantly. With an increased pressure drop in all coronary arteries, caused by the additional inertial pressure loss term B, the role of R_{col3} changes completely because this is the only collateral whose driving pressure (P_{ao}) is not hindered by any stenosis. A parameter estimation is also included in appendix B, where R_{col3} is lower in all patients. Considering the high connectivity of the elements in our model, this modification of R_{col3} causes some modifications of the other collateral resistances as well. In fact, all other collateral resistances are consistently higher in all but one patient. This discrepancy of the estimation results needs to be considered in future developments. One possible way to figure out which stenosis model is more accurate would be to augment the observability of the system by including, for example, intra-operative measurements of the coronary arterial flows.

6.4.3.3 Patient-specific arterial parameters

The model simulations and parameter estimations are currently based on generic geometric properties of the epicardial arteries and grafts, which generate the parameters of table 6.3. More precise estimations can be achieved using patient-specific measurements of these vessels, but clinical data used in this work does not include this information. Fortunately, the sensitivity analysis showed that these parameters present a lower effect compared to capillary and collateral resistances; the effect of assuming generic parameters for arteries and grafts should be minor.

6.4.3.4 Coronary phasic flow

The clinical data obtained for this application did not include full flow profiles for the measured graft flows. This strong limitation affected all studies of this coronary model, including this one, to only consider the mean values of the model outputs. Therefore, current results do not take into account the flow variations during diastole and systole that characterize coronary flow. Results should be considered relevant only when considering the mean values, but not phase dynamics, which explains the low effect of parameters related to capacitances and inductors. Similarly, parameters found during the estimation will correctly simulate mean clinical data under vasodilation, but not flow variations during the cardiac cycle.

Some work has already been initiated to overcome this limitation. First, the coronary model has been coupled to a pulsatile model based on (Smith et al., 2007) that generates full profiles for aortic, venous and ventricular pressures (Ojeda et al., 2011). Following a coupling procedure similar to the multi-resolution application of chapter 3, the cardiovascular model signals are coupled as the inputs of the coronary model (P_{ao} and P_v). An example of the flow profiles of this integrated model is shown in fig. 6.9.

Although coupling the coronary model with a cardiovascular model generates a pulsatile coronary flow, fig. 6.9 does not display the systolic and diastolic profiles typical of coronary flow. The lack of flow drop during systole (around $t = 1\,\mathrm{s}$ in fig. 6.2) can be explained a missing consideration of ventricular pressure or muscular contraction in the original coronary model. In the literature, three different lumped parameter formulations exist to explain the interaction between coronary flow and cardiac contraction: *i)* modulation of microvascular resistances due to their collapse during systole (Wang et al., 1989), *ii)* waterfall models, an approach where the vessel is considered a tube that collapses when the surrounding pressure (in this case, the ventricular pressure) is higher than the venous pressure (Downey et al., 1975), and *iii)* intramyocardial pump models, a description that focuses on the role of vascular capacitance, which stores fluid during diastole and pumps it away when the myocardium contracts (Spaan et al., 1981).

To include the coronary phasic flow profiles, two developments have been initiated during this thesis:

– First, a proof of concept was implemented to couple a cardiovascular model to an intramyocardial pump model proposed by (De Lazzari et al., 2010), illustrated in fig. 6.10.

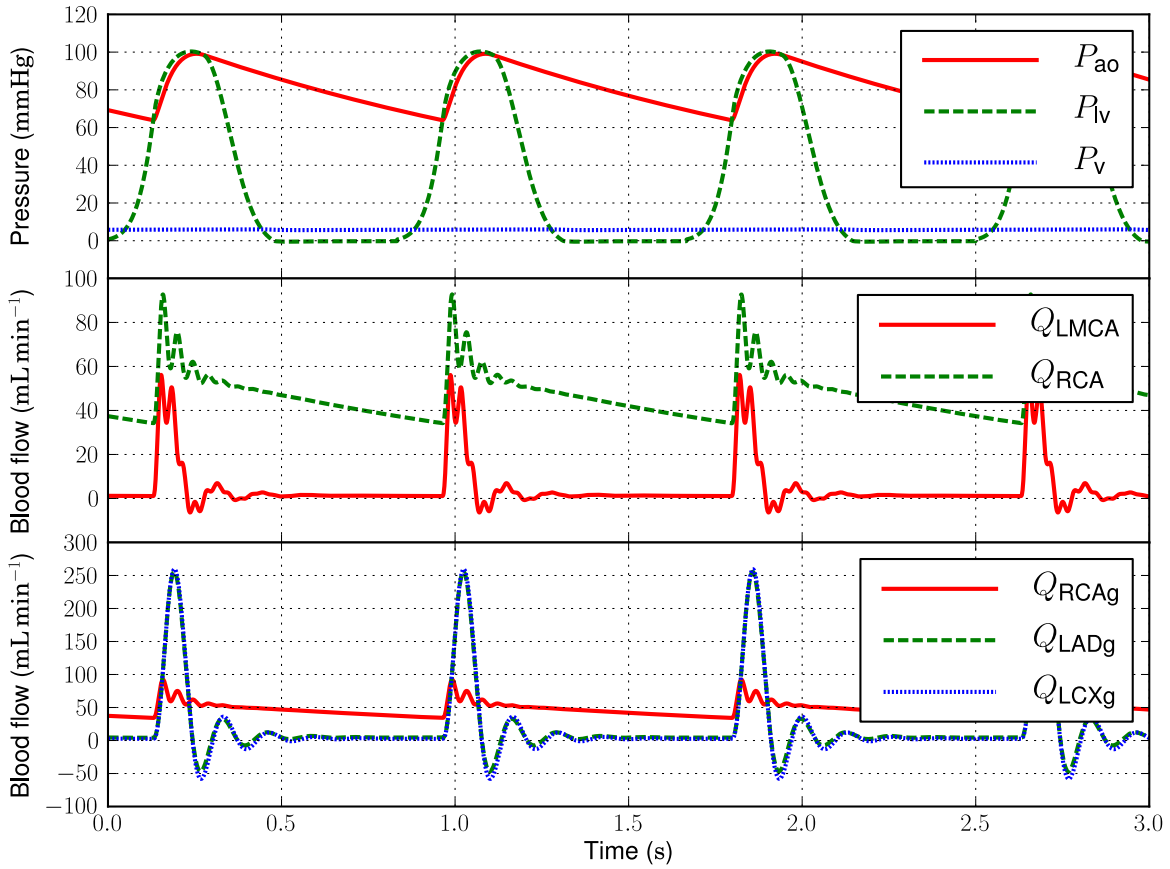

FIGURE 6.9– Flow profiles of the coronary model when coupled to a cardiovascular model. Signals correspond to patient 2 under the 3G case. Top panel shows cardiovascular pressures, middle panel shows left and right coronary flows, bottom panel shows graft flows.

Simulations of this model, shown in fig. 6.11, have been evaluated qualitatively: the systolic drop and subsequent diastolic flow are clearly visible; an encouraging preliminary result. However, multi-layered intramyocardial pump models rarely include collateral vessels and grafts, so a new design needs to combine the triple-vessel disease model used in this chapter, with an intramyocardial pump model.

– Second, motivated by the need of further developments towards a pulsatile coronary flow, the clinical protocol used to obtain intra-operative data is being redesigned. The main problem with the current protocol is that, even though the ultrasonic flow meter (Medistim Butterfly Flowmeter 2001) can save the graft flow profiles, this data was not preserved at the time of the study. During our new research efforts, we have proposed the preservation of this flow data and other hemodynamic signals, such as the arterial and venous pressures, and the electrocardiogram (ECG).

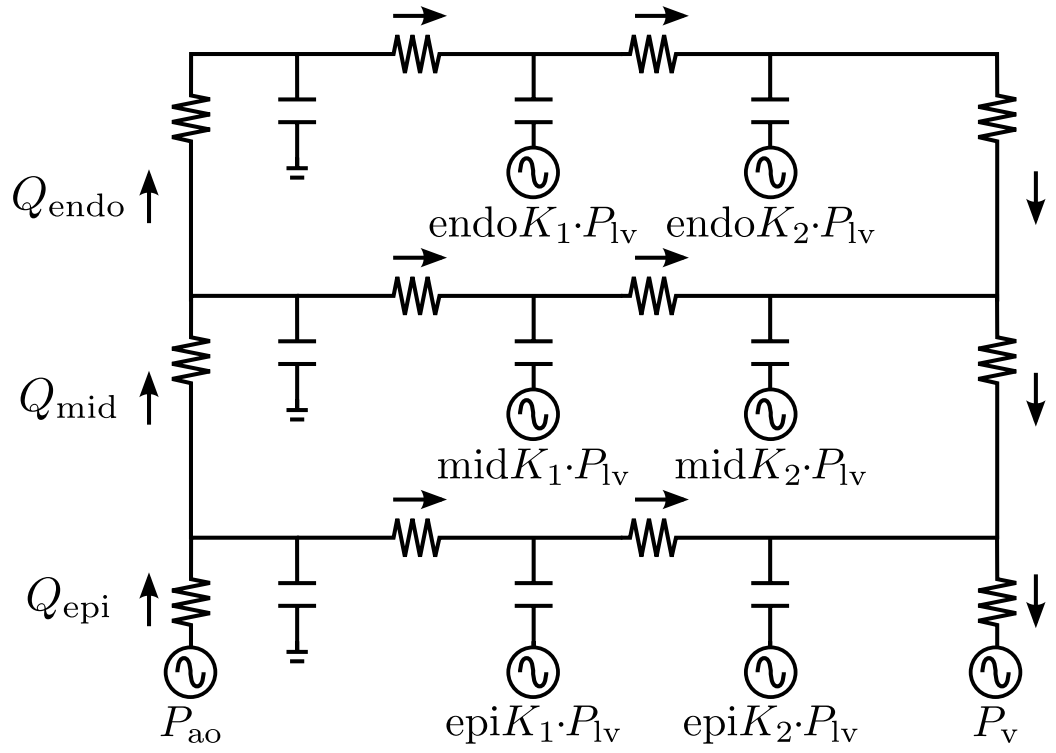

FIGURE 6.10– An intramyocardial pump model with three layers (epicardial, middle and endocardial), based on (DE LAZZARI et al., 2010).

6.5 Conclusions

The modeling application presented in this chapter presents introduced two original contributions towards the improvement of a coronary circulation model, devoted to patients with triple-vessel disease undergoing CABG surgery. First, an extensive parameter sensitivity analysis was presented, where it was determined that the capillary resistances are the most important parameters, followed by the collateral resistances. The disparity of the effect of collateral resistances for some of the model output variables, particularly the blood flow on the RCA, emphasizes the importance of considering heterogeneous, patient specific representations of the collateral circulation. Second, a multiobjective approach was proposed to estimate patient-specific parameters. This estimation is based on an original approach exploiting all available pre- and intra-operative data, without imposing any constraint regarding the parameters of the collateral vessels and considering a single parameter perturbation during the CABG. Results provide an estimation of the collateral and capillary development of a given patient, which may be a potentially useful marker for post-operative followup to CABG. Moreover, the estimated parameters showed an improvement with respect to an analytic approach (MAASRANI et al., 2008) and previous (mono-objective) evolutive algorithm optimization methods (OJEDA et al., 2012). However, a number of limitations persist in our model that need to be addressed in our future developments. Further

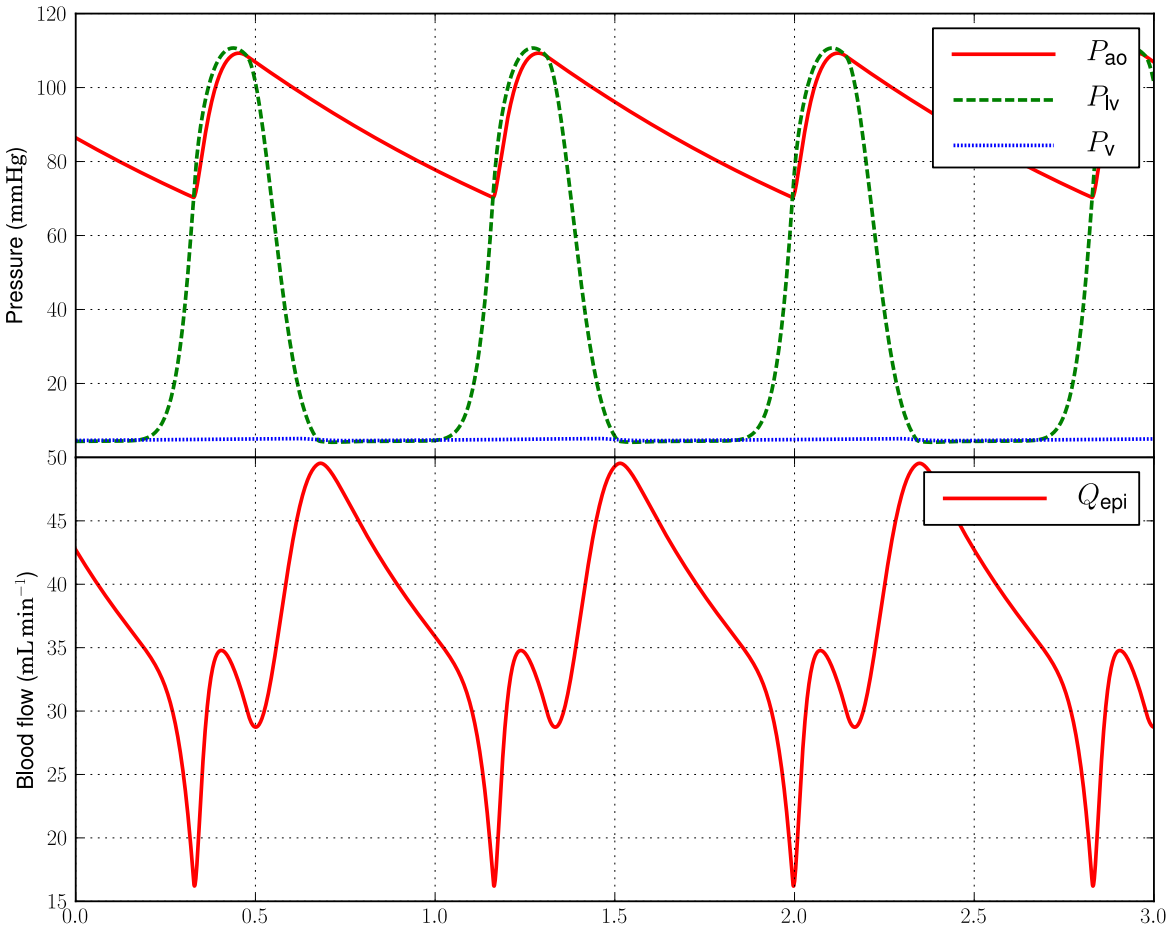

FIGURE 6.11– Example of coronary blood flow with intramyocardial pump. The diastolic phase coincides with a significant coronary flow.

work is thus directed towards: *i)* representation of flow-dependent resistances in arterial stenoses, which has been initially considered and where the sensitivity tendencies have been confirmed to follow the same observations presented in this work, *ii)* integration of coronary flow variations during the cardiac cycle with an extension of an intramyocardial pump model, and *iii)* better estimation of patient-specific stenosis resistances through semi-automatic analysis of coronary CT images (RINEHART et al., 2011). All this improvements are facilitated by the multiobjective identification approach proposed in this work, which can be more easily generalized than our previous analytical approaches.

References

ABOULIATIM, I. (2011). "Evaluation de la collateralité coronarienne entre le réseau gauche et la coronaire droite occluse: apport de la modélisation électrique". PhD thesis. Université de Rennes 1.

ABOULIATIM, I., M. HARMOUCHE, A. DROCHON, M. MAASRANI, H. CORBINEAU, and J.-P. VERHOYE (2011). "Coronary Flow in Patients with Three-Vessel Disease: Simulated Hemodynamic Variables in relation to

Angiographically Assessed Collaterality and History of Myocardial Infarction". In: *ISRN Vascular Medicine* 2011, pp. 1–10.

Bassingthwaighte, J., P. Hunter, and D. Noble (2009). "The Cardiac Physiome: perspectives for the future". In: *Experimental physiology* 94.5, pp. 597–605.

Berry, C., K. Balachandran, P. L'Allier, J. Lespérance, R. Bonan, and K. Oldroyd (2007). "Importance of collateral circulation in coronary heart disease". In: *European heart journal* 28.3, pp. 278–291.

Billinger, M., M. Fleisch, F. Eberli, B. Meier, and C. Seiler (2001). "Collateral and collateral-adjacent hyperemic vascular resistance changes and the ipsilateral coronary flow reserve: Documentation of a mechanism causing coronary steal in patients with coronary artery disease". In: *Cardiovascular research* 49.3, pp. 600–608.

Corbineau, H, J. P. Verhoye, T Langanay, P Ménestret, and A Leguerrier (2001). "Feasibility of the utilisation of the right internal thoracic artery in the transverse sinus in off pump coronary revascularisation: early angiographic results". In: *Eur J Cardiothorac Surg* 20.5, pp. 918–922.

De Lazzari, C., D. Neglia, G. Ferrari, F. Bernini, M. Micalizzi, A. L'Abbate, and M. Trivella (2010). "Computer simulation of coronary flow waveforms during caval occlusion". In: *Methods of Information in Medicine* 48.2, p. 113.

Deb, K. and D. Kalyanmoy (2001). *Multi-Objective Optimization Using Evolutionary Algorithms*. New York, NY, USA: John Wiley & Sons, Inc. isbn: 047187339X.

Downey, J. M. and E. S. Kirk (1975). "Inhibition of coronary blood flow by a vascular waterfall mechanism". In: *Circ Res* 36.6, pp. 753–760.

Finegold, J. A., P. Asaria, and D. P. Francis (2012). "Mortality from ischaemic heart disease by country, region, and age: Statistics from World Health Organisation and United Nations". In: *International journal of cardiology*.

Gould, K. L. (1985). "Quantification of coronary artery stenosis in vivo." eng. In: *Circ Res* 57.3, pp. 341–353.

Guyton, A. and J. Hall (2005). *Textbook of medical physiology*. 11th ed. Saunders.

Harmouche, M., M. Maasrani, H. Corbineau, J. Verhoye, and A. Drochon (2012). "A more sensitive pressure-based index to estimate collateral blood supply in case of coronary three-vessel disease". In: *Medical Hypotheses* 79.2, pp. 261–263.

Heusch, G., R. Schulz, and S. H. Rahimtoola (2005). "Myocardial hibernation: a delicate balance". In: *American Journal of Physiology-Heart and Circulatory Physiology* 288.3, H984–H999.

Hirai, T., M. Fujita, H. Nakajima, H. Asanoi, K. Yamanishi, A. Ohno, and S. Sasayama (1989). "Importance of collateral circulation for prevention of left ventricular aneurysm formation in acute myocardial infarction." eng. In: *Circulation* 79.4, pp. 791–796.

Johnson, P. C. (1991). "The Myogenic Response". English. In: *The Resistance Vasculature*. Ed. by J. A. Bevan, W. Halpern, and M. J. Mulvany. Vascular Biomedicine. Humana Press, pp. 159–168. isbn: 978-1-4612-6746-1. doi: 10.1007/978-1-4612-0403-9_10.

Jones, C., L Kuo, M. J. Davis, and W. M. Chilian (1996). "In vivo and in vitro vasoactive reactions of coronary arteriolar microvessels to nitroglycerin". In: *American Journal of Physiology-Heart and Circulatory Physiology* 271.2, H461–H468.

Kaul, S and A. R. Jayaweera (2008). "Myocardial capillaries and coronary flow reserve". In: *J Am Coll Cardiol* 52.17, pp. 1399–1401. doi: 10.1016/j.jacc.2008.07.039.

Koerselman, J, Y van der Graaf, P. P. de Jaegere, and D. E. Grobbee (2003). "Coronary collaterals: an important and underexposed aspect of coronary artery disease". In: *Circulation* 107.19, pp. 2507–2511. doi: 10.1161/01.CIR.0000065118.99409.5F.

Lee, C. W., S. W. Park, G. Y. Cho, M. K. Hong, J. J. Kim, D. H. Kang, J. K. Song, H. J. Lee, and S. J. Park (2000). "Pressure-derived fractional collateral blood flow: a primary determinant of left ventricular recovery after reperfused acute myocardial infarction." eng. In: *J Am Coll Cardiol* 35.4, pp. 949–955.

Lee, J. and N. P. Smith (2012). "The multi-scale modelling of coronary blood flow." eng. In: *Ann Biomed Eng* 40.11, pp. 2399–2413. doi: 10.1007/s10439-012-0583-7.

LEE, S. T., S. Y. KIM, G HUR, Y. J. HWANG, Y. H. KIM, J. W. SEO, S. J. CHA, and W. R. LEE (2008). "Coronary-to-bronchial artery fistula: demonstration by 64-multidetector computed tomography with retrospective electrocardiogram-gated reconstructions". In: *J Comput Assist Tomogr* 32.3, pp. 444–447. DOI: 10.1097/RCT.0b013e318123837c.

MAASRANI, M., J. VERHOYE, H. CORBINEAU, and A. DROCHON (2008). "Analog electrical model of the coronary circulation in case of multiple revascularizations". In: *Annals of Biomedical Engineering* 36.7, pp. 1163–1174.

MAASRANI, M., I. ABOULIATIM, M. HARMOUCHE, J. VERHOYE, H. CORBINEAU, and A. DROCHON (2011). "Patients specific simulations of coronary fluxes in case of three-vessel disease". In: *Journal of Biomedical Science and Engineering* 4.1, pp. 34–45.

MAASRANI, M., A. DROCHON, M. HARMOUCHE, H. CORBINEAU, and J.-P. VERHOYE (2013). "Theoretical study of the flow rate toward the right heart territory in case of total occlusion of the right coronary artery." eng. In: *Med Eng Phys* 35.1, pp. 103–107. DOI: 10.1016/j.medengphy.2012.04.005.

MANOR, D., S. SIDEMAN, U. DINNAR, and R. BEYAR (1994). "Analysis of coronary circulation under ischaemic conditions." eng. In: *Med Biol Eng Comput* 32.4 Suppl, S123–S132.

MOHR, F. W., M.-C. MORICE, A. P. KAPPETEIN, T. E. FELDMAN, E. STÅHLE, A. COLOMBO, M. J. MACK, D. R. HOLMES, M. ANGÈLE MOREL, N. V. DYCK, V. M. HOULE, K. D. DAWKINS, and P. W. SERRUYS (2013). "Coronary artery bypass graft surgery versus percutaneous coronary intervention in patients with three-vessel disease and left main coronary disease: 5-year follow-up of the randomised, clinical SYNTAX trial." eng. In: *Lancet* 381.9867, pp. 629–638. DOI: 10.1016/S0140-6736(13)60141-5.

MORRIS, M. (1991). "Factorial sampling plans for preliminary computational experiments". In: *Technometrics* 33.2, pp. 161–174.

OJEDA, D., V. L. ROLLE, and A. I. HERNÁNDEZ (2011). "A Model of the Cardiovascular System integrating the Coronary Circulation". In: *Recherche en Imagerie et Technologies pour la Santé (RITS 2011)*.

OJEDA, D., V. LE ROLLE, A. DROCHON, H. CORBINEAU, J.-P. VERHOYE, and A. I. HERNÁNDEZ (2012). "Sensitivity analysis and parameter estimation of a coronary circulation model for patients with triple-vessel disease". In: *Proceedings of The Virtual Physiological Human 2012 (VPH2012)*. London.

OJEDA, D., V. LE ROLLE, M. HARMOUCHE, A. DROCHON, H. CORBINEAU, J.-P. VERHOYE, and A. I. H. HERNÁNDEZ (2013). "Sensitivity analysis and parameter estimation of a coronary circulation model for triple-vessel disease". Submitted to IEEE transactions on biomedical engineering (Currently in minor revisions).

OLUFSEN, M. and A. NADIM (2004). "On deriving lumped models for blood flow and pressure in the systemic arteries". In: *Math Biosci Eng* 1.1, pp. 61–80.

PIETRABISSA, R., S. MANTERO, T. MAROTTA, and L. MENICANTI (Sept. 1996). "A lumped parameter model to evaluate the fluid dynamics of different coronary bypasses". In: *Medical Engineering & Physics* 18.6, pp. 477–484.

PIJLS, N. H., G. J. BECH, M. I. EL GAMAL, H. J. BONNIER, B DE BRUYNE, B VAN GELDER, H. R. MICHELS, and J. J. KOOLEN (1995). "Quantification of recruitable coronary collateral blood flow in conscious humans and its potential to predict future ischemic events". In: *J Am Coll Cardiol* 25.7, pp. 1522–1528.

RENTROP, K. P., M COHEN, H BLANKE, and R. A. PHILLIPS (1985). "Changes in collateral channel filling immediately after controlled coronary artery occlusion by an angioplasty balloon in human subjects". In: *J Am Coll Cardiol* 5.3, pp. 587–592.

RINEHART, S., G. VAZQUEZ, Z. QIAN, L. MURRIETA, K. CHRISTIAN, and S. VOROS (2011). "Quantitative measurements of coronary arterial stenosis, plaque geometry, and composition are highly reproducible with a standardized coronary arterial computed tomographic approach in high-quality {CT} datasets". In: *Journal of Cardiovascular Computed Tomography* 5.1, pp. 35 –43. ISSN: 1934-5925. DOI: 10.1016/j.jcct.2010.09.006.

ROCKSTROH, J and B. G. BROWN (2002). "Coronary collateral size, flow capacity, and growth: estimates from the angiogram in patients with obstructive coronary disease". In: *Circulation* 105.2, pp. 168–173.

SABISTON, D. C. and D. E. GREGG (1957). "Effect of cardiac contraction on coronary blood flow". In: *Circulation* 15.1, pp. 14–20.

Sagawa, K., R. Lie, J. Schaefer, et al. (1990). "Translation of Otto Frank's paper "Die Grundform des Arteriellen Pulses" Zeitschrift fur Biologie 37: 483-526 (1899)." In: *Journal of molecular and cellular cardiology* 22.3, p. 253.

Schaper, W (2009). "Collateral circulation: past and present". In: *Basic Res Cardiol* 104.1, pp. 5–21. doi: 10.1007/s00395-008-0760-x.

Seiler, C. (2003). "The human coronary collateral circulation". In: *Heart* 89.11, p. 1352.

Siebes, M., S. A. J. Chamuleau, M. Meuwissen, J. J. Piek, and J. A. E. Spaan (2002). "Influence of hemodynamic conditions on fractional flow reserve: parametric analysis of underlying model." eng. In: *Am J Physiol Heart Circ Physiol* 283.4, H1462–H1470. doi: 10.1152/ajpheart.00165.2002.

Siebes, M. and Y. Ventikos (2010). "The role of biofluid mechanics in the assessment of clinical and pathological observations". In: *Annals of biomedical engineering* 38.3, pp. 1216–1224.

Smith, B., S. Andreassen, G. Shaw, P. Jensen, S. Rees, and J. Chase (2007). "Simulation of cardiovascular system diseases by including the autonomic nervous system into a minimal model". In: *Computer methods and programs in biomedicine* 86.2, pp. 153–160.

Spaan, J. A., N. P. Breuls, and J. D. Laird (1981). "Diastolic-systolic coronary flow differences are caused by intramyocardial pump action in the anesthetized dog". In: *Circ Res* 49.3, pp. 584–593.

Steg, P. G., A Kerner, G. B. Mancini, H. R. Reynolds, A. C. Carvalho, V Fridrich, H. D. White, S. A. Forman, G. A. Lamas, J. S. Hochman, C. E. Buller, and OAT Investigators (2010). "Impact of collateral flow to the occluded infarct-related artery on clinical outcomes in patients with recent myocardial infarction: a report from the randomized occluded artery trial". In: *Circulation* 121.25, pp. 2724–2730. doi: 10.1161/CIRCULATIONAHA.109.933200.

Wang, J. Z., B Tie, W Welkowitz, J Kostis, and J Semmlow (1989). "Incremental network analogue model of the coronary artery". In: *Med Biol Eng Comput* 27.4, pp. 416–422.

Waters, S. L., J Alastruey, D. A. Beard, P. H. Bovendeerd, P. F. Davies, G Jayaraman, O. E. Jensen, J Lee, K. H. Parker, A. S. Popel, T. W. Secomb, M Siebes, S. J. Sherwin, R. J. Shipley, N. P. Smith, and F. N. van de Vosse (2011). "Theoretical models for coronary vascular biomechanics: progress & challenges". In: *Prog Biophys Mol Biol* 104.1-3, pp. 49–76. doi: 10.1016/j.pbiomolbio.2010.10.001.

Werner, G. S., M Ferrari, S Heinke, F Kuethe, R Surber, B. M. Richartz, and H. R. Figulla (2003). "Angiographic assessment of collateral connections in comparison with invasively determined collateral function in chronic coronary occlusions". In: *Circulation* 107.15, pp. 1972–1977. doi: 10.1161/01.CIR.0000061953.72662.3A.

WHO (2008). *World Health Statistics 2008*. World Health Organization.

CHAPTER 7

Patient-specific analysis of a cardiovascular model for CRT optimization

Résumé

Ce chapitre traite de l'application d'un modèle du système cardiovasculaire pour l'optimisation des thérapies de resynchronisation cardiaque (CRT). Le modèle proposé dans cette application inclut les descriptions de : *i)* l'activité électrique cardiaque, *ii)* un pacemaker bi-ventriculaire, et *iii)* l'activité mécanique cardiaque couplé aux circulations systémiques et pulmonaires. Afin d'appréhender la complexité de ce modèle, des analyses de sensibilités locales et globales ont pu être effectuées. Celles-ci ont notamment pu mettre en évidence l'importance des paramètres de précharge et ceux liés à la diastole. Les résultats préliminaires, concernant l'identification de paramètres spécifique-patient, mettent en évidence la proximité entre les débits mitraux simulés et ceux mesurés par échographie lors d'une séance d'optimisation des paramètres de la CRT.

In previous chapters, heart failure (HF) has been presented and analyzed with modeling approaches in order to understand the complex mechanisms that characterize this multifactorial pathology. Among the population affected by HF, 30 % to 40 % of patients show a significant cardiac ventricular desynchronization and are candidates for an implant-based therapy known as "Cardiac Resynchronization Therapy" (CRT). These cardiac implantable devices should be configured in a personalized manner in order to deliver an optimal therapy. However, the optimal, patient-specific configuration of these devices is a challenging task due to the complexity of the cardiovascular system. This chapter provides another example of the proposed model-based analysis methods, focused on the difficult problem of the definition of optimal, patient-specific therapies.

7.1 Pathophysiological aspects

Current therapeutic recommendations for symptomatic patients suffering from heart failure (HF) and presenting ventricular desynchronization (left ventricular systolic dysfunction, left ventricular ejection fraction $< 35\%$ and a QRS duration $> 120\,\text{ms}$), include the implant of a multisite cardiac stimulation device. This implant-based therapy, known as *cardiac resynchronization therapy* (CRT) is based on the electrical stimulation of the right atrium and both the right and left ventricles, at specific timings, in order to: *i)* improve left ventricular (LV) filling, by maximizing the contribution from the atrial systole, and *ii)* synchronize the mechanical activity of both ventricles, increasing the effective contribution of each ventricular wall to the ejection and, therefore, improving cardiac output. CRT has been shown to provide a significant improvement in most clinical markers of HF patients, promoting cardiac remodeling and to reducing hospitalizations (CAZEAU et al., 2001; LECLERCQ et al., 2002; MULLENS et al., 2009). However, the effectiveness of CRT is highly dependent on the implant configuration (particularly on the definition of the atrioventricular pacing delay—AVD), and this configuration has been shown to be patient-specific (COATRIEUX et al., 2005). The lack of a systematic and personalized optimization of these parameters may partly explain why approximately 30% of CRT patients do not respond correctly to this therapy (MCALISTER et al., 2007).

CRT optimization may be performed by analyzing a set of electrophysiological and echocardiographic markers of the cardiac response, acquired from an implanted patient while modifying the atrio-ventricular delay (AVD) and the intra-ventricular delay (VVD) within a given range (GOLD et al., 2007; JANSEN et al., 2006; RITTER et al., 1999). However, this is a long and tedious work that is seldom performed in clinical practice. Moreover, these analyses lead to large datasets of complex, multivariate data, which are very difficult to analyze, due to the multifactorial nature of this pathology. In order to ease this complex analysis, this chapter proposes a model-based approach, based on a lumped-parameter electro-mechanical model of the cardiovascular system, coupled with a simple model of a CRT device. To our knowledge, this application provides the first detailed sensitivity analysis of such a coupled model, integrating physiologically relevant parameter values. We estimate that these analyses can help to better understand the influence of the main CRT parameters on the patient response and may help the definition of new, streamlined CRT optimization procedures.

7.2 Problem statement and proposed approach

A model designed for the assistance of CRT optimization must take into account three elements: *i)* the electrical activity of the heart, *ii)* a biventricular pacemaker, and *iii)* the mechanical activity of the heart, as well as the pulmonary and systemic circulations. Consequently, the model proposed in this application is the integration of three main sub-models that represent these elements.

Models of the cardiac electrical and mechanical activity have been developed in our lab-

oratory, including implementation details and model validation with respect to real patient data (Hernández et al., 2002; Koon et al., 2010; Smith et al., 2007). In this occasion, a new coupling implementation is proposed, with a significant effort on the definition of appropriate pathophysiological values for model parameters. The following sections briefly describe each model component.

7.2.1 Electrical heart model

Since the 50's, the interest and knowledge of cardiac cell electrophysiology has been integrated in a wide range of models. These modeling efforts can be categorized in three groups: *i)* Realistic biophysical models of ion currents, defining the continuous dynamics of the flow of ions through the cardiac cell membranes (Hodgkin et al., 1952; Noble, 1962; Tusscher et al., 2006); these detailed biophysical models require a high number of state variables and parameters to describe the ionic currents and action potential of each cell, hindering their potential application in a global cardiovascular model, *ii)* Simplified ionic channel descriptions that are computationally cheaper models while reproducing the depolarization and repolarization oscillation of cardiac cells. These models are often based on the Hodgkin-Huxley simplification introduced by the FitzHugh-Nagumo model (FitzHugh, 1955; Karamcheti et al., 2012; Nagumo et al., 1962). *iii)* Simplified discrete models usually based on cellular automata, representing the electrical states of the action potential and their transitions (Fleureau, 2008; Hernández, 2000; Le Rolle, 2006).

The cardiac electrical system used for this application is based on the last group; the electrical conduction system is defined as a set of coupled cellular automata, adapted from (Hernández et al., 2002). Each cellular automata represents the electrical activation state of a given myocardial tissue, covering the main electrophysiological activation periods: slow diastolic depolarisation (T_{SDD}), upstroke depolarization (T_{UDP}), absolute refractory (T_{ARP}) and relative refractory (T_{RRP}), as shown in fig. 7.1. The state of the cellular automata cycles through these four stages, sending an output stimulation signal to neighboring cells when a given cell is activated (at the end of UDP phase). In this work, we consider three types of cardiac cells: the sinoatrial node (SAN), nodal cell automatas (NA) and myocardial cell automatas (MA).

The whole electrical model consists of 20 automata coupled as the illustration of fig. 7.2. This configuration was chosen because it can generate ventricular activations through a retrograde or lateral paths, specially under certain *VVD* configurations of a biventricular pacemaker, which cannot be simulated with simpler models. For this work, the depolarization of the AVN is fixed at an infinite value in order to represent atrioventricular block, which is a common inclusion criterion for CRT.

The model has four inputs: three stimulation inputs from the pacemaker (StimA, StimLV, StimRV), and the base heart rate (HR, in bpm), which determines the SSD period of the SAN. Lastly, the model generates five outputs: the stimulation generated after the atrial node, useful for the activation of the pacemaker, and four independent stimulations that trigger the mechanical

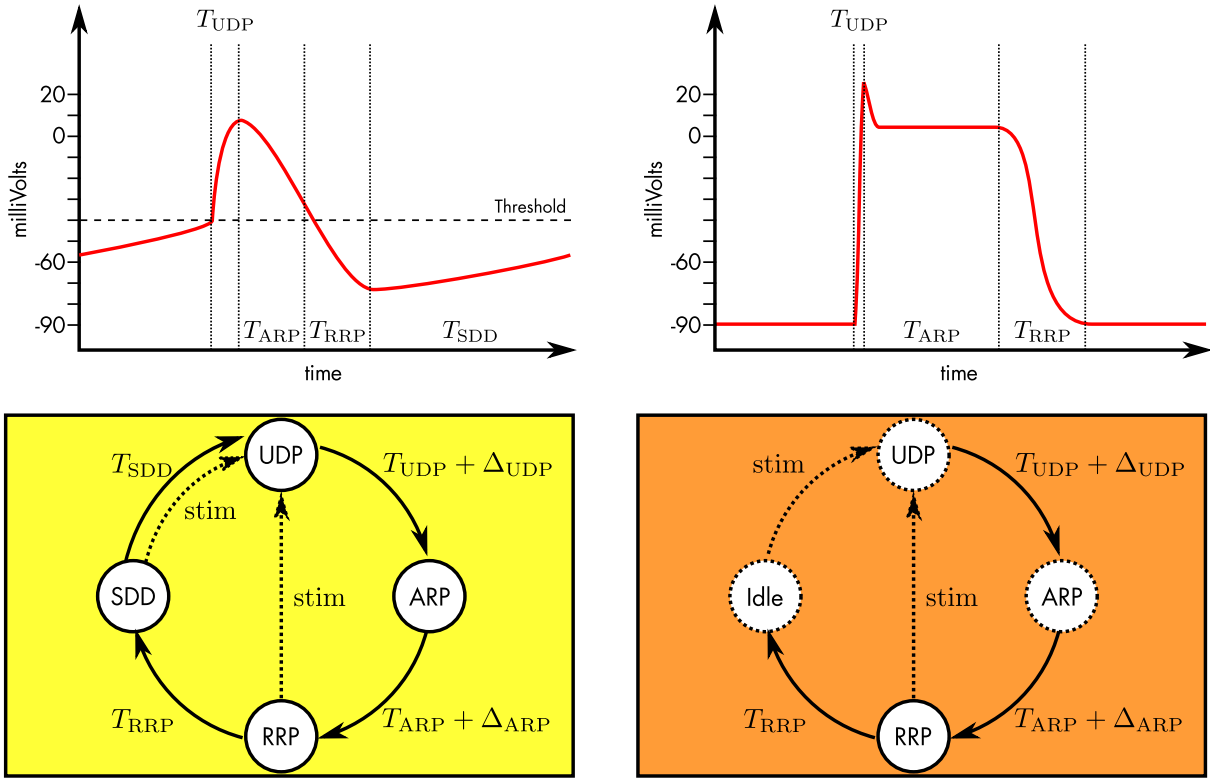

FIGURE 7.1– State diagram of the cellular automata that represent nodal cells (yellow, left) and myocardial cells (orange, right). The diagram at the top shows the correspondence of the automata's transition parameters with the myocardial action potential dynamics.

contraction of each heart chamber, as explained in the next sections. The values for all cell parameters are taken from (HERNÁNDEZ, 2000).

7.2.2 Simplified CRT pacemaker model

The pacemaker model simulates a CRT system with three independent stimulation electrodes in contact with the right atrium and both ventricles. Even though the device can control the heart rate by pacing the right atrium, it is used under the *sensor* configuration, which detects the spontaneous impulse in the atrium and then sends a stimulation to the ventricles. In this operational mode, the simplified CRT pacemaker model is composed of one input, two delays and two outputs. The input of the model (SenseAtrial) is the electrical impulse delivered by the FPSRA1 node of the cardiac electrical model. When the pacemaker input probe detects this impulse, it sends two independent electrical impulses to the left and right ventricles, according to the atrio-ventricular (AVD) and intra-ventricular (VVD) delays: The pacemaker can be summarized in the following equations:

$$\text{StimRV}(t + AVD + VVD) = \text{SenseAtrial}(t)\,, \tag{7.1}$$

$$\text{StimLV}(t + AVD) = \text{SenseAtrial}(t)\,. \tag{7.2}$$

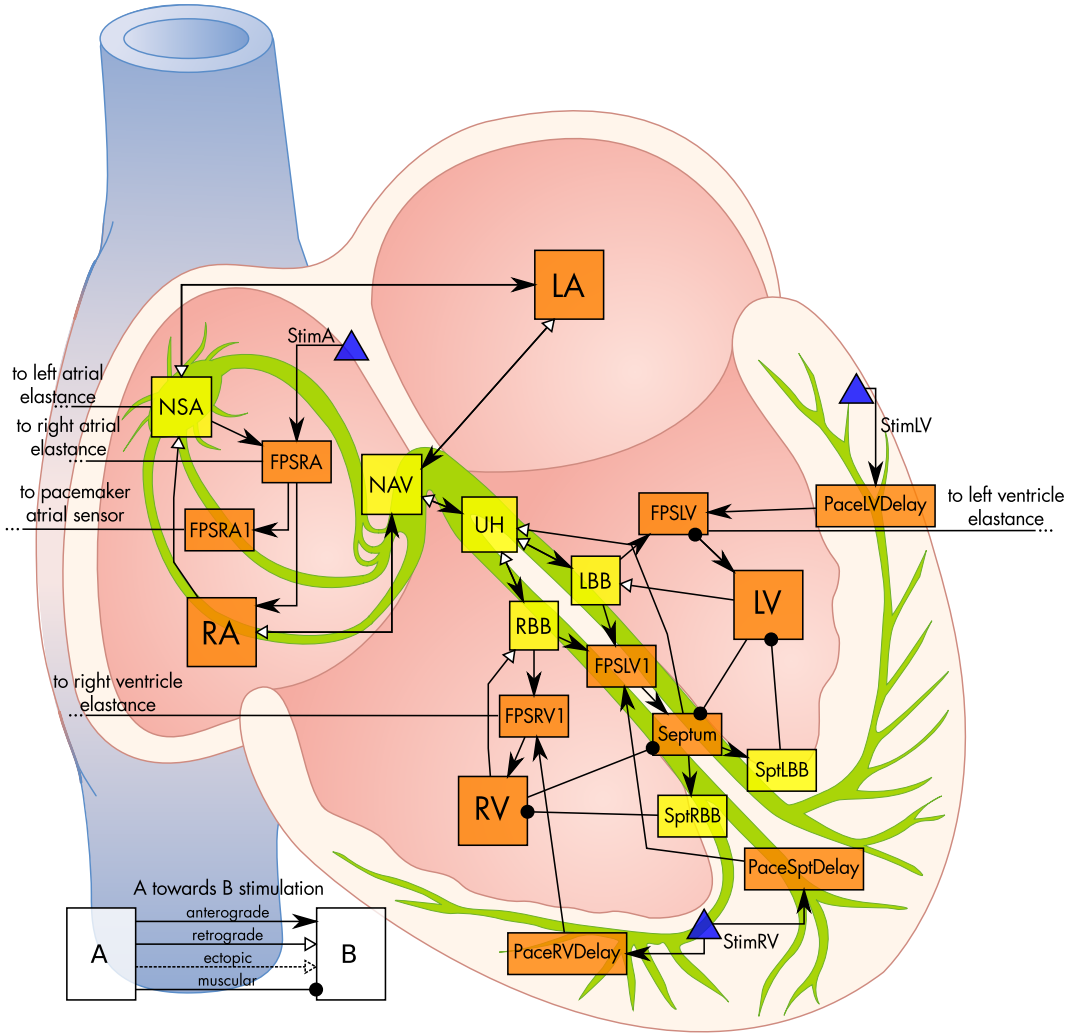

FIGURE 7.2– Cellular automata representation of the cardiac electrical conduction system. Yellow boxes represent nodal cell automatas; orange boxes represent myocardial cells.

7.2.3 Cardiac mechanics and circulatory model

The mechanical contraction of atria and ventricles is an effect of the shortening of the sarcomere fibers, the basic contractile structure of a myocardial cell. This fiber contraction is directly mediated by the electrical mechanisms at the cellular level, since the action potential across the cell membrane drives the flow of ions into the myocardial cell and activate the protein mechanisms that shorten the sarcomere. Therefore, the electrophysiological dynamics must be coupled with a mechanical description of the cardiac tissues. Further, the fiber contraction generated by this mechanical phenomenon must be coupled with a hydraulic model to calculate the generated pressure and volume variations of a cardiac chamber.

This electrical-mechanical and mechanical-hydraulic coupling has been largely addressed in the literature: from microscopic scales (HUNTER et al., 1998), to macroscopic approaches (GUARINI

et al., 1998; PALLADINO et al., 2001), including intermediary formulations (LE ROLLE et al., 2005). While fine scale models require an important amount of parameters and significant computational resources, lumped parameter models, on the other hand, offer a good compromise of complexity and accuracy. In this work, the electrical activation of four different elements of the cardiac electrical system trigger the outset of a corresponding elastance driving function. The cardiovascular model consists of a description of the passive and active elastic properties of the heart, based on the model of (SMITH et al., 2007), as illustrated in fig. 7.3, which includes all four cardiac chambers, and two circulatory networks.

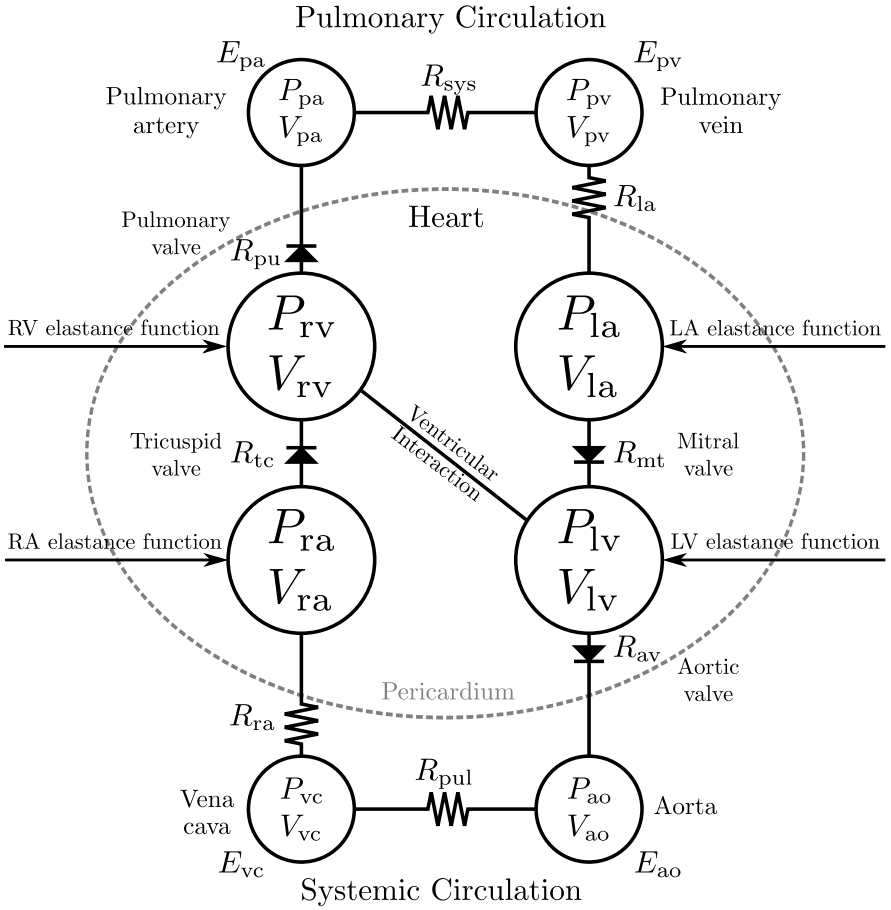

FIGURE 7.3– Circulatory and mechanical heart model.

The equations that describe the model dynamics have been presented in chapter 5; only two elements differ for this application: the inclusion of pulsatile atria and the design of a ventricular elastance driving function that is more adapted to HF. To account for the mechanical function of the atria, the left atrial pressure P_{la} is a linear function of its instantaneous volume V_{la}, whose slope E_{la} represents the elastic properties of the atrial wall:

$$P_{\mathrm{la}}(V_a, t) = E_{\mathrm{la}}(t) \cdot (V_{\mathrm{la}}(t) - V_{\mathrm{d,la}})\,, \tag{7.3}$$

$$E_{\mathrm{la}}(t) = E_{\mathrm{la,max}} \left(e_{\mathrm{la}}(t) + \frac{E_{\mathrm{la,min}}}{E_{\mathrm{la,max}}} \right)\,, \tag{7.4}$$

where $e_{\mathrm{la}}(t)$ is a Gaussian driving function that cycles between atrial diastole and systole:

$$e_{\mathrm{la}}(t) = \exp\left(-B_{\mathrm{la}}\left(\frac{\mathrm{HR}}{\mathrm{HRR}}\right)^2 \cdot \left(t - C_{\mathrm{la}}\frac{\mathrm{HRR}}{\mathrm{HR}}\right)^2\right). \tag{7.5}$$

Using B_{la} and C_{la}, it is possible to control the rise and peak of the atrial systole. Moreover, these parameters are adjusted to reduce or enlarge the systolic period when the heart rate is different than the baseline resting heart rate (HRR) of 60 bpm.

The driving function for the left ventricle is composed of two Gaussian functions with a common peak C_{lv}:

$$e_{\mathrm{lv}}(t) = \begin{cases} \exp\left(-B_{\mathrm{lv1}}\left(\frac{\mathrm{HR}}{\mathrm{HRR}}\right)^2\left(t - C_{\mathrm{lv}}\frac{\mathrm{HRR}}{\mathrm{HR}}\right)^2\right) & \text{if } t < C_{\mathrm{lv}}\,, \\ \exp\left(-B_{\mathrm{lv2}}\left(\frac{\mathrm{HR}}{\mathrm{HRR}}\right)^2\left(t - C_{\mathrm{lv}}\frac{\mathrm{HRR}}{\mathrm{HR}}\right)^2\right) & \text{if } t \geq C_{\mathrm{lv}}\,. \end{cases} \tag{7.6}$$

An asymmetric driver function permits to independently control the rise of the ventricular systole before (B_{lv1}) and after (B_{lv2}) its maximum value. This design is similar to existing elastance functions (Chung et al., 1997; Guarini et al., 1998), but permits to simulate a longer decay of the ventricular activation, which is typical for the abnormal ventricular activity of subjects with HF. For the right atrium and ventricle, the same eqs. (7.3) to (7.6) are used with subscript $_{\mathrm{r}}$.

The simultaneous consideration of atrial and ventricular dynamics permits the integrated model to generate typical mitral flow profiles, as shown in figs. 7.4 and 7.5(a) and discussed later. Mitral flow profiles present a particular shape during the cardiac cycle: along with the pressure drop of the left ventricle during diastole, the mitral valve opens and the ventricle is partially filled. The peak of flow due to this passive early filling is known as the E-wave. Immediately, the left atrium contracts and causes an additional blood flow observable by a second peak, the A-wave, which decays until the valve closes due to the increased pressure at the onset of ventricular contraction.

7.3 Simulation results

Depending on the parameter values, the model can produce the hemodynamics of different cardiovascular pathologies. This section presents two different situations: a normal healthy heart and a subject with HF with left ventricular dysfunction and preserved right ventricular function, undergoing CRT with an active pacemaker. The model parameters values were selected from the publications from which each model was originally based: ventricular and circulatory parameters were taken from (Smith et al., 2007), atrial parameters were adapted from (Heldt et al., 2002), and cardiac electrical conduction system from (Hernández et al., 2002). All parameter values are included in appendix C.

Subjects with HF often present a prolonged QRS duration (>120 ms) due to injuries of the heart electrical conduction system, which causes an inter and intra ventricular conduction delay. Furthermore, HF show an increased ventricular systole duration, an impaired diastolic ventricular function and a loss in ventricular contractility. Reduced diastolic function leads to increased

TABLE 7.1– Parameter values used for the simulation of a healthy and a HF subject

(a) Left cardiac parameters.

Parameter	**Healthy**	**HF**
$E_{\mathrm{la,min}}$ ($\mathrm{mmHg\,mL^{-1}}$)	0.3	0.045
$E_{\mathrm{la,max}}$ ($\mathrm{mmHg\,mL^{-1}}$)	1.2	2.0
$E_{\mathrm{es,lv}}$ ($\mathrm{mmHg\,mL^{-1}}$)	3.4	3.0
$V_{\mathrm{d,lv}}$ (mL)	30	100
$V_{\mathrm{o,lv}}$ (mL)	30	100
λ_{lv} ($\mathrm{mL^{-1}}$)	0.01	0.015
C_{lv} (s)	0.18	0.22

(b) Circulation parameters.

Parameter	**Healthy**	**HF**
R_{sys} ($\mathrm{mmHg\,s\,mL^{-1}}$)	1.05	2.05
E_{vc} ($\mathrm{mmHg\,mL^{-1}}$)	0.011	0.009
R_{pul} ($\mathrm{mmHg\,s\,mL^{-1}}$)	0.143	0.18
E_{pa} ($\mathrm{mmHg\,mL^{-1}}$)	0.34	2.81
E_{pu} ($\mathrm{mmHg\,mL^{-1}}$)	0.006	0.002
$V_{\mathrm{d,pu}}$ (mL)	200	245
Blood volume (L)	6	6.5

atrial contractility in order to compensate for the loss in early ventricular filling. Finally, HF also causes a reduced stroke volume as a result of a dilated ventricle and the stiffening of its walls. In order to consider these aspects, model parameters were manually adjusted as shown in tables 7.1(a) and 7.1(b).

Simulation results of the two subject profiles are shown in fig. 7.4. For both simulations, the heart rate was fixed at 60 bpm. For the healthy patient, the pacemaker was not included, while the HF subject had an enabled pacemaker at $AVD = 120$ ms and simultaneous biventricular stimulation ($VVD = 0$ ms). Simulated values are qualitatively coherent with clinical observations: the HF subject presents lower systolic and diastolic pressures (99/73 mmHg) than the healthy counterpart (124/72 mmHg), while the pulmonary arterial pressure shows the opposite trend (25/4 mmHg for healthy, 31/3 mmHg for HF). Ventricular volumes show an augmentation for HF, with significant reduction of the ejection fraction (23% HF, 54% healthy). Concerning ventricular filling, results show a significant change of mitral flow profile and its related clinical markers: the ratio of the peak E and A waves (E/A ratio) drops from a healthy 1.6 to 0.34, which is typical of systolic dysfunction HF. The ratio of mitral flow duration to RR-interval ($RMitRR$) is also reduced, from 0.54 to 0.44.

7.3.1 Simulation of AVD optimization of a CRT device

The choice of the appropriate AVD is of foremost importance during CRT. A common optimization procedure consists in determining the AVD with longest diastolic filling time without A-wave truncation (RITTER et al., 1999), which can be determined by changing the pacemaker delays and observing pulsed-wave doppler of the mitral inflow. Considering that the model is able to produce mitral flows, an AVD optimization procedure can be simulated for the HF subject by changing the AVD gradually from 40 ms to 300 ms.

Figure 7.5(a) shows some of the mitral flow profiles for this range. HR is kept constant at 60 bpm and flow profiles are centered around the ventricular stimulation, represented by the annotated vertical line. The other vertical lines show the beginning of atrial systole for each AVD configuration. When $AVD = 40$ ms, the A wave shows a clear truncation as a consequence of an

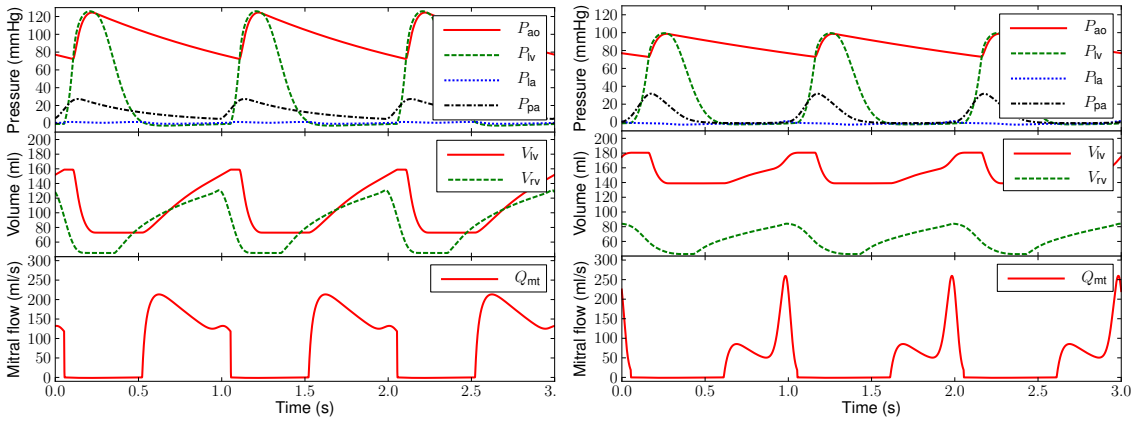

(a) Healthy subject.

(b) HF subject.

FIGURE 7.4– Simulated hemodynamic outputs for a healthy and a heart failure subject. Top panel shows pressures of left ventricle (P_{lv}), left atrium (P_{la}), aorta (P_{ao}) and pulmonary artery (P_{pa}). Middle panel shows left and right ventricular volumes (V_{lv}, V_{rv}). Bottom panel shows mitral valve flow (Q_{mt}).

early contraction of the left ventricle. On the other hand, an $AVD = 280\,\mathrm{ms}$ presents nearly a complete fusion of the E and A waves.

In addition to mitral flow profiles, some additional variables can be considered during AVD optimization, such as diastolic filling time, represented by the ratio of mitral flow to the RR segment ($RMitRR$). The velocity time integral (VTI) of the mitral flow, which corresponds to the mitral flow time integral ($MFTI$) can also provide information on the ventricular filling. Finally, one can consider the systolic blood pressure (SBP) and the maximum rate of change of left ventricular pressure (LV ${}^{dP}/_{dt}\mathrm{max}$), since they are markers of cardiac contractility and they have been considered in several atrio-ventricular delay optimization for CRT (AURICCHIO et al., 2002; JANSEN et al., 2006). The variation of these markers are presented in fig. 7.5(b). The analysis of their variations reveals some important points:

- The A-wave truncation seems to occur only with $AVD < 50\,\mathrm{ms}$, evidenced by the sudden drop of the blue curve in the bottom right plot. Configurations below this point would hinder the contribution of atrial contraction.
- The $RMitRR$ ratio, a surrogate of diastolic filling time, shows a sudden drop when $AVD > 130\,\mathrm{ms}$. Configurations over this limit produce a ventricular contraction that occurs too late, when the atrium has already finished its contraction, as evidenced by the AVD =200 ms and 280 ms curves in fig. 7.5(a). The contraction of the ventricle with such configuration would produce a high ventricular pressure with a relaxed atrium, causing the mitral valve to regurgitate if a patient presents some form of valve insufficiency.
- Although the $MFTI$ shows only an improvement of approximately 10 % for $AVD > 100\,\mathrm{ms}$, this delay configuration has a positive impact on the systolic blood pressure and left ventricle contractility. On the other hand, after a delay longer than 200 ms, the effect on $RMitRR$, SBP and LV ${}^{dP}/_{dt}\mathrm{max}$ is slightly detrimental. Although in this example the

effect is very modest, a similar parabolic effect can be observed in clinical *AVD* and *VVD* optimization (WHINNETT et al., 2006).

Considering the information presented above, for this virtual patient the simulation results suggest an optimal *AVD* around 110 ms to 130 ms.

7.4 Sensitivity analysis

Considering that the dynamics of the mitral flow and the choice of an optimal *AVD* depend on various internal mechanisms of the cardiovascular system, it would be interesting to Considering the interactions of different systems introduced by the integration of different models, three sensitivity analyses were performed to understand the effect of the model parameters on the simulated variables that play an important role during the CRT delay optimization procedure. These analyses are presented in the following sections, which are focused on the E and A wave peak values, *RMitRR* ratio, *MFTI*, and other hemodynamic variables such as the maximum rate of change of the left ventricular pressure (LV $^{dP}/_{dt}$max) and the systolic blood pressure (*SBP*).

7.4.1 Local sensitivity analysis

A first setting used to understand the influence of model parameters was based on a local sensitivity study. As explained in chapter 4, this type of analysis is performed by varying the value of a single parameter while fixing the rest. In this case, the working point parameter values were those of the HF subject in table 7.1 with $AVD = 120$ ms, which is long enough to avoid A wave truncation, while short enough to prevent fusion of E and A waves. These local analysis were concentrated on the left atrial and ventricular parameters since these two chambers, which are separated by the mitral valve, should be the predominant causes of variations in mitral flow profiles. The variations for each parameter followed the ranges of table 7.2.

Several local analyses were performed, but only one reference result is shown here (cf. fig. 7.6). The main findings of these analyses were:

- The effect of λ_{lv} (diastolic-related parameter) on mitral flow is very significant, on all selected variables, as shown in the example of fig. 7.6.
- In contrast to the diastolic properties, the systolic parameters ($E_{\mathrm{es,lv}}$) show a similar pattern, but not a significant effect on the A-wave.
- Timing-related parameters (C_{lv}, B_{lv1} and B_{lv2}) have an impact on the passive filling (E wave) in the same way as diastolic properties.
- After λ_{lv} and $E_{\mathrm{es,lv}}$, the maximum atrial elastance ($E_{\mathrm{la,max}}$) shows the most significant effect on the E wave and systolic blood pressure, but a minor effect on all other variables.

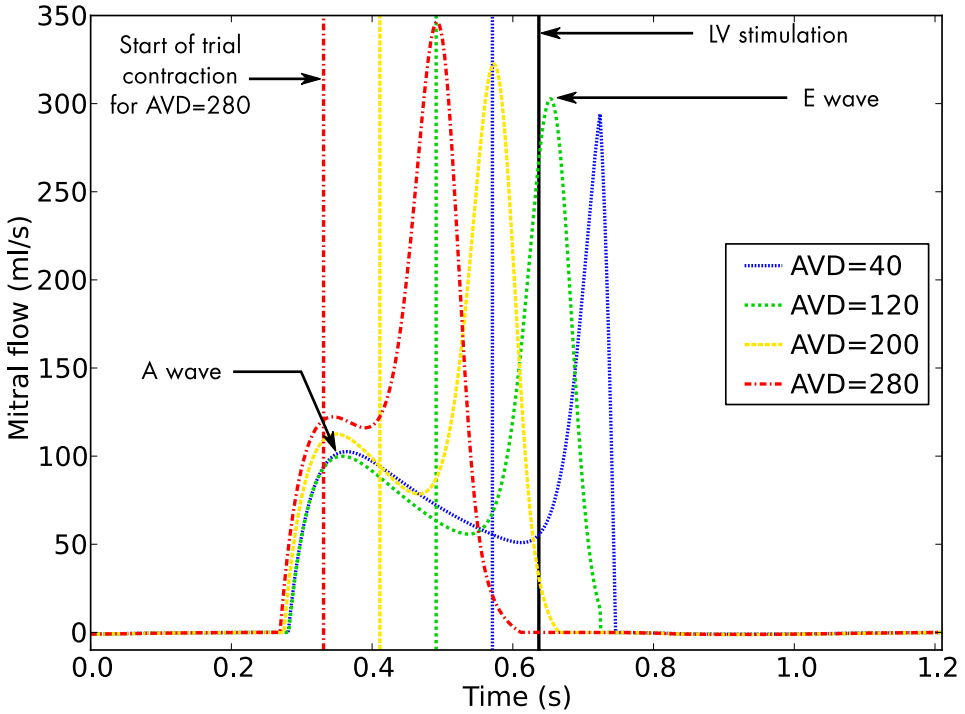

(a) Simulated mitral flow profiles for an *AVD* ranging from 40 ms to 280 ms at a fixed HR of 60 bpm. All flows have been synchronized with respect to their ventricular stimulation. Vertical lines indicate the onset of atrial contraction for each case.

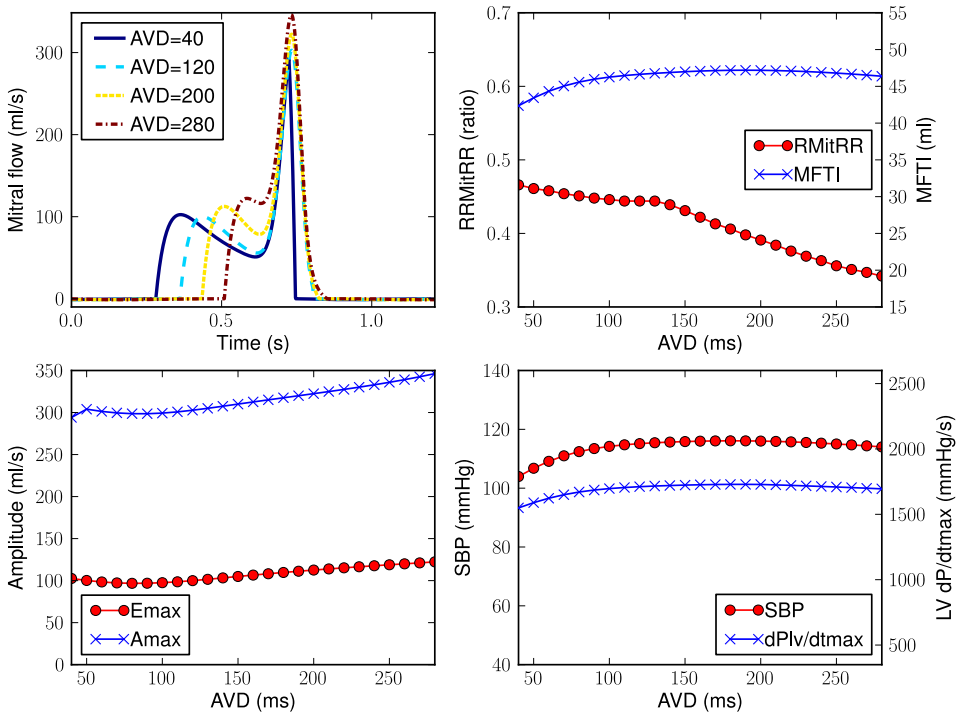

(b) Simulated mitral flow characteristics for different *AVD* values. Top left: flow profiles, top right: *RMitRR* and *MFTI*, bottom left: E and A waves amplitudes, and bottom right: systolic blood pressure (*SBP*) and LV $^{dP}/_{dt}$max.

FIGURE 7.5– Simulated mitral flow profiles and characteristics for *AVD* optimization of a CRT device.

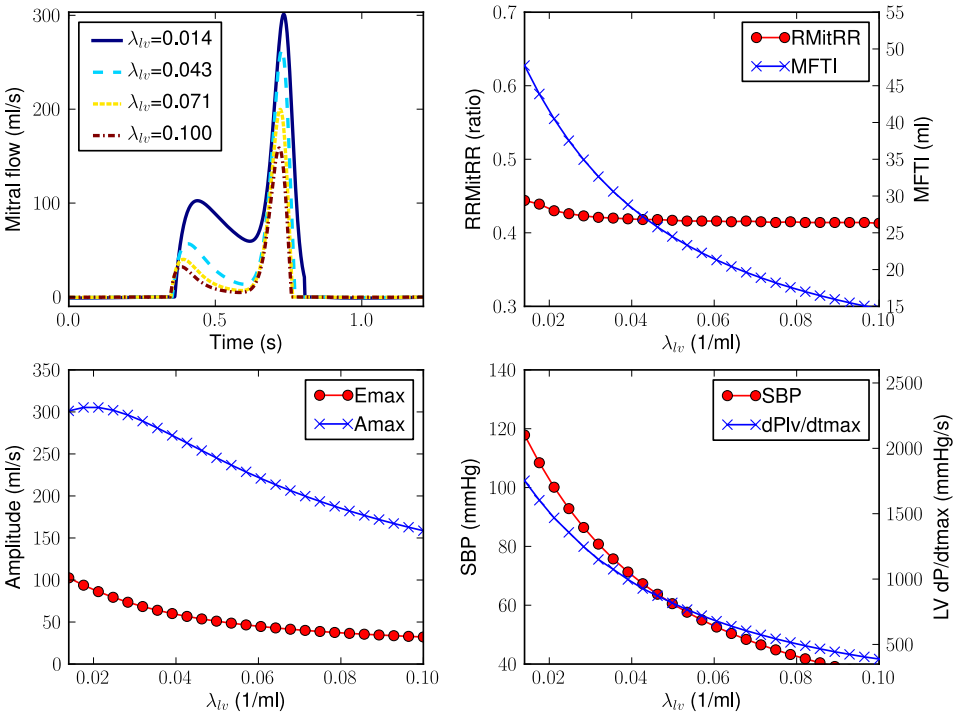

FIGURE 7.6– Local effect of variations of the diastolic elastance (λ_{lv}) on mitral flow profiles (top left), *RMitRR* and *MFTI* (top right), peak values of E and a waves (bottom left), *SBP* and LV $^{dP}/_{dt}$max (bottom right). λ_{lv} units are /mL

7.4.2 Parameter screening

Local sensitivity analysis provide good insights on how the dynamics of the model and how the mitral flow is sensitive to some parameters. However this approach is not exhaustive, it does not consider all model parameters and it can miss important influences that are only visible in other parameter value configurations. In order to observe the sensitivity of the model outputs to all parameters and to compare the extent of all parameter effects, the Morris elementary effects method (MORRIS, 1991) was used to screen the most important parameters. The details of this method have been presented in chapter 4.

In this work, the Morris method was applied to the model for all its parameters, each within physiologically consistent ranges that were determined from cardiovascular modeling literature, mainly from (CHUNG et al., 1997; HELDT et al., 2002; LU et al., 2001; SMITH et al., 2007). An exhaustive list of parameter values found in the literature is included in appendix C. Considering all the variability found in the literature, a list of parameter ranges was compiled and is presented in table 7.2.

Table 7.2: Parameter used for sensitivity analyses.

Parameter	Units	Minimum value	Maximum value
$E_{\mathrm{la,max}}$	$\mathrm{mmHg\,mL^{-1}}$	0.13	2.54
$E_{\mathrm{la,min}}$	$\mathrm{mmHg\,mL^{-1}}$	0.075	1.81
$V_{\mathrm{d,la}}$	mL	1.83	45.34
$E_{\mathrm{es,lv}}$	$\mathrm{mmHg\,mL^{-1}}$	0.1	8.0
$V_{\mathrm{d,lv}}$	mL	0	71.44
$V_{\mathrm{o,lv}}$	mL	0	71.44
λ_{lv}	$\mathrm{mL^{-1}}$	0.014	0.100
$P_{\mathrm{o,lv}}$	mmHg	0.2	4
R_{mt}	$\mathrm{mmHg\,s\,mL^{-1}}$	0.00045	0.016
R_{av}	$\mathrm{mmHg\,s\,mL^{-1}}$	0.005	0.045
R_{la}	$\mathrm{mmHg\,s\,mL^{-1}}$	0.001	0.015
$E_{\mathrm{ra,max}}$	$\mathrm{mmHg\,mL^{-1}}$	0.20	0.91
$E_{\mathrm{ra,min}}$	$\mathrm{mmHg\,mL^{-1}}$	0.15	0.38
$V_{\mathrm{d,ra}}$	mL	3	30
$E_{\mathrm{es,rv}}$	$\mathrm{mmHg\,mL^{-1}}$	0.34	2.87
$V_{\mathrm{d,rv}}$	mL	0	89
$V_{\mathrm{o,rv}}$	mL	0	89
λ_{rv}	$\mathrm{mL^{-1}}$	0.01	0.06
$P_{\mathrm{o,rv}}$	mmHg	0.35	1.2
R_{tc}	$\mathrm{mmHg\,s\,mL^{-1}}$	0.0013	0.007
R_{pv}	$\mathrm{mmHg\,s\,mL^{-1}}$	0.001	0.042
R_{ra}	$\mathrm{mmHg\,s\,mL^{-1}}$	0.008	0.075
λ_{pcd}	$\mathrm{mL^{-1}}$	0.005	0.030
P_{th}	mmHg	-4	-2
E_{ao}	$\mathrm{mmHg\,mL^{-1}}$	0.62	0.76
$V_{\mathrm{d,ao}}$	mL	425	973
E_{vc}	$\mathrm{mmHg\,mL^{-1}}$	0.010	0.015
$V_{\mathrm{d,vc}}$	mL	2300	3000
R_{sys}	$\mathrm{mmHg\,s\,mL^{-1}}$	0.77	1.53
E_{pa}	$\mathrm{mmHg\,mL^{-1}}$	0.0769	6.37
$V_{\mathrm{d,pa}}$	mL	50	160
E_{pu}	$\mathrm{mmHg\,mL^{-1}}$	0.006	0.125
$V_{\mathrm{d,pu}}$	mL	120	512

Continued on next page...

Table 7.2 – Parameter used for sensitivity analyses (continued from previous page).

Parameter	Units	Minimum value	Maximum value
R_{pul}	$\mathrm{mmHg\,s\,mL^{-1}}$	0.004	0.312
AVD	ms	40	200
VVD	ms	−40	60
B_{la}	$\mathrm{s^{-2}}$	60	1500
C_{la}	s	0.04	0.5
B_{ra}	$\mathrm{s^{-2}}$	60	1500
C_{ra}	s	0.04	0.5
C_{lv}	s	0.175	0.4
B_{lv1}	$\mathrm{s^{-2}}$	60	1500
B_{lv2}	$\mathrm{s^{-2}}$	60	1500
C_{rv}	s	0.175	0.4
B_{rv1}	$\mathrm{s^{-2}}$	60	1500
B_{rv2}	$\mathrm{s^{-2}}$	60	1500
UDP (PaceLVDelay)	ms	10	80
UDP (FPSRA1)	ms	10	80
HR	bpm	46	90
Blood volume	ml	3750	6890

The screening method was configured to calculate $r = 1000$ elementary effects for $n = 46$ parameters, with a grid of $p = 50$ levels and a variation $\Delta = 0.02$. In total, this configuration performed 47 000 simulations; each simulation lasted 60 s. After this time, the last beat was analyzed in order to determine the last mitral flow curve and the systolic and diastolic pressure and volume measurements. Results for the mitral flow E and A wave amplitudes are presented in figs. 7.7(a) and 7.7(b), and further results (*RMitRR*, *MFTI*) have been included in appendix C. For all results, the mean and standard deviation plane is presented in the top panel; the bottom panel shows the parameters ordered according to their rank. However, the results in this chapter only include the 30 most important parameters in order to improve the readability.

The main findings of the parameter screening results were:

– All studied outputs are mostly dependent of left heart parameters and pulmonary circulation elastances. Dependence to left heart parameters is not surprising, since the analyzed outputs are part of this subsystem. However, the pulmonary circulation effect on preloadis an important factor for mitral flow and should not be taken for granted in any CRT model.

– Although right heart parameters do not stand out as the most important group of parameters, their effect is still non negligible. Indeed, the right heart parameters can affect the left

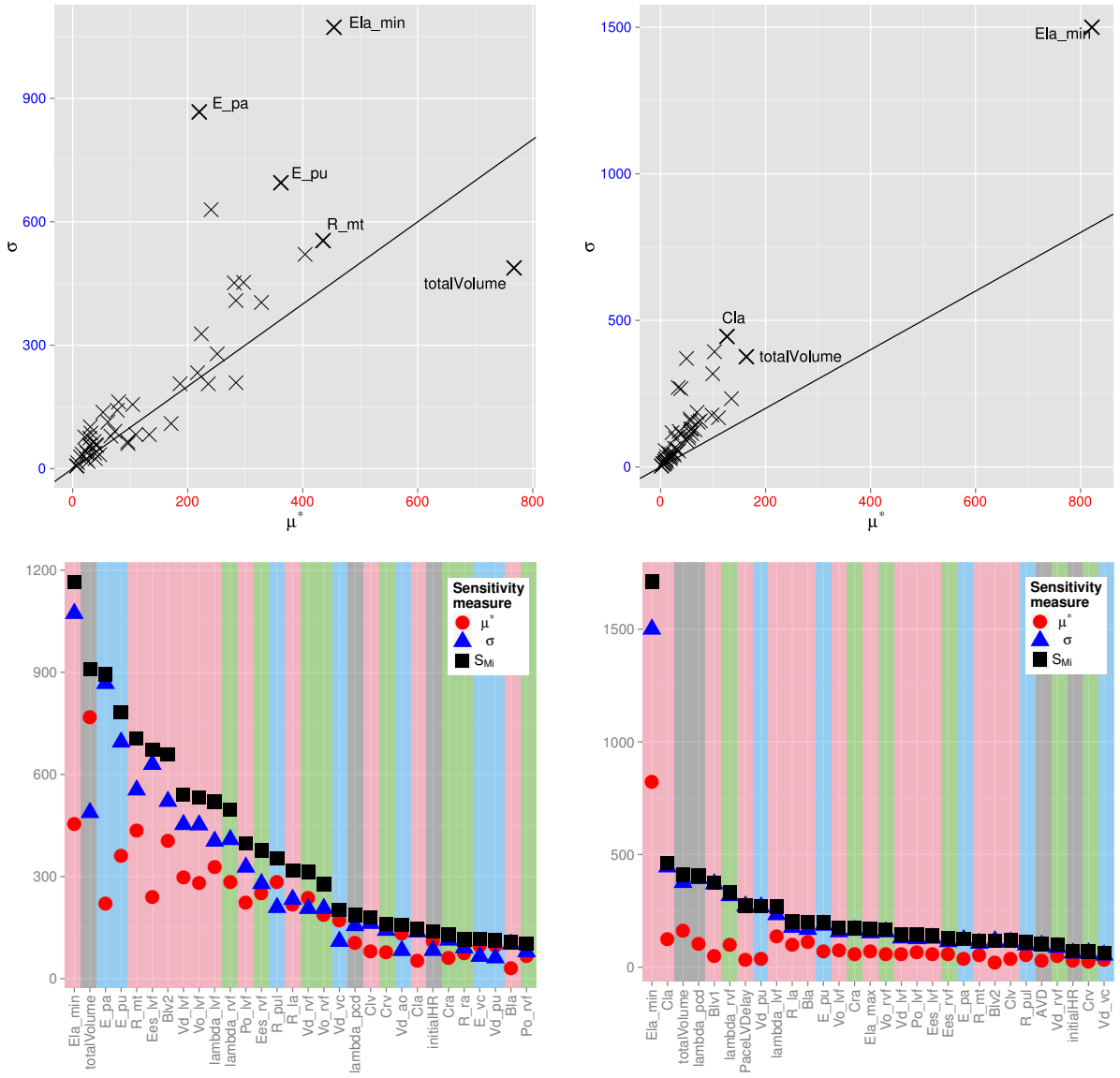

(a) Elementary effects for E wave amplitude.

(b) Elementary effects for A wave amplitude.

FIGURE 7.7– Results of Morris elementary effects method for E and A wave amplitudes. Top plots show the $\mu^* - \sigma$ plane. Bottom plots show the mean (μ^*), standard deviation (σ) and the Morris index (S_{Mi}) of the 30 most important parameters. Background of bottom plots are color-coded: red stripes are parameters of the left heart, green stripes are parameters of the right heart, blue stripes are parameters related to the circulation, and gray stripes are general or other parameters.

heart dynamics in two ways: through the inter-ventricular interaction due to the septum wall and pericardium, and through the effect in the closed loop of the circulation.

- Wave amplitudes and all pressure and volume variables are heavily affected by the total blood volume. Cardiovascular modeling publications, such as (BENEKEN et al., 1967; HELDT et al., 2002; SMITH et al., 2007) usually dismiss this parameter quite quickly and set its value from general human cardiovascular statistics. It is easy to forget that blood volume affects all chambers and vessels of the cardiovascular system, yet its consideration for HF patients should not be ignored; the control of blood (and plasma) volume is one of the key mechanisms of diuretics and other HF related drug therapies.
- The effect of *AVD* and *VVD* delays are masked by the overwhelming effects of all other parameters. This observation should be considered with caution: it does not suggest that these delays are unimportant for CRT optimization, but it may indicate a limitation of this modeling approach, since our model only considers the short-term effect of these parameters.
- The general distribution of the parameters on the μ^* vs. σ space indicates that the effect of most parameters is either nonlinear or caused by the interaction with other parameters. In particular, for the A wave amplitude (cf. fig. 7.7(b)), all parameters are situated above the $\mu^* = \sigma$ reference line, which indicates that the dynamics of this variable are more complicated than its E wave counterpart. On the other hand, parameters below $\mu^* = \sigma$ (i.e. parameters whose red circle is situated above the blue triangle on the lower panels) include blood volume, dead and zero-point volumes (V_d, V_o) and heart rate.

7.4.3 Global sensitivity analysis: Sobol indices

To complement the information revealed by the previous analysis, an additional sensitivity analysis was performed to explain the source to the high variability (σ) found in the elementary effects. At this point, since a global sensitivity analysis based on first and total order indices requires a high number of simulations, only the most important parameters were included.

The Sobol indices approach was selected for this global analysis, explained before in chapter 4. Further details on the Monte-Carlo method that estimates the Sobol indices are available in (SALTELLI et al., 2010). A total of 30 parameters were considered, with probability distributions considered as uniform in the ranges of table 7.2. To ensure a good estimation of the first and total order effects, a total of 320 000 simulations were performed. Results for E and A wave peak values and mitral flow duration and time integral are shown in fig. 7.8. The rest of the results are included in appendix C.

E wave results in fig. 7.8(a) show an important dependence on total blood volume and all left ventricle parameters. Right ventricle parameters show a significant effect, but only in their total effect, which implies that their effect is due to interactions with other parameters. Timing parameters, including *AVD*, do not have an important effect on the amplitude of the E wave, with the exception of B_lv2; the effect of the elastance after the left ventricular peak was already identified in the Morris screening results, but here this effect is mediated with the interaction of

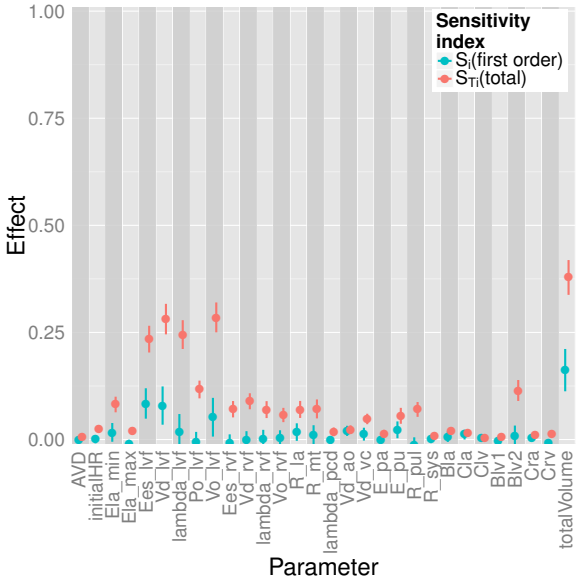

(a) Sobol indices for E wave amplitude.

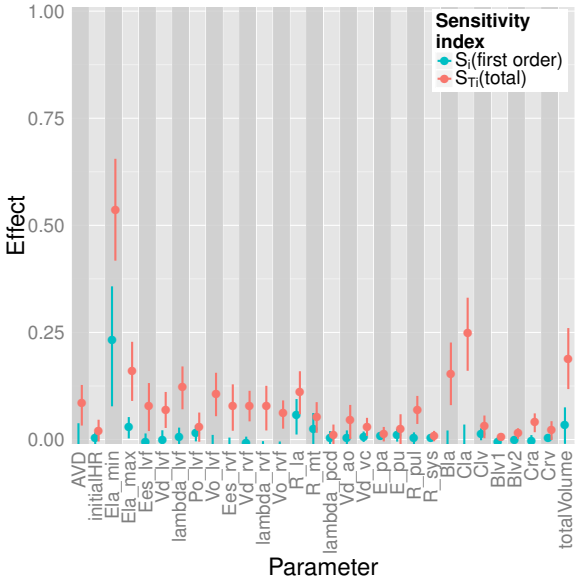

(b) Sobol indices for A wave amplitude.

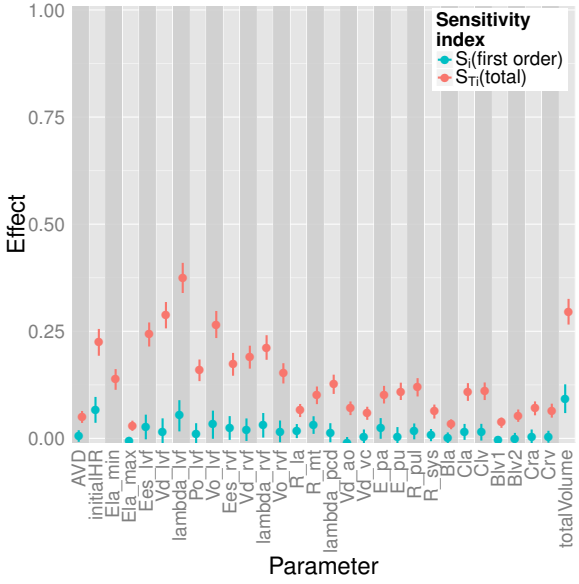

(c) Sobol indices for mitral flow duration.

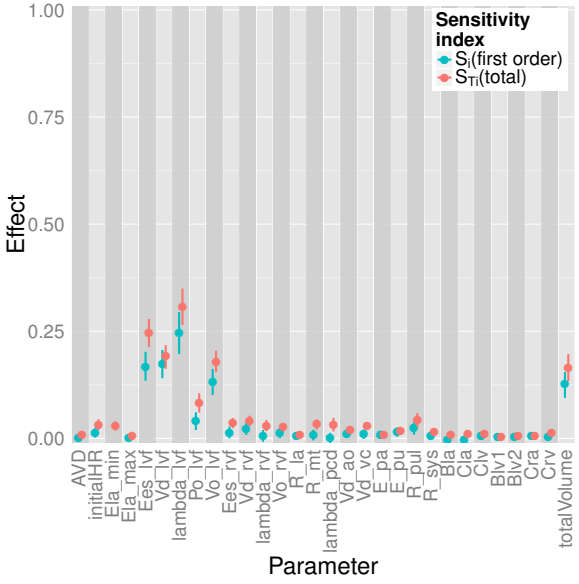

(d) Sobol indices for mitral flow time integral.

FIGURE 7.8– Results of a global sensitivity analysis using Sobol indices for E and A wave amplitudes, mitral flow duration and its time integral. Blue ranges indicate first order effects (sensitivity to parameter variations alone), red ranges indicate total order effects (sensitivity to parameter interactions). All points are accompanied by their 90 % confidence interval.

other parameters.

A wave results in fig. 7.8(b) show a high effect of atrial parameter $E_{\mathrm{la,min}}$, and an even more important effect when considering its interactions. Globally, the A wave amplitude is highly dependent of interactive effects, which complicates the understanding of the dynamics of this mitral flow marker. Most interactions are probably originated from left and right ventricle

parameters. The effects from the left ventricle is evident, but from the right ventricle is only possible if one considers the effect of the right heart on the pulmonary circulation and preload, or its interaction with the left ventricle through the septal wall. This uncertainty could be elucidated with a more detailed analysis of higher order effects.

Concerning the effect of timing and elastance-shape parameters on the A wave, a clear significant interaction is observed for the left atrium, but a low effect from the ventricle. Further, the *AVD* delay shows a non negligible effect, but only due to interactions with other parameters. This result suggests that *AVD* modulation only provokes a change in A wave under certain parameter configurations; a suggestion that needs further analysis and is potentially interesting for the investigation of non-responders of CRT.

Similarly to the A wave amplitude, the results for mitral flow time duration in fig. 7.8(c) show an example of a simulated variable that depends mostly on parameter interactions. In fact, all parameters have a low first-order effect accompanied with a total effect so significant that it is difficult to draw any conclusion. However, systolic and diastolic ventricle parameters seem to provide most of these interactions. More detailed analysis are needed to understand the effect on mitral flow duration, such as the calculation of higher order indices (2nd or 3rd order), but this needs more simulations and, more importantly, the possible combinations of groups of 2–3 parameters out of 30 parameters are 870 and 24360 respectively, which might be difficult to analyze later.

On the other hand, *MFTI* results in fig. 7.8(d) show an example of a variable with very few interactions, since their first order effects do not differ significantly from the total effects. Almost all variability is explained by six elements: left ventricle parameters and total volume. These results imply that cardiac output, which is directly related to *MFTI*, is mostly dependent on LV parameters, both systolic and diastolic.

7.5 Patient-specific parameter identification

The next step on the analysis of the model is the identification of the model parameters in order to reproduce real data of patients during CRT. A patient with HF without mitral regurgitation underwent an echographic examination for a post-operative CRT optimization. During this examination, different *AVD* configurations from 80 and 155 ms were tested; for each configuration, a thoracic ultrasound performed by a clinician assessed the mitral flow. The audio output of a General Electric®VIVID 7 scanner was connected to a data acquisition system that extracts the raw mitral flow audio signal, recorded at 10 kHz for at least three consecutive cardiac cycles with the same ECG morphology. A three way ECG was also recorded simultaneously at 1 kHz. For each *AVD* configuration, the audio signal was processed to extract the mitral flow contour for each cycle. With all extracted contours for a configuration, the average contour was calculated. In addition to mitral flow and ECG, the ejection volume and systemic pressures (systolic and diastolic) was also acquired.

In total, the obtained data from the CRT optimization session were: instantaneous heart

rate, averaged contour of mitral flow, left ventricular ejection volume (EV), systolic and diastolic blood pressures. Using the heart rate, *AVD* and the detected stimulation in the ECG leads permitted the exact synchronization of the clinical and simulated data. Then, the following functions were designed for an multiobjective optimization procedure:

$$g_\epsilon^{(1)} = \left\langle \mathrm{RMSE}(Q_{\mathrm{mt}}^{\mathrm{cli}}, Q_{\mathrm{mt}}^{\mathrm{sim}}) \right\rangle \quad , \tag{7.7}$$

$$g_\epsilon^{(2)} = \left\langle \left| \frac{P_{\mathrm{ao,s}}^{\mathrm{cli}} - P_{\mathrm{ao,s}}^{\mathrm{sim}}}{P_{\mathrm{ao,s}}^{\mathrm{cli}}} \right| \right\rangle , \tag{7.8}$$

$$g_\epsilon^{(3)} = \left\langle \left| \frac{P_{\mathrm{ao,d}}^{\mathrm{cli}} - P_{\mathrm{ao,d}}^{\mathrm{sim}}}{P_{\mathrm{ao,d}}^{\mathrm{cli}}} \right| \right\rangle , \tag{7.9}$$

$$g_\epsilon^{(4)} = \left\langle \left| \frac{V_{\mathrm{EV}}^{\mathrm{cli}} - V_{\mathrm{EV}}^{\mathrm{sim}}}{V_{\mathrm{EV}}^{\mathrm{cli}}} \right| \right\rangle , \tag{7.10}$$

where $^{\mathrm{cli}}$ and $^{\mathrm{sim}}$ denote clinical and simulated data respectively, RMSE is the root mean squared error of two signals, $P_{\mathrm{ao,s}}$ is systolic aortic pressure, $P_{\mathrm{ao,d}}$ is diastolic aortic pressure and V_{EV} is the ejection volume calculated as the difference between systolic and diastolic left ventricular volumes. The optimization functions consider all available *AVD*, which is why every function is expressed as the average $\langle\cdot\rangle$ of all *AVD* configurations.

Considering that the integrated CVS model consists of > 50 parameters, a complete identification from four clinical variables is unfeasible. Only the following 18 parameters were selected for the estimation phase, according to the results of the previous sensitivity analyses:

- Parameters that had an important total order indices for Q_{mt} indices: $E_{\mathrm{la,max}}$, $E_{\mathrm{la,min}}$, $E_{\mathrm{es,lv}}$, $V_{\mathrm{d,lv}}$, $P_{\mathrm{o,lv}}$, λ_{lv}, $V_{\mathrm{o,lv}}$, C_{lv}, C_{la} and total volume. Timing parameters of the left heart were also included: B_{la}, B_{lv1} and B_{lv2}.
- Parameters with a significant effect over aortic pressure: E_{pu} and R_{sys}.
- Some parameters that had a low effect but were consistently present in all variables: right ventricle parameters $E_{\mathrm{es,rv}}$ and λ_{rv}, and R_{mt}.

The parameter estimation approach consisted in the application of the multiobjective evolutionary algorithm presented in chapter 4 (NSGA-II). Parameter ranges were equal to sensitivity analysis ranges in table 7.2. The evolutionary algorithm was parametrized as follows: a population of 1800 individuals, during 100 generations and with crossover and mutation probabilities $p_c = 0.8$ and $p_m = 0.1$.

7.5.1 Parameter identification results

Statistics of the final population, consisting of 1800 individuals that estimate the Pareto region for the four objective functions, are shown in table 7.3. The evaluation of the objective functions for these individuals show a good estimation of the pressure-related objectives: in average, results have a relative error of 7.05 and 8.24 % for systolic and diastolic pressure estimations (i.e. $g_\epsilon^{(2)}$ and $g_\epsilon^{(3)}$). However, mitral flow and EV present relative errors of 15.56 and 11.11 %.

Due to the multiobjective nature of the problem, and considering that the results show an important variability in some parameters, it is not possible to determine which individual among

the final population represents the optimal solution. However, the *best* individual was selected as the one with the minimum value of:

$$\text{Euclid}\left(g_\epsilon^{(1)}, g_\epsilon^{(2)}, g_\epsilon^{(3)}, g_\epsilon^{(4)}\right) = \sqrt{\sum_{k=1}^{4}\left(g_\epsilon^{(k)}\right)^2}, \tag{7.11}$$

which is the Euclidean distance to the origin of the objective function space. This individual shows significantly better results for all objective functions, with a minor increase on $g_\epsilon^{(2)}$, as listed in table 7.3. From this individual, a comparison of the simulated and clinical data is shown in fig. 7.9. The simulated mitral flows show a good, but not perfect correspondence with clinical data. In general, A wave peaks and the start and end of the mitral flow are well estimated, but E wave shows some differences in AVD of 80, 95 and 110 ms. A significant part of this discrepancy between simulated and clinical data can be attributed to the segment between the E and A peaks: for this particular data, the decay of the passive mitral flow presents a decrease that is barely monotonous (see AVD =80, 95 and 155 ms). This effect could be the product of the averaging of several mitral flows; it suggests that the clinical data treatment may need to be revised.

Further analysis of the identification results requires the consideration of the entire Pareto region estimation. Figure 7.10 shows the points that estimate this region in the objective function space. The color of each point represents the point's evaluation of eq. (7.11). In other words, blue points are closer to the best individual and red points are farther. These plots provide some interesting insights when analyzing their distribution: blue dots are concentrated at near $g_\epsilon^{(1)}$, $g_\epsilon^{(3)}$ and $g_\epsilon^{(4)}$, but for $g_\epsilon^{(2)}$, these same points are situated around 0.09-0.10. This suggests that points in the Pareto can simultaneously minimize further the $g_\epsilon^{(2)}$ function, but with a negative impact on the other three objective functions, and viceversa.

When studying the distribution of the parameter values of the Pareto region, in fig. 7.11, some additional patterns can be observed. The densities of the parameters show that, in the Pareto region, the values of these parameters are well delimited to a certain range. This is the case for $E_{\text{la,min}}$, λ_{lv}, λ_{rv}, C_{la}, $P_{\text{o,lv}}$ and B_{lv2}. When interpreting a well defined range back to their physiological signification, it is possible to suggest some patient-specific interpretations. For example, the results for this patient present a λ_{lv} between 0.014 to 0.03 mL^{-1} and $P_{\text{o,lv}}$ between 0.2 to 1.2 mmHg. This implies that the left ventricle is particularly flexible during diastole. On the other hand, the same patient presents a high range for λ_{rv}: 0.05 to 0.06 mL^{-1}, indicating a stiff right ventricle and probably some right ventricle diastolic dysfunction due to an inadequate relaxation.

On the other hand, some parameters have a wide variability, such as $E_{\text{la,max}}$, $V_{\text{d,lv}}$, $V_{\text{o,lv}}$, $E_{\text{es,rv}}$, E_{pu}, B_{la} and B_{lv1}. This suggest that there are many different configurations for these parameters that produce good results. If the sensitivity of these parameters were low, they could be fixed to a value without much impact on the objective functions. Alas, these parameters were selected because of their clear effect. A lower variability can be obtained if the most important parameters are fixed, including those whose ranges are relatively well defined. Another approach would be to include more observable data in the optimization method or direct the evolutionary

TABLE 7.3– General results of the multiobjective estimation, including its estimated parameters and the evaluated objective functions. The pareto estimation column includes the mean and standard deviation of the individuals in the last generation. The best individual is calculated from the Euclidean distance to the origin in the objective function space.

Objective function	**Units**	**Pareto estimation** ($\mu \pm \sigma$)			**Best individual**
$g_\epsilon^{(1)}$	–	0.1556	$\pm$	0.0488	0.0526
$g_\epsilon^{(2)}$	–	0.0705	$\pm$	0.0249	0.0871
$g_\epsilon^{(3)}$	–	0.0824	$\pm$	0.0403	0.0531
$g_\epsilon^{(4)}$	–	0.1111	$\pm$	0.0537	0.0619
Euclid	–	0.2314	$\pm$	0.0473	0.1304
Parameter value	**Units**	**Pareto estimation** ($\mu \pm \sigma$)			**Best individual**
$E_{\mathrm{la,max}}$	$\mathrm{mmHg\,mL^{-1}}$	1.1928	$\pm$	0.5560	0.6503
$E_{\mathrm{la,min}}$	$\mathrm{mmHg\,mL^{-1}}$	0.1003	$\pm$	0.0351	0.0859
$E_{\mathrm{es,lv}}$	$\mathrm{mmHg\,mL^{-1}}$	5.4608	$\pm$	1.7251	6.0516
$V_{\mathrm{d,lv}}$	mL	23.2208	$\pm$	14.4405	42.1182
$V_{\mathrm{o,lv}}$	mL	43.7797	$\pm$	19.1904	25.8725
λ_{lv}	$\mathrm{mL^{-1}}$	0.0195	$\pm$	0.0058	0.0172
C_{lv}	s	0.3778	$\pm$	0.0141	0.3704
C_{la}	s	0.2526	$\pm$	0.0180	0.2770
Blood volume	mL	4942.4620	$\pm$	111.5063	5017.187
E_{pu}	$\mathrm{mmHg\,mL^{-1}}$	0.0485	$\pm$	0.0222	0.0341
R_{sys}	$\mathrm{mmHg\,s\,mL^{-1}}$	1.4400	$\pm$	0.0879	1.4829
$E_{\mathrm{es,rv}}$	$\mathrm{mmHg\,mL^{-1}}$	1.4068	$\pm$	0.7998	0.7463
λ_{rv}	$\mathrm{mL^{-1}}$	0.0538	$\pm$	0.0060	0.0452
R_{mt}	$\mathrm{mmHg\,s\,mL^{-1}}$	0.0131	$\pm$	0.0023	0.0140
$P_{\mathrm{o,lv}}$	mmHg	0.6679	$\pm$	0.4288	0.9355
B_{la}	$\mathrm{s^{-2}}$	545.5344	$\pm$	275.5533	118.2519
B_{lv1}	$\mathrm{s^{-2}}$	1086.3980	$\pm$	388.8994	1367.855
B_{lv2}	$\mathrm{s^{-2}}$	98.7465	$\pm$	14.8673	90.9478

algorithm towards solutions that are clinically coherent, which would need further assistance from clinicians.

7.6 Conclusion

The application presented in this chapter proposes a model composed of an integration of several lumped-parameter models that is capable of generating mitral flow profiles similar to those observed clinically during standard echographic examinations. After close examination of local and global parameter variations, sensitivity analyses showed how atrial and ventricular parameters impact on the main characteristics of mitral flow profiles. Moreover, the global analysis identified the most influential parameters on mitral flow profiles. In addition to the identification of atrial

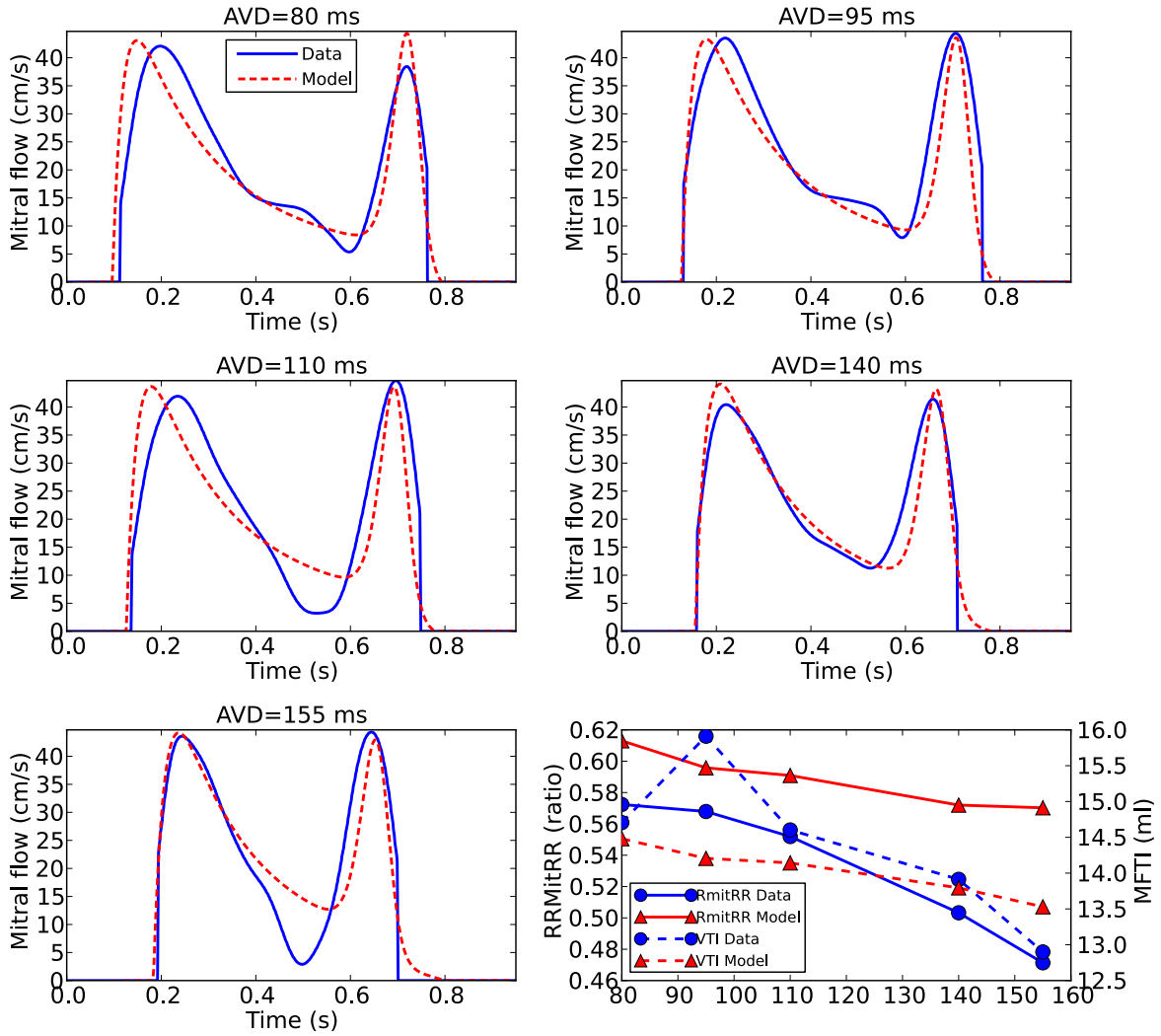

FIGURE 7.9– Simulated and clinical mitral flow profiles for a patient. Simulated data was generated with the parameter values of the best individual listed in table 7.3.

and ventricular properties (systolic and diastolic) among the most influential parameters, the importance of preload related variables (such as the pulmonary circulation parameters) and global parameters (including the total blood volume) was also revealed.

An initial step towards a patient-specific parameter identification based from data of a CRT optimization session was presented as well. Taking advantage of the improved understanding of the parameter effects, a multi-objective estimation was used to explore a physiologically relevant parameter space. The results of this estimation give opportunities for the improvement of the agreement between simulated and clinical mitral flow profiles. Nevertheless, the parameter analysis of the estimation results already provide important information that can be transposed to physiological interpretations.

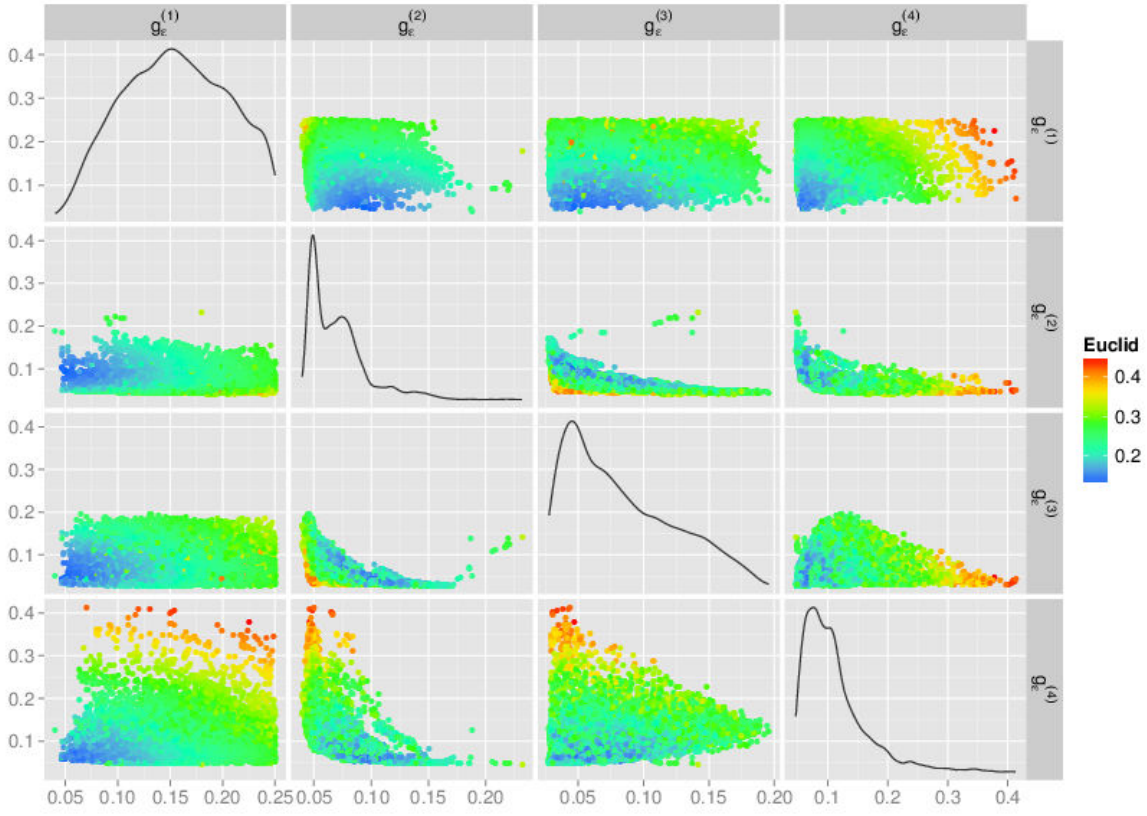

FIGURE 7.10– Scatterplot of the evaluation of all four objective functions for the individuals in the final Pareto region estimation. Plots in the diagonal show the estimation of the density function of the corresponding objective function. The color of each point represents the Euclid distance to the origin, calculated in the $g_\epsilon^{(1)} \times g_\epsilon^{(2)} \times g_\epsilon^{(3)} \times g_\epsilon^{(4)}$ hyperspace.

References

AURICCHIO, A., J. DING, J. C. SPINELLI, A. P. KRAMER, R. W. SALO, W. HOERSCH, B. H. KENKNIGHT, and H. U. KLEIN (2002). "Cardiac resynchronization therapy restores optimal atrioventricular mechanical timing in heart failure patients with ventricular conduction delay". In: *Journal of the American College of Cardiology* 39.7, pp. 1163–1169.

BENEKEN, J. E. and B. DEWIT (1967). "A physical approach to hemodynamic aspects of the human cardiovascular system". In: *Physical bases of circulatory transport: regulation and exchange*. Ed. by E. REEVE and A. GUYTON. Philadelphia: Saunders, pp. 1–45.

CAZEAU, S., C. LECLERCQ, T. LAVERGNE, S. WALKER, C. VARMA, C. LINDE, S. GARRIGUE, L. KAPPENBERGER, G. A. HAYWOOD, M. SANTINI, C. BAILLEUL, J. C. DAUBERT, and M. S. I. C. M. U. S. T. I. C. S. I. (2001). "Effects of multisite biventricular pacing in patients with heart failure and intraventricular conduction delay." eng. In: *N Engl J Med* 344.12, pp. 873–880.

CHUNG, D., S. NIRANJAN, J. CLARK, A. BIDANI, W. JOHNSTON, J. ZWISCHENBERGER, and D. TRABER (1997). "A dynamic model of ventricular interaction and pericardial influence". In: *American Journal of Physiology-Heart and Circulatory Physiology* 272.6, H2942.

COATRIEUX, J. L., A. I. HERNÁNDEZ, P. MABO, M. GARREAU, and P. HAIGRON (2005). "Transvenous path finding in cardiac resynchronization therapy". In: *Functional Imaging and Modeling of the Heart*. Springer, pp. 236–245.

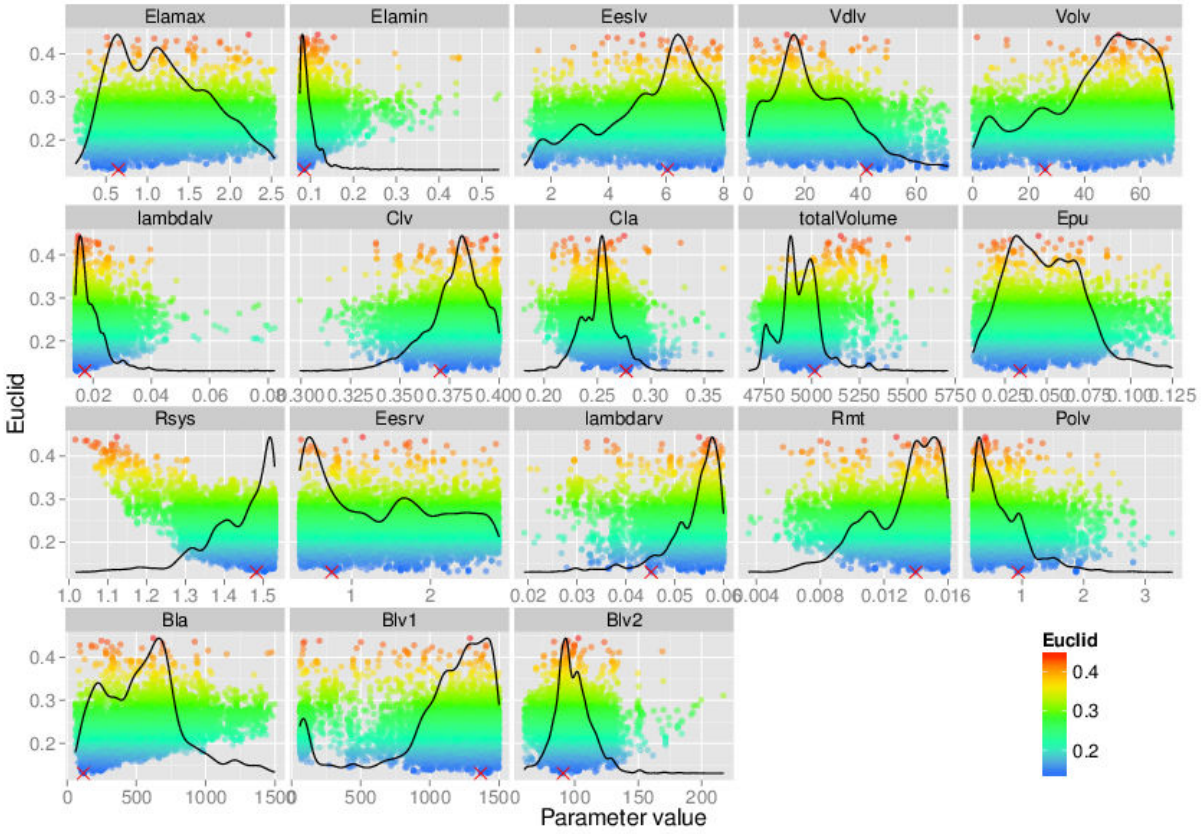

FIGURE 7.11– Scatterplot of the parameter values found in the final Pareto region estimation, with respect to their Euclid distance to the origin. A black curve in each plot shows the estimation of the density function for each parameter. A red cross indicates the best individual found, taking into account the minimum Euclid distance to the origin, calculated in the $g_\epsilon^{(1)} \times g_\epsilon^{(2)} \times g_\epsilon^{(3)} \times g_\epsilon^{(4)}$ hyperspace.

FITZHUGH, R. (1955). "Mathematical models of threshold phenomena in the nerve membrane". In: *The bulletin of mathematical biophysics* 17.4, pp. 257–278.

FLEUREAU, J. (2008). "Intégration de données anatomiques issues d'images MSCT et de modéles électrophysiologique et mécanique du coeur". PhD thesis. Universite de Rennes 1.

GOLD, M. R., I. NIAZI, M. GIUDICI, R. B. LEMAN, J STURDIVANT, M. H. KIM, Y. YU, J. DING, and A. D. WAGGONER (2007). "A prospective comparison of AV delay programming methods for hemodynamic optimization during cardiac resynchronization therapy". In: *Journal of cardiovascular electrophysiology* 18.5, pp. 490–496.

GUARINI, M, J URZÚA, A CIPRIANO, and W GONZÁLEZ (1998). "Estimation of cardiac function from computer analysis of the arterial pressure waveform". In: *IEEE Trans Biomed Eng* 45.12, pp. 1420–1428. DOI: 10.1109/10.730436.

HELDT, T, E. B. SHIM, R. D. KAMM, and R. G. MARK (2002). "Computational modeling of cardiovascular response to orthostatic stress". In: *J Appl Physiol* 92.3, pp. 1239–1254. DOI: 10.1152/japplphysiol.00241.2001.

HERNÁNDEZ, A., G. CARRAULT, F. MORA, and A. BARDOU (2002). "Model-based interpretation of cardiac beats by evolutionary algorithms: signal and model interaction". In: *Artificial Intelligence in Medicine* 26.3, pp. 211–235.

HERNÁNDEZ, A. I. (2000). "Fusion de signaux et de modèles pour la caractérisation d'arythmies cardiaques". PhD thesis. Université de Rennes 1.

HODGKIN, A. L. and A. F. HUXLEY (1952). "A quantitative description of membrane current and its application to conduction and excitation in nerve". In: *The Journal of physiology* 117.4, p. 500.

Hunter, P., A. McCulloch, and H. Ter Keurs (1998). "Modelling the mechanical properties of cardiac muscle". In: *Progress in biophysics and molecular biology* 69.2-3, pp. 289–331.

Jansen, A. H., F. A. Bracke, J. M. van Dantzig, A. Meijer, P. H. van der Voort, W. Aarnoudse, B. M. van Gelder, and K. H. Peels (2006). "Correlation of Echo-Doppler Optimization of Atrioventricular Delay in Cardiac Resynchronization Therapy With Invasive Hemodynamics in Patients With Heart Failure Secondary to Ischemic or Idiopathic Dilated Cardiomyopathy". In: *The American Journal of Cardiology* 97.4, pp. 552 –557. issn: 0002-9149. doi: http://dx.doi.org/10.1016/j.amjcard.2005.08.076.

Karamcheti, S. and J. Kravitz (2012). *Analyzing Cardiac Action Potentials with the Fitzhugh-Nagumo Model*. Tech. rep. California State Summer School for Mathematics & Science (Cluster 9).

Koon, K. T. V., C. Thebault, V. Le Rolle, E. Donal, and A. I. Hernández (2010). "Atrioventricular delay optimization in cardiac resynchronization therapy assessed by a computer model". In: *Computing in Cardiology, 2010*. IEEE, pp. 333–336.

Le Rolle, V. (2006). "Modélisation Multiformalisme du Système Cardiovasculaire associant Bond Graph, Equations Différentielles et Modèles Discrets". PhD thesis. Rennes: Université de Rennes 1.

Le Rolle, V., A. I. Hernandez, P.-Y. Richard, J. Buisson, and G. Carrault (2005). "A bond graph model of the cardiovascular system". In: *Acta Biotheoretica* 53.4, pp. 295–312.

Leclercq, C. and D. A. Kass (2002). "Retiming the failing heart: principles and current clinical status of cardiac resynchronization." eng. In: *J Am Coll Cardiol* 39.2, pp. 194–201.

Lu, K, J. W. Clark, F. H. Ghorbel, D. L. Ware, and A Bidani (2001). "A human cardiopulmonary system model applied to the analysis of the Valsalva maneuver". In: *Am J Physiol Heart Circ Physiol* 281.6, pp. 2661–2679.

McAlister, F. A., J. Ezekowitz, N. Hooton, B. Vandermeer, C. Spooner, D. M. Dryden, R. L. Page, M. A. Hlatky, and B. H. Rowe (2007). "Cardiac resynchronization therapy for patients with left ventricular systolic dysfunction: a systematic review." eng. In: *JAMA* 297.22, pp. 2502–2514. doi: 10.1001/jama.297.22.2502.

Morris, M. (1991). "Factorial sampling plans for preliminary computational experiments". In: *Technometrics* 33.2, pp. 161–174.

Mullens, W., R. A. Grimm, T. Verga, T. Dresing, R. C. Starling, B. L. Wilkoff, and W. W. Tang (2009). "Insights from a cardiac resynchronization optimization clinic as part of a heart failure disease management program". In: *Journal of the American College of Cardiology* 53.9, pp. 765–773.

Nagumo, J., S Arimoto, and S Yoshizawa (1962). "An active pulse transmission line simulating nerve axon". In: *Proceedings of the IRE* 50.10, pp. 2061–2070.

Noble, D. (1962). "A modification of the Hodgkin-Huxley equations applicable to Purkinje fibre action and pacemaker potentials". In: *The Journal of Physiology* 160.2, pp. 317–352.

Palladino, J. L. and A. Noordergraaf (2001). "A paradigm for quantifying ventricular contraction." In: *Cellular & molecular biology letters* 7.2, pp. 331–335.

Ritter, P., L. Padeletti, L. Gillio-Meina, and G. Gaggini (1999). "Determination of the optimal atrioventricular delay in DDD pacing. Comparison between echo and peak endocardial acceleration measurements." eng. In: *Europace* 1.2, pp. 126–130. doi: 10.1053/eupc.1998.0032.

Saltelli, A., P. Annoni, I. Azzini, F. Campolongo, M. Ratto, and S. Tarantola (2010). "Variance based sensitivity analysis of model output. Design and estimator for the total sensitivity index". In: *Computer Physics Communications* 181.2, pp. 259 –270. issn: 0010-4655. doi: http://dx.doi.org/10.1016/j.cpc.2009.09.018.

Smith, B., S. Andreassen, G. Shaw, P. Jensen, S. Rees, and J. Chase (2007). "Simulation of cardiovascular system diseases by including the autonomic nervous system into a minimal model". In: *Computer methods and programs in biomedicine* 86.2, pp. 153–160.

Tusscher, K. H. ten and A. V. Panfilov (2006). "Alternans and spiral breakup in a human ventricular tissue model". In: *American Journal of Physiology-Heart and Circulatory Physiology* 291.3, H1088–H1100.

Whinnett, Z. I., J. E. Davies, K Willson, C. H. Manisty, A. W. Chow, R. A. Foale, D. W. Davies, A. D. Hughes, J Mayet, and D. P. Francis (2006). "Haemodynamic effects of changes in atrioventricular and interventricular delay in cardiac resynchronisation therapy show a consistent pattern: analysis of shape,

magnitude and relative importance of atrioventricular and interventricular delay". In: *Heart* 92.11, pp. 1628–1634. DOI: 10.1136/hrt.2005.080721.

CHAPTER 8

Recursive identification of autonomic parameters in newborn lambs

french

Abstract

Ce chapitre traite de l'étude du baroréflexe en période néonatale. Un modèle de la réponse autonomique aux variations de pression artérielle a pu être proposé. La principale originalité de ce travail est d'appliquer un algorithme d'identification récursive pour l'évaluation des activités des voies vagale et sympathique. Des résultats préliminaires ont pu être présentés pour l'analyse de signaux obtenus chez l'agneau nouveau-né lors de manœuvres pharmacologiques de stimulation du baroréflexe. L'évaluation des activités sympathique et vagale montre une cohérence notable avec les connaissances actuelles sur ces systèmes. Les réponses des voies sympathique et parasympathique aux injections de vasodilatateurs et vasoconstricteurs ont notamment pu être estimées. Il est intéressant de noter que la diminution de la réponse sympathique, évaluée lors de l'injection de béta-bloquant, est cohérente avec les effets attendus.

Heart rate variability (HRV) is a commonly used indicator of the autonomic activity as it results of the complex mechanisms involved in the heart rate regulation. The baroreflex, whose function is to maintain arterial blood pressure, could explain a part of this variability. In fact, the heart rate results from the combined action of the sympathetic and parasympathetic nervous systems. In human adults, the Task force of the North American Society (Electrophysiology Task Force, 1996) defined the spectral characteristics of heart rate in order to determine the sympathovagal balance. However, these recommendations are not appropriate for neonates because there is a shift of the spectrum to the high frequencies. In fact, the neonatal heart rate may vary between 100 and 200 bpm and the respiratory rates could be included between 30 and 90 breaths/min (Andriessen et al., 2003). Different spectral divisions can be defined in neonatal studies but no consensus has been defined yet. The immaturity of neonates respiratory and autonomic nervous systems could explain the difficulty to find an agreement concerning the

method used to analyze neonatal signals. In this context, a model-based approach could ease the interpretation of heart rate variability because it helps to evaluate vagal and sympathetic activities.

Models of baroreflex can be classified in two categories: behavioral and representative models. Behavioral models, which are based on ARMA representation (BASELLI et al., 1988, 1994), are particularly useful to analyze the spectral characteristic of heart rate signal. On the other hand, representative models integrate an explicit description of vagal and sympathetic nervous systems (URSINO et al., 2003; VAN ROON et al., 2004). Most of these models are based on transfer functions (KAWADA et al., 2012). As these models describe the regulation of heart rate, contractility and peripheral resistance, they could be coupled to models of the cardiovascular systems (LE ROLLE et al., 2008a; LE ROLLE et al., 2005; SMITH et al., 2007). The hemodynamic and nervous influences could be studied during physiological tests, such as Valsalva maneuver (LE ROLLE et al., 2005; LU et al., 2001) and orthostatic tests (HELDT et al., 2002; LE ROLLE et al., 2008a).

Unfortunately, a large majority of these modeling approaches are applied to adults and are not adapted to the neonatal period. Moreover, it is particularly difficult to reproduce, in simulation, the whole variability contained in experimental heart rate signals. In fact, this variability is not only due to the baroflex response to blood pressure variations, but is also influenced by neuronal, humoral or other physiological control loops. In this chapter, a modeling approach is proposed in order to simulate experimental heart rate variability and to estimate the time-varying activities of vagal and sympathetic pathways. The complete process has been applied to analyze RR series acquired on one newborn lamb during the injection of a vasodilator and a vasoconstrictor. In the next section, the experimental protocol, the baroreflex model and the identification algorithm are described. Then, the results obtained are described and discussed.

8.1 Modeling of the autonomic activity

8.1.1 Autonomic regulation of cardiovascular variables

The autonomic nervous system (ANS) modulates the cardiovascular function through complex physiological control reflexes, involving receptors, an afferent pathway, a control system (usually located in the NTS), an efferent pathway and an effector (MONTANO et al., 2011). The heart is the main effector in these control loops, since the ANS is able to modulate all of its fundamental properties, which are: *i)* Chronotropic effect (modulation of the HR through the S-A node); *ii)* dromotropic effect (modulation of the conduction velocity of the A-V node); *iii)* bathmotropic effect (modulation of the myocite excitability); *iv)* inotropic effect (modulation of the cardiac contractility); and *v)* lusitropic effect (modulation of the cardiac relaxation). Another important effector is the vasculature, through the modulation of vasoconstriction.

In normal resting conditions, the main cardiovascular variable being controlled by the autonomic nervous system is the arterial blood pressure (ABP), through the arterial baroreceptor reflex (STEINBACK et al., 2009). In order to sense modifications on blood pressure, barorecep-

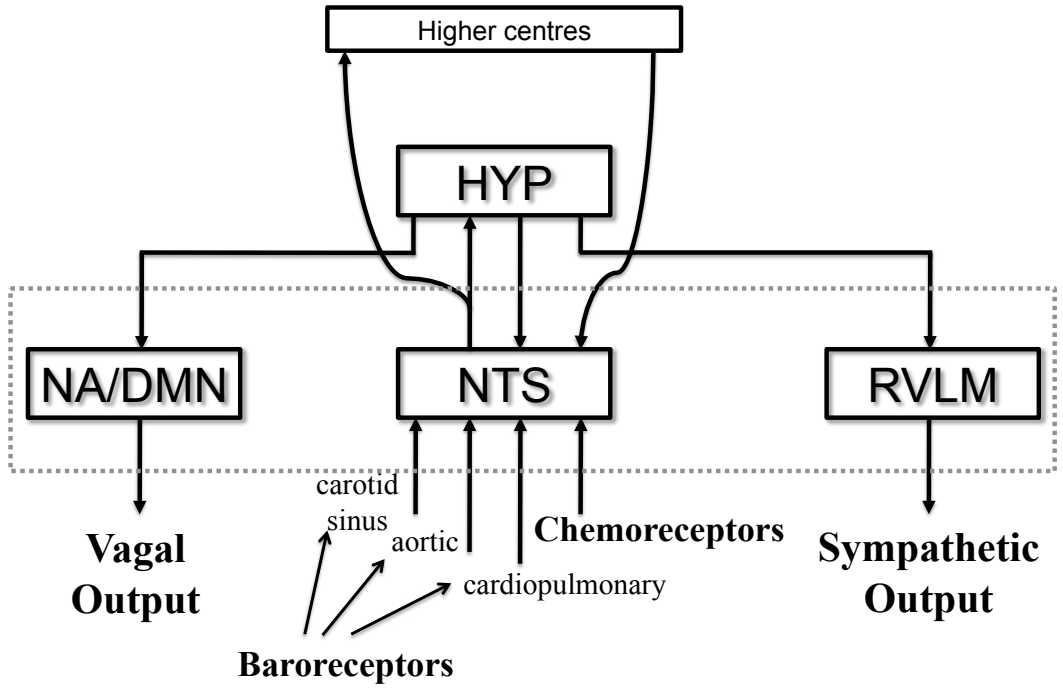

FIGURE 8.1– Structure of the cardiovascular control center. DMN=vagal Dorsal Motor Nucleus, HYP=Hypothalamus, NA=Nucleus Ambiguus, NTS= Nucleus Tractus Solitarii, RVLM= Rostral Ventrolateral Medulla.

tors are present in large arteries, including carotid sinuses, aortic arch, and right subclavian artery. These receptors are excited by the stretch of the blood vessels, which sends signals via afferent pathways to the central nervous system. An increase in ABP evokes a further reflex increase in cardiovagal activity, a decrease in sympathetic activity and a corresponding decreased chronotropic, dromotropic, inotropic, lusitropic and bathmotropic effects (COWLEY et al., 1973). Conversely, when blood pressure is reduced, cardiovagal activity is inhibited, sympathetic drive is increased, and the above-mentioned regulatory effects increase.

The cardiovascular control center is the link between afferent and efferent pathways. This complex structure, located in the medulla, includes the Nucleus Tractus Solitarius (NTS) that is connected to afferent nerves, the vagal motor center (Vagal Dorsal Motor Nucleus DMN, the Nucleus Ambiguus, NA) and the origin of sympathetic nerve (Rostral Ventrolateral Medulla RVLM) (VAN ROON et al., 2004). The different elements of this structure depend on the output from baroreceptors and are also under the direct influence of different brain structures like central nervous system, the hypothalamus or the respiratory control center (BORELL et al., 2007), as illustrated in fig. 8.1.

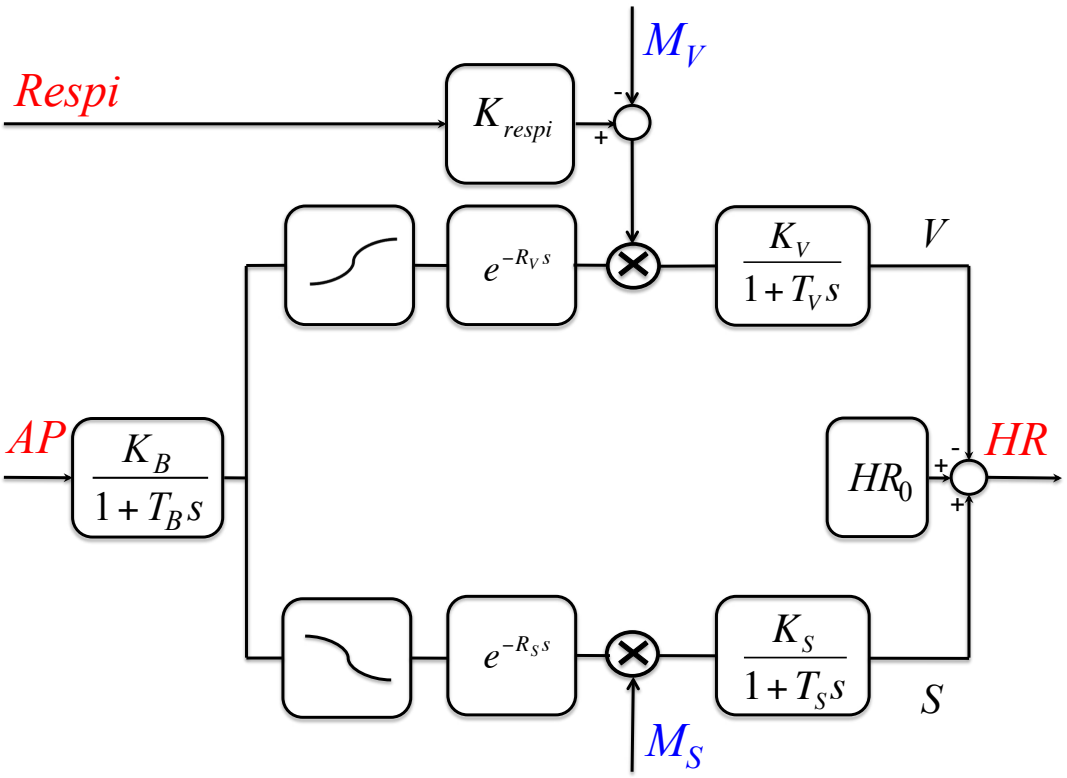

FIGURE 8.2– Block diagram of baroreflex control of arterial pressure. See text for abreviations.

8.1.2 Baroreflex Model

The baroreflex model is represented in fig. 8.2. It includes the receptors (baroreceptors) and afferent pathways, the cardiovascular control center and the efferent pathways (including the vagal and sympathetic branches).

The baroreceptor input is the arterial pressure (AP) and its dynamical properties are represented by a first-order filter, whose gain and time constant are denoted K_B and T_B. The cardiovascular control center is represented by sigmoidal functions and two delays (R_V and R_S are respectively the sympathetic and parasympathetic delays). Normalization and saturation effects are represented by sigmoidal input-output relationship :

$$N_x = a_x + \frac{b_x}{e^{\lambda_x (P_B - M_{x,0})} + 1}, \tag{8.1}$$

where the generic index $x \in \{V, S\}$ stands for the vagal and sympathetic pathways, P_B is the baroreceptor output, and the parameters a_x, b_x, λ_x and $M_{x,0}$ are used to adjust the sigmoidal shape.

The vagal and sympathetic activities are modulated by two time-varying variables $M_V(t)$ and $M_S(t)$ in order to take into account the influence of different brain structures on vagal and sympathetic pathways. The vagal activity is modulated by $M_V(t)$ and by *Respi* which is equal

to the plethysmography signal normalised in ordre to rescale its range in [0, 1]. It is important to understand that these two time-varying variables $M_V(t)$ and $M_S(t)$ aggregate all the influences, which are not due to blood pressure variations. It notably includes the impact of the closed-loop structure of the baroreflexe.

The efferent pathways are composed of two first-order filters characterized by a gain (K_V and K_S for the sympathetic and the vagal gains) and a time constant (T_V and T_S). The output signal of the heart rate regulation model (HR) is continuous and is obtained by adding the contributions from the sympathetic (S) and vagal (V) branches and a basal (intrinsic) heart rate (HR_0).

8.1.3 Identification Method

The identification process was performed using the experimental AP and *Respi* as input of the baroreflex model. The simulated RR interval signal is used as output and is compared to the experimental RR using the error functions described in this section. The identification procedure is composed of two steps:

1. the constant parameters [T_B, K_V,T_V,R_V, K_S,T_S,R_S] are first identified for each lamb,
2. the time-varying variables [M_V, M_S] are identified recursively on the complete RR signal, of duration T_{tot}.

These two steps are based on a recursive identification of parameters. At each step i of the algorithm, parameters are identified on intervals, which duration is equal to T_I, by minimizing an error function g_ϵ:

$$g_\epsilon = \sum_{t_e=iT_L}^{(i+1)T_L} \left|(\mathrm{RR}_{sim}(t_e) - \mathrm{RR}_{exp}(t_e))\right| + \sum_{t_e=iT_L}^{iT_L+T_I} \left|(\mathrm{RR}_{sim}(t_e) - \mathrm{RR}_{exp}(t_e))\right|, \quad i \in [0, \ldots, N], \tag{8.2}$$

where t_e corresponds to the time elapsed since the onset of the identification period, T_L is the overlag time between each interval and N is the number of identification intervals, which is equal to integer part of T_{tot}/T_L. The error function is composed of two parts in order to consider the slow and rapid components of the RR signals. These parts evaluated the difference between simulated and experimental RR. The first sum was realized on the overlag time to consider only rapid events and, in the second sum, the difference on the whole identification period was considered in order to reproduce the slow variations of the signals.

This error function is minimized on each interval i using an evolutionary algorithm (EA), as in our previous works (Le Rolle et al., 2008b, 2011), and as explained in chapter 4. Concerning the first interval, a set of random initial solutions was used to create the initial population. For the following intervals, the initial population was set equal to the population obtained from interval $i-1$ considering that the parameter variation between intervals is limited. Although this approach of attribution of initial populations limits the parameters changes, a mutation operator

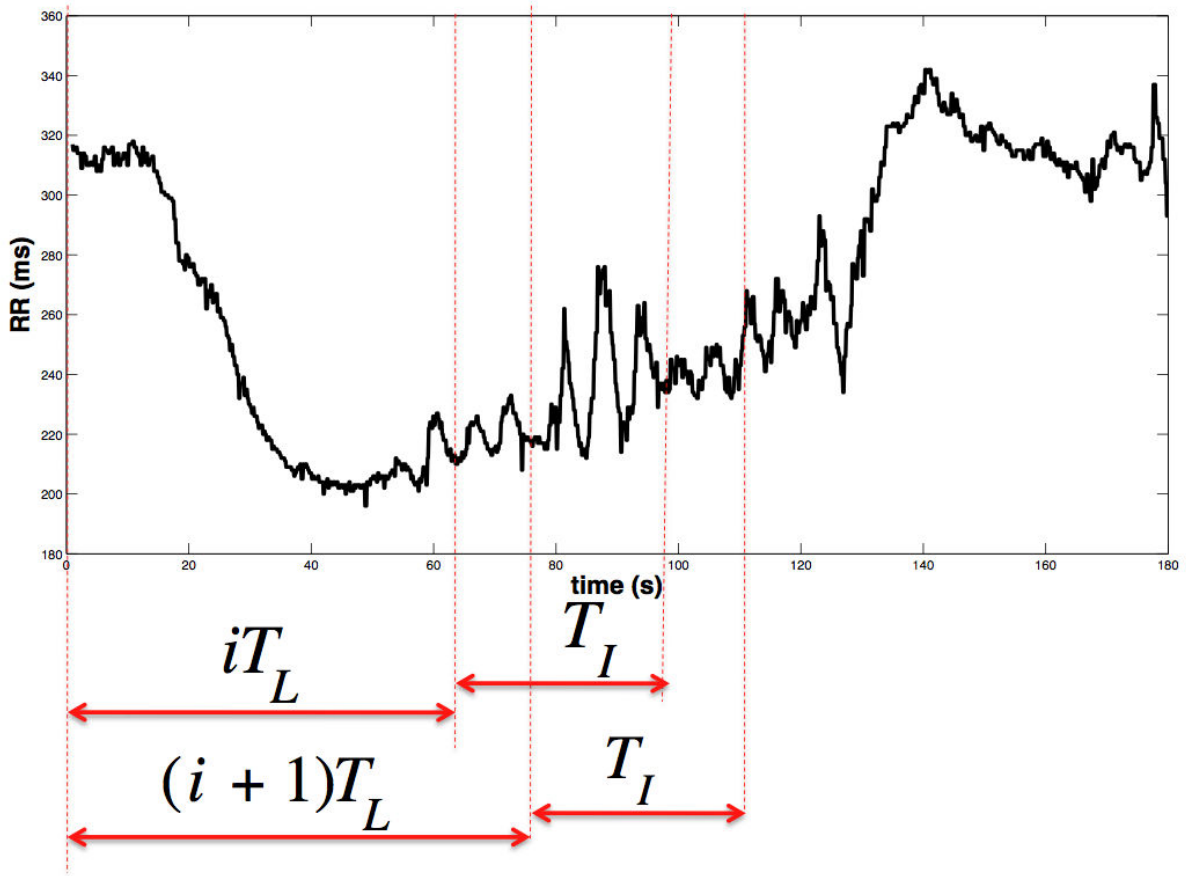

FIGURE 8.3– Example of an experimental RR signal used for the recursive identification. T_L: overlapping window. T_I: identification windows. T_L and T_I are used in the evaluation of the error function.

with probability $p_m = 0.2$ helps the process to explore the entire search space and prevent from convergence to a local minimum.

Concerning the first step, constant parameters ($[T_B, K_V, T_V, R_V, K_S, T_S, R_S]$) are identifying recursively. Uniform distribution bounded by feasibility intervals was defined to create the initial population for each parameters: [0.01, 1] for T_B (s), [0.01, 1.5] for T_V (s), [0.1, 0.5] for R_V (s), [0.01, 6] for K_V (bpm), [5, 20] for T_S (s), [2, 6] for R_S (s), [0.01, 6] for K_V (bpm). These intervals were defined to approximate previously published parameters (LU et al., 2001; VAN ROON et al., 2004; WESSELING et al., 1993) and large enough to assure an accurate research of the parameters values. Constant parameters were determined by setting their values equal to the mean value obtained after the reccurssive identification.

These constant parameters are used in the baroreflex model in order to realize the recursive identification of the time-varying variables $[M_V, M_S]$. The overlag time T_L was defined equal to the vagal delay and the indentification period T_I is equal to the sympathetic delay in order to consider the slow and rapid components of the RR signals. In fact, the identification period should be, at least, equal to the sympathtic delay to take into account slow changes due to the input variations and the overlag time T_L should be short enough to capture rapid events due to

the vagal response.

8.1.4 Experimental protocol

The in vivo experiments were performed in three mixed-breed lambs, born at term by spontaneous vaginal delivery and housed with their mother in our animal quarters. The protocol was approved by the Committee for Animal Care and Experimentation of the Université de Sherbrooke, Canada. Aseptic surgery was performed upon the day of arrival under general anesthesia (Isoflurane 1–2% + NO_2 30 %, balance O_2) after an intramuscular injection of atropine sulfate (0.1 mg/kg), ketamine (10 mg/kg), morphine (0.016 mg/kg) and antibiotics (5 mg/kg gentamicin and 0.05 mg/kg duplocilline, which were administered daily thereafter until the end of the experiment). One dose of ketoprofen (3 mg/kg, intramuscular) was systematically given immediately after induction of anesthesia for analgesia and repeated if needed the next day. Chronic instrumentation was performed as previously described (Duvareille et al., 2007) and included two needle-electrodes into the parietal cortex for electrocorticogram (ECoG) and two subcutaneous needle electrodes into the forelegs for electrocardiogram (ECG). One needle-electrode was also inserted subcutaneously on the scalp to serve as a ground. In addition, a supra-glottal catheter was inserted to allow testing for laryngeal chemoreflexes as previously described (Beuchée et al., 2009). Finally, an arterial catheter was introduced in the brachial artery for measuring blood gases. All lambs were returned to their mother after arousal from anesthesia. Additional instrumentation was extemporaneously performed prior to the experiments for recording nasal airflow (thermocouple), electro-oculogram (EOG, using two platinum needle electrodes), respiratory thoracic-abdominal movements (respiratory inductance plethysmography) and oxyhemoglobin saturation (pulse oximetry). Three platinum needle electrodes (two on the foreleg root and one on the left hind leg root) were inserted subcutaneously for recording electrocardiogram (ECG). Our custom-built radiotelemetry system (Létourneau et al., 2003) was used to continuously transmit signals of nasal flow, Arterial Blood Pressure, ECG, EOG and ECoG. All signals were sampled at 1000 Hz and recorded on a PC, using the MP100A data acquisition system and Acknowledge 3.7.3 software (Biopac Systems Inc. Goleta, CA, USA). Correct electrode positioning was systematically verified at autopsy.

Experiments were performed in non-sedated lambs at postnatal age 4 and 5 days. Throughout the recordings, the lambs were comfortably positioned in a sling with loose restraints and monitored with polygraphic recording. Ambient temperature was 22 °C. An observer was always present in the laboratory to note all events. The sequence of experiments started with a 3 min recording in basal condition while in quiet sleep, followed by a continuous perfusion of nitropussiate sodium for 360 seconds, subsequently, after a 30 min period of recovery, a second continuous perfusion of nitroprusside was started for 120 seconds and concluded by a single and bolus injection of phenylephrine. The same sequence of experimentations was repeated the following day started 5 minutes after the bolus administration of metoprolol 1 mg/kg repeated each 30 mins.

TABLE 8.1– Identified values for constant parameters.

	T_B	K_V	T_V	R_V	K_S	T_S	R_S
Lamb 1	0.50	2.04	0.84	0.29	3.56	14.22	4.16
Lamb 2	0.55	2.05	0.60	0.35	2.58	11.40	4.0
Lamb 3	0.60	1.44	0.82	0.32	2.27	12.11	3.82

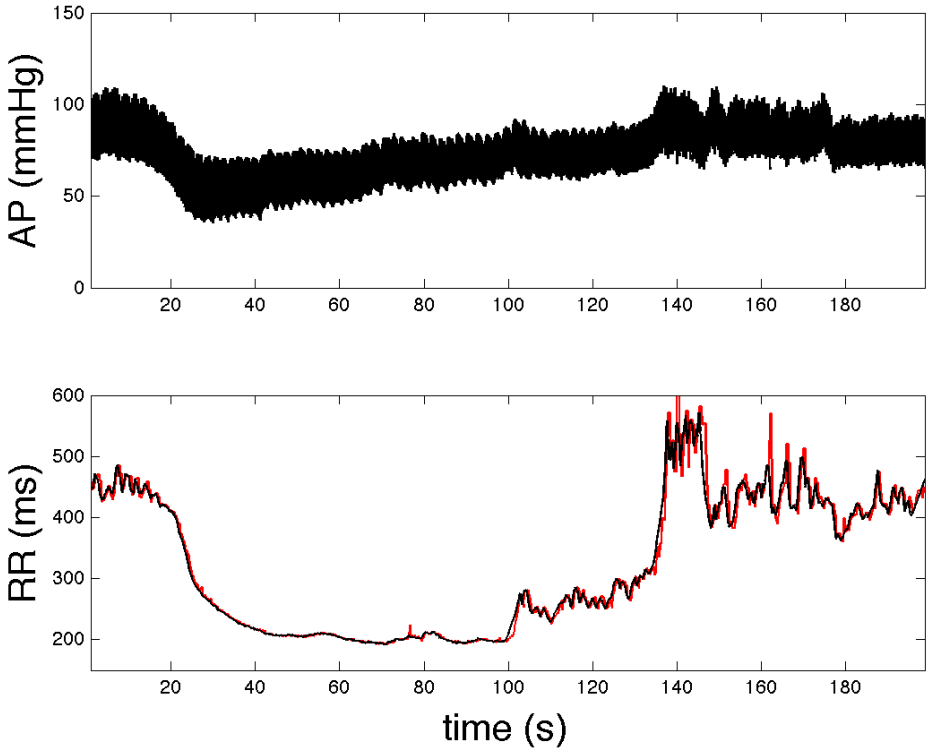

FIGURE 8.4– Simulated results and experimental data without autonomic blocking. (a) Experimental arterial pressure, (b) Comparison of model simulations (black lines) with experimental RR interval (grey lines). Deviations are given as RMSE in each lamb.

8.2 Results and discussion

The results obtained concerning the identification of constant parameters are exposed in table 8.1. Delays and time constants differ from the adults concerning both the vagal and sympathetic systems. This can be explained by the maturity of the autonomic nervous because parameters evolve rapidly during the first days of life. Identification results are in agreements with spectral analysis realised on neonates signals (ANDRIESSEN et al., 2003). Identified parameters values were used in the recursive identification of the time-varying variables [M_V, M_S].

Figure 8.4 shows an exemple of experimental arterial pressure and RR signals obtained on one lamb without any autonomic blocking drugs. The beginning of the RR series corresponds to the nitroprusside injection, and the phenylephrine bolus is injected after 120 seconds. The

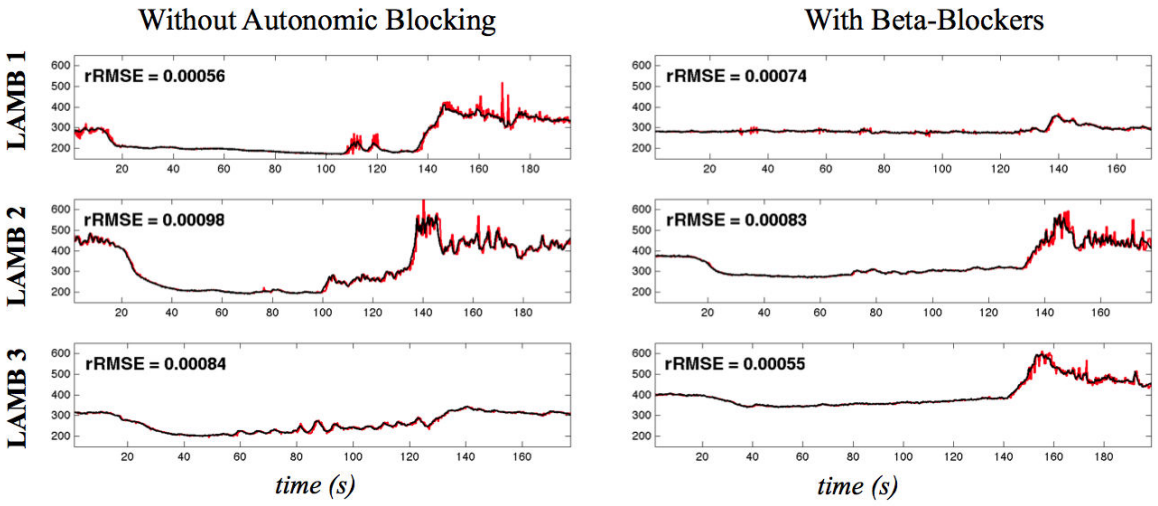

FIGURE 8.5– Simulated results and experimental data without autonomic blocking. Left: Experimental arterial pressure. Right: Comparison of model simulations (black lines) with experimental RR interval (grey lines). Deviations are given as RMSE in each lamb.

decrease of arterial pressure and RR interval, which can be observed in the first part of the signal, is the consequence of the vasodilatation induced by nitroprusside. Then, the RR increases following the baroreflex response and the injection of phenylephrine (at $t = 120\,\text{s}$) which induces a vasoconstriction.

Figure 8.5 depicts simulated and experimental data without autonomic blocking (day 1) and with beta-blockers (day 2). The root mean square error (RMSE) between simulated and experimental data was computed for each case. The comparison between simulated (black lines) and experimental (red lines) RR intervals after recursive identification shows a good adaptation of the model to real data because the average RMSE is equal to 7.48×10^{-4}. In fact, the global morphology of the curve is reproduced since RR signals increase and decrease in response to nitroprusside and phenylephrine. The high frequency component, which is also present in simulated signals, reflects the RR response to AP variations and the modulation of the cardiovascular control center.

The estimated activities of vagal and sympathetic pathways, without any autonomic blockade drugs and with beta-blockers, are shown in 8.6 and 8.7. During the first 100 s, these signals are characterized by a decrease of vagal activity and an increase of sympathetic activity when no autonomic blocking is introduced. Then, the parasympathetic contribution begins to rise and the sympathetic contribution falls because AP stabilizes. After the injection of phenylephrine occurring at 120 s, the vagal activity suddenly rise and, then, is maintained while sympathetic activities slowly decrease after the injection.

The second columns of 8.6 and 8.7 depicts the contributions of vagal and sympathetic pathways with beta-blockers. Although the injection of nitroprusside is realized at the beginning ($t = 0\,\text{s}$), vagal and sympathetic contributions are relatively stable until the injection of phenylephrine.

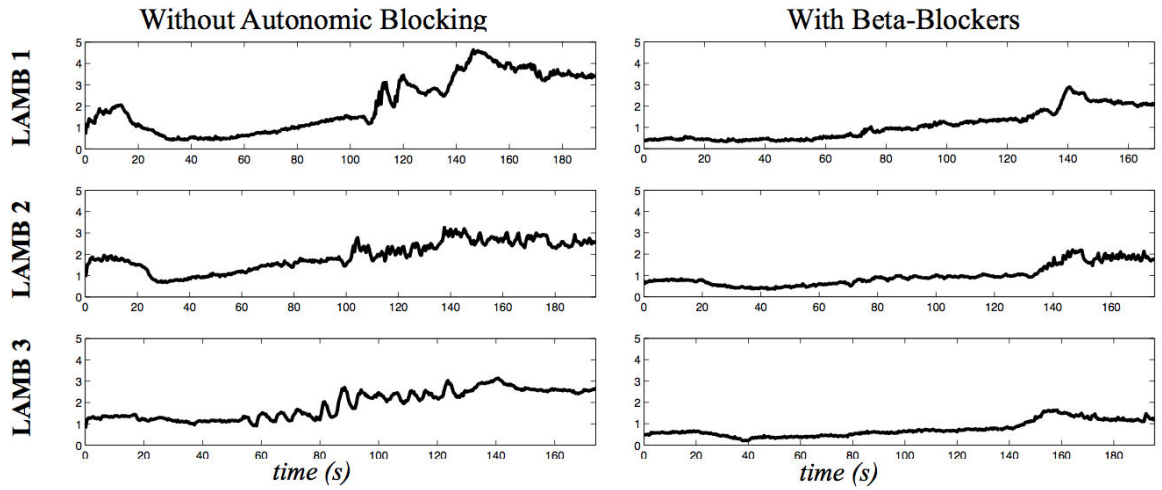

FIGURE 8.6– Contributions of the vagal pathway in baseline conditions and with beta-blockers.

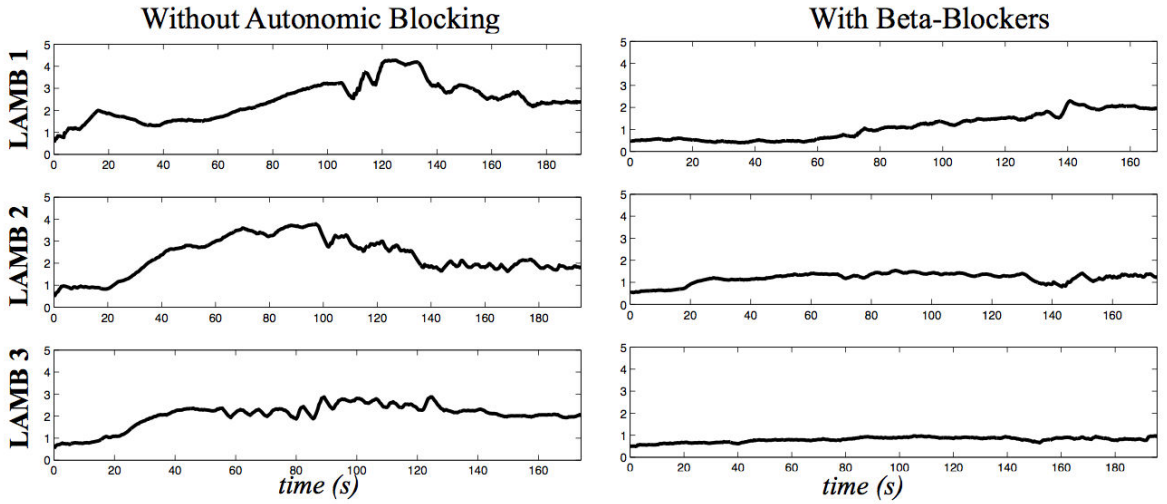

FIGURE 8.7– Contributions of the sympathetic pathway with beta-blockers and with beta-blockers.

After 120 s, parasympathetic activity rapidly increases and then stabilizes. The sympathetic activities maintain because beta-blockers block the action of the sympathetic nervous system

The variations of vagal and sympathetic pathways show different behaviors in the absence of an autonomic blockade drug and with beta-blockers. In fact, the baroreflex activity allows a stabilization of AP in the first case and, as expected, while vagal and sympathetic responses are reduced in the second case. So, simulations of vagal and sympathetic activities are particularly interesting because there are in agreements with physiological knowledge. The reduction of sympathetic action, due to beta-blockers, was estimated from the reccursive identification of vagal and sympathetic modulations.

8.3 Conclusion

In this chapter, a model-based approach is proposed to estimate the vagal and sympathetic contributions to heart rate. A simple baroreflex model is used to analyse RR signals obtained on newborn lambs during the injection of nitroprusside and phenylephrine. Signals acquisitions were realized under baseline conditions and beta-blockers. The main contribution is to propose a recursive identification algorithm, based on EA, to evaluate parasympathetic and sympathetic modulations during autonomic maneuvers. Results following the reccusive identification illustrate the similarity between simulated and experimental RR. Simulations of vagal and sympathetic activities show the different responses associated with baseline conditions and beta-blockers. It is particularly interesting to note that the model is able to estimate the reduction of sympathetic activity with beta-blockers

The results presented in this chapter are encouraging for the use of this model-based approach for the estimation of parasympathetic and sympathetic activities. These prelimenary results must now be further validated by comparing the model-based approach with conventionnal signal processing methods. The objective will be to validate the vagal and sympathetic estimations in comparison with results (obtained from spectral analysis applied on RR for example) that will constitute an accepted reference.

References

Andriessen, P., A. M. Koolen, R. C. Berendsen, P. F. Wijn, E. D. Ten Broeke, S. G. Oei, and C. E. Blanco (2003). "Cardiovascular fluctuations and transfer function analysis in stable preterm infants". In: *Pediatric research* 53.1, pp. 89–97.

Baselli, G, S Cerutti, S Civardi, A Malliani, G Orsi, M Pagani, and G Rizzo (1988). "Parameter extraction from heart rate and arterial blood pressure variability signals in dogs for the validation of a physiological model". In: *Computers in biology and medicine* 18.1, pp. 1–16.

Baselli, G, S Cerutti, F Badilini, L Biancardi, A Porta, M Pagani, F Lombardi, O Rimoldi, R Furlan, and A Malliani (1994). "Model for the assessment of heart period and arterial pressure variability interactions and of respiration influences". In: *Medical and Biological Engineering and Computing* 32.2, pp. 143–152.

Beuchée, A., G. Carrault, J. Y. Bansard, E. Boutaric, P. Bétrémieux, and P. Pladys (2009). "Uncorrelated randomness of the heart rate is associated with sepsis in sick premature infants". In: *Neonatology* 96.2, pp. 109–114.

Borell, E. von, J. Langbein, G. Després, S. Hansen, C. Leterrier, J. Marchant-Forde, R. Marchant-Forde, M. Minero, E. Mohr, A. Prunier, et al. (2007). "Heart rate variability as a measure of autonomic regulation of cardiac activity for assessing stress and welfare in farm animals — a review". In: *Physiology & behavior* 92.3, pp. 293–316.

Cowley, A. W., J. F. Liard, and A. C. Guyton (1973). "Role of the baroreceptor reflex in daily control of arterial blood pressure and other variables in dogs". In: *Circulation Research* 32.5, pp. 564–576.

Duvareille, C., M. Lafrance, N. Samson, M. St-Hilaire, P. Pladys, P. Micheau, V. Bournival, C. Langlois, and J.-P. Praud (2007). "Effects of hypoxia and hypercapnia on nonnutritive swallowing in newborn lambs". In: *Journal of Applied Physiology* 103.4, pp. 1180–1188.

Electrophysiology Task Force, T. (1996). "Heart Rate Variability: Standards of Measurement, Physiological Interpretation, and Clinical Use". In: *Circulation* 93.5, pp. 1043–1065. doi: 10.1161/01.CIR.93.5.1043.

HELDT, T, E. B. SHIM, R. D. KAMM, and R. G. MARK (2002). "Computational modeling of cardiovascular response to orthostatic stress". In: *J Appl Physiol* 92.3, pp. 1239–1254. DOI: 10.1152/japplphysiol.00241.2001.

KAWADA, T., K. UEMURA, S. SHIMIZU, A. KAMIYA, M. J. TURNER, M. MIZUNO, K. SUNAGAWA, and M. SUGIMACHI (2012). "Consideration on parameter determination of a new model describing dynamic vagal heart rate control in rats". In: *Engineering in Medicine and Biology Society (EMBC), 2012 Annual International Conference of the IEEE*. IEEE, pp. 3809–3812.

LE ROLLE, V., A. HERNÁNDEZ, P. RICHARD, and G. CARRAULT (2008a). "An autonomic nervous system model applied to the analysis of orthostatic tests". In: *Modelling and Simulation in Engineering* 2008, p. 2.

LE ROLLE, V., A. I. HERNANDEZ, P.-Y. RICHARD, J. BUISSON, and G. CARRAULT (2005). "A bond graph model of the cardiovascular system". In: *Acta Biotheoretica* 53.4, pp. 295–312.

LE ROLLE, V., A. I. HERNÁNDEZ, P.-Y. RICHARD, E. DONAL, and G. CARRAULT (2008b). "Model-based analysis of myocardial strain data acquired by tissue Doppler imaging". In: *Artificial Intelligence in Medicine* 44.3, pp. 201–219.

LE ROLLE, V., D. OJEDA, and A. I. HERNÁNDEZ (2011). "Embedding a cardiac pulsatile model into an integrated model of the cardiovascular regulation for heart failure follow-up". In: *IEEE transactions on biomedical engineering* 58.10, pp. 2982–2986.

LÉTOURNEAU, P. and J.-P. PRAUD (2003). "A radiotelemetry system for polysomnographic recordings in lambs". In: *Methods* 30.2, pp. 115–121.

LU, K, J. W. CLARK, F. H. GHORBEL, D. L. WARE, and A BIDANI (2001). "A human cardiopulmonary system model applied to the analysis of the Valsalva maneuver". In: *Am J Physiol Heart Circ Physiol* 281.6, pp. 2661–2679.

MONTANO, N., E. TOBALDINI, and A. PORTA (2011). "The Autonomic Nervous System". In: *Stress Challenges and Immunity in Space: From Mechanisms to Monitoring and Preventive Strategies*, pp. 71–86.

SMITH, B., S. ANDREASSEN, G. SHAW, P. JENSEN, S. REES, and J. CHASE (2007). "Simulation of cardiovascular system diseases by including the autonomic nervous system into a minimal model". In: *Computer methods and programs in biomedicine* 86.2, pp. 153–160.

STEINBACK, C. D., D. SALZER, P. J. MEDEIROS, J KOWALCHUK, and J. K. SHOEMAKER (2009). "Hypercapnic vs. hypoxic control of cardiovascular, cardiovagal, and sympathetic function". In: *American Journal of Physiology-Regulatory, Integrative and Comparative Physiology* 296.2, R402–R410.

URSINO, M. and E. MAGOSSO (2003). "Role of short-term cardiovascular regulation in heart period variability: a modeling study". In: *American Journal of Physiology-Heart and Circulatory Physiology* 284.4, H1479–H1493.

VAN ROON, A., L. MULDER, M. ALTHAUS, and G. MULDER (2004). "Introducing a baroreflex model for studying cardiovascular effects of mental workload". In: *Psychophysiology* 41.6, pp. 961–981.

WESSELING, K. and J. SETTELS (1993). "Circulatory model of baro-and cardio-pulmonary reflexes". In: *Blood pressure and heart rate variability*, pp. 56–67.

CHAPTER 9

Conclusion

This thesis was defined around the proposal of new multi-resolution modeling methods for the analysis and interpretation of physiological signals, with concrete applications on different cardiovascular pathologies. It presented three main contributions:

The first contribution is the generalization and the extension of the multi-formalism and multi-resolution modeling methodologies that has been previously proposed in our team. This methodology is formalized and presented in chapter 3 and was part of a journal paper (Hernández et al., 2011).

As a complement to these theoretical aspects, a second contribution is related to the improvement and creation of a set of software tools for modeling and simulation, dedicated to the identification, analysis, implementation and sharing of complex mathematical models (the M2SL toolkit). These tools, presented in chapter 4 have been registered with the French agency of software protection. Additionally, due to the utility of hybrid system simulations, parameter analysis and identification, this toolkit has been licensed to several laboratories and is now part of the tools identified in the European Network of Excellence on the "Virtual Physiological Human" (VPH NoE).

The third contribution concerns the application of the proposed methods and tools to improve the diagnostic and therapeutic strategies on real clinical applications involving the cardiovascular system: heart failure (HF) and coronary heart disease (CAD). Moreover, two prospective applications on cardiac resynchronization therapy (CRT) and the identification of autonomic responses of premature newborns are also proposed. These applications required the creation of hybrid models, including highly heterogeneous and dynamic mathematical formalisms, as well as data acquisition. The four clinical applications that conform this contribution were:

1. The Guyton model (Guyton et al., 1972) was examined for its pioneering description of the long term regulation of blood pressure. This horizontal integration model was extended through a selective vertical integration of a more detailed pulsatile heart, that operates under a shorter temporal scale. The obtained model demonstrated the interest of the development of a multi-resolution approach, from a modeling and computational

perspective. From a clinical perspective, this original model may assist on the analysis of contractility modulations in the long-term regulation of the cardiovascular system. This application resulted in the publication of a conference and a journal paper (LE ROLLE et al., 2011; OJEDA et al., 2013a).

2. The second application of this work was the study of the coronary circulation on patients suffering from coronary artery disease. The objective was to provide a new mathematical model and model-based tools allowing for a more complete and patient-specific analysis of per-operative data obtained during a coronary artery bypass graft surgery (CABG). Complete parameter analysis and patient-specific parameter identification were performed on the proposed model, revealing the importance of the collateral vessels and their heterogeneous development. Four conference contributions and an international journal publication are associated with this work (OJEDA et al., 2011, 2012a,b, 2013b,c).
3. The third modeling application of this thesis was designed to assist the clinician on the optimization of patient-specific CRT pacemaker parameters. The proposed modeling methodology and tools are once again applied to integrate models of: *i)* the electrical activity of cardiac tissue, *ii)* atrial and ventricular mechanical activities, *iii)* the systemic and pulmonary circulations and *iv)* a simplified model of an implantable CRT device. The sensitivity analysis of the coupled model underlines the significant role of the diastolic properties of the failing heart, as well as the importance of the atrial activity and preload modulation, which are often underestimated when applying modeling methods to the analysis of CRT. The model can produce different patterns of mitral flows with changes in AVD values. Parameter identification results show coherent variations when reproducing real data from one HF patient, for different pacing configurations. In this sense, this model may be useful, during post-operative optimization phases, to reduce the number of AVD-VVD combinations tested and to provide, via the identified parameters, new quantitative estimators of the patient's response. These results have been presented in an international conference (OJEDA et al., 2013d).
4. The fourth and final prospective application is defined in the context of neonatology. Here, a recursive identification method is proposed and applied to obtain time-varying estimates of the sympathetic and parasympathetic components of the autonomic nervous system. Data from newborn lambs during pharmacological maneuvers were analyzed. Results obtained after recursive parameter identification are coherent with the expected physiological responses induced by the applied pharmacological maneuvers. To our knowledge, this is the first non-linear model-based method allowing for a time-varying estimation of the autonomic components in non-stationary conditions. We expect a number of potential clinical applications of this method, in particular in the field of neonatology. The initial results related to this application have been presented in an international conference as well (LE ROLLE et al., 2013).

The future directions of this work are organized in two different axes: improvements of the M2SL toolkit and the prospects for each clinical application.

The M2SL toolkit already provides three temporal synchronization strategies that are useful for the management of models with different time dynamics: the individual time step of each simulator can be calculated, providing two possible adaptive simulation strategies. The horizontal and vertical integration shown for the Guyton models implementation showed the interest of these adaptive step strategies from a computational point of view. The next logical step for such adaptive simulations is to enhance the current strategies with the calculation of the optimal synchronization step.

The second axis for future directions are:

- Since the Guyton model has been extended with a pulsatile heart, the short and medium-term dynamics of the regulatory mechanisms, such as the baroreflex, can now be integrated in this model. Currently, the Guyton model only includes simplified descriptions of the baroreflex mechanism. Therefore, a natural step of this modeling application would be to extend this model.
- The prospects related to the CAD application are clearly directed towards *i)* the consideration of flow-dependent resistances for the stenotic segments, *ii)* the estimation of patient-specific arterial parameters from clinical imaging techniques, and *iii)* the modification of the current model to improve the diastolic phase dynamics of coronary flow. In order to fulfill these future objectives, the current clinical protocol must be redefined to obtain the full phasic flow profiles during CABG.
- The prospective application of a cardiovascular model for CRT optimization will be directed to the evaluation of the parameter identification for more patients and further analysis of the parameter values found with the estimation method. More importantly, the results of the sensitivity analyses will provide important knowledge for the PSPC INTENSE project, whose objective is the development of implantable neurostimulation devices that stimulate the vagal nerve for the treatment of HF.
- Finally, the future work related to the identification of autonomic parameters in newborn lambs is the validation with classical indices of sympathetic and vagal activities, and the coupling of this baroreflex model with a closed-loop cardiovascular model.

In addition to these technical perspectives, the approach adopted in this work, combining multi-resolution physiological modeling, sensitivity analysis and parameter identification, as well as their application to concrete medical problems, is particularly promising. The maturation and upcoming evolution towards the clinics of international initiatives such as the VPH or the IUPS Physiome are an evidence of the interest of this strongly interdisciplinary field. These model-based approaches may well gradually lead to significant changes in the way of healing, but also in the way of understanding the origins of disease.

References

Guyton, A., T. Coleman, and H. Granger (1972). "Circulation: overall regulation". In: *Annual review of physiology* 34.1, pp. 13–44.

HERNÁNDEZ, A. I., V. LE ROLLE, D. OJEDA, P. BACONNIER, J. FONTECAVE-JALLON, F. GUILLAUD, T. GROSSE, R. G. MOSS, P. HANNAERT, and S. R. THOMAS (2011). "Integration of detailed modules in a core model of body fluid homeostasis and blood pressure regulation". In: *Progress in Biophysics and Molecular Biology* 107, pp. 169–182. DOI: 10.1016/j.pbiomolbio.2011.06.008.

LE ROLLE, V., D. OJEDA, and A. I. HERNÁNDEZ (2011). "Embedding a cardiac pulsatile model into an integrated model of the cardiovascular regulation for heart failure follow-up". In: *IEEE transactions on biomedical engineering* 58.10, pp. 2982–2986.

LE ROLLE, V., D. OJEDA, A. BEUCHEE, J.-P. PRAUD, P. PLADYS, and A. I. HERNANDEZ (2013). "A model-based approach for the evaluation of vagal and sympathetic activities in a newborn lamb". In: *Engineering in Medicine and Biology Society (EMBC), 2013 35th Annual International Conference of the IEEE*, pp. 3881–3884. DOI: 10.1109/EMBC.2013.6610392.

OJEDA, D., V. L. ROLLE, and A. I. HERNÁNDEZ (2011). "A Model of the Cardiovascular System integrating the Coronary Circulation". In: *Recherche en Imagerie et Technologies pour la Santé (RITS 2011)*.

OJEDA, D., V. LE ROLLE, and A. I. HERNÁNDEZ (2012a). "Analyse de Sensibilité d'un modèle de la circulation coronarienne sur des patients présentant une maladie coronarienne tri-tronculaire". In: *32ème Séminaire de la Société Francophone de Biologie Théorique*. **Awarded oral presentation: Prix Delattre 2012**.

OJEDA, D., V. LE ROLLE, A. DROCHON, H. CORBINEAU, J.-P. VERHOYE, and A. I. HERNÁNDEZ (2012b). "Sensitivity analysis and parameter estimation of a coronary circulation model for patients with triple-vessel disease". In: *Proceedings of The Virtual Physiological Human 2012 (VPH2012)*. London.

OJEDA, D., V. LE ROLLE, G. CARRAULT, and A. I. HERNÁNDEZ (2013a). "Intégration d'un modèle cardiaque pulsatile dans un modèle complet de la régulation cardiovasculaire". In: *Recherche en Imagerie et Technologies pour la Santé (RITS 2013)*.

OJEDA, D., V. LE ROLLE, A. DROCHON, M. HARMOUCHE, H. CORBINEAU, J.-P. VERHOYE, and A. I. HERNANDEZ (2013b). "Multiobjective patient-specific estimation of a coronary circulation model for triple vessel disease". In: *Engineering in Medicine and Biology Society (EMBC), 2013 35th Annual International Conference of the IEEE*, pp. 3877–3880. DOI: 10.1109/EMBC.2013.6610391.

OJEDA, D., V. LE ROLLE, M. HARMOUCHE, A. DROCHON, H. CORBINEAU, J.-P. VERHOYE, and A. I. H. HERNÁNDEZ (2013c). "Sensitivity analysis and parameter estimation of a coronary circulation model for triple-vessel disease". Submitted to IEEE transactions on biomedical engineering (Currently in minor revisions).

OJEDA, D., V. LE ROLLE, K. TSE VE KOON, C. THEBAULT, E. DONAL, and A. I. HERNÁNDEZ (2013d). "Towards an atrio-ventricular delay optimization assessed by a computer model for cardiac resynchronization therapy". In: *Proceedings of the 9th International Seminar on Medical Information Processing and Analysis*. Ed. by S. D. LIBRARY.

APPENDIX A

List of associated publications

International journals

Hernández, A. I., V. Le Rolle, D. Ojeda, P. Baconnier, J. Fontecave-Jallon, F. Guillaud, T. Grosse, R. G. Moss, P. Hannaert, and S. R. Thomas (2011). "Integration of detailed modules in a core model of body fluid homeostasis and blood pressure regulation". In: *Progress in Biophysics and Molecular Biology* 107, pp. 169–182. doi: 10.1016/j.pbiomolbio.2011.06.008.

Le Rolle, V., D. Ojeda, and A. I. Hernández (2011). "Embedding a cardiac pulsatile model into an integrated model of the cardiovascular regulation for heart failure follow-up". In: *IEEE transactions on biomedical engineering* 58.10, pp. 2982–2986.

Ojeda, D., V. Le Rolle, M. Harmouche, A. Drochon, H. Corbineau, J.-P. Verhoye, and A. I. H. Hernández (2013c). "Sensitivity analysis and parameter estimation of a coronary circulation model for triple-vessel disease". Submitted to IEEE transactions on biomedical engineering (Currently in minor revisions).

International conferences

Le Rolle, V., D. Ojeda, A. Beuchee, J.-P. Praud, P. Pladys, and A. I. Hernandez (2013). "A model-based approach for the evaluation of vagal and sympathetic activities in a newborn lamb". In: *Engineering in Medicine and Biology Society (EMBC), 2013 35th Annual International Conference of the IEEE*, pp. 3881–3884. doi: 10.1109/EMBC.2013.6610392.

Ojeda, D., V. Le Rolle, A. Drochon, H. Corbineau, J.-P. Verhoye, and A. I. Hernández (2012b). "Sensitivity analysis and parameter estimation of a coronary circulation model for patients with triple-vessel disease". In: *Proceedings of The Virtual Physiological Human 2012 (VPH2012)*. London.

Ojeda, D., V. Le Rolle, A. Drochon, M. Harmouche, H. Corbineau, J.-P. Verhoye, and A. I. Hernandez (2013b). "Multiobjective patient-specific estimation of a coronary circulation model for triple vessel disease". In: *Engineering in Medicine and Biology Society (EMBC), 2013 35th Annual International Conference of the IEEE*, pp. 3877–3880. doi: 10.1109/EMBC.2013.6610391.

Ojeda, D., V. Le Rolle, K. Tse Ve Koon, C. Thebault, E. Donal, and A. I. Hernández (2013d). "Towards an atrio-ventricular delay optimization assessed by a computer model for cardiac resynchronization therapy". In: *Proceedings of the 9th International Seminar on Medical Information Processing and Analysis*. Ed. by S. D. Library.

National conferences

OJEDA, D., V. L. ROLLE, and A. I. HERNÁNDEZ (2011). "A Model of the Cardiovascular System integrating the Coronary Circulation". In: *Recherche en Imagerie et Technologies pour la Santé (RITS 2011)*.

OJEDA, D., V. LE ROLLE, and A. I. HERNÁNDEZ (2012a). "Analyse de Sensibilité d'un modèle de la circulation coronarienne sur des patients présentant une maladie coronarienne tri-tronculaire". In: *32ème Séminaire de la Société Francophone de Biologie Théorique*. **Awarded oral presentation: Prix Delattre 2012**.

OJEDA, D., V. LE ROLLE, G. CARRAULT, and A. I. HERNÁNDEZ (2013a). "Intégration d'un modèle cardiaque pulsatile dans un modèle complet de la régulation cardiovasculaire". In: *Recherche en Imagerie et Technologies pour la Santé (RITS 2013)*.

APPENDIX B

Sensitivity analysis of the coronary model with stenoses

This appendix contains the results of a sensitivity analysis of the coronary model with the inclusion of the stenosis area reductions. The percentage of three stenoses in three arteries (left main coronary artery, left anterior descending artery and left circumflex artery) was defined within the range (1 to 99) %. Two sets of results are included in this appendix: Figures B.1 to B.3 are the sensitivity analysis results for a modification of the resistance that does not account for turbulent flow, as expressed in eq. (6.4). figs. B.4 to B.6 are the results when considering the turbulent flow, according to (Manor et al., 1994; Siebes et al., 2002) and expressed in eqs. (6.9) to (6.11).

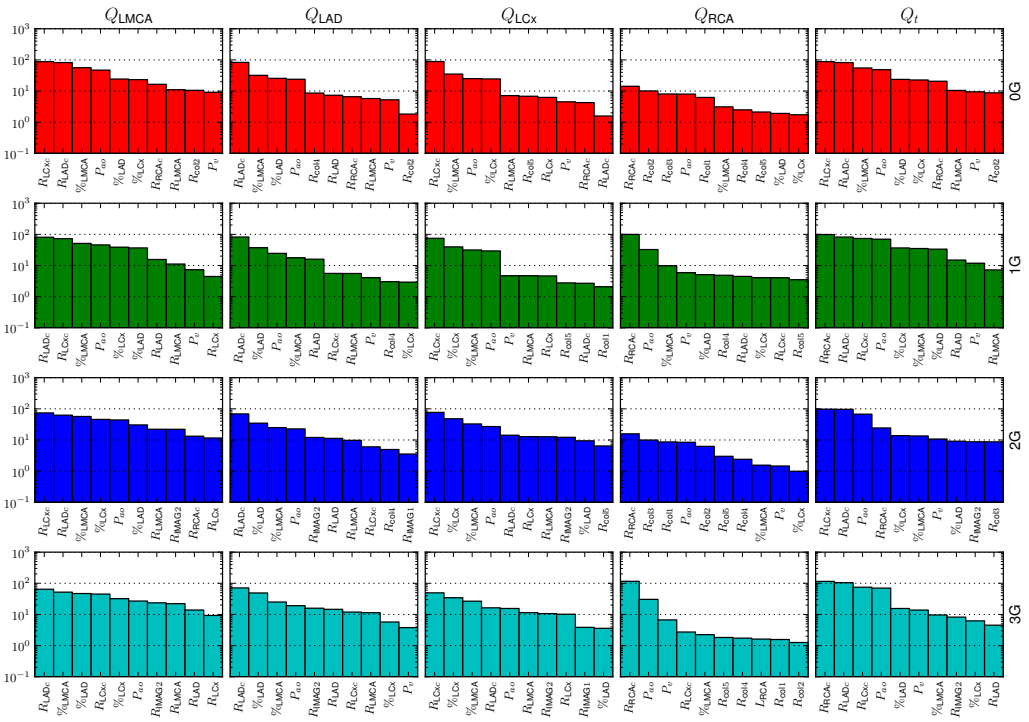

FIGURE B.1– Morris sensitivity results with linear stenoses for arterial flows (Q_{LMCA}, Q_{LAD}, Q_{LCx}, Q_{RCA}) and total coronary flow (Q_t). The Morris parameters used were $p = 20$, $\Delta = {}^{p}/_{2(p-1)} = 0.526$ and $r = 1000$ repetitions. Graphs are organized by graft cases (rows) and output variable (columns). Each graph contains only the ten most important parameters, where a bar represents the value S_{Mi} as defined in eq. (4.16) (the higher the bar, the higher the influence of the parameter).

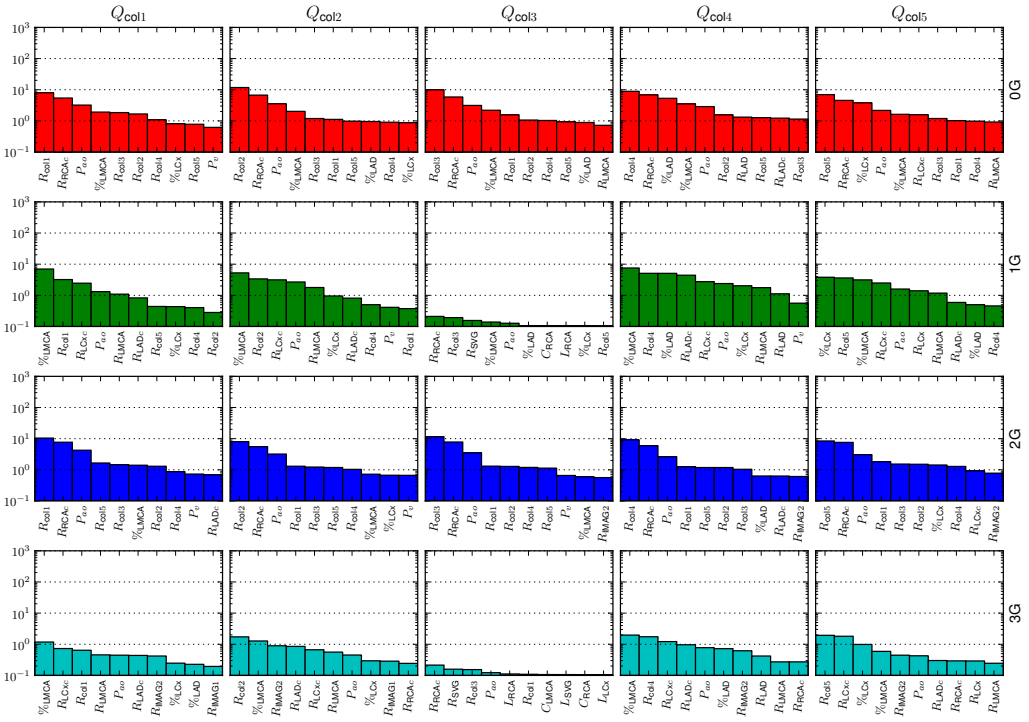

FIGURE B.2– Morris sensitivity results with linear stenoses for collateral flows (Q_{col1}, Q_{col2}, Q_{col3}, Q_{col4}, Q_{col5}). The Morris parameters used were $p = 20$, $\Delta = p/2(p-1) = 0.526$ and $r = 1000$ repetitions. Graphs are organized by graft cases (rows) and output variable (columns). Each graph contains only the ten most important parameters, where a bar represents the value S_{Mi} as defined in eq. (4.16) (the higher the bar, the higher the influence of the parameter).

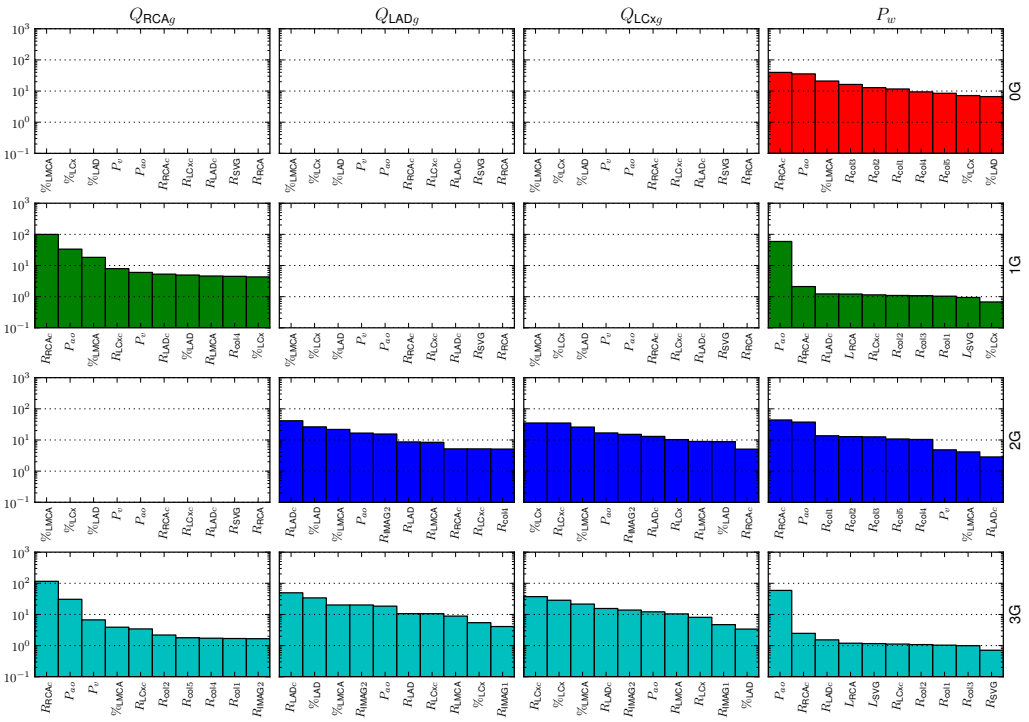

FIGURE B.3– Morris sensitivity results with linear stenoses for the coronary graft flows (Q_{RCAg}, Q_{LADg}, Q_{LCxg}) and coronary wedge pressure (P_{w}). The Morris parameters used were $p = 20$, $\Delta = p/2(p-1) = 0.526$ and $r = 1000$ repetitions. Graphs are organized by graft cases (rows) and output variable (columns). Each graph contains only the ten most important parameters, where a bar represents the value S_{Mi} as defined in eq. (4.16) (the higher the bar, the higher the influence of the parameter).

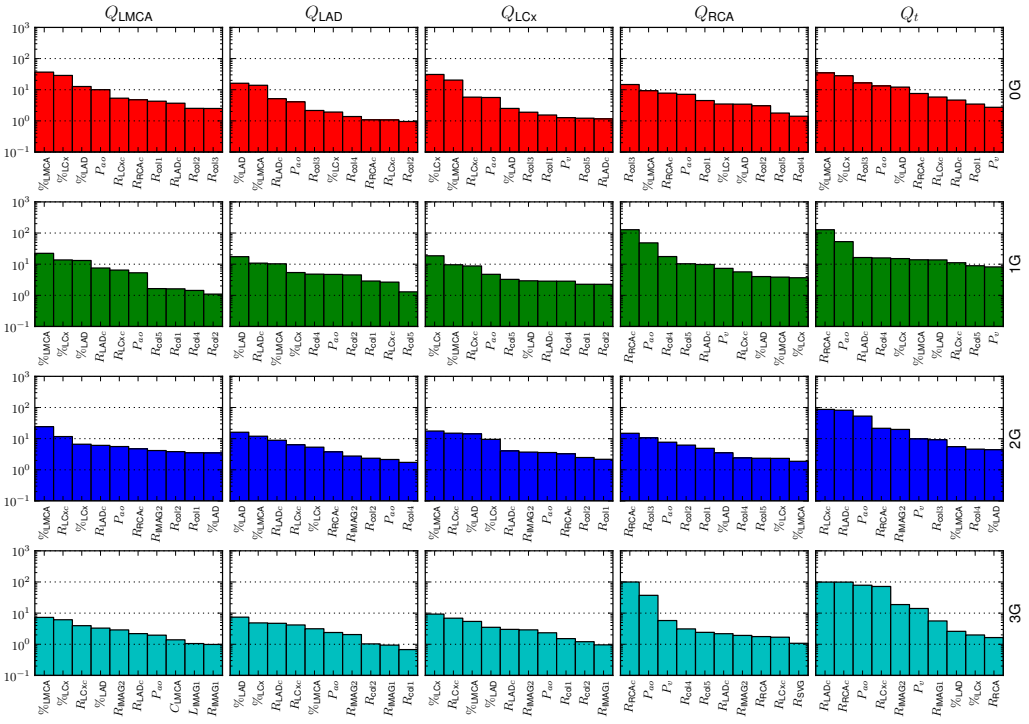

FIGURE B.4– Morris sensitivity results with nonlinear stenoses for arterial flows (Q_{LMCA}, Q_{LAD}, Q_{LCx}, Q_{RCA}) and total coronary flow (Q_t). The Morris parameters used were $p = 20$, $\Delta = p/2(p-1) = 0.526$ and $r = 1000$ repetitions. Graphs are organized by graft cases (rows) and output variable (columns). Each graph contains only the ten most important parameters, where a bar represents the value S_{Mi} as defined in eq. (4.16) (the higher the bar, the higher the influence of the parameter).

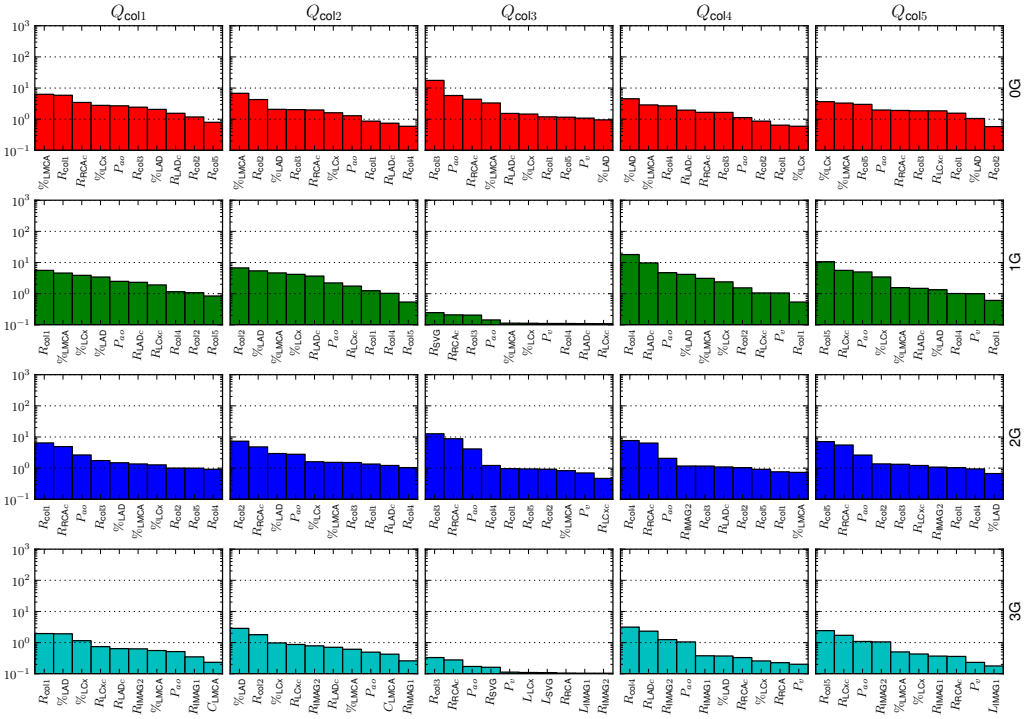

FIGURE B.5– Morris sensitivity results with nonlinear stenoses for collateral flows (Q_{col1}, Q_{col2}, Q_{col3}, Q_{col4}, Q_{col5}). The Morris parameters used were $p = 20$, $\Delta = p/2(p-1) = 0.526$ and $r = 1000$ repetitions. Graphs are organized by graft cases (rows) and output variable (columns). Each graph contains only the ten most important parameters, where a bar represents the value S_{Mi} as defined in eq. (4.16) (the higher the bar, the higher the influence of the parameter).

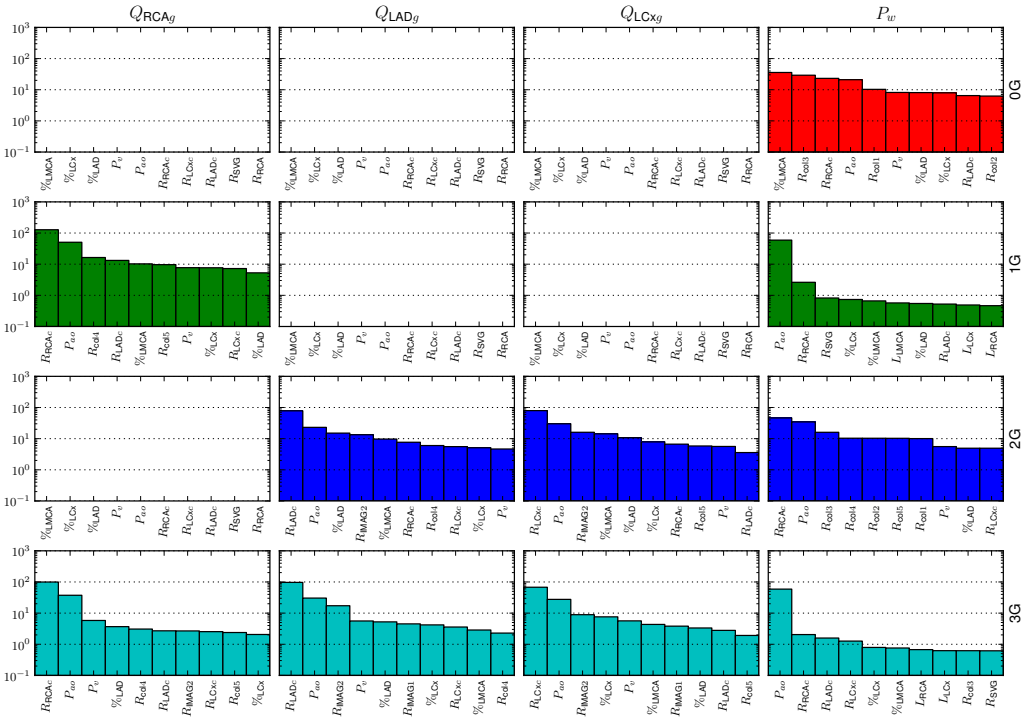

FIGURE B.6– Morris sensitivity results with nonlinear stenoses for the coronary graft flows (Q_{RCAg}, Q_{LADg}, Q_{LCxg}) and coronary wedge pressure (P_{w}). The Morris parameters used were $p = 20$, $\Delta = {}^{p}/_{2(p-1)} = 0.526$ and $r = 1000$ repetitions. Graphs are organized by graft cases (rows) and output variable (columns). Each graph contains only the ten most important parameters, where a bar represents the value S_{Mi} as defined in eq. (4.16) (the higher the bar, the higher the influence of the parameter).

TABLE B.1– Values identified for ten patients using the multiobjective optimization method with a nonlinear formulation of the stenoses. Each row represents the $\mu \pm \sigma$ of the best 10% individuals in the final population. All resistances values are given in mmHg s/mL.

(a) Capillary resistances (R_{LADc}, R_{RCAc}, R_{LCxc}), the right coronary capillary for the 1G revascularization case ($R_{\text{RCAc-1G}}$).

Patient	R_{LADc}	R_{RCAc}	$R_{\text{RCAc-1G}}$	R_{LCxc}
1	82.9±0.0	54.3±0.0	171.0±0.0	240.0±0.0
2	200.9±0.0	96.9±0.0	112.1±0.0	222.9±0.0
3	237.1±0.0	63.4±0.0	393.5±0.0	95.7±0.0
4	60.3±0.0	148.5±0.0	524.0±0.0	120.8±0.0
5	202.7±0.0	58.5±0.0	153.3±0.0	73.8±0.0
6	383.4±0.0	117.6±0.0	244.6±0.0	353.7±0.0
7	176.4±0.0	76.7±0.0	94.3±0.0	106.4±0.0
8	93.3±0.0	358.9±0.0	524.0±0.0	233.7±0.0
9	174.5±0.0	81.3±0.0	61.5±0.0	83.7±0.0
10	158.3±0.0	215.0±0.0	451.6±0.0	524.0±0.0

(b) Collateral resistances ($R_{\text{col1}} = R_{\text{col2}}$, R_{col3}, R_{col4}, R_{col5}).

Patient	RS	R_{col1}	R_{col3}	R_{col4}	R_{col5}
1	3	104.0±0.0	104.0±0.0	2000.0±0.0	104.0±0.0
2	2	2000.0±0.0	104.0±0.0	2000.0±0.0	2000.0±0.0
3	3	1991.6±0.0	104.0±0.0	570.3±0.0	380.3±0.0
4	3	2000.0±0.0	140.3±0.0	2000.0±0.0	2000.0±0.0
5	3	199.8±0.0	104.0±0.0	142.0±0.0	104.0±0.0
6	2	2000.0±0.0	158.7±0.0	2000.0±0.0	2000.0±0.0
7	3	2000.0±0.0	235.7±0.0	2000.0±0.0	642.3±0.0
8	1	2000.0±0.0	183.6±0.0	2000.0±0.0	2000.0±0.0
9	1	2000.0±0.0	104.0±0.0	2000.0±0.0	2000.0±0.0
10	2	2000.0±0.0	104.0±0.0	2000.0±0.0	2000.0±0.0

References

MANOR, D., S. SIDEMAN, U. DINNAR, and R. BEYAR (1994). "Analysis of coronary circulation under ischaemic conditions." eng. In: *Med Biol Eng Comput* 32.4 Suppl, S123–S132.

SIEBES, M., S. A. J. CHAMULEAU, M. MEUWISSEN, J. J. PIEK, and J. A. E. SPAAN (2002). "Influence of hemodynamic conditions on fractional flow reserve: parametric analysis of underlying model." eng. In: *Am J Physiol Heart Circ Physiol* 283.4, H1462–H1470. DOI: 10.1152/ajpheart.00165.2002.

APPENDIX C

Parameter values of cardiovascular models and further sensitivity analysis results

In this appendix, a detailed list of the cardiovascular model parameters are presented with their associated publications. Additionally, some results of the sensitivity analyses that were mentioned in chapter 7 are also included here.

C.1 Parameter value list found in cardiovascular model literature

The list of values shown next in table C.1 represents a thorough research of the state of the art in cardiovascular models. These reference values were used to determine the parameter ranges for sensitivity analyses and parameter estimations in chapter 7 and presented in table 7.2. Although in this work, a more extensive list was compiled for this matter, here, we only show the higher and lower values found in the literature. This selection shows how different parameter values are found in the literature, but also it permits to define a wide, yet physiologically sound range for each parameter.

Table C.1: Cardiovascular model parameter values found in literature.

Parameter	Unit	Value/Range	Reference
$E_{\mathrm{la,max}}$	$\mathrm{mmHg\,mL^{-1}}$	0.22 ± 0.05	(Dernellis et al., 1998)
		2.5	(Luo et al., 2011)

Continued on next page...

Table C.1 – Cardiovascular parameters found in the literature (continued from previous page)

Parameter	Unit	Value/Range	Reference
$E_{\mathrm{la,min}}$	$\mathrm{mmHg\,mL^{-1}}$	1.22 ± 0.36	(DERNELLIS et al., 1998)
		0.052	(URSINO, 1998)
$V_{\mathrm{d,la}}$	mL	3.05 ± 0.74	(DERNELLIS et al., 1998)
		$[7.0, 40.0]$	(LUO et al., 2011)
$E_{\mathrm{es,lv}}$	$\mathrm{mmHg\,mL^{-1}}$	7.7	(CHUNG et al., 1997)
		$[0.1, 2.5]$	(DAVIS, 1991)
$V_{\mathrm{d,lv}}$	mL	40	(LU et al., 2001)
		0	(BURKHOFF et al., 1993)
$V_{\mathrm{o,lv}}$	mL	25	(LU et al., 2001)
		0	(URSINO, 1998)
λ_{lv}	$\mathrm{mL^{-1}}$	0.014	(URSINO, 1998)
		0.5	(LUO et al., 2011)
$P_{\mathrm{o,lv}}$	mmHg	0.35	(BURKHOFF et al., 1993)
		2	(LUO et al., 2011)
R_{mt}	$\mathrm{mmHg\,s\,mL^{-1}}$	0.00045	(SMITH et al., 2007)
		0.016	(DAVIS, 1991; SATO et al., 1974)
R_{av}	$\mathrm{mmHg\,s\,mL^{-1}}$	0.007 ± 0.002	(HELDT, 2004)
		$[0.03, 0.045]$	(URSINO, 1998)
R_{la}	$\mathrm{mmHg\,s\,mL^{-1}}$	0.01	(LU et al., 2001)
		0.0056	(URSINO, 1998)
R_{ra}	$\mathrm{mmHg\,s\,mL^{-1}}$	0.010	(LU et al., 2001)
		0.075	(KORAKIANITIS et al., 2006)
$E_{\mathrm{ra,max}}$	$\mathrm{mmHg\,mL^{-1}}$	0.74 ± 0.1	(HELDT, 2004)
		0.25	(KORAKIANITIS et al., 2006)
$E_{\mathrm{ra,min}}$	$\mathrm{mmHg\,mL^{-1}}$	0.30 ± 0.05	(HELDT, 2004)
		0.15	(KORAKIANITIS et al., 2006)
$V_{\mathrm{d,ra}}$	mL	30.0	(BENEKEN et al., 1967)
		4.0	(KORAKIANITIS et al., 2006)
$E_{\mathrm{es,rv}}$	$\mathrm{mmHg\,mL^{-1}}$	$[0.62, 2.87]$	(DELL'ITALIA et al., 1988)
		$[0.05, 0.834]$	(DAVIS, 1991)
$V_{\mathrm{d,rv}}$	mL	46.0 ± 21.0	(HELDT, 2004)
		0	(BURKHOFF et al., 1993)
$V_{\mathrm{o,rv}}$	mL	25	(LU et al., 2001)
		0	(URSINO, 1998)
λ_{rv}	$\mathrm{mL^{-1}}$	0.0587	(CHUNG et al., 1997)

Continued on next page...

Table C.1 – Cardiovascular parameters found in the literature (continued from previous page)

Parameter	Unit	Value/Range	Reference
		0.01	(Luo et al., 2011)
$P_{o,rv}$	mmHg	1.2	(Smith et al., 2007)
		0.35	(Burkhoff et al., 1993)
R_{tc}	$\mathrm{mmHg\,s\,mL^{-1}}$	0.0013	(Smith et al., 2007)
		0.08	(Beneken et al., 1967; Davis, 1991)
R_{pv}	$\mathrm{mmHg\,s\,mL^{-1}}$	0.021	(Chung et al., 1997)
		0.003	(Davis, 1991)
$E_{es,spt}$	$\mathrm{mmHg\,mL^{-1}}$	48.75	(Chung et al., 1997; Smith et al., 2007)
		40	(Luo et al., 2011)
$V_{d,spt}$	mL	2	(Chung et al., 1997; Smith et al., 2007)
		0	(Luo et al., 2011)
$V_{o,spt}$	mL	2	(Chung et al., 1997; Smith et al., 2007)
		0	(Luo et al., 2011)
λ_{spt}	$\mathrm{mL^{-1}}$	0.435	(Chung et al., 1997; Smith et al., 2007)
		0.05	(Luo et al., 2011)
$P_{o,spt}$	mmHg	1.11	(Chung et al., 1997; Smith et al., 2007)
		1.5	(Ursino, 1998)
$V_{o,pcd}$	mL	200	(Lu et al., 2001)
		20	(Chung et al., 1997)
λ_{pcd}	$\mathrm{mL^{-1}}$	0.03	(Smith et al., 2007)
		0.005	(Luo et al., 2011)
$P_{o,pcd}$	mmHg	0.5	(Smith et al., 2007)
		1.0	(Chung et al., 1997)
E_{ao}	$\mathrm{mmHg\,mL^{-1}}$	0.758	(Burkhoff et al., 1993)
		0.625	(Davis, 1991)
$V_{d,ao}$	mL	800	(Smith et al., 2007)
		425	(Beneken et al., 1967)
E_{vc}	$\mathrm{mmHg\,mL^{-1}}$	0.0143	(Burkhoff et al., 1993)
		0.01	(Davis, 1991)
$V_{d,vc}$	mL	2665 ± 218	(Heldt, 2004)
		2500	(Davis, 1991)
R_{sys}	$\mathrm{mmHg\,s\,mL^{-1}}$	$[0.77, 1.52]$	(Heldt, 2004)
		0.9	(Burkhoff et al., 1993)
E_{pa}	$\mathrm{mmHg\,mL^{-1}}$	$[0.67, 3.55]$	(Reuben, 1971)
		0.0769	(Burkhoff et al., 1993)

Continued on next page...

Table C.1 – Cardiovascular parameters found in the literature (continued from previous page)

Parameter	Unit	Value/Range	Reference
$V_{\mathrm{d,pa}}$	mL	160 ± 20	(HELDT, 2004)
		50	(BENEKEN et al., 1967)
E_{pu}	$\mathrm{mmHg\,mL^{-1}}$	9.0 ± 3.7	(HELDT, 2004)
		0.006	(SMITH et al., 2007)
$V_{\mathrm{d,pu}}$	mL	120	(URSINO, 1998)
		490	(DAVIS, 1991)
R_{pul}	$\mathrm{mmHg\,s\,mL^{-1}}$	$[0.01, 0.16]$	(HELDT, 2004)
		0.312	(KORAKIANITIS et al., 2006)
P_{th}	mmHg	-3 ± 0.5	(HELDT, 2004)
		-4	(SMITH et al., 2007)
AVD	ms	$[40.0, 200.0]$	(WHINNETT et al., 2006)
VVD	ms	$[-40.0, 60.0]$	(WHINNETT et al., 2006)
B_{la}	$\mathrm{s^{-2}}$	$[60.0, 120.0]$	(KOON et al., 2010)
		1531	(KORAKIANITIS et al., 2006)
C_{la}	s	$[0.2, 0.3]$	(HELDT, 2004)
		0.045	(KORAKIANITIS et al., 2006)
B_{ra}	$\mathrm{s^{-2}}$	$[60.0, 120.0]$	(KOON et al., 2010)
		1531	(KORAKIANITIS et al., 2006)
C_{ra}	s	$[0.2, 0.3]$	(HELDT, 2004)
		0.045	(KORAKIANITIS et al., 2006)
C_{lv}	s	$[0.34, 0.39]$	(HELDT, 2004)
		0.175	(BURKHOFF et al., 1993)
C_{rv}	s	$[0.34, 0.39]$	(HELDT, 2004)
		0.175	(BURKHOFF et al., 1993)
T_{UDP}	ms	$[70.0, 80.0]$	(HERNÁNDEZ, 2000, for PaceLVDelay)
T_{UDP}	ms	$[70.0, 80.0]$	(HERNÁNDEZ, 2000, for FPSRA1)
HR	bpm	$[46.0, 89.0]$	(HELDT, 2004)
		60	(KORAKIANITIS et al., 2006)
Blood volume	L	5.5	(SMITH et al., 2007)
		$[3.75, 6.89]$	(HELDT, 2004)

C.2 Detailed results of the Morris screening method

In chapter 7, the Morris elementary effects results only included the top 30 most important parameters, in order to improve the readability of this chapter. Here, we present the complete results of all parameters and for each output variable of the model: E and A wave amplitude (fig. C.1), mitral flow time duration and time integral (fig. C.2).

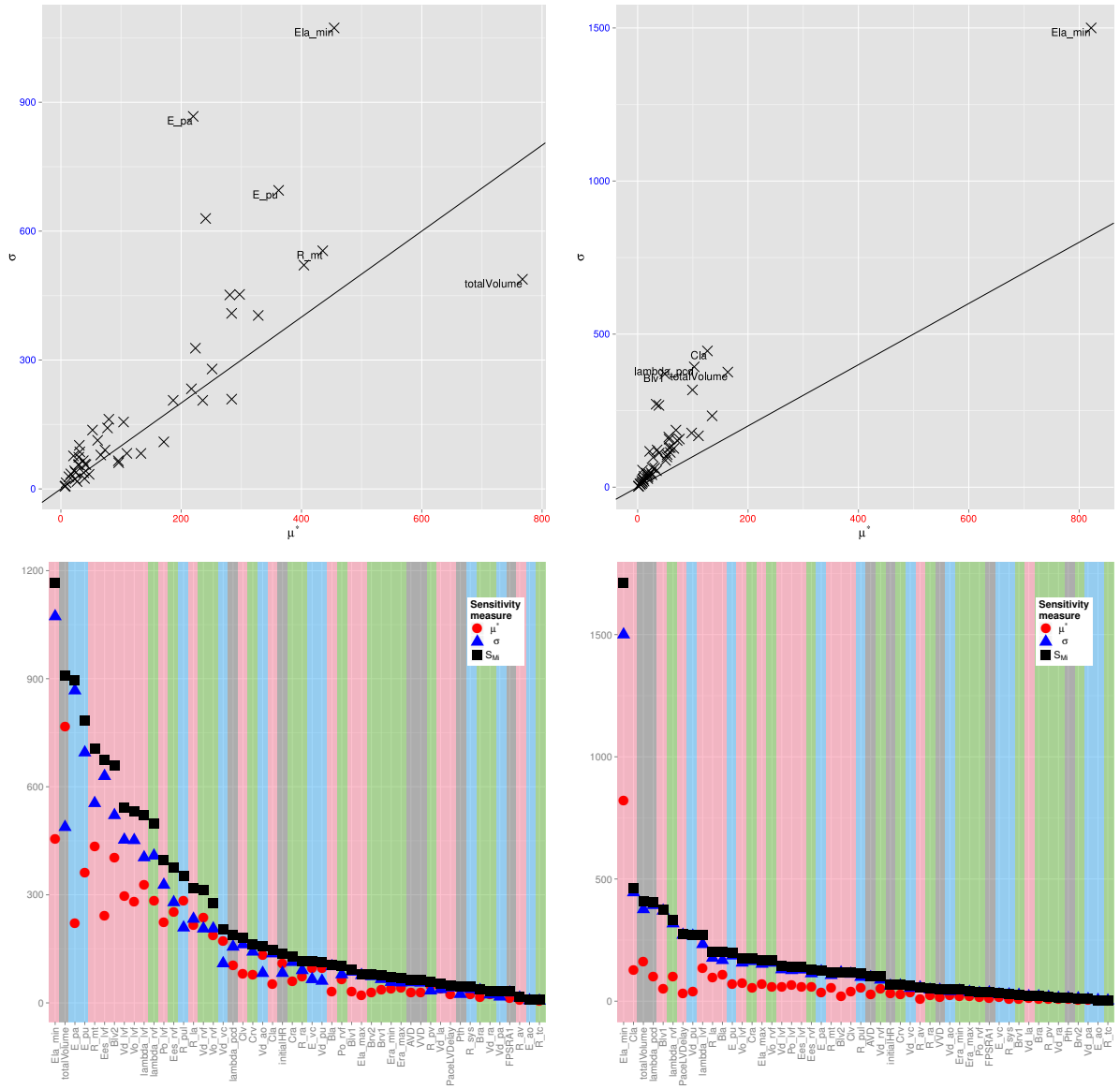

(a) Elementary effects for E wave amplitude.

(b) Elementary effects for A wave amplitude.

FIGURE C.1– Results of Morris elementary effects method for E and A wave amplitudes. Top plots show the $\mu^* - \sigma$ plane. Bottom plots show the mean (μ^*), standard deviation (σ) and the Morris index (S_{Mi}). Background of bottom plots are color-coded: red stripes are parameters of the left heart, green stripes are parameters of the right heart, blue stripes are parameters related to the circulation, and gray stripes are general or other parameters.

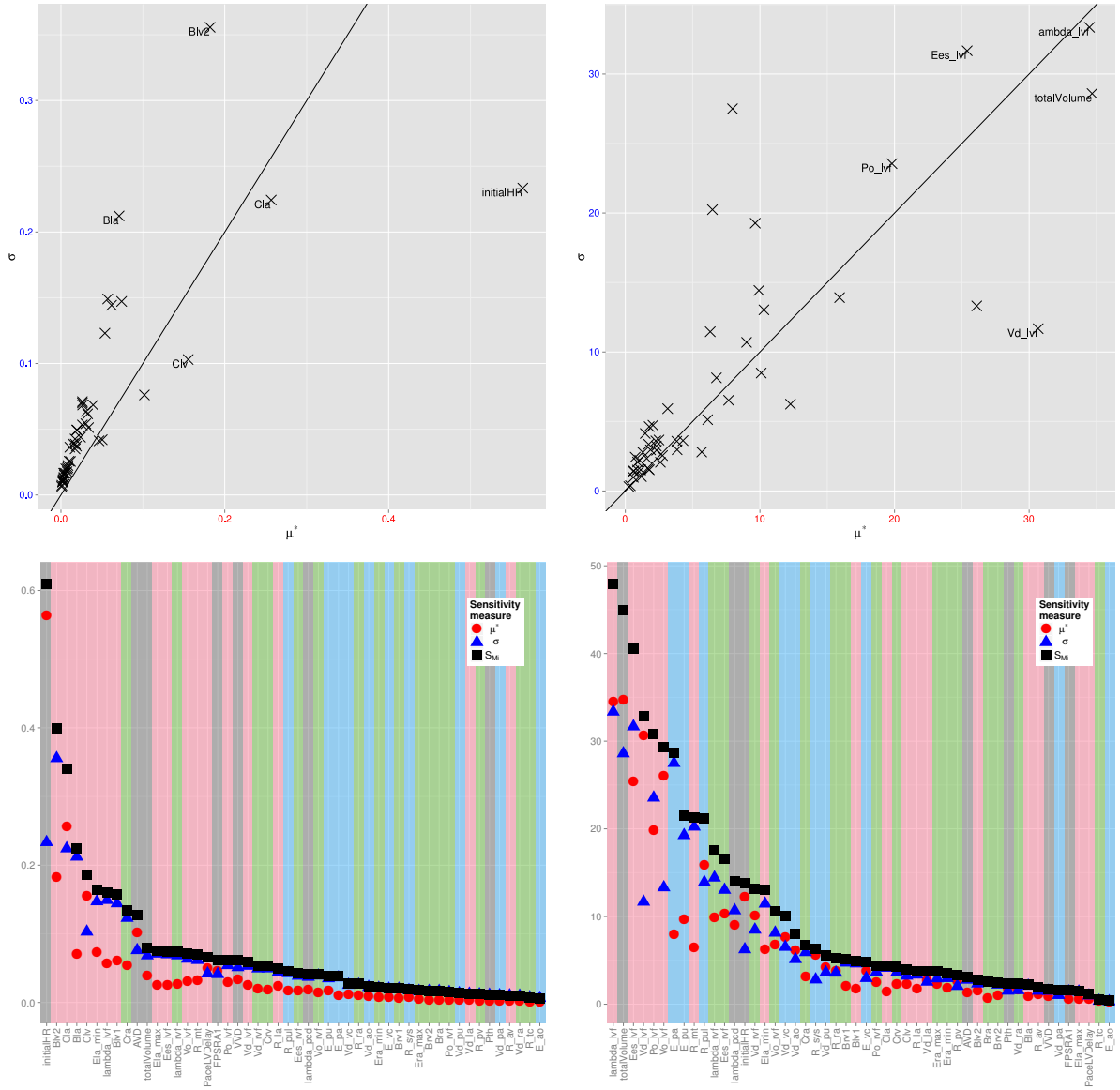

(a) Elementary effects for mitral flow duration.

(b) Elementary effects for mitral flow time integral.

FIGURE C.2– Results of Morris elementary effects method for mitral flow time duration and time integral. Top plots show the $\mu^* - \sigma$ plane. Bottom plots show the mean (μ^*), standard deviation (σ) and the Morris index (S_{Mi}). Background of bottom plots are color-coded: red stripes are parameters of the left heart, green stripes are parameters of the right heart, blue stripes are parameters related to the circulation, and gray stripes are general or other parameters.

References

Beneken, J. E. and B. DeWit (1967). "A physical approach to hemodynamic aspects of the human cardiovascular system". In: *Physical bases of circulatory transport: regulation and exchange*. Ed. by E. Reeve and A. Guyton. Philadelphia: Saunders, pp. 1–45.

Burkhoff, D. and J. V. Tyberg (1993). "Why does pulmonary venous pressure rise after onset of LV dysfunction: a theoretical analysis." eng. In: *Am J Physiol* 265.5 Pt 2, H1819–H1828.

Chung, D., S. Niranjan, J. Clark, A. Bidani, W. Johnston, J. Zwischenberger, and D. Traber (1997). "A dynamic model of ventricular interaction and pericardial influence". In: *American Journal of Physiology-Heart and Circulatory Physiology* 272.6, H2942.

Davis, T. L. (1991). "Teaching physiology through interactive simulation of hemodynamics". MA thesis. Massachusetts Institute of Technology.

Dell'Italia, L. J. and R. A. Walsh (1988). "Application of a time varying elastance model to right ventricular performance in man". In: *Cardiovascular Research* 22.12, pp. 864–874. doi: 10.1093/cvr/22.12.864. eprint: http://cardiovascres.oxfordjournals.org/content/22/12/864.full.pdf+html.

Dernellis, J. M., C. I. Stefanadis, A. A. Zacharoulis, and P. K. Toutouzas (1998). "Left atrial mechanical adaptation to long-standing hemodynamic loads based on pressure-volume relations." eng. In: *Am J Cardiol* 81.9, pp. 1138–1143.

Heldt, T. (2004). "Computational models of cardiovascular response to orthostatic stress". PhD thesis. MIT Division of Health Sciences and Technology: Harvard University.

Hernández, A. I. (2000). "Fusion de signaux et de modèles pour la caractérisation d'arythmies cardiaques". PhD thesis. Université de Rennes 1.

Koon, K. T. V., C. Thebault, V. Le Rolle, E. Donal, and A. I. Hernández (2010). "Atrioventricular delay optimization in cardiac resynchronization therapy assessed by a computer model". In: *Computing in Cardiology, 2010*. IEEE, pp. 333–336.

Korakianitis, T and Y Shi (2006). "A concentrated parameter model for the human cardiovascular system including heart valve dynamics and atrioventricular interaction". In: *Med Eng Phys* 28.7, pp. 613–628. doi: 10.1016/j.medengphy.2005.10.004.

Lu, K, J. W. Clark, F. H. Ghorbel, D. L. Ware, and A Bidani (2001). "A human cardiopulmonary system model applied to the analysis of the Valsalva maneuver". In: *Am J Physiol Heart Circ Physiol* 281.6, pp. 2661–2679.

Luo, C., D. Ramachandran, D. L. Ware, T. S. Ma, and J. W. Clark (2011). "Modeling left ventricular diastolic dysfunction: classification and key indicators." eng. In: *Theor Biol Med Model* 8, p. 14. doi: 10.1186/1742-4682-8-14.

Reuben, S. R. (1971). "Compliance of the human pulmonary arterial system in disease." eng. In: *Circ Res* 29.1, pp. 40–50.

Sato, T., S. M. Yamashiro, D. Vega, and F. S. Grodins (1974). "Parameter sensitivity analysis of a network model of systemic circulatory mechanics". In: *Annals of Biomedical Engineering* 2.3, pp. 289–306.

Smith, B., S. Andreassen, G. Shaw, P. Jensen, S. Rees, and J. Chase (2007). "Simulation of cardiovascular system diseases by including the autonomic nervous system into a minimal model". In: *Computer methods and programs in biomedicine* 86.2, pp. 153–160.

Ursino, M. (1998). "Interaction between carotid baroregulation and the pulsating heart: a mathematical model." In: *Am J Physiol* 275.5 Pt 2. issn: 0002-9513.

Whinnett, Z. I., J. E. Davies, K Willson, C. H. Manisty, A. W. Chow, R. A. Foale, D. W. Davies, A. D. Hughes, J Mayet, and D. P. Francis (2006). "Haemodynamic effects of changes in atrioventricular and interventricular delay in cardiac resynchronisation therapy show a consistent pattern: analysis of shape, magnitude and relative importance of atrioventricular and interventricular delay". In: *Heart* 92.11, pp. 1628–1634. doi: 10.1136/hrt.2005.080721.

List of Figures

List of Tables

VU:

VU:

Le Directeur de Thèse
ALFREDO I HERNÁNDEZ

Le Responsable de l'école doctorale

VU pour autorisation de soutenance
Rennes, le

Le Président de l'Université de Rennes 1

Guy CATHELINEAU

VU après soutenance pour autorisation de publication:

Le Président de Jury